Redox Characteristics of Shallow Groundwater in the Tararua Ground Water Management Zone

A thesis presented in partial fulfilment of the requirements for the degree of

Master of Science in Earth Science

at Massey University, Manawatū, New Zealand

Peter Grant McGowan

2018

Abstract

Groundwater redox conditions have a major influence on transport and transformation of nutrients such as nitrate from farms to rivers and lakes. This study focused on measurement and analysis of chemical and physical characteristics of groundwater to determine the spatial distribution of redox characteristics across the Tararua Ground Water Management Zone in the Manawatu River catchment. The influence of catchment characteristics such as soil texture and drainage, and rock type have on groundwater chemistry and its redox characteristics across the Tararua GWMZ is investigated using multivariate statistical analysis.

Existing geographical information was collated and analysed to map spatial distributions of landuse, soil characteristics and lithologies across the study area. This information was utilised to identify potential site locations for sampling and analysis of shallow groundwater in the Tararua GWMZ. A direct-push system capable of penetrating a range of substrates including deep, imbricated, and coarse gravels was developed. Using this system, shallow groundwater samples were recovered from contrasting hydrogeological settings, areas where water wells are rarely installed; such as along the margins of the axial ranges, and from areas considered not to have groundwater; e.g. the mudstone country on the east of the Tararua District.

Data collected with the direct-push method was combined with similar data collected from existing wells by Rivas et al. (2017) and classified according to redox status. The data was subjected to multivariate statistical assessment using Hierarchical Cluster Analysis to determine the water type, and Principle Component Analysis to determine the influence of discrete catchment characteristics on redox reactions occurring in shallow groundwater of the Tararua GWMZ.

The in-field and chemical analysis revealed significant variation of groundwater quality parameters and redox characteristics across the Tararua GWMZ. The regional trend was for reducing conditions in gravel aquifers in the north western areas of the Tararua GWMZ and oxidising in gravel aquifers of the south western; although statistically significant variations of redox characteristics is also recognised within these areas. Groundwater samples were collected from mudstone where little, if any, groundwater research has been conducted previously. Groundwater characteristics from mudstone are generally classified as anoxic and strongly reducing, with very high specific conductivity and analyte levels such as bromide, chlorine, sodium, fluorine, dissolved inorganic carbon and magnesium. Identifying the influence of discrete catchment characteristics on groundwater chemistry and redox characteristics was complex and difficult to quantify. Extrapolation of the principal component inferred to be associated with redox characteristics provides a useful means to evaluate the influence of discrete catchment characteristics on redox conditions in shallow groundwater of the Tararua GWMZ. The direct-push method provided an opportunity to compare groundwater chemistry between samples collected proximal and distal to production wells. Statistically significant differences in redox related parameters such as DOC, *Eh*, Fe^{2+}, Mn^{2+}, NH_4^+-N, and NO_2^--N were detected in groundwater samples collected from existing wells compared to groundwater samples collected with the direct-push method. Factors contributing to this effect were explored but found to be difficult to isolate.

Acknowledgements

Massey University is an amazing institution, without the extramural program and financial support via generous scholarships I would have never been able to complete this thesis. I would also like to thank Horizons Regional Council who provided generous financial support for the analysis of my groundwater samples. I sincerely appreciate the confidence my supervisors placed in me to progress and develop my thesis as I saw fit; yet were always there to provide incisive direction when necessary, thank you Ranvir and Alan.

I gratefully acknowledge the farmers who kindly granted permission for me wander on their land and poke holes through their pasture. Nitrate contamination of groundwater, particularly for the dairy industry is a hot topic at present, yet the farmers were welcoming and keen to establish what was happening on a local and regional basis.

Sincere thanks must go to Terrance from Perry Geotech who kindly provided expensive drill rods for the project and never blinked an eye when I lost an entire string down a hole…twice. Also to David Feek who's technical, engineering and problem solving abilities were outstanding, and his mordant comments on my fieldwork aspirations never failed to jolt me back to reality.

I also would like thank my close friends, Shaun and Fiona, and Bruce and Debbie who over a beer and dinner would often quietly sit and listen to my ramblings of experiences and newfound geological knowledge. I could see your eyes, glazed at times, but never closed, thank you.

My very dear mentor and friend, Monty Blomfield guided and supported me over the last 25 years for which I am eternally grateful. Unashamedly from the "old school" Monty taught me so much and encouraged me to take the plunge into academia. Our many fishing and hunting adventures were awesome, but simply spending time in his presence counted more than anything; more so now that he has passed on.

Over the course of my studies both my parents also passed away. Truly wonderful parents and friends, they always encouraged me to remain positive, develop an enquiring mind, look for the good in everyone, and enjoy life's every moment. I feel so sad that they weren't able to see to where my journey has led.

To our children Krystie, Jarrad, and Ryan, you guys are simply the most amazing young people, and if you ever agree to go in the car with me again, I promise not to hold you hostage and waffle on about subduction, obduction, rocks, minerals, plate tectonics, back arc volcanism, turbidites, ultramafics, ophiolites, hydrothermal alteration, mineralization, aquifers, hydraulic conductivity, etc. etc. etc.

Finally I would like to thank my wonderful wife Julie for putting up with me over these long years. I may have been a tad temperamental on the odd occasion, and living apart for 2 ½ years was very difficult for both of us. But you understood that although times were tough, I was following my dream and you never complained. Thank you so much, I will make it up to you.

Frontispiece: The Mangatewainui Stream. This image captures the essence of the Tararua GWMZ; swift flowing streams, vast quantities of greywacke gravels, and tectonically deformed marine sediments that underlie shallow gravel aquifers often mantled with a veneer of loess.

Table of Contents

List of Figures

List of Tables

List of Equations

List of Abbreviations and Acronyms

Major Inorganic Constituents

Abbreviation	units	Parameter Name
Ca^{2+}	mg L^{-1}	Dissolved calcium
Cl^{-}	mg L^{-1}	Dissolved chlorine
DIC	mg L^{-1}	Dissolved inorganic carbon
DOC	mg L^{-1}	Dissolved organic carbon
HCO_3^{-}	mg L^{-1}	Dissolved bicarbonate
K^{+}	mg L^{-1}	Dissolved potassium
Mg^{2+}	mg L^{-1}	Dissolved magnesium
Na^{+}	mg L^{-1}	Dissolved sodium
SiO_2	mg L^{-1}	Dissolved silica

Minor Inorganic Constituents

Abbreviation	units	Parameter Name
As	mg L^{-1}	Dissolved arsenic
B	mg L^{-1}	Dissolved boron
Br^{-}	mg L^{-1}	Dissolved bromide
Cd	mg L^{-1}	Dissolved cadmium
CH_4	mg L^{-1}	Dissolved methane (gas)
CO_2	mg L^{-1}	Dissolved carbon dioxide (gas)
F^{-}	mg L^{-1}	Dissolved fluoride
Fe(II)	mg L^{-1}	Dissolved Iron; ferrous (oxidation state $^{+}2$)
Fe(III)	mg	Iron; ferric (oxidation state $^{+}3$)
HS^{-}	mg L^{-3}	Dissolved bisulphide
H_2S	mg L^{-1}	Dissolved hydrogen sulphide
Mn(II)	mg L^{-1}	Dissolved manganese (oxidation state $^{+}3$)
Mn(IV)	mg	Manganese (oxidation state $^{+}4$)
NaCl	mg L^{-1}	Sodium chloride
TA_meq/L	meq L^{-1}	Alkalinity milliequivalents

TATemp	°C	Temperature at total alkalinity analysis
TitrantVol	ml	Titrant volume
TApH	pH	Total alkalinity; titrant analysis pH
TA_mgCaCO$_3$	mg L^{-1}	Total alkalinity as calcium carbonate

Nutrients

Abbreviation	units	Parameter Name
NH_4^+	mg L^{-1}	Ammonium cation (atomic mass = 18)
NH_4^+ -N	mg L^{-1}	Ammoniacal nitrogen (atomic mass = 14)
NO_3^-	mg L^{-1}	Nitrate anion (atomic mass = 62)
NO_3^- -N	mg L^{-1}	Nitrate as nitrogen (atomic mass = 14)
NO_2^-	mg L^{-1}	Nitrite anion (atomic mass = 46)
NO_2^- -N	mg L^{-1}	Nitrite as nitrogen (atomic mass = 14)
N_r	n/a	Reactive nitrogenous compound
SO_4^{2-}	mg L^{-1}	Sulphate
TON	mg L^{-1}	Total organic nitrogen
TRP	mg L^{-1}	Total reactive phosphorus
TOC	mg L^{-1}	Total organic carbon

Physical Characteristics

Abbreviation	units	Parameter Name
Baro	kPa	Barometric pressure
DO	mg L^{-1}	Dissolved oxygen
DOsat	%	Dissolved oxygen; percentage saturation
EC	µS cm^{-1}	Electrical conductivity
Eh	µS cm^{-1}	Electrical conductivity (hydrogen electrode)
O_2	n/a	Oxygen gas
N_2	n/a	Nitrogen Gas
ORP	mV	Oxidation-reduction potential
pH	pH	The acidity or basicity of an aqueous solution
SPC	µS cm^{-1}	Specific conductivity; EC temperature corrected

SpActual	µS cm^{-1}	Actual conductivity
TDS	ppm	Total dissolved solids
Temp	°C	Temperature

QMap, Geological, and GIS

Abbreviation	Parameter Name
Cong	Conglomerate
Coq	Coquina
Grv	Gravel
GrW	Greywacke
LST	Limestone
MST	Mudstone
SST	Sandstone
KEY_NAME	Combines stratigraphic age, stratigraphic name, and lithological information
MAIN_ROCK	Mainrocks QMap class derived from the most commonly encountered rocks in an particular area (scale 1:250,00)
QMap	Geological map series of N.Z.
SIM_NAME	Combines stratigraphic age and depositional environment
SUBROCK	subrocks QMap A class derived from subordinate rock types found with main rock types (scale 1:250,00)
SUBROCK_ Simple	Sub rocks simplified and condensed

Statistical

Abbreviation	Parameter Name
ANNOVA	Analysis of variance
Cmp	Principal component derived by PCA
HCA	Hierarchal cluster analysis
IDF	Inverse-DF function used to normalise data
KMO	Kaiser-Meyer-Olkin measure of adequacy
PCA	Principal component analysis

SPSS	Statistics software from IBM

General

Abbreviation	Parameter Name
AirTemp	Ambient temperature at time of sampling
ATP	ATP adenosine triphosphate
CBE	Charge Balance Equation
CNC	Computer Numerical Control
CPT	Cone Penetration test
DEA	Denitrifying enzyme activity
DEM	Digital Elevation model
DL	Detection limit
DNRA	Dissimilatory nitrate reduction to ammonia
DRASTIC	Drastic
FSL	FSL fundamental soil layers
GIS	Geographic information systems
GNS	New Zealand Crown Research Institute; formerly Institute of Geological and Nuclear Sciences
GPS	Global positioning system
PPK	Post Processing Kinematic GPS
GV	Guideline value
ha	Hectares
HRC	Horizons Regional Council (HRC)
KML	File extension registered with Google Earth software
LCDB	Land Cover Database version 4.1.
LRIS	Land Resource Information Systems Portal
MAV	Maximum allowable value
MP	Multi-purpose
NIWA	The National Institute of Water and Atmospheric Research Ltd.
NOF	National Objectives Framework which defines upper and

	lower limits for water quality parameters including nitrates
OC	Organic carbon
OM	Organic matter
OSH	Occupational Safety and Health
PET	Polyethylene terephthalate (thermoplastic polymer resin containers)
Redox	Oxidation-reduction reaction
smarTROLL	Handheld multi-parameter water quality instrument
Soln	solution
SOM	Soil organic matter
Tararua GWMZ	Tararua Groundwater Management Zone
TEAP	Terminal electron acceptor process
Tg	1 x 10^6 tonne
TVZ	Taupo Volcanic Zone
WHO	World Health Organization

Chapter 1: Thesis Overview

1.1 Introduction

Nitrate (NO_3^-) is one of the most pervasive water pollutants associated with modern anthropogenic activities (Spalding & Exner, 1993). It is highly soluble, stable when dissolved, and will not bind to soil particles (Killpack & Buchholz, 2008). Nitrogen saturation in the soil occurs when the capability of plants, soils and microorganisms to assimilate the additional nitrogen is exceeded (Saggar et al., 2013). When the soils field capacity is exceeded and water cannot be held within the soil zone, dissolved nitrate will either be transported downwards into groundwater, or across the surface as runoff (Killpack & Buchholz, 2008; Saggar et al., 2013). Elevated rates of NO_3^- are widely encountered in surface water and groundwater settings, both fresh and marine, throughout inland and coastal regions across the globe (Howarth & Marino, 2006). Global NO_3^- levels vary widely but peak concentrations tend to be associated with areas of high population density and/or high levels of agricultural activity (Howarth & Marino, 2006). The nature of New Zealand's nitrogen outputs are distinctive due to our large, and often highly intensive, agricultural sector (Parfitt, Schipper, Baisden, & Elliott, 2006).

The main source of nitrate in New Zealand's ground and surface water is reputed to originate from dairy cow excreta where up to 25% of grazed pasture may be contaminated by urine patches containing around 600 to 1000 kg N ha^{-1} (Moir, Cameron, Di, & Fertsak, 2011). However, Woodward, Stenger, and Bidwell (2011) maintain that nitrate inputs from dry-stock farms should not be discounted; although generally considered less intensive than dairy on a stock-unit per hectare basis, sheep and beef farms may also contribute significantly to nitrate levels due to their large area. Other inputs of NO_3^- may occur as non-point sources of nitrates originating from

nitrogenous fertilizers, legume crops, irrigation flow returns, and weathering of nitrogen bearing rocks, while point sources of NO_3^- may arise from cesspits, septic tanks and occasionally from thermal waters (Aksever, Davraz, & Karagüzel, 2015). Within New Zealand, up to 5% of monitored water supplies exceed World Health Organisation (WHO, 2011) water quality (nitrate) standards of 11.3 mg nitrate-nitrogen (NO_3^--N) L^{-1}, and from 1994 to 2013 nitrate-nitrogen concentrations worsened at 55.3% of all monitored sites; 68.1% of sites are located in the pastoral land-cover class (Statistics New Zealand, 2017).

Growing awareness of consequences from losses of nitrogen occurring between the agricultural soils and the receiving waters is driving further research to better quantify pathways and trends of nitrogen transport in the subsurface environment (e.g. Elwan et al., 2016; Parfitt et al., 2012; Rivas et al., 2017; R Singh et al., 2017). However, not all nitrogen rich leachate entering the subsurface environment will inevitably discharge to and contaminate surficial waters (McMahon & Chapelle, 2008; Rivas et al., 2017; Stenger et al., 2005; Stenger, Barkle, Burgess, Wall, & Clague, 2008; Stenger, Clague, Woodward, Moorhead, Wilson, Shokri, Wohling, et al., 2013). In specific hydrogeologic settings, a series of microbial facilitated oxidation-reduction reactions may result in step wise reduction of NO_3^- to relatively inert dinitrogen gas in a process known as denitrification (McMahon & Chapelle, 2008). The hydrochemical conditions required for denitrification to occur in groundwater are now relatively well understood (e.g. Barkle, Clough, & Stenger, 2007; Korom, 1992; McMahon & Chapelle, 2008; Schüring et al., 2013), but the hydrogeological factors that control the spatial diversity of groundwater chemistry and its redox status are still poorly known (Rivas et al., 2017).

This research therefore attempts to address some of the gaps in current knowledge relating to the influence of different soils and rocks types on the redox characteristics of shallow groundwater in the Tararua Ground Water Management Zone (Tararua GWMZ), located in southern Hawkes Bay and Northern Wairarapa.

The Tararua GWMZ is seen as an ideal study area for a variety of reasons. Encompassing the Pahiatua Basin and bounded to the west and east by uplifted and tilted greywacke ranges, reasonable assessment of nitrogen inputs and outputs is possible. This is due to the majority of infiltrated precipitation (less evapotranspiration) is believed to discharge from the Tararua GWMZ via the Manawatu gorge (Rawlinson & Begg, 2014), (Figure 1). A diverse range of sedimentary rocks such as mudstones, sandstones, limestones, greywackes and alluvial gravel deposits are widespread throughout the region (Lee & Begg, 2002; Lee et al., 2011). As parent materials for the regions soils, these rocks provide for a diverse range of soil chemistry, textures, and drainage. The large gravel deposits are associated with relatively impermeable underlying facies (which serve as aquitards), resulting in extensive aquifers underlying the alluvial plains (Rawlinson & Begg, 2014). The expansive alluvial plains and significant groundwater reserves prove ideal for dairy farming operations; the predominant landuse in the flat to undulating terrain of the Tararua GWMZ. The environmental impact of modern dairy farming systems, particularly with regard to nitrogenous leachate is well documented (e.g. Barkle et al., 2013; Jha et al., 2013; Ledgard, Penno, & Sprosen, 1999; Moir et al., 2011; Singleton et al., 2007; Stenger et al., 2008). Bearing in mind the physical characteristics of the area such as shallow, often unconfined, productive aquifers (Rawlinson & Begg, 2014), the potential negative influence of farming has resulted in considerable focus on water quality management in the Tararua GWMZ by Horizons Regional Council (McArthur, Roygard, Ausseil, & Clark, 2007). Earlier studies supported in part by HRC, reveal significant differences between estimates of nitrate loss from farms to nitrate loads in the rivers (e.g. Elwan, Singh, Horne, Roygard, & Clothier, 2015; R. Singh, Rivas, et al., 2014a, 2014b). Further studies (e.g. Elwan, 2015; Rivas, Singh, Horne, et al., 2014; Rivas et al., 2017; R. Singh, Rivas, et al., 2014b) reveal redox conditions, and therefore the level of denitrification, vary widely across the district. However, despite growing knowledge of groundwater redox characteristics of the Tararua GWMZ, greater understanding of the

hydrogeologic influence on the variability of redox conditions in the areas groundwater was required and therefore pivotal to initiating this study.

Previous studies in the Tararua GWMZ assess water quality from samples abstracted from existing wells, but the distribution of wells tend to follow aquifer characteristics of high water quality and productivity (Stenger et al., 2008). To further support research into hydrogeologic influences on groundwater redox conditions, it was considered necessary to analyse samples from geological settings across the region where wells might not exist. Direct-push methodology is seen as a cost effective and practical means of collecting these samples. However, most proprietary technology is developed for use in unconsolidated soils, sands and silts (McBeth, Morgenstern, Toews, Feek, & Begg, 2015) and not sufficiently robust to withstand prolonged use in gravel facies. The direct-push system developed in this study is able to survive sustained use in the challenging conditions encountered in the Tararua GWMZ and facilitated the collection of a number of groundwater samples from areas not believed to have been analysed previously.

Figure 1: The Head of the Manawatu Gorge. Practically all infiltrated precipitation (minus evapotranspiration) in the Tararua GWMZ will discharge via the Manawatu Gorge thereby creating an ideal location for hydrogeological study. (Rawlinson & Begg, 2014).

1.2 Thesis Aims and Objectives

This research aims to:

(i) Develop a direct-push method to effectively sample shallow groundwater from a wide range of hydrogeological settings;

(ii) Analyse chemical and physical characteristics of groundwater and determine their redox characteristics and distribution; and

(iii) Identify the influence catchment characteristics such as soil texture and drainage, and rock types have on groundwater chemistry and its redox characteristics across the Tararua Groundwater Management Zone.

1.3 Thesis Outline

This thesis is presented in seven chapters and begins with the first chapter on introduction, rationale and the study objectives. Chapter 2, Concepts of Denitrification describes fundamental characteristics of the nitrogen cycle, nitrification and denitrification processes encountered in shallow groundwater. Chapter 3, the Literature Review presents a summary of basic principles and key research related to redox conditions prevailing within shallow groundwater in New Zealand, before a more focused investigation into the evolution of this research relevant to denitrification in the Tararua GWMZ is undertaken. The location and characteristics of the Tararua GWMZ are introduced in Chapter 4, followed by a discussion of the regions geological history and sediments. Chapter 5, Methods and Materials, describes the site selection process, the development of the direct-push method, the method used to abstract the water and a discussion of the chemical analysis used and the statistical methodology applied. The results section (Chapter 6) presents key findings and preliminary discussions of the groundwater analyses, and is followed by the summary and

conclusions from this research (Chapter 7). The section concludes with suggestions for further work that may prove useful in further developing our understanding of redox processes and characteristics of shallow groundwater.

Chapter 2: Fundamental Concepts of Nitrogen Cycle and Subsurface Denitrification

2.1 Characteristics of Nitrogen Compounds

Nitrogenous compounds that are biologically, chemically, and radiatively active such as nitrate (NO_3^-), nitrite (NO_2^-), nitrous oxide (NO_2^-), ammonia and ammonium (NH_3 and NH_4 respectively) are collectively known as reactive nitrogen compounds (N_r). N_r are key components of nitrification and denitrification transformation pathways (Figure 2; caption on following page) and are essential for plant growth (Clague, 2013). Prior to the development of Haber-Bosch process in 1909 and the subsequent industrial manufacture of nitrogenous fertilisers (Smil, 1999), nitrogen fluxes along transformation pathways were restricted by relatively static nitrogen levels in the system (Fowler et al., 2015). Microbial nitrogen fixation, and to a lesser degree lightning fixation and nitrogen deposition via rainfall, are the principal means for gaseous N_2 to be converted to inorganic nitrate and ammonium (Fowler et al., 2015).

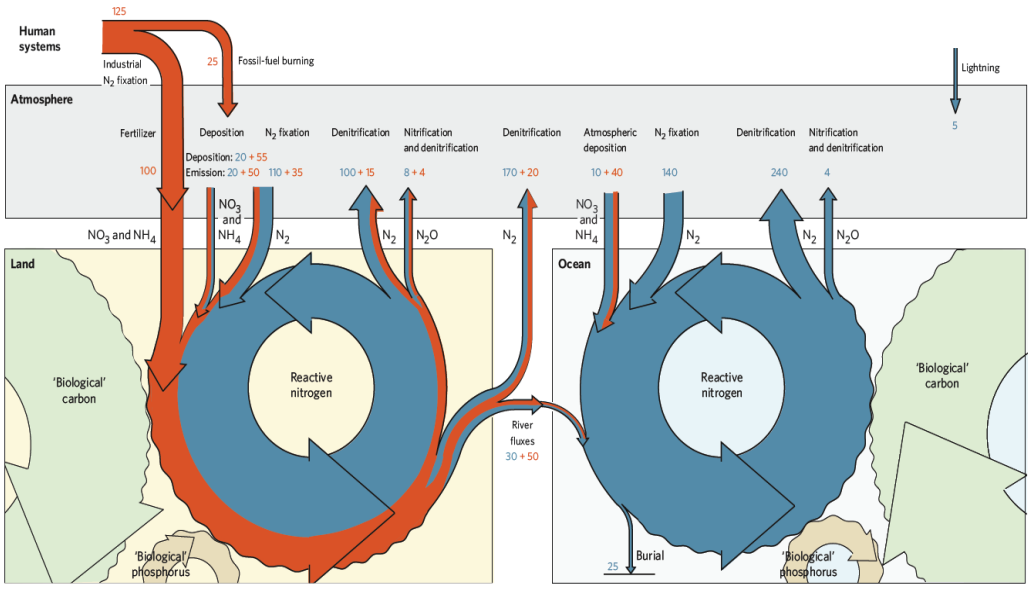

Figure 2: The Global Nitrogen Cycle for the land (left panel) and the ocean (right panel) *(continued on following page).*

Figure 2 *continued*: The Global Nitrogen Cycle for the land (left panel) and the ocean (right panel). The major processes fundamental to conversion of N_r to N_2 and vice versa are illustrated. Natural fluxes of nitrogenous compounds are blue, while fluxes attributed to anthropogenic influences are orange. The values in blue or orange represent Tg N y^{-1} for 1990 data (1 Tg = 10^6 Tonne); accuracy of these data are sketchy at best with few estimates bettering ± 20% and many exceeding ± 50% (Gruber & Galloway, 2008, p. 28). The closely linked carbon and phosphorus cycles are shown but are not elaborated upon.

Post 1909, rapid increase of anthropogenic contributions of N_r, i.e. NO_x from combustion, ammonia/ammonium from industrial fertiliser production, and increased planting of nitrogen fixing crops resulted in disruption of the natural balance; to the point where over 65% of reactive N entering the system over the past century is believed to have originated from anthropogenic activities (Fowler et al., 2015). The large increases in N_r have resulted in a range of severe and unintended environmental consequences including contamination of groundwater, eutrophication of surface water and threats to human health (Fowler et al., 2015; WHO, 2011).

2.2 Elements of the Nitrogen Cycle

The cycling of nitrogen occurs during four principal processes: nitrogen fixation, ammonification, nitrification, and denitrification (Figure 3), and is facilitated by microorganisms that obtain energy (as adenosine triphosphate (ATP) and nitrogen compounds essential for cell growth via biochemical reactions (Rivett et al., 2008). During these biochemical reactions, transformation of one form of nitrogen to another occurs via inter-compound electron-transfer along specific pathways (Rivett et al., 2008).

Figure 3: Schematic diagram of the nitrogen cycle and its close association with the hydrosphere. Key factors of the nitrogen cycle are discussed below (Saggar et al., 2013, p. 1).

2.2.1 Nitrogen Fixation

Nitrogen fixation is the conversion from gaseous N_2 to reactive nitrogen (N_r); i.e. compounds of nitrogen arising from fixation of molecular nitrogen (Bothe, Ferguson, & Newton, 2007). Nitrogen fixation is the only natural means of transforming atmospheric N_2 into a bioavailable form (Bothe et al., 2007). Fixation of N_2 may occur biologically via leguminous plants, or physically during lightning flashes. Equation 1 presents a simplified reaction where molecular nitrogen is reduced to an ammonium ion.

$$N_2 + 6\,e^- + 8H^+ \rightarrow 2NH_4^+ \qquad \text{Equation 1}$$

2.2.2 Ammonification

Ammonification is the process where organically bound nitrogen present in biomass is converted by fungi or bacteria to ammonia (NH_3) or ammonium (NH_4^+). The microbes gain energy from the process and assimilate NH_4^+, while excess NH_4^+ is subsequently excreted and becomes available to plants. Equation 2 represents the conversion of urea and water to ammonium and carbon dioxide.

$$CO(NH_2)_2 + 3H_2O \rightarrow 2NH_4^+ + CO_2$$ Equation 2

2.2.3 Nitrification

Nitrification is a significant process in agriculture that converts nitrogenous fertilizers, often applied in the form of NH_4^+, into plant available forms. Equation 3 represents nitrification; the biological oxidation of NH_4^+ to nitrite (NO_2^-) by *Nitrosomonas spp.* bacteria and then subsequent conversion to nitrate (NO_3^-) by bacteria from the genus *Nitrobacter* (Clague, 2013, p. 5). The processes of nitrification and ammonification combine to form a mineralization process which serves to decompose organic material with the subsequent release of N available forms (Bothe et al., 2007).

$$2NH_4^+ + 4O_2 \rightarrow 2NO_3^- + 4H^+ + 2H_2O$$ Equation 3

2.2.4 Mineralisation

Mineralisation occurs where organic nitrogen found in living tissue is rendered into bioavailable forms of inorganic nitrogen compounds such as NO_3^-, NO_2^- and NH_4^+ during decomposition. Mineralisation rates are controlled by soil temperature and moisture content, as well as the level of organic nitrogenous compounds and biomass of microbes. Equation 4 portrays the biogeochemical process where "R" represents an organic compound is transformed into a reactive nitrogenous product (Bothe et al., 2007).

$$R - NH_2 \rightarrow NH_4^+ \; or \; NO_3^-$$ Equation 4

2.2.5 Volatilisation

Volatilisation is commonly associated with sublimation of solid nitrogenous material into gaseous forms. The process is driven by urease enzymes found in plants and soils and occurs principally following application of fertilizers (such as urea) during warm and windy conditions, but also from animal excreta during storage and spreading of cesspit and herd home waste (Bishop & Manning, 2010). Volatilisation rates are affected by soil moisture and temperature, and high soil pH >7.0, and may be accelerated post fertiliser application where conditions favour rapid accumulation of NH_3 and NH_4^+, notably when fertilisers are combined with lime applications (Bishop & Manning, 2010). Volatilisation of ammonium is illustrated in Equation 5.

$$2NH_4^+ + 4O_2 \rightarrow 2NO_3^- + 4H^+ + 2H_2O \qquad \text{Equation 5}$$

2.2.6 Nitrogen Attenuation

Breakdown (reduction) of reactive nitrogen compounds within the subsurface environment is referred to as nitrogen attenuation. Nitrogen attenuation may occur by: nitrate assimilation by microbial biomass; dissimilatory nitrate reduction to ammonium; plant uptake; dilution by mixing with low-nitrate recharge; or denitrification, the breakdown of nitrate via a series of steps to relatively inert molecular nitrogen gas (N_2) (Korom, 1992). Although these attenuation processes may all occur in the subsurface environment, denitrification is considered the only nitrogen attenuation factor of significance (Rivett et al., 2008); that is, denitrification is the only process that actually removes nitrogen from the subsurface environment as opposed to diluting or storing it (Stenger et al., 2012).

2.3 Denitrification

Denitrification (Equation 6), is the stepwise reduction of nitrate by a large group of anaerobic bacteria that may ultimately but not necessarily, yield N_2 (Korom, 1992). The microbes involved in denitrification tend to facilitate a single reaction in the process, and the reaction may be arrested at any of the intermediate stages. Therefore, complete reduction and release of stable N_2 at the conclusion of the reaction series is not inevitable (Rivett et al., 2008).

$$NO_3^- \rightarrow NO_2^- \rightarrow NO \rightarrow N_2O \rightarrow N_2 \qquad \text{Equation 6}$$

The denitrifying bacteria are of two major classes, either heterotrophic that utilize organic matter (OM) as both their energy source and source of cellular carbon, or autotrophic that obtain energy from reduced inorganic substrates such as sulphides (S_2^-) or ferrous iron (Fe(II) and utilise inorganic carbon (generally HCO_3^-) for cell construction (Rivett et al., 2008). Bacteria that are able to create energy via aerobic respiration in oxic conditions and are able to anaerobically respire in anoxic conditions are referred to as facultative anaerobes (Korom, 1992), while those which exist only in environments with no oxygen are known as obligate anaerobes. Denitrification is typically facilitated by heterotrophic facultative anaerobes (Korom, 1992). Denitrification occurs when microbes facilitate exchange of an electron from a donor (Figure 4) such as carbon or sulphur, to a terminal electron acceptor such as NO_3^-; the bacteria gain energy from the process and produce NO_2^- as a by-product (Korom, 1992). In addition oxygen is released at each step in the form of bicarbonate ions (HCO_3^-), carbon dioxide (CO_2), or sulphate ions (SO_4^{2-}),(Rivett et al., 2008).

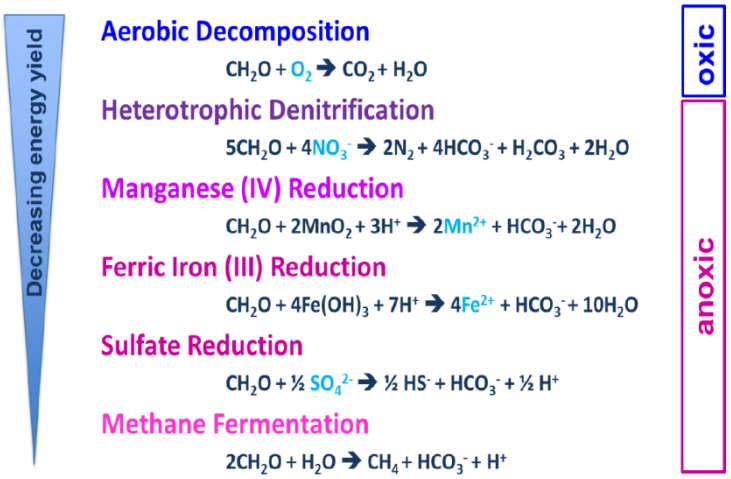

Figure 4: The Ecological succession of oxidation and reduction processes that occur in groundwater. Denitrification will occur in anoxic conditions and when nitrate levels reach a certain threshold, manganese will be then be reduced, despite the lower energy yield to anaerobes (Stenger et al., 2015, p. 3).

Electron transfers involving oxidation of carbon and reduction of oxygen yield the highest amount of energy, and are preferentially exploited by aerobic bacteria until O_2 levels become so low due to groundwater's isolation from direct atmospheric contact and therefore low O_2 replenishment potential (Rissmann, 2011) that facultative anaerobic bacteria become active and NO_3^- becomes the preferred electron acceptor (Korom, 1992). The reduction of NO_3^- to N_2 (denitrification) proceeds via a series of stages as each level of preferred electron donor become depleted (Equation 6). As the process continues, all available oxygen eventually get consumed and bacteria that only survive in the absence of oxygen (obligate anaerobes) supersede the facultative anaerobes and preferentially oxidise manganese, then iron, and finally sulphides (Korom, 1992; McMahon & Chapelle, 2008; Rivett et al., 2008). The sequence of thermodynamic electron acceptors involved during oxidation of organic carbon (OC) within a saturated environment is illustrated in Figure 5. It should be noted that although the thermodynamic sequence of progressively lower energy yielding reactions is controlled by the availability of electron donors, the heterogeneity of aquifer conditions can result in a range of reactions occurring simultaneously (Korom, 1992). This phenomena is commonly encountered in microbial biofilms coating the substrate

where a range of different redox reactions may occur simultaneously due to microbial communities exploiting pore-scale heterogeneities within the aquifer matrix (Rivett et al., 2008).

Complete denitrification to N_2 gas tends to occur under relatively stable redox conditions found in reduced groundwater zones, while incomplete denitrification often encountered in the vadose zone tends to favour production of N_2O (Stenger, Clague, Woodward, Moorhead, Wilson, Shokri, Wohling, et al., 2013). From an environmental perspective, incomplete reduction is undesirable due to the production of:

- Nitrite (NO_2^-) which has a profoundly negative effect on stratospheric ozone levels and is significantly more toxic than NO_3^- (Luo, 1996)
- mono-nitrogen oxides (NO_x)
- nitrous oxide (N_2O), a recognised greenhouse gas (Forster et al., 2007).

The rate of NO_3^- to N_2 transformation, and the level to which it occurs is reliant on a range of factors including pH, temperature, availability of carbon, and the concentrations of other ions (Rivett et al., 2008).

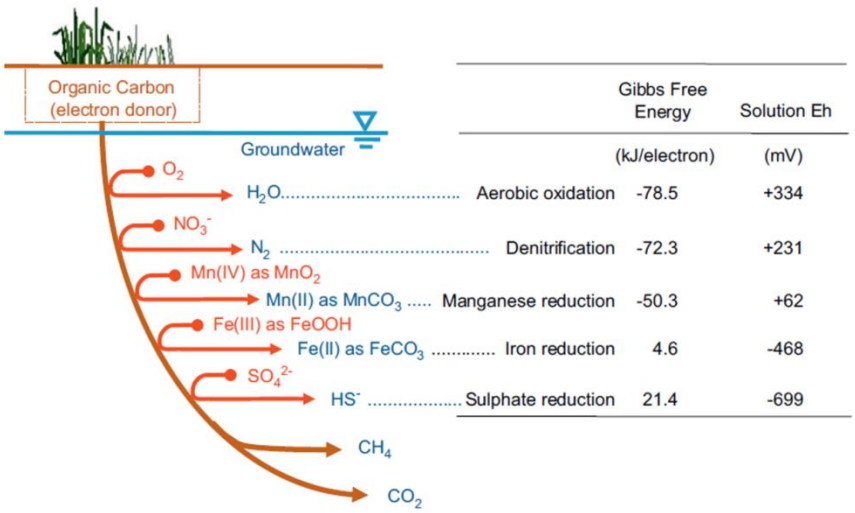

Figure 5: Thermodynamic sequence of electron acceptors when organic carbon is oxidised within the saturated zone *(continued on following page)*.

Figure 5 *continued*: Thermodynamic sequence of electron acceptors when organic carbon is oxidised within the saturated zone. Redox reactions involving organic carbon and oxygen provide the greatest energy to the aerobic bacteria. When the supply of O_2 becomes limited, facultative bacteria will then will utilise NO_3^- as an electron acceptor and so on through the series of lower energy yielding reactions involving Mn(IV), Fe(III), SO_4^{2-}, CH_4 and finally CO_2 (Rivett, Buss, Morgan, Smith, & Bemment, 2008, p. 4217).

Note: in this thesis the terms anoxic, suboxic, and mixed oxic follow the definitions used by McMahon and Chapelle (2008). Depending on the conditions encountered, researchers (e.g. McMahon & Chapelle, 2008; Rissmann, 2011; Rivas et al., 2017) consider oxic water to have a DO content >0.5 to 2 mg L^{-1}, Mn^{2+} <0.05 mg L^{-1} and Fe^{2+} <0.1 mg L^{-1}. Anoxic relates not only to the absence of dissolved oxygen (DO) and presence of hydrogen sulphide (H_2S) and methane (CH_4), but is extended to include reduction of NO_3^-, manganese (Mn(IV) and iron (Fe(III) within the body of water. Table 1 presents the thresholds to identify denitrification potential in groundwater originally defined by McMahon and Chapelle (2008) across the USA . McMahon and Chapelle (2008) describe suboxic conditions as being low in DO but require further data to identify which redox processes are occurring.

Table 1: Parameters defined by McMahon and Chapelle (2008, p. 262) to determine and classify denitrification potential in groundwater.

Threshold Concentrations for Identifying Redox Processes in Regional Aquifer Systems

Redox Process	Water Quality Criteria (mg/L) O_2	NO_3-N	Mn^{2+}	Fe^{2+}	SO_4^{2-}	Comments
Oxic						
O_2 reduction	≥0.5	—	<0.05	>0.1	—	—
Suboxic						
—	<0.5	<0.5	<0.05	<0.1	—	*Further definition of redox processes not possible*
Anoxic						
NOS reduction	<0.5	≥0.5	>0.05	<0.1	—	—
Mn(IV) reduction	<0.5	<0.5	≥0.5	<0.1	—	—
Fe(III) / SO_4^{2-} reduction	<0.5	<0.5	—	≥0.1	≥0.5	—
Methanogenesis	<0.5	<0.05	—	≥0.1	<0.5	—
Mixed						
—	—	—	—	—	—	*Criteria for more than one redox process are met*

2.3.1 Factors that Regulate Denitrification

The level of denitrification may be regulated by proximal or distal factors. Proximal regulators have an immediate effect on denitrification rates and include availability of N oxides (NO_3^-, NO_2^-, NO, and N_2O) as terminal electron acceptors, carbon availability, oxygen concentration, and temperature, and the existence of certain inhibitory compounds (Beauchamp, Gale, & Yeomans, 1980). Distal regulators have a greater effect on the nature of denitrifying bacterial communities both temporally and spatially (Groffman & Tiedje, 1989). Distal regulators include the abundance and species of denitrifying bacteria, pH, the presence of essential trace elements, and may include cultivation and farming practices. Optimal conditions for complete denitrification to occur are warm groundwater temperatures, basic to neutral pH, limited dissolved oxygen, and presence of suitable electron donors such as organic carbon, glauconite or iron pyrite (Hiscock, Lloyd, & Lerner, 1991; Korom, 1992; McMahon & Chapelle, 2008).

2.3.2 Presence of Suitable Bacteria

Although denitrifying bacteria are considered ubiquitous within the subsurface environments of agricultural regions (McMahon & Chapelle, 2008; Rivett et al., 2008), the absence of such bacteria may occasionally limit denitrification. For example, in some soils underlying indigenous forest and not exposed to agricultural runoff, denitrifying bacteria are conspicuously absent (Verchot, Franklin, & Gilliam, 1998). The type of overlying vegetation also influences the type of microbes present in the subsurface environment; Steele, Bonish, and Sarathchandra (1984) note higher levels of denitrifying bacteria *R. lupini* in hill soils where leguminous plants such as gorse and lupins are present. However, the major factors that generally limit denitrification

potential are the availability and concentration of DO and electron donors, not the availability of the denitrifying bacteria (Rivett et al., 2008).

2.3.3 Dissolved Oxygen Content

Depending on salt levels, temperature, and atmospheric pressure the DO levels in groundwater tend to lie between 7-10 mg DO L^{-1} (fully oxidised) and 0 mg DO L^{-1} (fully anoxic), (Rose & Long, 1988). Microbes preferentially oxidise O_2 until DO levels are so low that it becomes more energetically advantageous for them to reduce NO_3^- instead. The upper threshold value of DO for anaerobic reduction of NO_3^- to occur is estimated to vary from around 0.5 mg DO L^{-1} (McMahon & Chapelle, 2008) to 2 mg DO L^{-1} (Rissmann, 2011; Stenger, Clague, Woodward, Moorhead, Wilson, Shokri, Wöhling, et al., 2013), however Böhlke and Denver (1995) observed denitrification occurring in a plume of agricultural fertilizer at 4 mg DO L^{-1}. The DO content of groundwater is not static and may be increased by O_2 rich recharge water or decreased by microbial consumption, particularly with extended aquifer residence time (McMahon & Chapelle, 2008; Rose & Long, 1988).

2.3.4 Dissolved Carbon Content

The rate of denitrification is also dependent on the availability of a suitable electron donor; generally dissolved organic carbon (DOC) is oxidised, but if present iron pyrite (FeS_2)(McMahon & Chapelle, 2008) or glauconite ($(K,Na)(Fe^{3+},Al,Mg)2(Si,Al)_4O_{10}(OH)_2$) may feature in low carbon environments (Chapelle et al., 1995). Other sources of carbon such as the solid fraction organic carbon (f_{oc}) or solid organic matter may be found in local rocks, but do not contribute significantly to the amount of carbon in the

groundwater (including pore-water) (Rivett et al., 2008). The level of DOC within an aquifer is primarily dependent on the volume and nature of the carbon source, but may be influenced by other factors such as mineralization, DOC attenuation, sorption, and dilution effects of recharge (Rivett et al., 2008).

2.3.5 pH

Optimum pH values for heterotrophic denitrification lie between pH 5.5 and 8.0 (Hiscock et al., 1991 suggest 7.0 to 8.0) and pH's beyond this range are likely to hinder or arrest the process (Rivett et al., 2008). However Peyton, Mormile, and Petersen (2001) observed complete reduction of NO_3^- at pH 9.0 by the bacteria *Halomonas campisalis* in industrial wastewater and regeneration fluids, and Van Den Heuvel, Van Der Biezen, Jetten, Hefting, and Kartal (2010) reported denitrification in soils by *Rhodanobacter* species at pH 4.0; albeit with low N_2 and significant N_2O production.

2.3.6 Temperature

Temperature has a strong influence on the rate of denitrification, where low temperatures are related to low denitrification rates (Pfenning & McMahon, 1997). Hiscock et al. (1991) observed denitrification occurring in groundwater at detectable levels from 0 to 5 °C, which then was found to double at successive 10 °C intervals. The relationship between temperature, O_2, and denitrification is synergistic; i.e. combined these factors enhance the rate of denitrification to a level greater than would be enabled by each individual factor (Hiscock et al., 1991). Rivett et al. (2008) suggest that in order for denitrifying bacteria to flourish in extremes of temperature or pH they must undergo acclimation and/or adaption to the conditions.

2.3.7 Nutrient Availability

Macro and micro nutrients are essential for microbial metabolism and cell growth, and typically groundwater possesses adequate minerals to support this biosynthesis (Hiscock et al., 1991), except perhaps in nutrient poor, low productivity oligotrophic systems such as strongly leached soils, or deep aquifers (Rivett et al., 2008). Denitrification may be inhibited by excess sulphides or salt (natural marine environments notwithstanding). However, in an extreme case of salt tolerance in laboratory experiments, Peyton et al. (2001) found the halophytic bacteria *Halomonas campisalis* was able to function in solutions up to 12.5% sodium chloride (NaCl). Biological inhibition of denitrification is understood to occur, although little is known of the actual mechanisms involved (Bardon et al., 2016).

2.3.8 Nitrate-N Concentrations

The concentration of nitrates influence the extent to which denitrification may occur. Luo (1996) identified that at high NO_3^- -N concentrations, the predominant denitrification end product as N_2O, while at low NO_3^- -N concentrations as N_2. High levels of NO_3^- are implicated in decreasing denitrification rates by inhibiting reduction of N_2O, Lalisse-Grundmann, Brunel, and Chalamet (1988) suggest a threshold of NO_3^- around 113 mg N g^{-1} will have this effect but is dependent on aquifer characteristics and the species of bacteria (Lalisse-Grundmann et al., 1988).

2.4 Redox in Groundwater Environments

2.4.1 Introduction

Chemical reactions that involve simultaneous transfer of electrons from one chemical species to another are referred to as oxidation and reduction (redox) reactions. The oxidised species gain electron/s and becomes more electro-negative, while the reduced species loose electron/s and so become more electro-positive (Schüring et al., 2013). This concept can be difficult to understand, particularly when considered in terms of oxidising and reducing agents and is clarified by Clark (2013):

- Oxidation is the loss of electrons,
- A chemical species that donates an electron is oxidised,
- The oxidising agent is the chemical species which oxidises another species.
- The oxidising agent accepts an electron,
    - Therefore the oxidising agent is reduced,
- In a half equation should the free electron lie to the left of the equation, the species will be oxidised.

Conversely

- Reduction is the gaining of electrons,
- A chemical species which accepts an electron is reduced,
- The reducing agent is the chemical species which reduces another species,
- The reducing agent loses an electron,
    - Therefore the reducing agent is oxidised.
- In a half equation should the free electron/s lie to the right of the equation, the species will be reduced.

This is illustrated by the oxidisation and reduction of methane (Equation 7). Note: redox reactions are typically written as half equations which dissect the reaction and analyse either only the oxidised or the reduced components of interest.

Full reaction	$\boldsymbol{C^{4+}H_4^+ + 2O_2 \rightarrow C^{4+}O_2^{2-} + 2H_2^+O^{2-}}$	Equation 7
Half equation for C		
C loses electrons *C is oxidised by O*	$C^{4-} \rightarrow C^{4+} + 8\,e^-$	6.1
O is the reducing agent		
Half equation for H *No Redox*	$H_4^+ \rightarrow 2H_2^+$	6.2
Half equation for O		
O gains electrons *O is reduced by C*	$2O + 8e^- \rightarrow 2O_2^{2-}$	6.3
C is the reducing agent		

2.4.2 Redox Potential

The redox potential (*E*) is the measure in volts (V, typically millivolts mV) of a chemical species affinity for electrons (electronegativity). *E* is measured with an electrochemical cell consisting of a reference electrode (generally hydrogen) and an inert platinum electrode. Positive redox potentials are generated by oxidising substances (Figure 6), while negative redox potentials are generated by reducing substances (Schüring et al., 2013). The redox potential may be written *Eh*, when *E* is measured with reference to the reduction of hydrogen ions (of a hydrogen electrode) to hydrogen gas at standard state conditions (i.e. 25 °C at 1 atmospheric pressure with 1 unit activity for all chemical species). To facilitate comparison with other datasets the oxidation reduction potential (*ORP*) measured in this study with the smarTROLL Multi Parameter handheld instrument was converted to *Eh* by adding 200 mV (Rice, Baird, Eaton, & Clesceri, 2012).

Figure 6: Schematic diagram of a natural systems redox potential (at near neutral pH). A greater difference between the two potentials equates to a more vigorous electron flow from the less electronegative to the higher electronegative substance. Strong oxidants have a positive redox potential which may be as high as +800 mV, while strong reductants can have a negative redox potential of up to -400 mV (Schüring, Schulz, Fischer, Böttcher, & Duijnisveld, 2013, p. 26).

2.4.3 Limitations of Redox Potential Measurements

Although easily measured with a handheld instrument, redox potential may not be a reliable means *per se* to assess the redox potential of an aquifer. This is due to the most significant groundwater redox reactions such as $O_2 \rightarrow H_2O$, $NO_3^- \rightarrow N_2$, $NO_3^- \rightarrow NH_4^+$, $SO_4^{2-} \rightarrow HS$, and $CO_2 \rightarrow CH_4$ being kinematically very slow and dependent on microbial catalysis (Schüring et al., 2013). The influence of these factors tend to result in very low exchange currents and unstable potential measurements (Schüring et al., 2013). In addition, to accurately establish the redox potential, equilibrium is required between the various redox couples in both the solution and at the electrode; but in nature this is rarely achieved (Schüring et al., 2013; Stefánsson, Arnórsson, & Sveinbjörnsdóttir, 2005). Schüring et al. (2013) also suggest that due to seasonal changes in the water table, measurements are required over a sufficient temporal period to account for natural variations in groundwater redox characteristics. Stefánsson et al. (2005) maintain that for natural waters (which typically display redox disequilibrium), the *Eh* could be determined by quantifying the oxidation state of each of the redox couples (Fe^{3+}/Fe^{2+}; O_2/H_2O; H_2S/SO_4^{2-}; NO_3^-/NO_2^-; NO_3^-/NH_4^+; NO_2^-/NH_4^+), and ideally separate mass balance and mass action equations should be performed for each oxidation state.

2.4.4 Redox in Groundwater

If conditions are favourable, redox reactions may occur throughout the subsurface environment from the soil and unsaturated zone, to within deep aquifers. Redox processes have a profound effect on water quality by: facilitating or restricting movement of metals (e.g. arsenic, chromium and iron); attenuating a range of contaminants derived from anthropogenic activities e.g. volatile organic compounds and nitrates (Figure 7); as well as generating environmentally detrimental substances

such as NO_2^-, CH_4 and dissolved Fe^{2+} (e.g. Chapelle, Haack, Adriaens, Henry, & Bradley, 1996; Korom, 1992; Lovley, 1993; McMahon & Chapelle, 2008; Ramesh Kumar & Riyazuddin, 2012; Wang, Bush, Sullivan, & Jianshe, 2013). Redox reactions in groundwater may also involve tetrachloroethene, tricloroethene as electron acceptors, and dichloroethene, ethene and vinyl chloride as electron donors (McMahon & Chapelle, 2008). Studies of redox processes in subsurface environments are not restricted to groundwater, and include a diverse range of settings such as acid mine drainage, connate water in marine sediments, and bioremediation of contaminant plumes (e.g. Aravena & Robertson, 1998; Wang et al., 2013; Zapata-Peñasco, Salazar-Coria, Saucedo-García, Villa-Tanaca, & Hernández-Rodríguez, 2016). Ramesh Kumar and Riyazuddin (2012) state as the chemical species sensitive to redox and redox processes differ from the other processes and reactants found within aquifers, knowledge of the redox status of a groundwater system facilitates understanding of a wide range of scenarios encountered in these environments (Figure 7). To this end, quantifying redox processes by analysis of a consistent suite of chemical characteristics (Chapelle, Bradley, Thomas, & McMahon, 2009; McMahon & Chapelle, 2008; Mendizabal, Stuyfzand, & Wiersma, 2011) have been undertaken at the national (Mendizabal et al., 2011), regional (Close et al., 2016; Rissmann, 2011), catchment (Clague, 2013; Collins et al., 2016; Rivas et al., 2015) and plume level (Christensen et al., 2000; Liotta, D'Alessandro, Bellomo, & Brusca, 2016) .

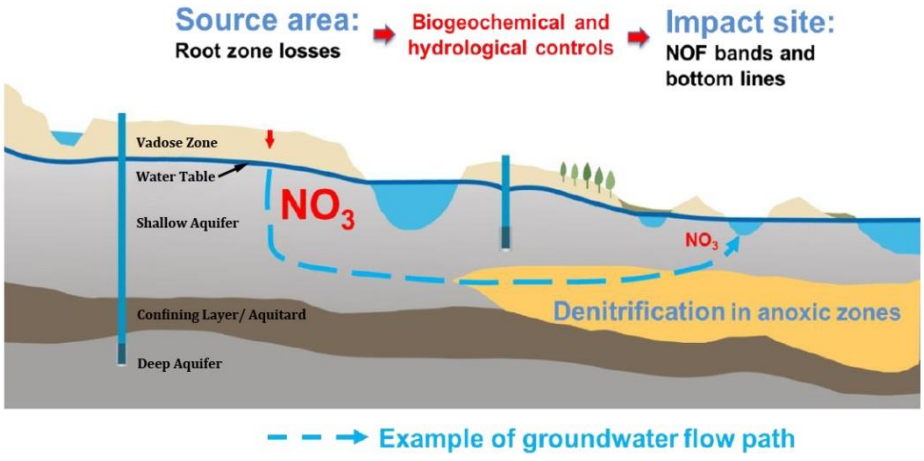

Figure 7: Conceptual diagram of nitrogen sources and flow paths (adapted from Stenger et al., 2015, p. 2), *(continued on following page).*

Figure 7 *continued*: Conceptual diagram of nitrogen sources, flow paths, the denitrification zone, and eventual discharge to a surficial water body. NOF = National Objectives Framework which defines upper and lower limits for various water quality parameters including nitrates (adapted from Stenger et al., 2015, p. 2).

2.4.6 Redox Fronts

The relationship between groundwater redox chemistry and denitrification is complex, where redox fronts and gradients may be marked by levels of dissolved chemical species (Schüring et al., 2013). The transition through the series of Terminal Electron Accepting Processes (TEAP's) appears to occur in a systematic fashion (Figure 5) and where this transition is associated with an abrupt change in groundwater chemistry, it is referred to as the redoxcline (Tesoriero, Liebscher, & Cox, 2000). In the Abbotsford-Sumas aquifer of southwestern British Columbia, Canada, and northern Washington State, United States of America, Tesoriero et al. (2000) identified increased SO_4^{2-} and Fe^{2+} (and Mn^{2+}, albeit at lower levels) concentrations proximal to the redoxcline which decreased farther downgradient, thereby indicating the loss from the solution by precipitation of minerals rich in these elements. Pedersen, Bjerg, and Christensen (1991) measured the redox front in a shallow sandy aquifer near Vejen, Denmark, they determined this zone to be 30 cm wide, and that although they detected NO_3^-, SO_4^{2-} and O_2 above the redoxcline, they were unable to do so within redox front. They suggested denitrification was occurring in the anaerobic microenvironments above the front. Although depicted as a series of distinct chemical reactions occurring at distinct intervals in the water column Figure 5, this is not always the case due to aquifer recharge, or dissolution of aquifer matrix increasing concentrations of electron donors or acceptors along groundwater flow paths; thereby allowing a range of redox reactions to occur simultaneously (Tesoriero et al., 2000).

2.4.5 Redox and Denitrification in Groundwater

Work done initially by Korom (1992) and subsequently developed by McMahon and Chapelle (2008) recognised that the reagents and products of redox reactions in groundwater could provide a means to assess the level of denitrification occurring at a specific site. The level of denitrification could be determined by the presence of key chemical parameters such as dissolved oxygen (DO), nitrate (NO_3^-), manganese (Mn^{4+}), ferric iron (Fe^{3+}); with sulphate (SO_4^{2-}) and carbon dioxide (CO_2) becoming common when DO, NO_3^-, Mn(IV) and Fe(III) have been depleted (McMahon & Chapelle, 2008). As described in the sections above, microbes that catalyse redox reactions have to compete for limited resources within the groundwater and preferentially favour the redox process that generates the greatest energy per mole of organic carbon oxidised (McMahon & Chapelle, 2008). However, due to poor contact with the atmosphere, consumption of oxygen via reduction in certain groundwater settings tends to surpass oxygen replenishment, and O_2 levels decline to such a level where microbes utilise less energetically favourable, but more abundant chemical species (McMahon & Chapelle, 2008). This stepwise reduction of a series of chemical species results in a formal sequence of preferential electron exchange known as the ecological succession of terminal electron-accepting processes (TEAP) which proceeds from $O_2 \rightarrow NO_3 \rightarrow Mn \rightarrow Fe \rightarrow SO_4 \rightarrow CO_2$ (McMahon & Chapelle, 2008). Half equations for each of the reactions (Banchuen, 2002) are presented in Equation 8.

Equation 8

i $$\frac{1}{4}O_2(g) + H^+(w) + e^- = \frac{1}{2}H_2O$$

ii $$\frac{1}{5}NO_3^- + \frac{6}{5}H^+(w) + e^- = \frac{1}{10}N_2(g) + \frac{3}{5}H_2O$$

iii $$\frac{1}{2}MnO_2(s) + 2H^+(w) + e^- = \frac{1}{2}Mn^{2+}(s) + H_2O$$

iv $$Fe(OH)_3(s) + 3H^+ + e^- = Fe^{2+} + 3H_2O$$

v $$\frac{1}{8}SO_4^{2-} + \frac{9}{8}H^+ + e^- = \frac{1}{8}HS^- + \frac{1}{2}H_2O$$

vi $$\frac{1}{4}CO_2 + H^+ + e^- = \frac{1}{4}CH_2O + \frac{1}{4}H_2O$$

2.4.7 Identifying Redox Processes Occurring In Groundwater

The succession of terminal electron-accepting processes and the inherent tendency for particular reactions to segregate into discrete zones with distinctive end products such as N_2, NH_4^+, Fe^{2+}, H_2S, and CH_4 allows ambient redox processes to be determined from groundwater quality data (McMahon & Chapelle, 2008). The framework developed by McMahon and Chapelle (2008) to quantify redox status was based principally on threshold concentrations of O_2, NO_3^-- N, Mn^{2+}, Fe^{2+}, SO_4^{2-} which allowed groundwater to be classed as oxic, anoxic, mixed oxic, and suboxic. This framework was modified by Rivas et al. (2015) who adapted the thresholds to those considered more appropriate for conditions found in the Tararua GWMZ (Table 2). As knowledge of redox in the Tararua GWMZ increased, the DO thresholds were further refined by Rivas et al. (2017) to 1 mg L^{-1} which were subsequently applied in this study.

Table 2: Parameters and sources applied by Rivas et al. (2015, p. 3) to determine and classify denitrification potential in New Zealand groundwater.

Parameters assessed to determine denitrification potential in groundwater.

Parameter	Criteria	Relevance to Denitrification	References
Dissolved Oxygen (DO)	< 2 mg L^{-1}	Denitrification occurs in an anaerobic condition	Rivett et al., 2008; Rissmann, 2011; Thayalakumaran et al., 2008
pH	5.5 -8.0	Indicator of acidity or alkalinity in water	Rust et al., 2000
Oxidation-Reduction Potential (ORP)	< 150 mV	Low redox potential indicates strong reducing tendency of groundwater	Jahangir et al., 2012
Temperature	2 - 50 °C	Temperature affects microbial activities, including denitrification	Brady and Weil, 2002
Dissolved Organic Carbon (DOC)	> I mg L^{-1}	Electron donor (heterotrophic denitrification)	Rivett et al., 2008
Ferrous iron (Fe^{2+})	> I mg L^{-1}	Electron donor (autotrophic denitrification)	Thayalakumaran et al., 2008

McMahon and Chapelle (2008) highlighted limitations of their framework which included the sampling scale and the variation of threshold concentrations in groundwater which were controlled by availability of electron donors and the number and/or species of microbes. The authors recognised that although they had established the onset of denitrification by DO threshold concentrations of 0.2 to 0.3 mg L^{-1}, in some conditions, denitrification occurred with O_2 levels exceeding 2.0 mg L^{-1}. McMahon and Chapelle (2008) attributed this large variation in DO threshold concentrations to the convergence of multiple flow paths of dissimilar chemistry modifying the chemical characteristics of the groundwater. Defining precise threshold concentrations for sulphate, ferrous iron and manganese is also considered challenging due to precipitation and sorption processes, and differentiating between Fe(III) and SO_4^{2-} reduction. However when applied to a range of different groundwater systems at a regional scale, this methodology is able to identify redox characteristics in both homogenous and heterogeneous aquifer settings (McMahon & Chapelle, 2008). Other approaches to estimate groundwater redox status include measurement of *Eh* and TEAPs. *Eh* tends to be effective for identifying progressively increasing reducing conditions and distinguishing between the oxic and anoxic status, but *Eh* is not able to determine between the specific redox processes taking place (Schüring et al., 2013). Identification of the dominant TEAP may be more effective, but is constrained by intensive data collection requirements and analysis, as well as overlap of Mn(IV) and Fe^{2+} TEAPs, SO_4^{2-} reduction, and CH_4 production within the aquifer. The issue of overlapping TEAPs may be mitigated to some degree by measurement of dissolved H_2 which is an intermediate product of the reactions (Gao, Tanji, Scardaci, & Chow, 2002). Should the groundwater chemistry indicate the redox status transitioned from oxic to anoxic over a relatively short distance, it could be inferred that within this distance NO_3^- is probably also likely to be reduced (Korom, 1992; McMahon & Chapelle, 2008).

2.4.8 Groundwater Quality Measurements to Determine Redox Status

The redox status of groundwater can therefore be relatively successfully estimated by the analysis of dissolved oxygen, nitrate nitrogen and manganese and further supported by analysis of sulphate and ferrous ions in groundwater. Dissolved oxygen levels are a simple diagnostic marker to initially assess whether denitrification is possible in the prevailing aquifer conditions; i.e. denitrification is unlikely to occur in oxic conditions where DO is greater than 2.0 mg L^{-1}, and is likely to occur when DO levels are lower (Close et al., 2016). Mixed oxic conditions prevail when high DO levels are associated with Mn^{2+} and Fe^{2+} concentrations that exceed their respective threshold values (McMahon & Chapelle, 2008). Mixed redox conditions, in which key threshold concentrations of dissolved components are consistent with multiple TEAPs, are attributed to either mixing of waters with different redox conditions adjacent to well screens, or to local diversity of redox processes related to lithologic heterogeneity (McMahon & Chapelle, 2008).

A recent study by Close et al. (2016) attempted to predict only whether or not denitrification is likely to occur in the incumbent conditions within aquifers of Waikato and Canterbury, and applied an simplified version of McMahon and Chapel's (2008) framework. They used three criteria in their analysis; NO_3^- -N, Mn and DO. Nitrate threshold levels are set at 0.05 mg L^{-1}. Due to difficulties in measuring low DO at low levels encountered in wells, the threshold criteria for dissolved oxygen is set at 1.0 mg L^{-1}; and as manganese was considered more reliable than iron due to concerns of iron particulate contamination (originating from ferrous well casings), a threshold of 0.5 mg Mn L^{-1} was adopted. The redox status was assessed as oxidised, mixed or reduced, and the authors believe such a system provides a simple yet relatively robust method of determining whether denitrification may potentially occur. As the literature demonstrates, defining the groundwater quality parameters thresholds at which

denitrification occur is strongly controlled by local conditions, this study follows the criteria reviewed and applied by Rivas et al. (2017) in the Tararua GWMZ (Table 2) to determine the redox status and processes occurring in the shallow groundwater.

Chapter 3: Literature Review

3.1 Nitrogen and Denitrification Research in New Zealand

Nitrate contamination of some New Zealand aquifers was detected early in the 1970's (Baber & Wilson, 1972) yet research into the transport, fate and consequences of this environmental threat appeared to gather momentum slowly. Steele et al. (1984) recognised that not only were reactive nitrogen compounds leaching into the groundwater, but also a degree of denitrification was occurring concurrently in some northern pastoral soils. They recognise the bacteria *Rhizobium lupini* is a key factor in denitrification processes, and denitrification potentials (dependent on availability of organic carbon) vary significantly in the soils of the study. Cooke and Cooper (1988) investigated the role of soils and lithologies in the transport of nitrates and noted NO_3^- transport is dependent on soil porosity and nitrate is particularly mobile in well aerated soils derived from greywacke rocks and gravels or volcanic ashes.

The impetus of research into denitrification increased in the mid 1990's. In laboratory experiments, Luo (1996) incubated soil (from Massey University No. 4 dairy-farm, Palmerston North) within a closed system and using acetylene inhibition methodology. He concludes denitrification varies spatially and temporally, is greatest in the upper root zone, and that it decreased with soil profile depth. Luo suggested decreased enzyme activity, or availability of carbon and/or NO_3^- as the key factors that control denitrification. Rosen and McNeill (1996) studied NO_3^- transport and the hydrogeology of the unconfined aquifers of the Ngaruroro River terraces (Maraekakaho, Hawkes Bay). Compared to modern water analysis (e.g. Rivas et al., 2017), the chemical analysis of pH, HCO_3^-, Cl^-, and NO_3^- was rudimentary. Two distinct water types in the study area were recorded; low alkalinity groundwater, and high alkalinity (HCO_3^- and calcium) water that flows from the Maraekakaho River. Rosen and McNeill (1996)

attribute the high alkalinity and calcium in the water to dissolution of nearby limestone facies

As knowledge increased, it became evident that intensive farming practices could produce a significant negative impact on groundwater quality. McLarin, Bekesi, Brown, and McConchie (1999) identified the major source of nitrates in an unconfined Manawatu gravel aquifer, (later substantiated by Luo, Tillman, and Ball (2000), to be principally from animal excreta rather than fertilizer inputs, and that the distribution of NO_3^- inputs at the individual farm scale was highly variable, both spatially and temporally.

A report on the consequences of agricultural intensification from analysis of National Groundwater Monitoring Program data (NGMP) (Daughney & Reeves, 2005) reinforced the link between intensive farming practices and declining groundwater quality throughout New Zealand. Zemansky (2007) then conducted an assessment of groundwater in the predominantly dairy (farmed) Kowhitirangi and Kokatahi plains, West Coast. He notes elevated nitrate sensitivity, particularly along the margins of gravel aquifers, although low levels of nitrates were generally detected. Zemansky (2007) suggests despite high potential nitrate sensitivity, the low nitrate levels detected may be due to very high precipitation rates of the West Coast that flush nitrate rapidly through the very permeable gravel aquifers, before discharge to surface water and ultimately into the Tasman Sea.

Barkle et al. (2013) tracked transport and transformation of nitrogen arising from urine patches in a loamy sand soil with a stratified volcanic vadose zone within a sub-catchment of Lake Taupo. Fluxes of Organic N, NH_4^+, and NO_3^- were measured from the root zone down to 5.1 m below the ground surface. The authors observe that variations in soil texture and hydrophobicity combine to create significant heterogeneity within the vadose zone and that beyond depths of 1.0 m, all detected

nitrogen was in the form of NO_3^- -N. They also note little denitrification was observed in the deeper horizons.

The paradox of economics versus environmental accountability became apparent with the dairy boom of the early 2000's (Bowman & Conway, 2013), as the relatively fertile alluvial plains (generally underlain by highly productive aquifer systems and thus irrigable) are ideal for dairy development and thus farmed more intensively. However, the desired properties of the fertile, gravelly, well drained soils are also associated with high nutrient leaching losses and rapid subsurface transport of contaminants, particularly when the augmented by large irrigation systems (Carrick, Palmer, Webb, Scott, & Lilburne, 2013). These physical characteristics present significant difficulties for the farmers to operate and remain within water quality frameworks (Carrick, Palmer, et al., 2013).

Understanding, identifying, mapping, and predicting the level of natural denitrification, particularly in vulnerable areas became paramount. To this end a variety of studies were initiated that examined in a diverse range of settings, the processes, transport and pathways involved with denitrification and the fate of nitrogen in New Zealand's subsurface environments. Research has been focused on the susceptibility of microbes to NO_3^- toxicity, the nature of chemical and redox reactions, the availability of electron and acceptors donors in the context of NO_3^- contamination of aquifers, and the consequences of intensive dairy farming practices. Sirisena, Daughney, Moreau-Fournier, Ryan, and Chambers (2013) investigated the structure of the bacterial communities in New Zealand's groundwater. They confirmed a diverse range of species are present and that the microbial community structures are strongly correlated to groundwater redox potential, anthropogenic impacts on water quality (intensive farming, and point source pollution such as sewerage from clustered septic tanks), and mean groundwater residence time. Jha et al. (2013) studied the community structure of denitrifying bacteria and observed their inherent variability in soils of differing characteristics in the Manawatu. They also noted that populations of

denitrifying bacteria in soils tend to rapidly increase following surficial application of bovine urine.

Determining the physical factors associated with denitrification require a broad range of studies. Taylor, Trompetter, Brown, and Bekesi (2001) used isotope analysis to determine the source of carbon in some Manawatu aquifers. They established that replenishment of inorganic carbon in shallow aquifers is due to decay of organic matter, while in deeper settings in the Pohangina aquifer, the carbon source originates primarily from carbonate dissolution.

Kensington, Richards, Murray, and Peake (2003) analysed *Eh*, pH, organic N, and total dissolved Fe and Mn in the Taieri Plain Aquifer, Canterbury. They observed extensive alluvial fans present in the northern margins as being key pathways for rapid infiltration of contaminants into the unconfined aquifer. They also note that the movement of organic N, NO_3^-, and NH_4^+ into the central aquifers is impeded by aquicludes of interbedded sand/silts deposited by marine transgressions. The large spatial variability of NO_3^- levels (11.36 g m^{-3} in alluvial gravel fans to 0.6 g m^{-3} in confined aquifers) prompted further work to identify and account for NO_3^-, NO_2^-, and NH_4^+ distribution (Kensington et al., 2003). Kensington et al. (2003) recommended landuse intensity in the areas underlain by alluvial gravel fans to be restricted in order to protect groundwater quality.

Barkle et al. (2007) investigated biologically mediated denitrification in the vadose at three sites (Kinloch, Waihora, and Rangitea, Lake Taupo catchment). The authors recognise relict vegetative matter buried in ignimbrite flows may be a source of carbon for microbial facilitated denitrification in the Taupo region. However, much of this relict material may have been carbonised rather than organic, and therefore of limited availability as a source of carbon for microbial action. Although they were able to identify denitrification decreases rapidly with depth, it was difficult to correlate results from laboratory experiments to actual denitrification occurring in situ.

The spatial and temporal trends in groundwater chemistry at a national level were investigated by Daughney and Reeves (2005). They used hierarchical cluster analysis to identify a set of parameters able to represent temporal patterns of change in groundwater quality. Their analysis reveals that key factors in temporal changes to groundwater quality are aquifer lithology, redox potential, level of confinement and the degree of rock-water interaction. The authors note variations in groundwater quality exhibit little relationship to landuse in overlying properties. The relationship between landuse and groundwater chemistry was later explored by Stenger et al. (2008) in the Toenepi Catchment, Taupo. They analysed shallow groundwater only, which they believe is likely to provide a stronger connection between landuse and groundwater quality. Stenger et al. (2008) concede that although knowledge of recharge and local and regional flow paths was limited, such knowledge is fundamental to correlating landuse with groundwater quality. In a later study Woodward, Stenger, and Bidwell (2013) established that seasonal variability of groundwater flow paths in conjunction with heterogeneous redox environment can have a strong temporal effect on nitrate fluxes in the same catchment. Stenger et al. (2008) also point out that most studies rely on data collected from existing domestic or production wells that typically located in high productivity aquifers and that dependence on such data may not present a representative sample of the spatial variability of groundwater hydrochemistry. However, they acknowledge that despite the benefits to science, the cost of installing wells purely for monitoring purposes is prohibitive. For example conventional water well drilling rates currently in Tauranga (not including transport to site) currently are in the vicinity of $200.00 to $300.00 per metre depending on local conditions (T. Perry, personal communication, March 12, 2018; M. Carlyle, personal communication, March 12, 2018).

Taylor et al. (2001) applied a multidisciplinary environmental tracer approach in aquifers of Manawatu and determined that isotopes ($\delta^{18}O$, $\delta^{3}H$, $\delta^{13}C$, and $\delta\ ^{14}C$), hydrochemistry (pH, Fe^{2+}, Mn^{2+}, SO_4^{2-}, Na^{+}, K^{+}, Mg^{2+}, and Cl^{-}) and potentiometric data

provide a suite of mutually consistent parameters to identify groundwater sources and flow paths, yet isotopic analysis of groundwater quality has been used over a number of years in the Waikato with limited success (Clague, 2013). The limitations of this method to quantify denitrification potential is identified by Clague, Stenger, and Clough (2015). They recognise very low concentrations of NO_3^- in the groundwater proved difficult to detect. Although their research identifies some spatial variability of denitrification in the catchment, lack of knowledge and understanding of flow paths in the catchment was a significant constraint.

Carrick, Fraser, Dennis, Knight, and Tabley (2013) confirm the spatial variability of leaching rates at the farm scale are due to variability in slope, soil water holding capacity, infiltration and soil wetness. These characteristics are compounded by management practices such as irrigation, cultivation, cropping and grazing. They determined that the level of soil drainage as one of the most critical factors in controlling the rate of nutrient leaching; yet obtaining reliable measurements of soil drainage and nutrient leaching particularly from undisturbed alluvial sedimentary soils appears extremely difficult. While research and development of techniques to quantify nitrate levels is being conducted, similar efforts to create reliable models to extrapolate these data to a range of scales has been being undertaken.

3.1.1 Modelling

It should be appreciated that although the goal is generally to produce highly accurate models. This is rarely achieved due to the complexity of processes that govern nutrient concentrations and transport in both groundwater and surface water (Anastasiadis, Kerr, Nauleau, Cox, & Rutherford, 2014). However, despite their limitations, some consider models superior to other alternatives such as the use of proxies, and expert or local knowledge (Anastasiadis et al., 2014). Therefore, modelling may be considered a

convenient means of increasing understanding of denitrification in groundwater systems; provided due scientific process of documentation, validation, and review is adhered to (Etheridge & Scott, 2015).

As awareness of the magnitude of environmental issues related to nitrate leaching have grown, a range of methods to map and predict the presence and movement of nitrogen in the subsurface have been developed. Modelling of nitrate levels in New Zealand in groundwater was undertaken initially by Webb, Claydon, and Harris (2000) in a study that investigated physical soil characteristics. This work was hindered at the time by technological limitations and data quality issues, including the resolution of existing soil maps. Although significant advances in computing power have facilitated the use of more complex modelling software, the spatial resolution of soil and geological units and boundaries still prove to be a limiting factor in increasing the accuracy of models based on them. Woods et al. (2004) produced nitrogen leaching risk maps at the national and regional scale. Soil maps with 200 m resolution provide adequate detail at the national scale, and although 25 m resolution soil maps provide acceptable detail at the regional scale at the time not all areas in New Zealand had been mapped at this higher resolution. This holds true for the present day where the Landcare Research series of fundamental soil layer maps (FSL) are being superseded by the S-map series, but, despite nationwide coverage of the (reputed) S-maps more reliable data is still not available (Landcare Research, 2018).

Woods et al. (2006) maintain the impact of anthropogenic activities should be considered when modelling groundwater flows. For example, although natural groundwater flowing through riparian zones is noted for high denitrification (e.g. Carlyle & Hill, 2001; Puckett, 2004; Spruill, 2004; Vidon & Hill, 2005) such zones may be bypassed by common land drainage systems. Woods et al. (2006) allow for this effect in their model by reducing the attenuation factor in Gley Soils under intensive landuse regimes in New Zealand, a practice Webb, Hewitt, Lilburne, McLeod, and Close (2010)

deemed reasonable, but declined to include in their model due to uncertainties of the actual effect of subsurface drainage on denitrification potential in Canterbury.

Daughney (2008) applied multivariate statistical methods such as hierarchal cluster analysis (HCA) and discriminant analysis (DA) to classify groundwater chemistry and provenance in the Waiareka and Deborah aquifers of Otago. The analysis was based solely on the groundwater's major ion concentrations and was conducted with no input from physical hydrogeological parameters such as bore location, depth or hydrostratigraphic unit. Daughney consider differences in Cl^-, K^+, Mg^{2+}, Na^+, HCO_3^-, and SO_4^{2-} ions the most reliable to distinguish differences in aquifer lithology, while Fe^{2+}, NO_3^-, and NH_4^+ were discounted as their relative concentrations are the product of redox reactions rather than aquifer lithology. More recently Stenger, Clague, Woodward, Moorhead, Wilson, Shokri, Wohling, et al. (2013) acknowledged redox-sensitive parameters such as the concentrations of dissolved iron (Fe^{2+}), manganese (Mn^{2+}) and DO can be used to ascertain the denitrification capacity within a groundwater system. The four hydrochemical categories Daughney (2008) identified with HCA were consistent with the Otago Regional Council's hydrostratigraphic models, but HCA alone was unable to accurately correlate the hydrogeology of a well to the expected hydrostratigraphic unit; and required further evaluation with discriminant analysis (DA). Provided the additional step of applying DA was included in the process, Daughney (2008) claimed that multivariate statistical methods as a valid and practical means of developing or refining conceptual hydrological models. Daughney, Guggenmos, et al. (2009) applied similar methodology in aquifers of the Wairarapa and were also able to differentiate spatial variations in groundwater chemistry.

The DRASTIC model was used by Baalousha (2010) to map aquifer vulnerability to nitrate contamination in the Hawkes Bay. This model is based on weighting factors, such as depth to water table (D), recharge (R), aquifer media (A), soil media (S), topography (T), influence of vadose zone (I) and hydraulic conductivity (C), to calculate a vulnerability index. The DRASTIC method highlighted the importance and

challenges of determining and selecting the optimum numbers of monitoring sites at an appropriate spatial distribution (Baalousha, 2010). The authors maintained a balance needed to be established between having poorly distributed or too few sites against the cost of monitoring too many sites and problems analysing redundant or superfluous data. Furthermore as stated by Carrick, Fraser, et al. (2013) although computer models are used regularly to simulate and forecast nitrogen losses, it is essential that they are validated with accurate field data to ensure the reliability of any computed predictions.

Rissmann (2011) attempted to correlate nitrogen attenuation within Southland's shallow aquifers with the geomorphology, lithology and chemical composition of their hydrostratigraphic units. He considered the major aquifers in terms of nitrate sensitivity, i.e. low sensitivity aquifers possess high denitrification potential, and those classified as high sensitivity possess low denitrification potential. He referred to the main-rock and sub-rock units in the 1:250,000 QMap geological maps, then classified both datasets in terms of reduced chemical species present in each lithological unit; i.e. organic carbon (OC), and iron bearing minerals such as glauconite and iron sulphides. A regional scale map of the denitrification potential of Southland soils was then developed by Killick, Rissmann, and Stenger (2014). Using 1:50,000 soil maps, the authors developed a classification system founded on soil-horizon datasets. This soil horizon information enabled assessment of the degree of water saturation, which in turn allowed evaluation of redox conditions possible in that particular soil horizon. Although Killick et al.'s maps provide a reasonable assessment of soil denitrification potential occurring in the region, a scale of 1:50,000 is so large that many critical soil zones where either leaching is high, or denitrification is taking place, e.g. ephemeral water channels is likely to be omitted (Killick et al., 2014). By combining soil characteristics with the geological and hydrogeological data used by Rissman (2011), Killick et al. (2014) believe greater resolution and accuracy may be attained.

Close et al. (2016) adopted a more holistic approach in their study of the redox status of the groundwater of 568 wells in the Waikato and 2223 wells in Canterbury. The authors

asserted that as reducing conditions are a requisite for denitrification to occur, the redox status of groundwater provide a reliable means to identify the spatial patterns of significant denitrification in groundwater. They identified the redox status of each region's wells as oxic, reduced, or mixed and then related the redox status to topography, geology and soil characteristics. Models developed with linear discriminant analysis (LDA) from the point source data were able to distinguish between the three redox states, and were subsequently analysed using GIS where the data was extrapolated across the entire region. Close et al. (2016) maintained their models are an effective and reliable means of predicting reducing groundwater conditions as well as estimating the level of denitrification at a regional scale.

Rivas et al. (2017) undertook a different approach to identifying key denitrification elements in the Tararua GWMZ. As with previous studies they classified water types using HCA, but preferred to use principal component analysis (PCA) to identify significant factors and discard those which had little influence on the groundwater's redox potential. Five significant components were identified and three accounted for nearly 65% of the variance between variables. The processes associated with Component-1 and Component-3 were not clearly identified, however, Component-2 showed strong association with redox processes. By plotting Component-1 vs Component-2 and shading the values with factors of interest such as soil texture, drainage class, aquifer material and rock type Rivas et al. (2017) identified these as the most influential on the areas hydrochemistry.

3.2 Manawatu Studies

This study is preceded by, and builds on, a range of work done specifically in the Manawatu region. Initial research on the fate of nitrogen in soils of this region gave rise

to nitrogen budgeting at the catchment scale, which eventually led to investigations into the denitrification potential and capacity of groundwater at a range of scales.

An early study by Magesan (1992) used tracers, acetylene inhibition techniques, soil cores, and suction cup experiments to investigate the leaching of solutes from Manawatu soils. With the limited technology of the day, Magesan (1992) was unable to accurately identify the levels of nitrate in the leachate. Later work by Luo (1996) was more successful and they were able to ascertain that denitrification is the greatest in the surface soils and decrease with depth in soil profile. Luo, Tillman, White, and Ball (1998) noted carbon availability as a significant (denitrification) limiting factor and that enzyme activity in the soil (if not limited by C or NO_3^- -N availability) vary seasonally. Luo et al. (2000) identified that highest denitrification rates were observed in warm wet soils with high levels of organic carbon and NO_3^- particularly in poorly drained soils where compaction by stock had severely restricted aeration.

Concerns had been raised with regard to nitrogen transport of the effect of drainage practices on naturally waterlogged soils in the Manawatu. For example, Woods et al. (2006) noted groundwater entering freshly excavated drains in a poorly drained location exhibited NO_3^- levels of 5 to 50 mg N L^{-1} but following heavy rainfall only 2.6 mg of N L^{-1} was recorded in groundwater in a new drain in Manawatu. The authors believed the artificial drainage systems provide a pathway that for leachate to bypass natural attenuation thereby allowing NO_3^- rich water to be directly delivered to the surface water systems, rather than be retained for longer within effective denitrification zones.

Daughney, Meilhac, and Zarour (2009) examined routinely monitored groundwater parameters, and determined that a large proportion of the groundwater in the Manawatu and Wanganui regions is anoxic and associated with the accumulation of products of denitrification such as dissolved Fe^{2+}, Mn^{2+}, NH_4^+, and SO_4^{2-} The high spatial variability in groundwater encountered in the Manawatu Wanganui region

reflect the diverse provenance and type of aquifer materials. The authors suggested 3D modelling of aquifer units as pivotal to increase understanding of the variability of groundwater chemistry.

At this stage much of denitrification work in the Manawatu has been limited to studies of denitrification in surface soils (Jha, Sagger, Tillman, & Giltrap, 2011; Luo, 1996; Luo, Tillman, & Ball, 1999; Luo et al., 2000; Luo et al., 1998) and little had been done on fate of nitrogen in the deeper subsurface environments of the Manawatu and Rangitikei Rivers. A series of ongoing studies in these catchments that began in 2014 are establishing foundations for understanding the potential for denitrification and the significance of quantifying and assessing the redox characteristics of groundwater (e.g. Collins et al., 2016; Elwan, 2015; Elwan et al., 2016; Elwan et al., 2015; Rivas, Singh, Horne, et al., 2014; R. Singh, Rivas, Espanto, Elwan, Horne, Roygard, Matthews, et al., 2014).

Inconsistencies from estimates of nitrogen leaching from the root zone when compared to calculated nitrogen river loads in sub catchments of the Tararua GWMZ, indicated that nitrogen attenuation rates of up to 50% may be occurring (R. Singh, Rivas, et al., 2014a). Rivas et al. (2014) expanded the study to survey 56 wells in the Tararua GWMZ. The aim was to ascertain the redox characteristics of the groundwater and classify it as either oxidised or reduced (Rivas, Singh, Horne, et al., 2014). From this analysis, a spatial distribution pattern became obvious; the groundwater in northern and central Tararua GWMZ tends to be reduced, while groundwater in southern regions of the Tararua GWMZ tends to be oxidised. The authors hypothesised that high DO and low DOC content as the key factors that moderate the capability of the aquifers in the southern regions to attenuate NO_3^- to any significant degree.

At the same time Rivas, Singh, Bishop, et al. (2014) attempted to develop effective methods for quantifying denitrifying enzyme activity (DEA) in the subsoil, and to test the practicality and reliability of push-pull tests to quantify denitrification in shallow

groundwater in the Manawatu River catchment. Single well push pull tests were refined to quantify of potential denitrification rates in the field, while the laboratory incubations allowed assessment of soils and subsoils denitrification potential (when carbon and nitrate are added to an incubation experiment (Yeomans, Bremner, & McCarty, 1992) and denitrification capacity (when nitrate is added at a constant temp of 28 °C (Yeomans et al., 1992)).

Burkitt, Bretherton, and Singh (2015) investigated temporal changes to sediments and nitrogen and phosphorus concentrations in the Tuapaka grazed hill country of the Manawatu Region, although levels of these nutrients are generally lower than those observed in the low lying regions, the authors identify nitrogen attenuation does occur in the hill country.

Work done by fellow MSc students also contributes to the understanding of the fate of nitrogen in subsurface environments of the Manawatu. In a study of the Rangitikei River, Collins (2015) identified a dynamic connection between groundwater and the river which not only recharge the aquifer, but also identify that significant discharge occurs from groundwater into the river around the Bulls area. He also confirmed that the shallow groundwater flow patterns are controlled by the regional topography and that reduction of NO_3^- occurs in the shallow groundwater. Using bromide tracer tests Espanto (2015) identified the existence of preferential flow paths in soil profiles at the Massey Dairy No. 1 site near Palmerston North. Analysing NO_3^- -N, DO, Fe^{2+}, Mn(IV), and SO_4^{2-} Espanto (2015) also determined that the groundwater is mixed oxic-anoxic from 5.8 to 51 m below ground level (bgl) and that groundwater deeper than 51 m bgl is generally anoxic at the Te Matai site.

In order to better understand the spatial variability of denitrification potential in the Tararua GWMZ, Rivas et al. (2015) conducted a survey that examined the hydrochemical properties of shallow groundwater from 56 wells. They observed a negative correlation between NO_3^- -N and silica, which they attribute to increasing

denitrification potential with groundwater age, but concede may simply be due to lack of nitrates in the deeper groundwater. Furthermore, they were unsure how physical factors such as geology and soil types influence the degree of denitrification. This research also reveals that despite the Upper Manawatu and the Mangatainoka catchments having different landuse characteristics, the average estimated amount of nitrates leached from their root zones were similar; yet their river loads of NO_3^- were significantly different. The authors demonstrated a correlation between denitrification and the redox status of groundwater, with the groundwater of the Upper Manawatu catchment generally proving to be reducing with lower NO_3^-, while the Mangatainoka sub-catchments typically being oxic with higher NO_3^- levels.

Research began establishing a correlation between river water quality and the catchment characteristics of soil texture, soil drainage, base flow index and geology Rivas et al., (2015), but their relationship with nitrogen attenuation is still poorly understood. Therefore, Elwan (2015) investigated how the spatial reduction in nitrogen is influenced by its relationship with a catchment's hydrogeological characteristics. By applying the nitrogen attenuation factor (derived by R. Singh, Rivas, et al., 2014a) Elwan (2015) demonstrated that the spatial variability of denitrification within the Tararua GWMZ as a function of catchment characteristics. Elwan (2015) confirmed that of the catchment characteristics, soil drainage is a key factor in determining the level of denitrification where low NO_3^- concentrations are related to poorly drained soils and high NO_3^- concentrations are found in areas with rapidly draining soils. Rivas et al., (2014), using Principal Component Analysis, also recognise that dissolution of carbonate minerals from aquifer rocks and oxidation-reduction (redox) processes directly influence the DO levels of the regions groundwater.

Research by Rivas et al. (2017) is the latest published article on the groundwater of the Tararua GWMZ. The authors applied comprehensive statistical analysis to groundwater samples and confirmed that although significant variation in denitrification potential exists throughout the Tararua GWMZ, broadly the southern

areas tend to be oxic while the northern and central areas generally exhibit reducing conditions. Furthermore with innovative use of principal component analysis (PCA) and analysis of variance (ANOVA), the authors demonstrated that denitrification in the area is heavily influenced by soil texture and drainage class, which control the rate of movement of groundwater through the soils. Poor soils drainage is associated with low DO and NO_3^- levels, while higher levels of DO and NO_3^- are associated well-drained soils developed in gravels; particularly in conjunction with intensive farming practices.

3.3 Influence of Geology, Soils, and Climate on Redox Status

Groundwater chemical composition and therefore the nature of redox processes that occur in groundwater are influenced by the local geology, aquifer properties and climate (Rissmann, 2011). This is due principally to geological and hydrological controls on groundwater residence time, geochemistry and electron donor availability, combined with climatic controls on precipitation, recharge, vegetation, soil development and weathering (McMahon & Chapelle, 2008).

The spatial distribution at local or regional scales of different types of aquifer materials i.e. gravels, marine, lacustrine, or volcanic sediments, peat, lignite, and fractured limestone or greywacke may be highly variable and as a consequence the denitrification potential of an aquifer may also be equally variable (Rissmann, 2011). Therefore, it is important to clearly identify the local geological units and their boundaries when attempting to classify and delineate the denitrification potential of an aquifer (Rissmann, 2011).

Aquifer forming rocks vary in terms of lithology, age, degree of weathering, mineralogy, and chemical reactivity, as well as hydrogeological properties such as neck and pore size, sorting of the matrix, porosity, permeability, and the nature of fractures

and joints (Younger, 2007). These factors may combine to directly affect groundwater chemistry, but may also modify groundwater chemistry indirectly by controlling residence time thereby influencing the time available for dissolution of aquifer rocks and minerals to occur via chemical weathering (Younger, 2007). The rocks and soils are, therefore, able to significantly modify the chemical composition of the groundwater and consequently the groundwater's redox characteristics and its ability to attenuate nitrates (Aksever et al., 2015). In general, dissolved oxygen and dissolved organic carbon concentrations in groundwater may be correlated to local lithologies, while concentrations of other electron acceptors and donors may be linked to the sediment's provenance and depositional history (McMahon & Chapelle, 2008).

The lithology also controls the topography, where slope may exert a strong influence on aquifer recharge rates by affecting precipitation, infiltration, runoff characteristics, hydraulic gradient, which in turn control groundwater flow rates and residence time (Aksever et al., 2015). Aspect also influences precipitation, interception and vegetation characteristics (Younger, 2007) which ultimately may influence infiltration and groundwater recharge. However, Close et al. (2016) suggested the contribution of aspect was significantly overshadowed by slope, therefore it was not represented in their model designed to predict redox status in the Waikato and Canterbury regions. The influence of lithology on the denitrification potential of various aquifers has been studied in some New Zealand settings. From a groundwater redox perspective, Rissmann (2011) considered well-indurated sedimentary rocks such as greywacke (Figure 8) with the exception of calcareous lithologies, possessed stable, unreactive mineralogy, with pore spaces sealed by interstitial cementation. Rissmann (2011) assert these rock types contribute little in the way of organic carbon to groundwater systems as they generally contain low inherent organic carbon levels, or the carbon is locked up within the mineral structure of the rocks. In some settings carbon may be present but in a form (recalcitrant carbon) that is unavailable to microbial metabolism (Close et al., 2016).

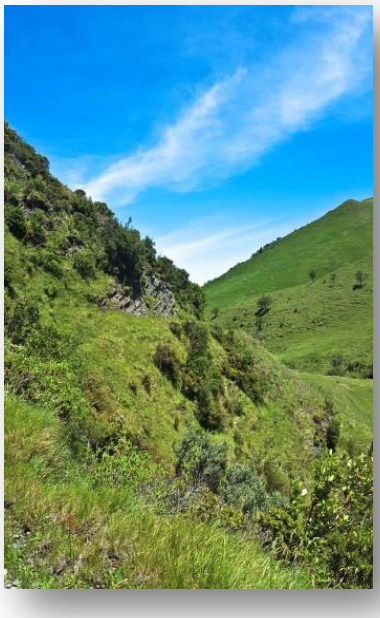

Figure 8: Esk Head Belt outcropping in a hillside (Tamaki East Road, Dannevirke 40°06'16.2"S 176°04'10.9"E). Steep topography and thin soils underlain by greywackes, result in low infiltration of precipitation and subsequent rapid water movement through the catchment. This allows little opportunity for the groundwater to interact with the rocks and soils and therefore has little effect on the local groundwater chemistry (Beyer et al., 2016a; Daughney, Guggenmos, McAlister, Begg, & Jackson, 2009).

Rivas et al. (2017) studied the redox characteristics of groundwater collected from 56 wells in the Tararua GWMZ during February to March 2014. The authors determine that freely draining soils combined with aquifer materials such as gravels with high hydraulic conductivity are associated with oxic conditions.

Rivas et al. (2017) also identified that reducing conditions prevail where carbon rich lithological facies (such as lignite) are commonly encountered, for example in the northern areas of the Tararua GWMZ. In this research, all gravels found in the Tararua GWMZ were considered as alluvium. The physical characteristics of gravels such as clast size, orientation and permeability are governed by the depositional environments (Klingbeil, Kleineidam, Asprion, Aigner, & Teutsch, 1999). However, Rivas (2017) gave little consideration to differences in physical characteristics such as age, depositional environments, and clast to matrix ratios of the gravels. Opportunity exists for future work to compare redox characteristics between gravels of differing hydrogeological properties (Figure 9), rather than compare them as a single entity.

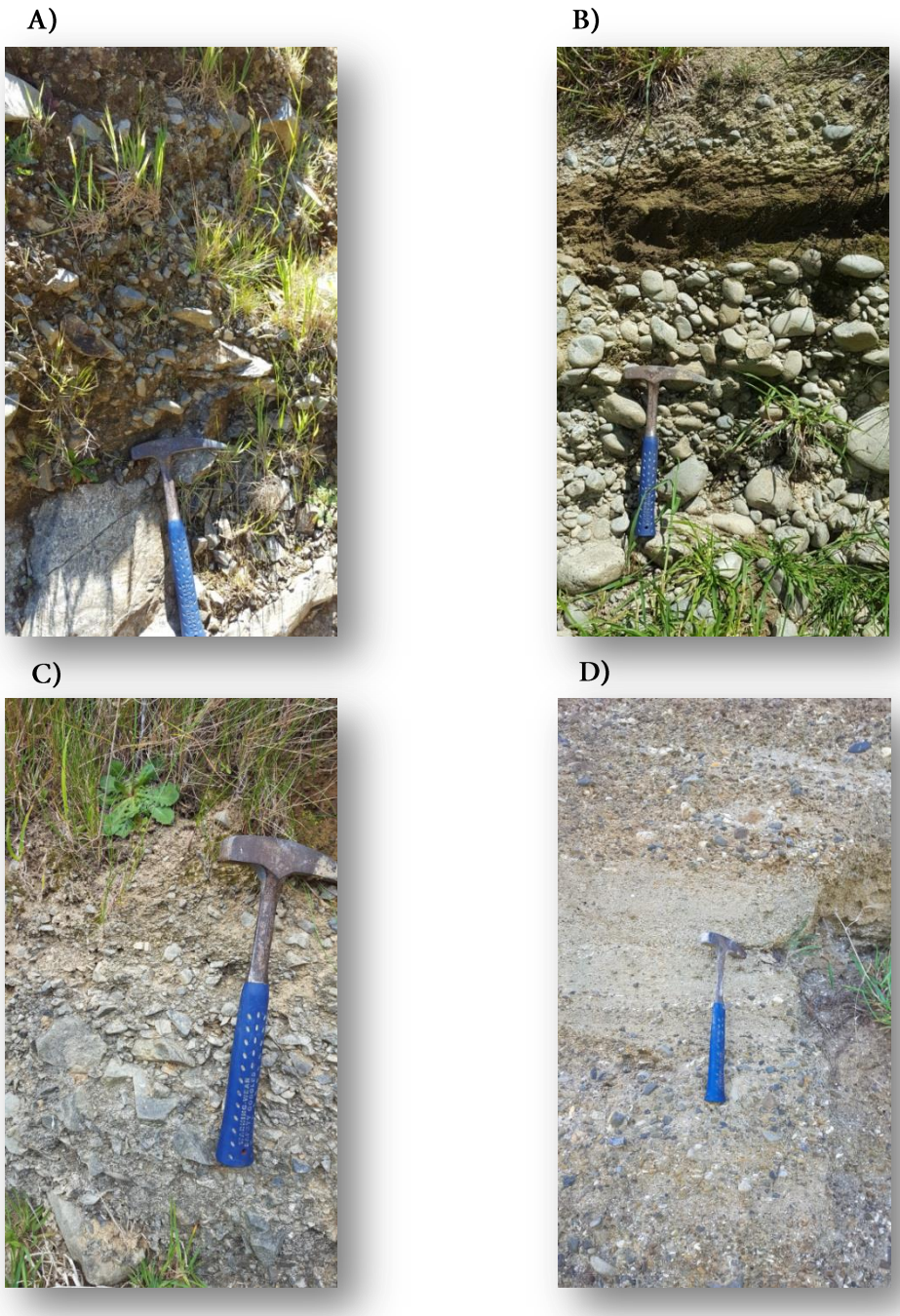

Figure 9: Four distinct gravel types observed in the Tararua GWMZ. The images above show the diversity of gravels and are by no means a complete representation of all types encountered during this study. The physical characteristics of the gravels reflect differing transport distances, depositional environments and water bearing properties. A) Colluvium in road cutting (40°13'40.2"S, 176°05'20.9"E, Tamaki East Road, Dannevirke) showing poorly indurated, clast supported, sub-angular, medium to coarse pebbles. B) Gravel in farm track (40°40'51.7"S, 175°88'62.3"E, Namu Road, Mangatainoka) showing poorly indurated, clast supported, sub-rounded to rounded, coarse pebble to cobbles. C) Outcrop in unnamed stream bank (40°15'31.1"S 176°00'38.3"E, Graham Road, Dannevirke) showing clast supported, indurated, angular, fine to coarse pebbles. D) Gravel in quarry (40.227935, 176.130352, Cowper Road, Dannevirke) showing matrix supported, indurated, sub-rounded to rounded very fine to medium pebbles.

Many of New Zealand's high yielding aquifers such as those located in Southland, Canterbury, Marlborough, Hutt Valley, Wairarapa, and Hawkes Bay are formed from greywacke derived gravels eroded from the Alps or Axial Ranges and deposited by glacial or fluvial actions (Daughney, Guggenmos, et al., 2009; Dravid & Brown, 1997; Gyopari, 2014; Rissmann, 2011). Typically these aquifers initially tend to have subdued hydrochemistry (Daughney, Guggenmos, et al., 2009).

Close et al. (2016) state the waters within the greywacke gravel aquifers of the Canterbury Plains are typically oxic with low organic carbon, due to the organic material generally being stripped by high stream flows in high hydraulic gradient environments. Peterson, Curtin, Thomas, Clough, and Meenken (2013) investigated the denitrification potential of alluvial gravels for a Canterbury aquifer and noted the low availability of organic carbon generally resulted in poor natural attenuation of nitrate. However, lenses of organic rich carbon sediments within the gravels (similar to that found in the Tararua GWMZ, Figure 10) are apparent and Peterson et al. (2013) conclude these carbon rich sediments could be responsible for the variable denitrification rates throughout the gravels in the gravel aquifers of Canterbury. They also suggested although the overall denitrification potential is low but when organic carbon is artificially introduced the denitrification capacity could be significantly enhanced; indicating the availability of organic carbon (OC) strongly limiting denitrification capability of the alluvial gravels in Canterbury.

Figure 10: Greywacke derived gravels overlying lignite, and blue-grey lacustrine sediments (Mangatewainui Stream, Matamau 40°07'16.6"S 176°12'21.2"E). The sea regressed in climatic cycles and combined with ongoing tectonic uplift, resulted in a transition from shallow marine to lacustrine settings, and deposition of lignite which provides a rich source of organic carbon throughout the northern regions of the Tararua GWMZ. These areas of the Tararua GWMZ consistently exhibit reducing conditions which are linked to the availability of DOC (Rivas et al., 2017).

The mudstone/siltstone marine sediments, deposited by long-term marine inundation of New Zealand can be vast units of tens to hundreds of meters thick, are often massively bedded, and possess poor hydrogeological characteristics (Rissmann, 2011). These large stratigraphic units generally contribute little in the way of reagents or chemicals required to modify the redox characteristics of the groundwater (Rissmann, 2011). However, the marine sediments deposited during marine transgressions in the Quaternary tend to be thinner and less extensive and may be interbedded within the gravel aquifers (Rissmann, 2011).

The characteristics of these younger sediments often reflect an evolving hydrological regime controlled by repeated eustatic sea level fluctuations and subduction driven uplift which affect sediment supply, provenance and the nature and level of vegetation

along the coastal margins (Rissmann, 2011). This results in a range of marine and lacustrine sediments being interbedded with the gravels such as found in northern areas of the Tararua GWMZ (Figure 11), (Begg & Johnston, 2000; Begg, Palmer, & Gyopari, 2005; Close et al., 2016; Lee & Begg, 2002; Lee et al., 2011; Rawlinson & Begg, 2014). Marginal marine sediments may often contain organic carbon (in the form of peats and lignite and iron (as pyrite); key sources of electrons used during the reduction of nitrates within aquifers. Alluvial sediments particularly in lower meandering reaches of fluvial systems are considered excellent sources of OC and are often associated with flat, peat rich, swampy land; Close et al. (2016) asserted that groundwater in these conditions are typically reduced or mixed oxic.

Figure 11: Road cutting north of the Whakaruatapu River (40°14'81.7"S 176°15'27.7"E). The eastward dipping alternating beds of lacustrine sediments, lignite and reworked pumice sands dominate the underlying geology, and have been overlain by younger unconsolidated alluvial gravels and soil.

Many fractured rock aquifers in New Zealand exist in limestone units and may significantly influence the hydrochemistry of the groundwater by contributing carbonate ions (Rissmann, 2011). McMahon and Chapelle (2008) concluded that in aquifers located within calcareous lithologies the predominant redox characteristic was suboxic. Rissmann (2011) also observed in the Southland Region many local limestone units contained iron in the form of glauconitic iron clays which he considered important electron donors. Volcanic rocks and volcanoclastic sediments typically have little organic carbon; however voluminous eruptions such as ignimbrite eruptions of the Taupo Volcanic Zone (TVZ) tend to rapidly burn and bury vegetation and soils which become an integral component of the subsurface environment. Therefore, buried soils and lignite's (and perhaps, charcoal) commonly associated with pumices in the Tararua GWMZ sits may be rich sources of OC for denitrification in areas such as the Waikato and the TVZ (Hadfield & Gibbs, 2007).

Soils are a product of the parent lithology, climate, organisms, relief, and time (McLaren & Cameron, 1990) and as infiltrated precipitation migrates through the soil profile, various chemicals and compounds fundamental to the redox and denitrification status such as particulate carbon and nitrates may be leached from the soil (e.g. Killick et al., 2014; Rissmann, 2011). Soils are a key factor in determining groundwater geochemistry where soil horizon characteristics allow assessment of the degree of water saturation and redox conditions possible in that particular soil horizon (Killick et al., 2014). Killick et al. (2014) note that mottled horizons indicate seasonal or periodic saturation conditions conducive to Fe(III) reduction, while predominant Fe(II) ions found in gleyed horizons indicate a higher degree of reducing conditions, and that soils with an "r" horizon classification are indicative of permanently saturated conditions of an intensely gleyed horizon. They noted that denitrification occurring within the gleyed horizons could be controlled primarily by the rate of water movement through the soils and that the organic matter found in the L, F, H (found in forest floors) and O (peat) organic horizons often reflected the level of dissolved organic carbon in the lower

mineral horizons. Woods et al. (2006), as part of a National initiative to classify the effects of landuse on water quality (Catchment Land Use for Environment Sustainability (NIWA, 2016), ranked poorly drained organic soils as having the highest ability to attenuate nitrogen, with peaty gley soils assessed as having 80% denitrification potential, gley soils 50%, and 20% for other poorly drained soils (see Figure 12 which shows two diverse soil types found in the Tararua GWMZ).

Killick et al. (2014) note that in the "Topoclimate South" soil profile descriptions accumulation of humus within mineral soils is documented by the index "h". However, anthropogenic modification generally by cultivation has resulted in many A horizons (whether they are tagged with the h index or not) having a high level of organic matter (OM). Therefore, in the Killick et al. (2014) study, such horizons are referred by the percentage of carbon rather than being classified with the h index. Significant factors used in their soil denitrification potential classification are determined to be organic matter (OM), and degree of saturation of mineral soil horizons.

Figure 12: Soil cores revealing quite different properties. The Dannevirke silt loam (upper image) exhibits larger particle size and is freer draining than the Mangamahu series core (lower image). Recovered from the mudstone country east of Eketahuna (Tane Road, Pahiatua 40°34'45.7"S 175°51'24.6"), the gleyed horizon in the upper 300 mm in the lower image indicates significant ponding with little infiltration to lower horizons.

3.4 Anthropogenic Influences on Groundwater Recharge and Quality.

Exacerbating the influence of natural factors are anthropogenic factors such as changing landuse patterns which may modify the nature of vegetation, surface roughness, and soil properties, and influence interception, evapotranspiration and infiltration capabilities (Black, 1996). Forested areas have lower runoff coefficients and overland flows than un-forested catchments, while pugging from stock and poor cultivation methods decrease soil permeability (Black, 1996). Urban areas with large impervious surfaces, drains and culverts allow rapid movement of water across surfaces and into watercourses thereby reducing concentration time, lag-times and lessening infiltration (Charlton, 2007). All the above anthropogenic factors serve to affect infiltration and recharge and consequently aquifer flow and groundwater residence time, furthermore fertiliser applications and pollution may modify the levels of electron acceptors and/or donors within the aquifer (McMahon & Chapelle, 2008; Figure 13).

Figure 13: An old style well installed in a productive artesian spring (Kohinui Road, Mangatainoka 40°25'03.8"S 175°52'27.2"E). Large volumes of water were withdrawn from this well to supply the nearby (disused) Dairy Factory.

3.5 Summary and Conclusions

The preceding sections describe and define the supporting principles of hydrogeology, the processes and components of the nitrogen cycle and fundamentals of nitrogen attenuation. This is followed by illustrating how knowledge of the fate and transport of nitrogen in the subsurface zones has evolved both globally, and within specific regions of New Zealand. It is now clear that not all nitrogen leachate transported into the subsurface zones is discharged to surficial water. Denitrification via stepwise reduction in groundwater is an important natural nitrogen-attenuation process occurring in a wide range of geological settings throughout New Zealand. Classifying the redox characteristics of groundwater has been demonstrated to be a practical, economic, and relatively reliable (at regional scales) proxy to quantify denitrification potential. It is expected that in anoxic groundwater conditions where poorly draining soil limits the rate of water movement, and in conjunction with underlying lithologies where peat, lignite (and possibly pyrite and glauconite) predominate, denitrification rates should be greatest. Conversely, in rapidly draining soils developed in relatively homogenous greywacke gravels, oxic conditions, with low concentrations of electron donors may prevail and therefore little denitrification should occur. However the actual influence of the physical and chemical characteristics of soils and lithologies on the denitrification potential of groundwater still remains to be satisfactorily resolved.

The literature reveals our understanding of the influence of rocks and soils on redox characteristics of shallow groundwater is limited and more work is required. Identifying the spatial distribution of redox characteristics throughout the Tararua GWMZ has not been fully addressed. Nor has the influence of rocks and soils on the redox characteristics of shallow groundwater in the Tararua GWMZ been fully identified. Opportunities exist to further expand our understanding of how the characteristics of shallow (and accordingly younger) groundwater might present a clearer linkage between nitrogen inputs and denitrification rates. More work is also

required to determine whether characteristics of deeper, nitrate poor, and perhaps older groundwater (some of which potentially pre-date European settlement), may mask denitrification characteristics of shallow younger groundwater. Furthermore, to date there has been little research into the geochemistry of shallow groundwater that is not constrained by the location of wells or piezometers in New Zealand; and none at all in the Tararua GWMZ. This study will attempt to bridge some of the gaps described above in current scientific knowledge by sampling (with direct push technology) and analysing with multivariate statistical methods, the shallow groundwater redox characteristics from a diverse selection of lithologies and soils encountered within the Tararua GWMZ (Figure 14).

Figure 14: The suite of alluvial terraces in mid-centre of the image are testimony to tectonic uplift, changes in climatic regime and erosion, down cutting, and depositional processes (Mangahei Road, Te Uri 40°14'15.1"S 176°12'35.3"E). The rolling hills are also expressions of tectonic deformation, as are the axial ranges in the far distance. The terraces are often cropped or farmed intensively and the underlying geology is such that waterways are vulnerable to the effects of nutrient rich leachate.

Chapter 4: The Tararua GWMZ

4.1 Introduction

This chapter provides a brief overview of the location and physical characteristics of the Tararua GWM. A more detailed chronological review of the rocks and soils commonly encountered in the area and their water bearing properties is then presented.

4.2 Location and Description

The Tararua Ground Water Management Zone (Figure 15) covers 3,163 km^2 between southern Hawkes Bay and northern Wairarapa, extending from Norsewood and Ormondville in the north, to Alfredton in the south.

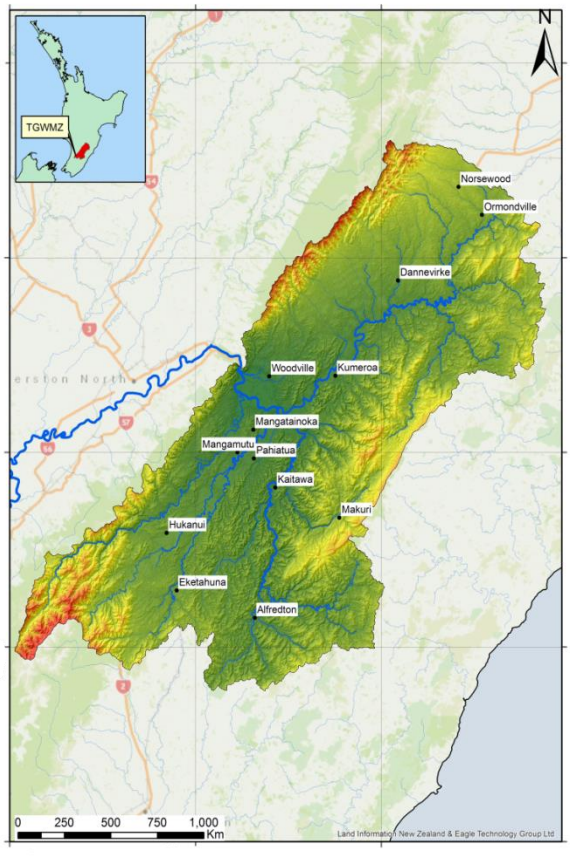

Figure 15: The Tararua Ground Water Management Zone (Tararua GWMZ) (Map generated in ArcGIS 10.2 using shapefiles from Land Information New Zealand, 2011b, 2013; Landcare Research, 2010d).

The Tararua GWMZ is bordered to the east by the Puketoi Ranges, and to the west by the Ruahine and Tararua Ranges. Elevation ranges from 60 to 1497 m, the topography is steep along the ranges and moderates to rolling hill country along the margins of expansive central alluvial plains (Elwan et al., 2015; Horizons Regional Council, 2016). The major population centres are Dannevirke, Woodville, Pahiatua and Eketahuna.

4.3 Landuse

Landuse is generally controlled by topography; and dairy farming is significant on the plains, sheep and beef on rolling country, and radiata and native forest predominate on the steeper areas. Landuse data obtained from LCBD v4.1 (Landcare Research, 2015) (Figure 16).

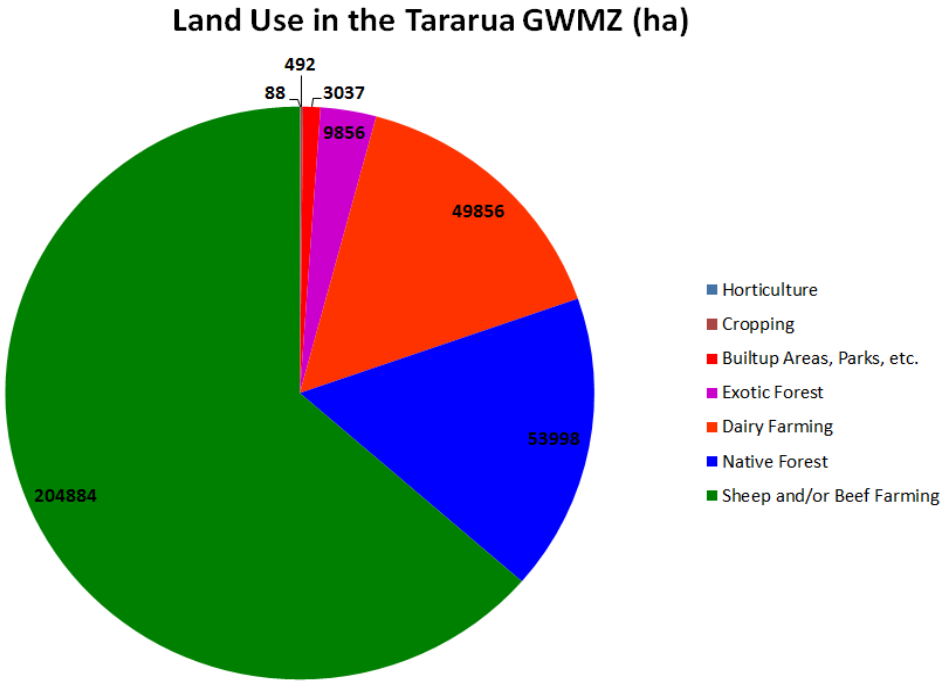

Figure 16: Area of the various land use categories of the Tararua GWMZ (labels indicate area in hectares). Almost the entire 3000km^2 is farmed or under forest cover. (Landcare Research, 2015).

4.3 Precipitation

Precipitation varies with altitude (Figure 17); an annual average of > 2000 mm falls along the Ruahine Ranges, and around 1400 mm along the Waewaepa Ranges and Eastern hill country. The plains are strongly affected by the rain shadow of both ranges where the annual rainfall decreases to around 800 mm - 1200 mm (Molloy, 1988).

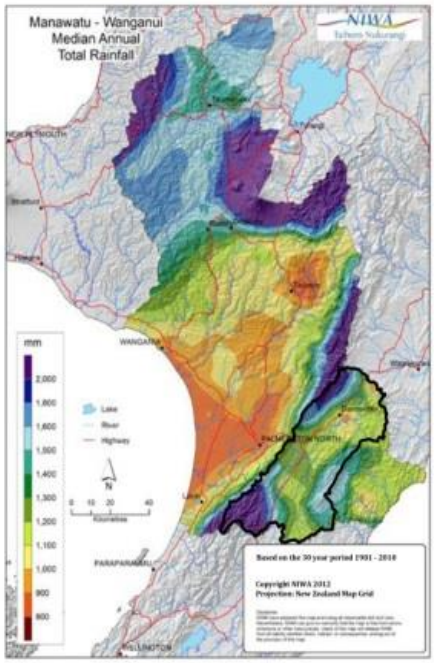

Figure 17: 30 year (1981-2010) mean rainfall for the Manawatu–Wanganui Regions; Tararua GWMZ is outlined in black. The Orographic precipitation effect is obvious about the higher elevation of the ranges. Overall rainfall in the Tararua GWMZ appears higher than west of the ranges (Chappell, 2015).

4.4 Hydrology

Drainage of the Tararua GWMZ (Figure 18) is via the NE–SW flowing Manawatu River which converges with its major tributaries, the Tiraumea, Mangatainoka, and Mangahao Rivers near the township of Mangatainoka before exiting the Tararua GWMZ westwards via the Manawatu Gorge towards the Tasman Sea (Vale, Fuller, Procter, Basher, & Smith, 2015). The morphology of the major rivers varies from semi-braided to pseudo-meandering, before evolving to form single-thread, laterally confined channels proximal to the gorge (Vale et al., 2015).

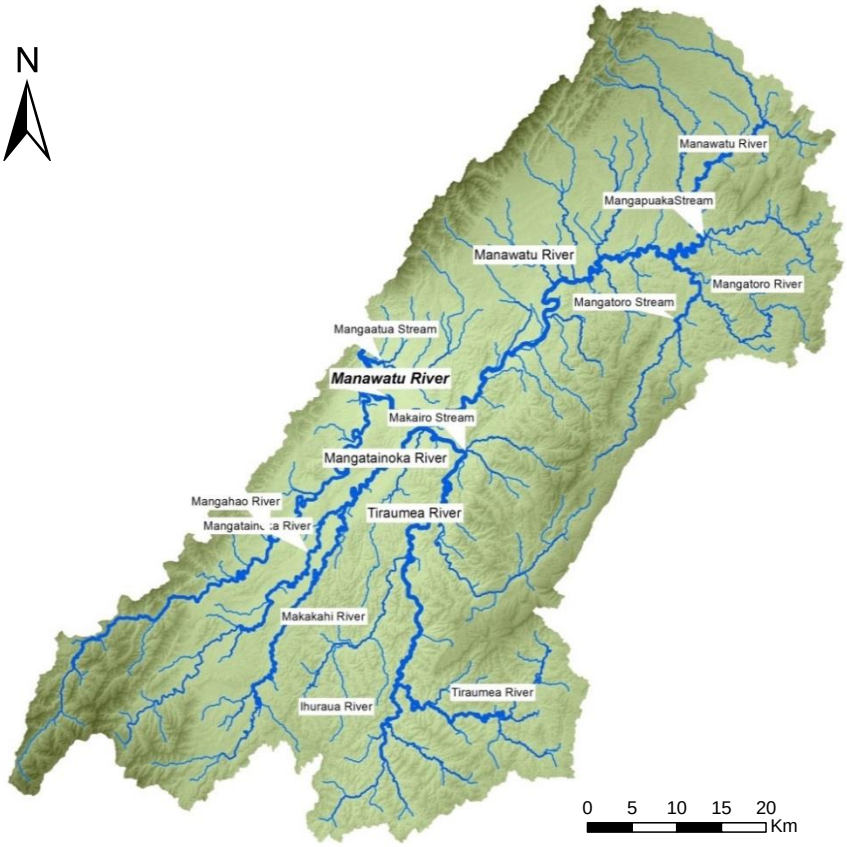

Figure 18: Main river systems and drainage pattern of the Tararua GWMZ. Drainage of the area westwards via the Manawatu River is occurring prior to uplift of the axial ranges and still continues, as down cutting of the river match or slightly exceed the rate of uplift and produce a classic example of antecedent drainage. The basement greywackes of Ruahine and Tararua Ranges form a relatively impermeable barrier in the west of the area forcing practically the entire basin's output to exit as surficial water via the Manawatu Gorge (Map generated in ArcGIS v10.2 using shapefiles from Land Information New Zealand, 2011b; Landcare Research, 2010d).

4.5 Potentiometric surface

Using depth to water table data from HRC, Rawlinson and Begg (2014) developed potentiometric contours of the Upper Manawatu and Mangatainoka Catchments. ArcGIS v10.2 was used to extrapolate these potentiometric contours to create a potentiometric surface, which was then extended to cover the extent of the Tararua GWMZ. The regional flowpaths tend to follow that of the rivers and streams and points

of interest are explained in Figure 19. It should be noted, as areas outside the boundary are extrapolated, they may not accurately represent actual water levels.

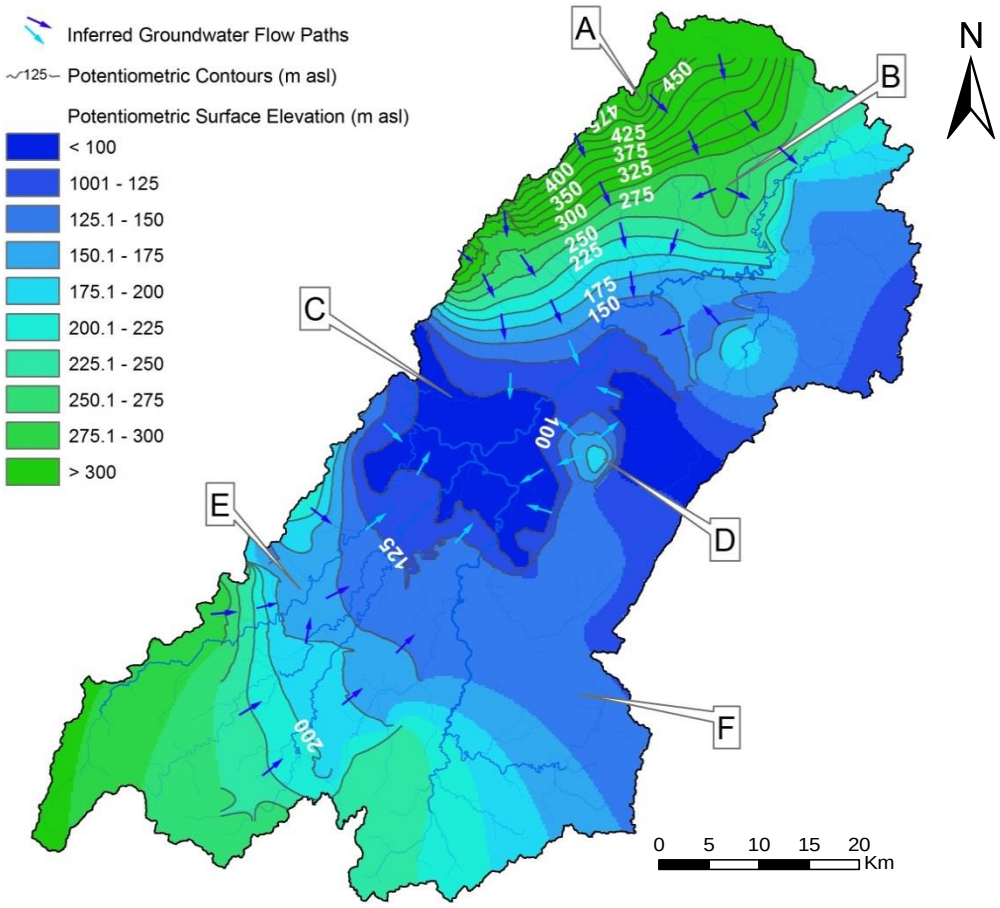

Figure 19: Potentiometric map indicating regional groundwater flow paths. Groundwater flow generally tends to parallel surficial water movement (Rawlinson & Begg, 2014). Key points of interest A). High hydraulic gradient adjacent to the axial ranges with SE flow. B). Topographic high spur around which groundwater flows are diverted. C). Area along the plains directly east of the head of the Manawatu Gorge where groundwater has low hydraulic gradient and ponds prior to discharge via the gorge. D). Topographic high point which controls groundwater flow E). Change in hydraulic gradient and generally northward flow paths. F). In areas where contour lines do not extend, the potentiometric surface has been extrapolated to encompass areas with very few wells and little knowledge of groundwater regimes (adapted using ArcGIS 10.2 from Rawlinson & Begg, 2014, p. 22).

4.6 Rocks of the Tararua GWMZ

4.6.1 Introduction

The geological history of the Tararua GWMZ is both complex and intriguing and although a full description exceeds the scope of this thesis, a brief summary is provided in Appendix A: Geological History of the Tararua GWMZ.

The geological processes have not only created several key geomorphological features including the Tararua, Ruahine, Waewaepa and Puketoi Ranges, the Pahiatua Basin, the Manawatu Gorge, but also deposited diverse and sometimes vast, sedimentary facies within the Tararua GWMZ (Figure 20). The characteristics of the rocks, their water bearing properties and how they influence the hydrogeology of the study area is discussed in the following section.

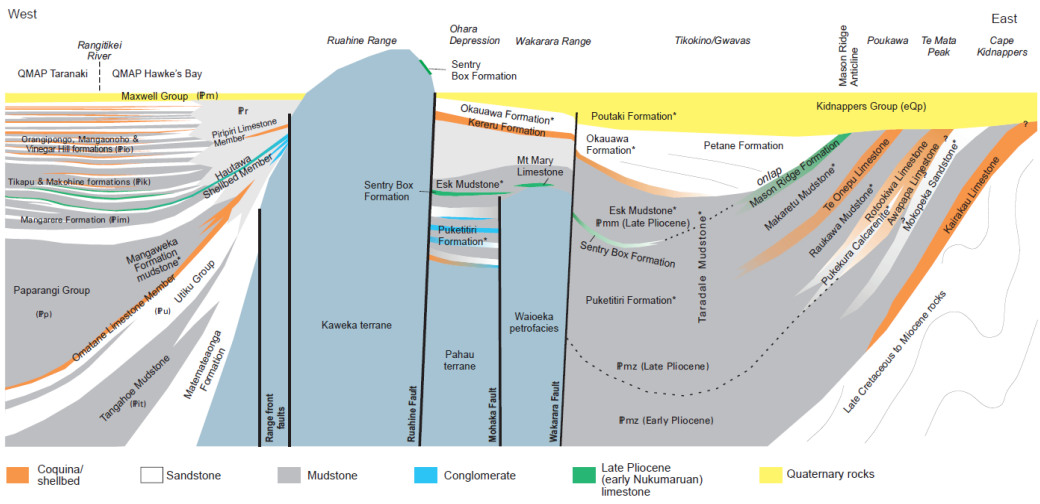

Figure 20: Schematic cross section of the eastern margin of the Wanganui Basin through the axial ranges to the eastern margin of the East Coast basin. The cross section represents an area north of the Tararua GWMZ and some of the folds/faults and rock units may differ slightly, nevertheless this diagram provides an excellent illustration of the effects of tectonic compression and deformation, as well as age, deposition and distribution of sediments in the Tararua GWMZ (Lee et al., 2011, p. 33).

The rocks of the region are predominantly sedimentary and are examined in chronological groupings based on the time of deposition and nature of depositional conditions (Figure 21; Figure 22). Although some rocks may only outcrop sporadically in the study area it is reasonable to expect (bar massive unknown unconformities) that they underlie a large portion of the Tararua GWMZ (Lee & Begg, 2002; Lee et al., 2011; Lillie, 1953).The groundwater in the region is predominantly encountered in two major porosity regimes, (i) the intergranular porosity of the alluvial fan and basin fill deposits and (ii) within the fracture porosity dominated limestone, coquina, and to a lesser degree, the greywacke basement rocks.

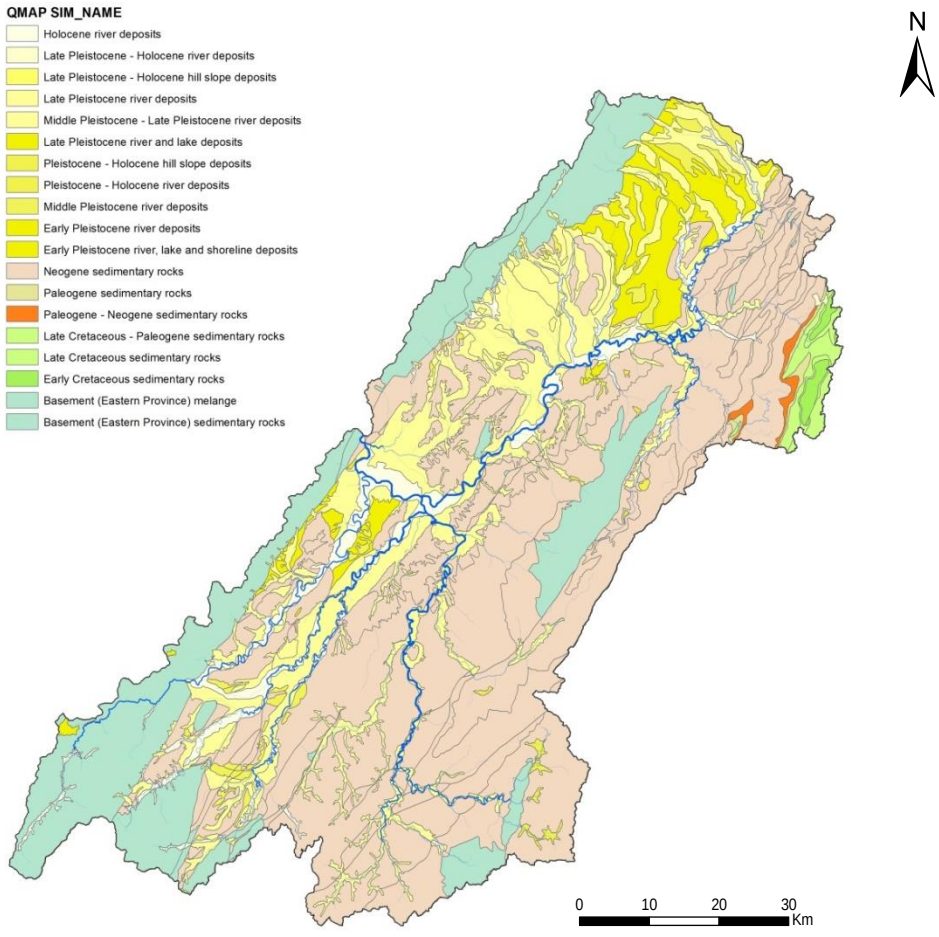

Figure 21: Main geological units of the Tararua GWMZ. Symbology follows that of the QMap series (GNS Science, 2012). A wide variety of sedimentary rocks are encountered in the area from ancient greywackes (basement rocks and melange) to Holocene gravels derived from them (Map generated in ArcGIS 10.2 using shapefiles from Heron, 2014; Land Information New Zealand, 2011b).

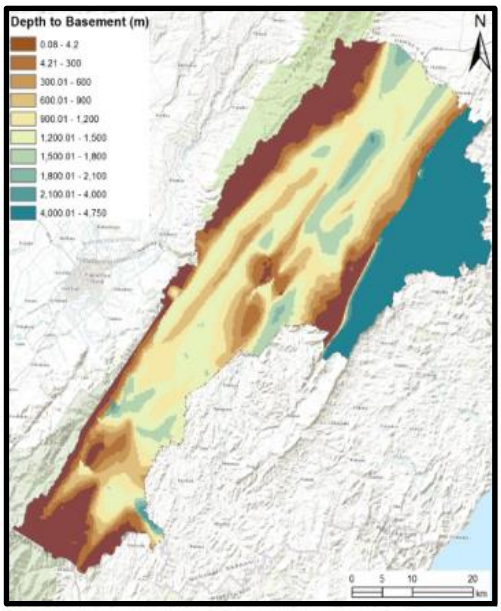

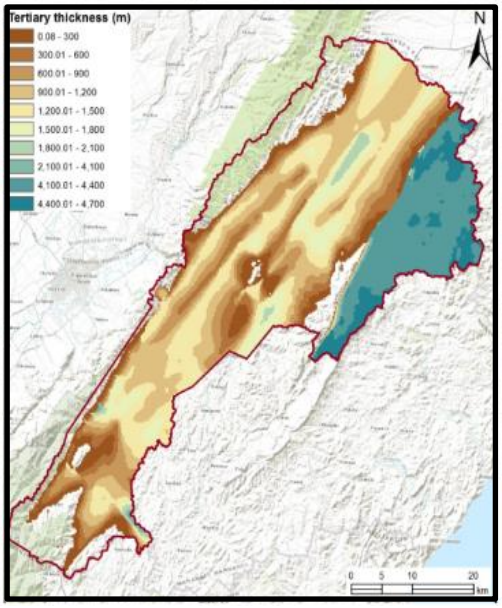

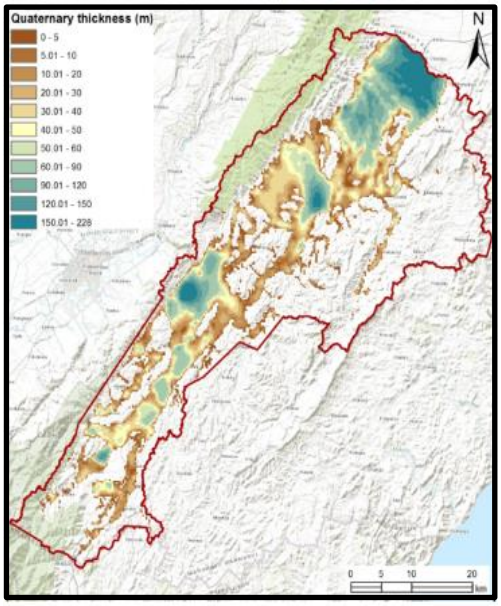

Figure 22: Depth to basement rocks (top), Tertiary (centre) and Quaternary rocks (bottom) (Rawlinson & Begg, 2014). These maps illustrate the NE dipping synclinal structure of the basement rocks of the Tararua GWMZ as well as the vast thicknesses of sedimentary rocks. The map does not encompass the entire Tararua GWMZ due to the model focussing on the Upper Manawatu and Mangatainoka Catchments, and is also due to few wells being installed in the south eastern area (Land Information New Zealand, 2011b, 2013; Rawlinson & Begg, 2014). Note: Well locations are mapped in Figure 32.

4.6.2 Basement Rocks

The basement rocks of the Tararua GWMZ (Figure 23) are greywacke-argillites of the Torlesse Composite terrane (Lee & Begg, 2002). Quartzo-feldspathic sandstone and argillite rocks, the Torlesse Terrane tends to be complexly deformed and often regionally metamorphosed (Lee & Begg, 2002; Rawlinson & Begg, 2014). The provenance of these well indurated sandstone, mudstone assemblages date to the Permian to late-early Cretaceous where they were deposited as muds and sands in a marine environment east of a tectonically accreting margin along continental Gondwana (Rawlinson & Begg, 2014). Bedding within the Torlesse Composite Terrane is steep to sub-vertical and indicative of intense tectonic uplift and deformation (Lee & Begg, 2002; Mortimer, 1994). Subgroups of the Torlesse Composite Terrane that outcrop within the study area are the Esk head Belt, Pahau Terrane, and Pohangina Melange. The predominant subgroup of the Torlesse Composite Terrane in the Tararua GWMZ is the Esk Head belt, a late Jurassic to early Cretaceous tectonically heavily sheared and fractured unit comprised of alternating sandstone and mudstone with allochthonous occurrences of limestone, chert and volcanics believed to be derived from adjacent terranes (Lee et al., 2011). Lying along the Eastern margins of both the Tararua and Ruahine ranges (within the study area) is the early Cretaceous Pahau Terrane; elongate, NE-SW trending belts of thinly bedded quartzo feldspathic, often carbonaceous, sandstone and mudstone (Lee et al., 2011). Also outcropping in the Waewaepa Ranges in the centre-east of the Tararua GWMZ, the Pahau Terrane is significantly more structurally intact than the Esk Head belt (Lee & Begg, 2002; Lee et al., 2011). In the Ruahine Ranges west of Norsewood and briefly intersecting the Tararua GWMZ boundary lies the Pohangina Melange, an elongate belt of heavily sheared black mudstone with finely bedded sandstone/mudstone and blocks of sandstone with occasional concretions, chert, limestone and volcanics (Lee et al., 2011).

The high degree of induration of the basement rocks coupled with significant mineralised intergranular cementation ensures little to no porosity or permeability is evident (Rawlinson & Begg, 2014). However, deformation (shear zones, fractures and joints) of these units leads to localised secondary permeability with some aquifer potential (Rawlinson & Begg, 2014). From well information provided by Horizons Regional Council, Rawlinson and Begg (2014) deduced that only two wells in the Tararua GWMZ were installed in Torlesse rocks. However, the authors struggled to determine whether these wells were actually located in greywacke due to the two wells their locations being estimated and their geographical proximity to younger lithologies. Site 50.9 (sampled in this study) according to QMap appeared to be situated in greywacke rocks overlain by silt loam, but upon field inspection of the geology, a more appropriate classification would be stony, silt loam overlying shallow greywacke derived gravels.

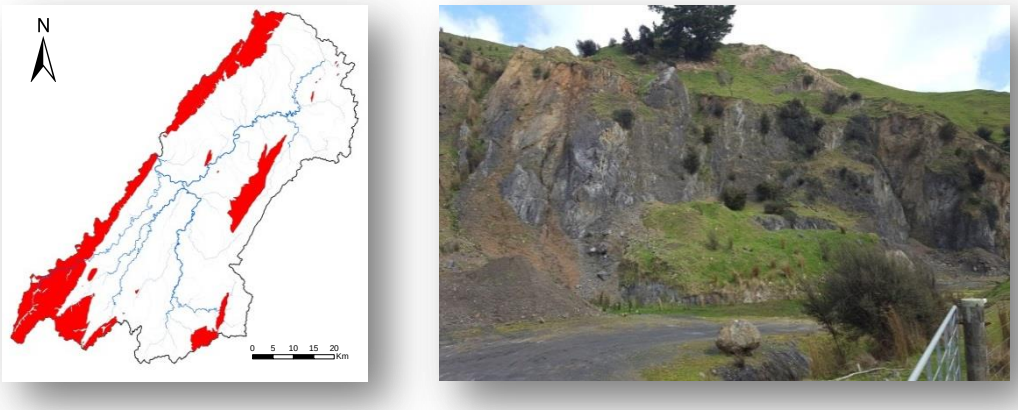

Figure 23: Extent of basement rocks in the Tararua GWMZ (left). Pahau Terrane (right) exposed by quarrying for aggregate (Central Mangaone Road, Pahiatua 40°62'7.94"S 175°76'77.3"E). Pahau terrane is encountered in the central east and southeast of the study area, while Torlesse Composite terrane forms the axial ranges in the west of the Tararua GWMZ. In the image (right), Pahau terrane is exhumed by the inactive, reverse NE-SW striking Rongomai Fault which lies around 100 m behind the photographer (Map generated in ArcGIS 10.2 using shapefiles from Heron, 2014; Land Information New Zealand, 2011b).

4.6.3 Cretaceous Rocks

Overlying the basement rocks are the Cretaceous Mangapurupuru Group (including the Springhill Formation) which occasionally crops out east of Dannevirke. Found in the core of a series of faulted anticlines (Rawlinson & Begg, 2014), these massive mudstone and alternating sandstone and mudstone beds of the Springhill Formation are believed to be submarine landslide sediments deposited in mid-outer shelf to bathyal environments (Lee et al., 2011; Rawlinson & Begg, 2014). Other minor units in this formation include conglomerate and pebble beds and occasionally some limestone (Lee et al., 2011). The Springhill Formation (Figure 24) can be up to 750 m thick (Lee et al., 2011) and the fine grained, well indurated sediments have low permeability, and unless heavily fractured do not transmit any groundwater (Rawlinson & Begg, 2014). According to Rawlinson and Begg (2014) no wells in the Tararua GWMZ are located in this formation.

Unconformably overlying the Springhill Formation are the Tinui Group comprising of sediments believed to have been deposited in an anoxic oceanic basin. The Tinui Group consists of the Tangaruhe and Whangai formations, the lower Tangaruhe unit can be up to 280 m thick and is comprised of a basal pebbly sandstone and mudstone overlain by mudstone with intermittent glauconitic sandstone and mudstone (Lee et al., 2011). The Upper Whangai Formation can be up to 500 m thick and conformably overlies the Tangaruhe Formation (Lee et al., 2011). The well indurated Whangai Shale is quite distinctive, fractures in the dark grey-brown (weathering to light-grey brown), poorly bedded siliceous mudstone are often rusty brown iron-stained with fine surficial deposits of the powdery yellow sulphurous mineral jarosite (Lee et al., 2011). Recognised for its hydrocarbon content, the Whangai Shale occasionally emits a distinctive hydrocarbon odour when rubbed. These formations have little water bearing capacity and Rawlinson and Begg (2014) reported no wells are located in either of these lithologies within the Tararua GWMZ.

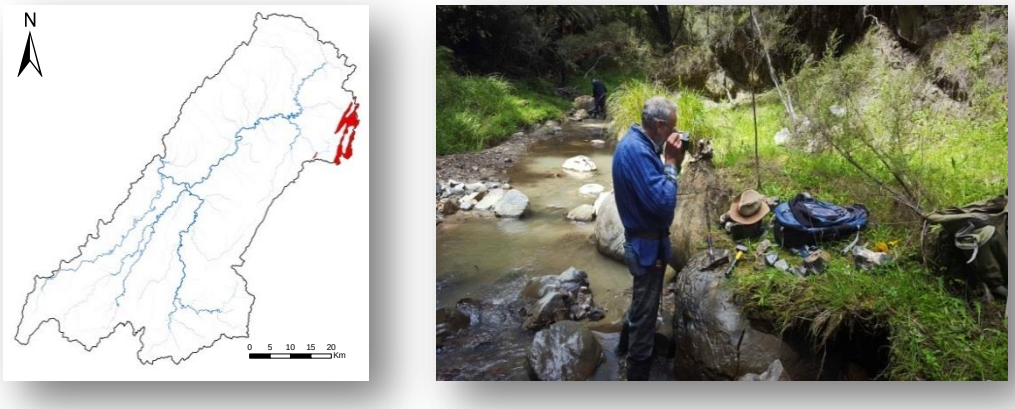

Figure 24: Cretaceous rocks are not commonly found outcropping at the surface in the Tararua GWMZ (left). Springhill formation (right) exposed in the Te Uri stream (Mangaorapa 40°17'31.5"S 176°27'22.3"E). The well indurated mudstone is found at the surface on the north eastern extent of the study area and should be considered an aquitard (Map generated in ArcGIS 10.2 using shapefiles from Heron, 2014; Land Information New Zealand, 2011b).

4.6.4 Paleogene (Paleocene to Oligocene) Rocks

The physical characteristics of the Palaeocene to middle Eocene, Mangatu Group (Wanstead Formation of the study area) vary throughout its range. This is due depositional conditions ranging from mid-bathyal to lower bathyal-abyssal depths in the easternmost sediments , rising to shallower depths for sediments that lie west of the Whangai Range (Lillie, 1953). Up to 300 m thick, the Wanstead Formation is typically a soft green-grey to reddish mudstone but tends to be a hard blue-grey to brown sandy mudstone in the Dannevirke area. Farther north and north east greensands and calcareous mudstone are prominent (Figure 25), and out of the study area north towards Te Hoe it will also include glauconitic, calcareous and micaceous mudstones (Lee et al., 2011; Lillie, 1953).

Overlying the Wanstead Formation is the Weber Formation, a cream-brown to light-brown calcareous well bedded mudstone/sandstone (Lillie, 1953). Inferred to have been deposited in shallower mid-bathyal depths, this formation can be up to 500 m thick in

the Dannevirke area. Foraminifera dating suggests an age ranging from early Oligocene to earliest Miocene (Lee et al., 2011; Lillie, 1953). As these fine grained sediments all exhibit low permeability and are considered aquitards it is not surprising that no wells in the study area are located in these rocks (Rawlinson & Begg, 2014). The presence of glauconite is observed in these formations and may be a locally significant electron donor in redox reactions occurring in carbon poor, anoxic environments (Rissmann, 2011).

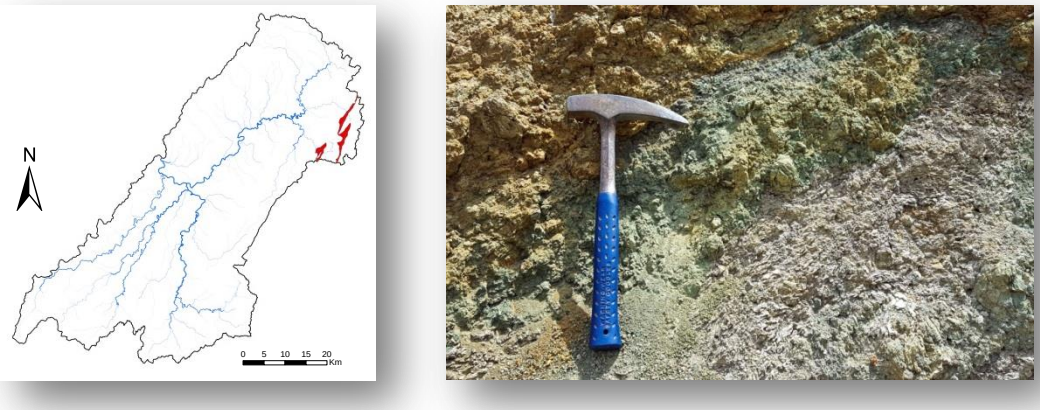

Figure 25: Paleogene rocks observed in a road cutting (Weber Road, Waitahora S40°21'24.3" E176°17'09.6"). A lens of green glauconite overlying pale grey-brown Wanstead Formation is visible beneath the geological hammer. Glauconite is considered to be a significant electron donor should organic carbon be limited (McMahon & Chapelle, 2008; Rissmann, 2011) Map generated in ArcGIS 10.2 using shapefiles from Heron (2014); Land Information New Zealand (2011b).

4.6.5 Neogene (Miocene to Early Pliocene) Rocks

Unconformably overlying the Weber Formation is the Tolaga group of undifferentiated Miocene sedimentary rocks. Widely distributed (from Wairarapa north to East Cape), the Tolaga group is immense with beds up to 5000 m thick in some localities (Lee et al., 2011). Grainsize characteristics of the sediments vary both temporally and spatially. Calcareous sandy silts predominate in the middle Miocene sediments of the north

eastern Tararua GWMZ. Late Miocene sediments around Dannevirke may include pebbly mudstone, limestone, sandstone, and mudstone. Similarly aged units around Eketahuna and Alfredton are comprised of calcareous mudstones and sandstones with localised conglomerate (Figure 26), and bioclastic limestones (Lee & Begg, 2002; Lee et al., 2011; Rawlinson & Begg, 2014).

The pore size, and effective permeability of sandstones potentially allow for storage and transmission of groundwater, but Rawlinson and Begg (2014) suggest this is compromised in the Miocene units by the presence of silts occurring in tandem with the sandstones. However, the conglomerates found in the southern area of the Tararua GWMZ are locally exploited for groundwater with six wells installed in this lithology, although uncertainties exist as to which rock unit the water is drawn from (Rawlinson & Begg, 2014).

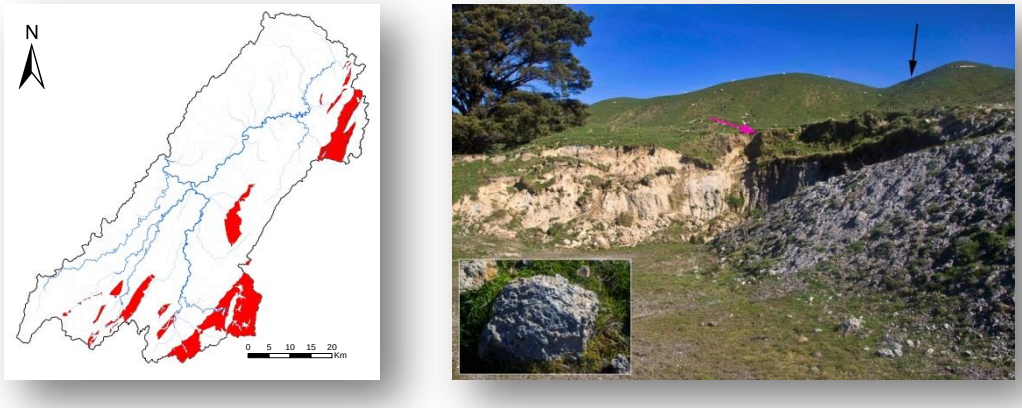

Figure 26: The Alfredton Fault (which ruptured during the 1934 7.6 magnitude Pahiatua Earthquake) is exposed in a quarry (Bartons Line, Ihuraua 40°42'54.9"S 175°49'25.4"E). Conglomerate has been juxtaposed against younger sediments by west side up, dip slip displacements up to two km. The fault trace on the horizon (black arrow) runs NE to the quarry (pink arrow). Six wells are installed in conglomerate in the Tararua GWMZ but this particular unit appears well cemented with no interstitial pores or fracture porosity (inset). Note: The light grey conglomerate in the foreground has been broken out by quarrying (Map generated in ArcGIS 10.2 using shapefiles from Heron, 2014; Land Information New Zealand, 2011b).

4.6.6 Neogene (Mid to Late Pliocene) Rocks

The Pliocene rocks of the Mangaheia Group were deposited while the Ruataniwha strait (see Appendix A: Geological History of the Tararua GWMZ) was shallowing and eventually drained by tectonically driven thrusting and uplift (Trewick & Bland, 2012). Early Pliocene sediments are predominantly siltstone, mudstone, sandstones and bioclastic limestones along with some conglomerate and pumiceous sands and silts (Figure 27; Figure 26; Figure 28). Late Pliocene rocks of the Mangaheia group are siltstone, mudstone, and bioclastic limestone with localised areas of sandstone (Lee et al., 2011). The sandstones of this group do have water bearing properties but not to the same level as the similarly aged limestones. Rawlinson and Begg (2014) determined that 91 wells in the study area are installed in Mangaheia group sediments but whether the water is abstracted from this group or the overlying or underlying sediments was not confirmed.

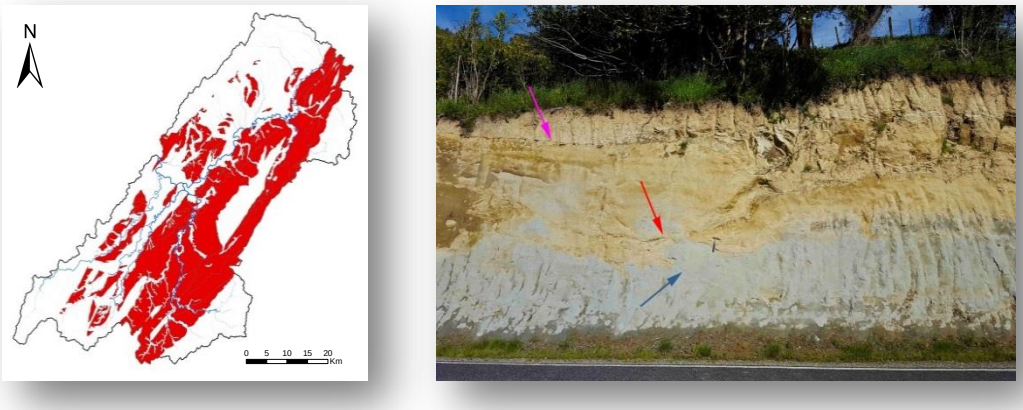

Figure 27: Pliocene sediments are widely distributed at the surface, particularly in the eastern hill country of the Tararua GWMZ. The Pliocene Mangaheia Group includes a range of sediments such as fine grained blue-grey mudstone (Mangaone Valley Road, Pahiatua 40°34'42.9"S 175°50'38.9"). Erosional surfaces/contacts are indicated by red and pink arrows whilst westward dipping bedding planes (typical of the area) is indicated by the grey arrow. The blue-grey mudstone is an effective aquitard, whilst the yellow- brown, fine-grained sandstone may store and transmit a little groundwater (Map generated in ArcGIS 10.2 using shapefiles from Heron, 2014; Land Information New Zealand, 2011b).

Figure 28: The Mangaheia Group is a diverse collection of different sediment types. Vast deposits of blue-grey mudstone (Figure 27 above) are bounded by beds of sandstone (left) such as those exposed in a road cutting (Bluff Road, Pahiatua 40°22'58.3"S 175°55'13.2"E) and limestone such as that outcropping at the ridge crest (Mangatoro Stream, Waitahora 40°21'34.1"S 176°09'09.7"E). Both facies are regarded as water bearing, although the sandstone is relatively limited in this regard. Note: black arrows indicate small bivalve fossils, and pink arrows indicate limestone in both the ridge and also large boulders in the stream.

4.6.7 Quaternary (Early Pleistocene to Holocene) Rocks

The early Quaternary rocks of the Kidnappers Group, encountered in the north to northeast of the study area consist of silt, sand, gravels with lignite, peat and some rhyolitic ignimbrites as well as pumiceous sands and silts. Mid to late Quaternary rocks are found in more central locations east of Dannevirke to south of Mangatainoka. The gravels of this age are recognised by Krieger (1992) to be deposited in expansive alluvial fans by rivers draining the axial ranges, the finer sediments indicating fluvially deposited gravelly-sand and sand. The large gravel areas in the plains have been formed not only from meanderings of the major rivers, but also due to right-lateral strike- slip movement of around 7mm y^{-1} along the Wellington and Ruahine faults (up to 15 mm y^{-1} in the Dannevirke area), (Neall & Hanson, 1995). This movement displaced streams, created new courses and abandoned the existing fans allowing new fans to form (Palmer, 2009). Krieger (1992) maintained interbedded silts originated from overbank

flood deposits, while fossiliferous silt and fine sand indicated deposition in an estuarine tidally dominant shallow environment. Furthermore Krieger (1992) established the poorly fossiliferous, centimetre bedded silts to have been deposited in a subsiding interfluvial-lacustrine environment. The carbonaceous material found within Quaternary sedimentary facies are indicative of lacustrine settings where swampy conditions prevailed prior to complete exhumation of the land (Figure 29). Pumice sands up to 30m thick interbedded with the Pleistocene sediments are locally significant, Krieger (1992) analysed the depositional structures and concluded the pumices were rapidly deposited as hyperconcentrated flow and overbank flood deposits of a meandering fluvial system. The sediments and analysis of paleo-shoreline data suggests the overall trend in the study area was that of marine regression driven by tectonic compressing and uplift which was punctuated by at least ten instances of marine transgressions due to changes in eustatic sea levels Krieger (1992).

Figure 29: Pleistocene sediments tend to be distributed in the expansive central plains of the Tararua GWMZ and the rolling hill country north of Dannevirke (left). The complex sequence of lacustrine and fluvial sediments (right, road cutting north of Whakaruatapu River 40°14'81.7"S 176°15'27.7"E) is indicative of the latter stages of the demise of the Ruataniwha Strait.. Arrows indicates peat and lignite (black arrow), lacustrine mudstone (chartreuse), pumice sands (blue), eastward dipping bedding planes (red) and angular unconformity between Pliocene and Pleistocene sediments (Map generated in ArcGIS 10.2 using shapefiles from Heron, 2014; Land Information New Zealand, 2011b).

The Quaternary sediments present at the surface throughout the study area are the most significant water bearing rocks (Figure 30; Figure 31). Of these, the older gravels and sands tend to be associated with some clay (arising from weathering) that restricts their water transmitting properties. However, the Pleistocene gravels are less likely to have such a high clay fraction and are capable of storing and transmitting significant volumes of water (Rawlinson & Begg, 2014).

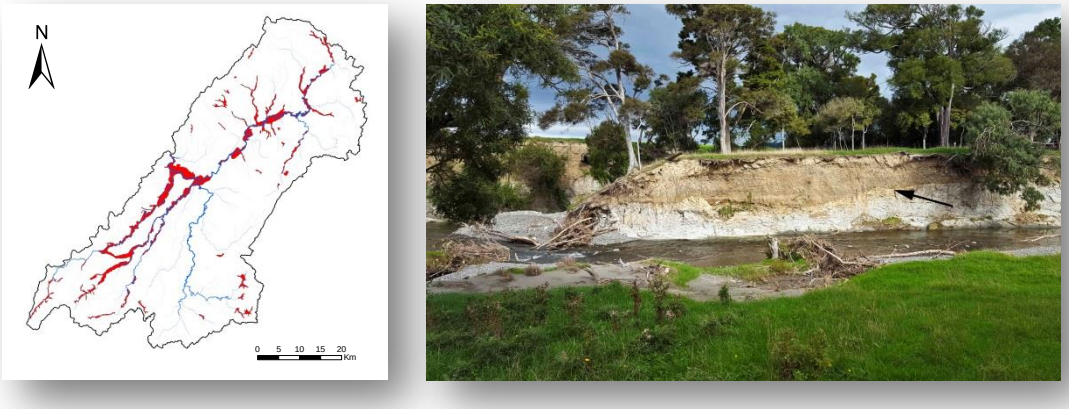

Figure 30: Holocene gravels are associated with the major fluvial systems of the Tararua GWMZ (left). The shallow aquifers in the region are typically unconfined gravels underlain by impervious marine sediments such as seen in the bank of an unnamed stream (Jackson Rd, Kumeroa 40°19'24.3"S 175°59'46.8"E). Arrow marks a strath; an erosional surface cut by fluvial processes prior to deposition of the gravels (Map generated in ArcGIS 10.2 using shapefiles from Heron, 2014; Land Information New Zealand, 2011b).

Figure 31: Gravels range from (left) large, sub angular clasts with high hydraulic conductivity such as the facies found in the Mangatainoka Plains (Namu Road, Mangatainoka ,40°24'18.9"S 175°53'11.1"E), to fine rounded to sub-rounded pebble sized clasts with poor hydraulic conductivity (right), (*continued on following page)*.

Figure 31 *continued*: Gravels range from (left) large, sub angular clasts with high hydraulic conductivity such as the facies found in the Mangatainoka Plains (Namu Road, Mangatainoka ,40°24'18.9"S 175°53'11.1"E), to fine rounded to sub-rounded pebble sized clasts with poor hydraulic conductivity (right). The clays and iron minerals in the deep "red gravels" found east of Dannevirke (40°19'26.7"S 176°01'35.7"E) further restrict their water bearing ability. Pink arrow indicates a small lens of fine silt interpreted to be an overbank flood deposit or possibly a small channel in the gravels.

The majority (92%) of bores in the Tararua GWMZ are installed in Quaternary sediments, and despite Rawlinson and Begg (2014) being unable to substantiate whether all the wells draw from Quaternary sediments, data from Horizons Regional Council's database (Rawlinson & Begg, 2014) shows the bores in these areas are generally less than 20 m deep (Figure 32), suggesting it is highly likely that the most productive lithological units are indeed Quaternary.

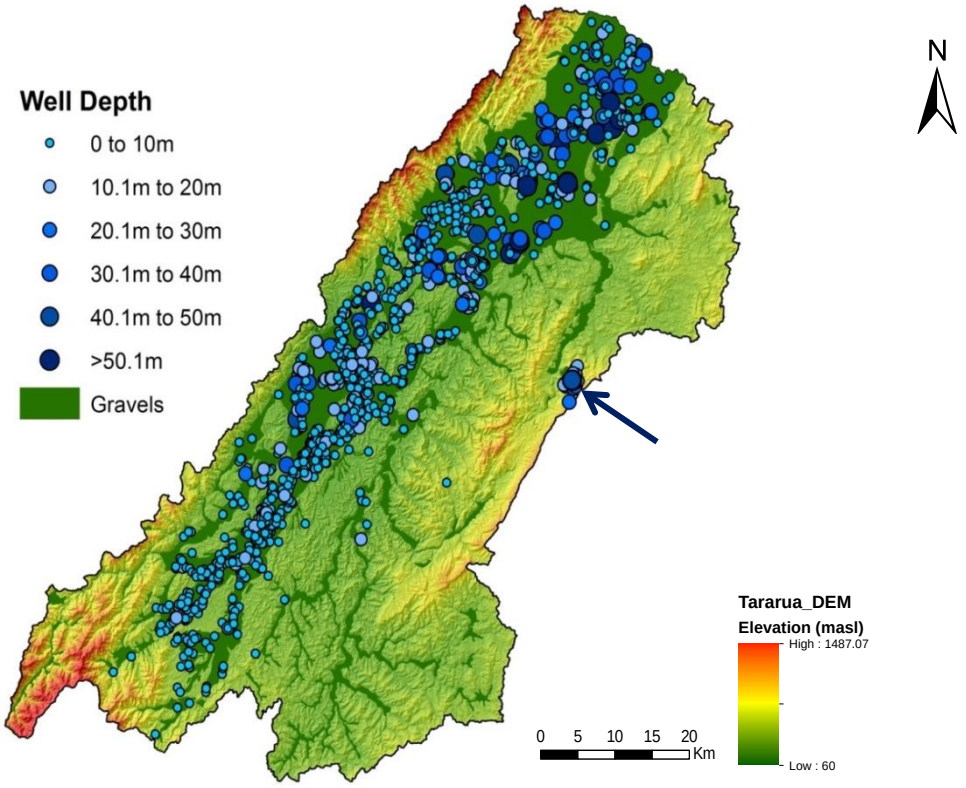

Figure 32: Location of bores in the Tararua GWMZ from the Horizon Regional Councils Database. The majority of wells are less than 10 m deep and are located in late Pleistocene to Holocene gravels. The area in the SE of the map with no wells is the mudstone country with no recognised aquifers. The small cluster of wells along the mid-eastern margin of the map (black arrow), are located in coquina in the Waitahora Valley area, but may be associated with hydrocarbon exploration (Map generated in ArcGIS 10.2 using shapefiles from Heron, 2014; Land Information New Zealand, 2011b).

4.7 Soils of the Tararua GWMZ

4.7.1 Introduction

The combination of diverse of landforms, rocks and parent materials with a distinct W-E trending climate gradient have served to produce a complicated pattern of soils in the Tararua GWMZ (Molloy, 1988). Broadly speaking, the soils may be classed as those developed from the Eastern hill country, basement rocks, and those from older river terraces, younger river terraces, and flood plains (Palmer, 2009). Palmer (2009) identifies that soils found adjacent to the ranges have developed in eroded greywacke-argillite colluvium with minor loess and tephra deposits. This contrasts with the soils developed from the eastern hill country which may have parent rocks of mudstone, sandstone or limestone. Some loess and tephra have been retained on the flat to gentle slopes, while valleys are infilled by colluvium at the foot-slopes, and alluvium is prominent on narrow river terraces. The soils on the rolling ridges and slopes are more complex and reflect the varied nature of the underlying strata combined with the more resilient of loess and tephra deposits, while soils on the steep slopes are often little more than a very thin veneer subject to regular slips and landslides (Figure 33).

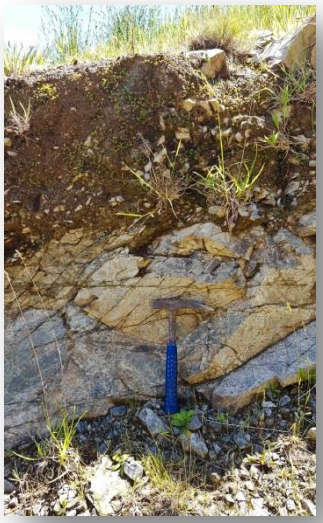

Figure 33: Soils of the Tararua GWMZ *(continued on following page).*

Figure 33 *continued*: Soils of the Tararua GWMZ. Soils on mudstone hills (left) were often extremely thin (red arrow) and very prone to erosion (Pa Valley Road, Alfredton 40°38'36.4"S 175°51'53.7"E) while soils in steep greywacke country (right) although often slightly deeper are also vulnerable to erosion (Tamaki East Road, Dannevirke 40°08'00.8"S 176°03'08.2"E). Steep topography, thin soils, and bedrock proximal to the surface result in rapid movement of runoff through the catchment and little chemical modification by contact with the soils and rocks.

The older river terraces tend to be draped with loess and tephra grading to thick poorly drained colluvium at the base of the hills. In areas proximal to the axial ranges, terraces formed during the Last Glacial tend to consist of loamy alluvium, (colluvium adjacent to steeper slopes) and gravels to the surface. The younger, lower terraces have a more complex soil pattern, where characteristics of the fluvial system such as stony river-bars, and loamy alluvium filled paleochannels are overlain by intricate flood deposits (Figure 34). Soils found on frequently flooded zones are regularly overlain by fresh alluvium and have little time for development, while those in areas less frequently affected by flooding have deeper topsoil and more evolved profiles. Of interest to this study is to what extent the chemical compositions and drainage properties of the soils exert some influence on the redox characteristics of the Tararua GWMZ's groundwater.

Figure 34: The presence of a paleochannel of the Mangatainoka River is indicated by the thick deposit of large gravel clasts (centre to left of the image) which are typical of the younger, lower terraces (Mangatainoka 40°36'07.4"S 175°39'37.6"E).

4.7.3 Soil Texture

The soil texture nomenclature in this study follows that defined in Lilburne, Hewitt, and Webb (2012). Texture may be expressed as single texture e.g. loam, or compound texture e.g. silty loam. Textures range from coarse free draining sand, and sand and stony gravel, to poorly draining silt loam and clay loam. The dominant soil textures (Figure 37) found in the Tararua GWMZ are silt loam (167,277 ha), sandy loam (51,400 ha), stony loam (23,911 ha) and stony silt loam (17,173 ha); areas calculated from the FSL shapefile (Landcare Research, 2010b). The small areas of soil textures not well represented in the Tararua GWMZ such as mottled sandy loam (22 ha), peaty loam (135 ha) peaty silt loam (407 ha) are not considered in this study.

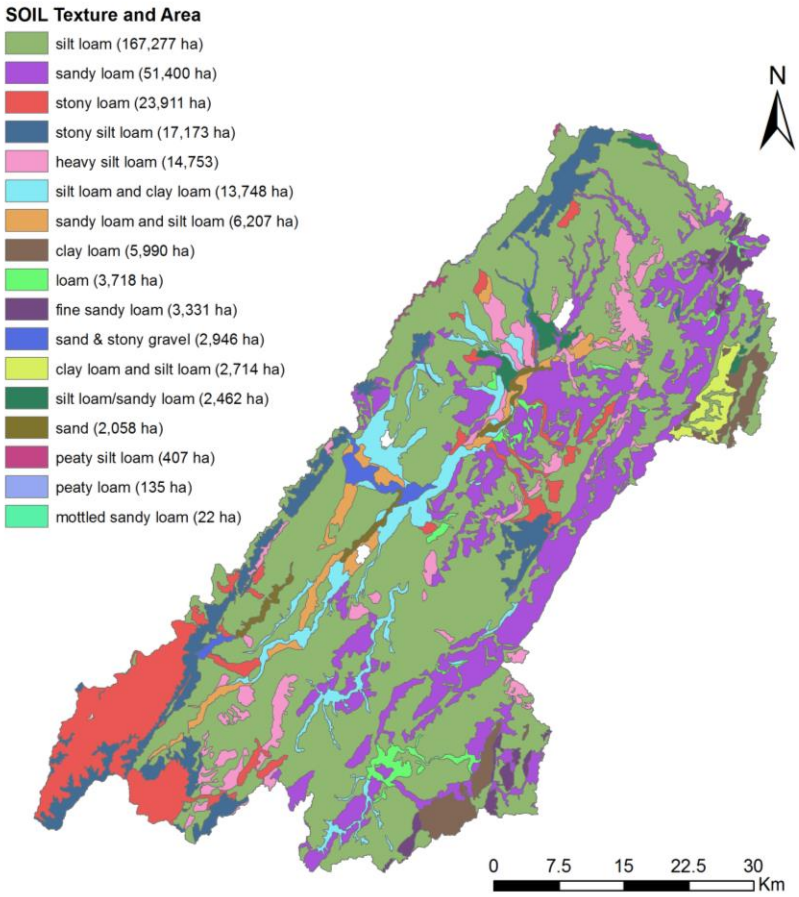

Figure 35: Fundamental soil layer (FSL) soil textures. Silt loam is clearly the dominant soil type in the Tararua GWMZ, and is found throughout the central plains flat to moderate slopes in the eastern regions. Soil textures with areas less than 2000 ha are not considered further in this study (Map generated in ArcGIS 10.2 using shapefiles from Heron, 2014; Land Information New Zealand, 2011b).

4.7.2 Soil Drainage and Soil Carbon

Soil drainage is estimated using the FSL drainage class (Figure 36a). The Tararua GWMZ is predominantly classed moderately well drained (235,595 ha) and imperfectly drained (65,289 ha) while only 17,376 ha are classed as poorly drained. Poorly drained soils tend to be located along the floodplains of the larger rivers such as the Manawatu, Mangatainoka, and Mangamaire Rivers. Soil carbon is estimated using the FSL carbon class (Figure 36b). Carbon levels in the Tararua GWMZ are predominately medium especially in the eastern areas (168,955 ha), and low in the central plains (132,406 ha) with small areas of high carbon irregularly dispersed through the western areas.

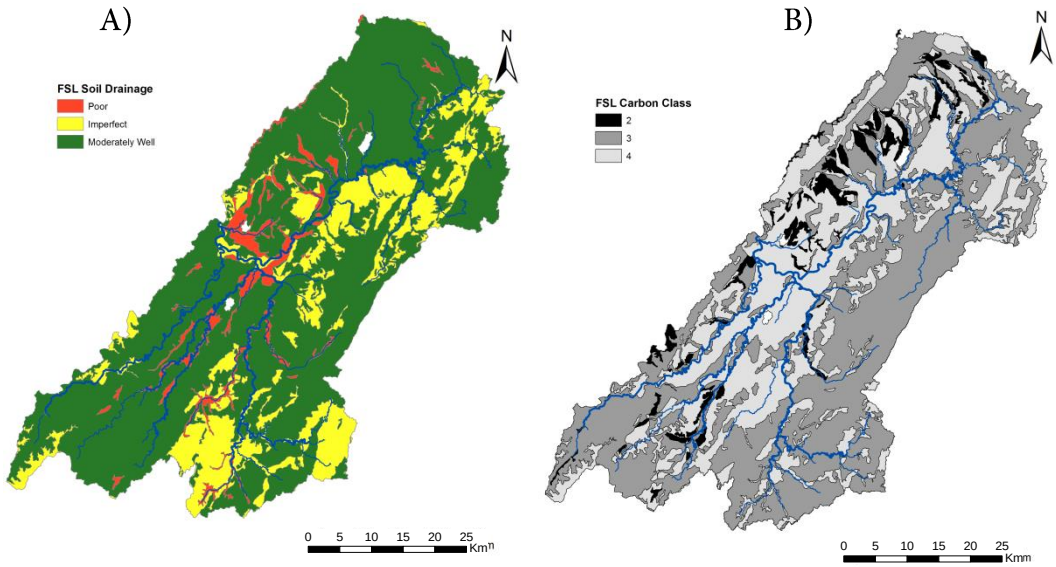

Figure 36: FSL soil drainage and carbon levels in the Tararua GWMZ. The central plains where the majority of samples were collect from in this study tend to be moderately well drained with medium to low levels of carbon (Map generated in ArcGIS 10.2 using shapefiles from Heron, 2014; Land Information New Zealand, 2011b; Landcare Research, 2010a, 2010c).

4.8 Summary

The complex geological history of the Tararua GWMZ has resulted in a diverse range of sedimentary facies that reflect specific geological settings and depositional conditions. The soils are predominantly moderately well drained silt loam and sandy loam with medium to low levels of soil carbon determined from FSL shapefiles (Landcare Research, 2010a). The prevalence of fine grained mudstones with very poor water transmitting and storage potential restricts available groundwater to the limestones, sandstones, gravels and sands (Rawlinson & Begg, 2014). In addition, lignite and peat theoretically provide a rich source of carbon; an essential component of the denitrification process (Rivas et al., 2017). Therefore the principal aquifers of the Tararua GWMZ tend to be gravel facies underlain by aquitards of fine grained marine sediments and possibly overlain to some degree by loess; it is from these aquifers that most of the samples in this study are collected. Figure 37 shows stratigraphy typical of the central plains of the Tararua GWMZ. The method used to identify appropriate sites, collect and analyse the samples and the statistical analysis are described in the next chapter.

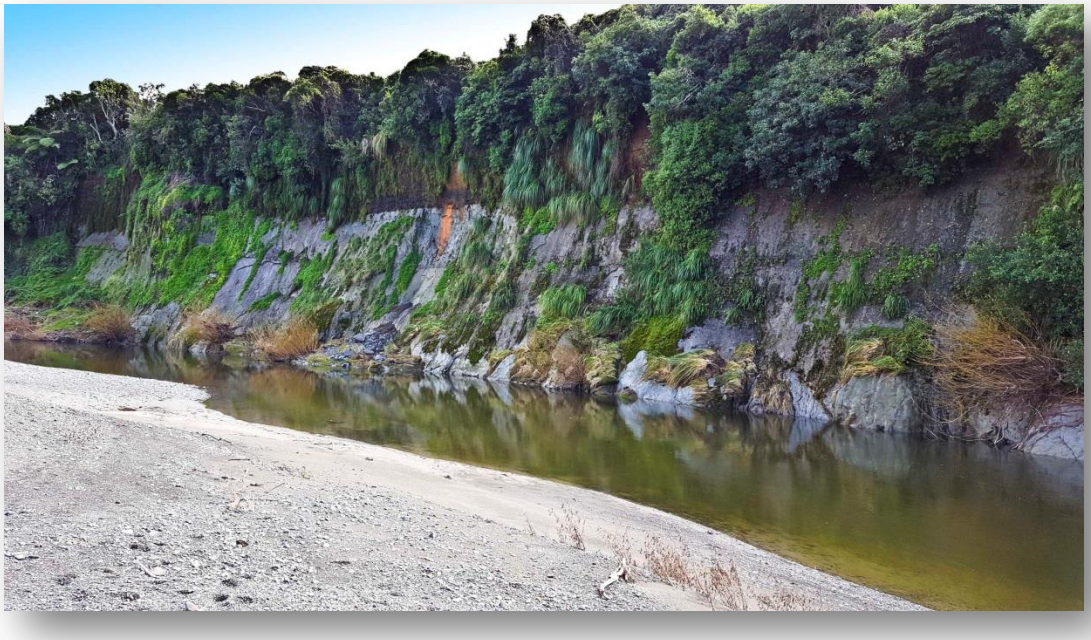

Figure 37: The upper Manawatu River at Otope Road, Dannevirke (40°14'56.2"S 176°05'18.8"E). This stratigraphy was observed to be representative of that underlying the plains from Dannevirke to Eketahuna. The river has cut down through the marine mudstones and as it meanders will build a new terrace and overlay it with gravels. Bright orange mark in centre of image is due to iron precipitating from groundwater that is discharging at the base of the gravels.

Chapter 5: Methods and Materials

5.1 Introduction

The research project involved five distinct phases;

- Site selection,
- Development of a direct-push system to sample shallow groundwater from specific locations not constrained by existing wells,
- Collection of shallow groundwater samples,
- Laboratory analysis of groundwater samples for major cations and anions, metals and nutrients,
- Statistical analysis of groundwater characteristics using HCA, and physical factors using PCA.

This chapter begins with a brief explanation of how Geographical Information Systems (GIS) were utilised to identify main-rock, sub-rock and soil types, select the shallow groundwater survey sites and delineate the most efficient routes prior to the fieldwork. This is followed by a description of the direct-push method as it evolved, a brief commentary of practical points that enhanced the success of the system, and the methodology used to collect shallow groundwater samples. The technical aspects of chemical analysis of the groundwater samples are then discussed, before concluding with a statistical analysis with the aim to establish the influence (if any) of rocks and soils on the groundwater's redox characteristics.

Note:

- In order to bolster the spatial resolution of this study and enhance the statistical analysis, data from 56 wells in the Tararua GWMZ collected by Massey University PhD student A. Rivas (Rivas et al., 2017) were included in the statistical analysis.
- The location of wells in the region established from the Horizons Regional Council (HRC) well database is presented at times. This data has been recorded over many years and many well locations are estimated from topographic maps or aerial photographs (S. Collins, personal communication, March 25, 2017). Furthermore, over 50% of the wells did not have well depth, or depth to water table documented. Therefore, it is assumed the locations and attributes of wells presented in these maps may not be accurate.
- Limestone and claystone are represented by very small areas in the Tararua GWMZ. Due to the similarity of their physical characteristics with coquina and mudstone respectively, and to simplify statistical analysis, these units are combined.

5.2 Digital Data

This project used ArcGIS v10.2 to analyse collected hydrogeological and geographical information to identify and locate shallow groundwater sample sites that lay within the different combinations of rocks and soils of the Tararua GWMZ (see key data sources in Appendix B: Digital Data Sources). The small scale 1:250,000 GNS QMap series and the larger scale 1:50,000 New Zealand DEM and LRIS Fundamental Soil Layers (FSL) provided the framework for spatial analysis of the geology and soils of the Tararua GWMZ. Supplementary soil information data such as soil pH and carbon levels were also obtained via the LRIS portal. These maps and layers were selected due to their

availability and spatial coverage at a national level, and were manipulated to create polygons of the various combinations of main rocks and soil types present in the Tararua GWMZ. The potentiometric map used in this study was generated from HRC bore information database by Rawlinson and Begg (2014) and extrapolated with ArcGIS v10.2 to the entire Tararua GWMZ.

5.3 Site Selection

As discussed, the hydrogeological properties of many rock units in the study zone were very similar. Therefore considering the size and the envisaged spatial resolution of the study area, it was considered reasonable to classify rocks by main-rocks and sub-rocks (a classification used exclusively by QMap to describe subordinate rock types found in conjunction with the principal rock type), rather than use specific geological group or formation names. Similarly, soils are classified by soil type rather than the soil series. The use of these broad categories rather than specifically named geological formations and units may also allow findings from this project to be extrapolated to other regions. Using ArcGIS v10.2 *dissolve tool,* boundaries within the main-rock polygons were dissolved by rock type, another shapefile was created by dissolving boundaries between subrock, and similarly the FSL polygons by soil type. The three shapefiles were combined using the *union tool* to produce a map that with appropriate classification was capable of displaying main-rock and soil type or should greater detail be required on main-rock, soil type and sub-rocks.

To better analyse the distribution of aquifers in the region, the locations of existing wells were overlaid over the geology-soils map, classified to show depth to the watertable, then exported and analysed in Microsoft Excel. These data (Table 3) reveal the water table in the central plains aquifers tended to be relatively shallow, and unsurprisingly, most wells are located in gravels.

Table 3: Water table depth and surficial geology of the Tararua GWMZ

Depth to Water Table	Number of Wells (m)	Number of Wells in Rock Type					
		Cong	Coq	Grv	GrW	MST	SST
Artesian	5	–	–	5	–	–	–
0 – 9.9 m	468	–	–	459	–	–	9
10 – 19.9 m	29	–	–	27	–	–	1
20 – 29.9 m	9	–	–	8	–	–	1
30 – 40 m	0	–	–	–	–	–	–
Not Recorded	673	–	–	–	–	–	–

Cong = Conglomerate, Coq = Coquina + Limestone, Grv = Gravel, GrW = Greywacke
MST = Mudstone, SST = Sandstone.

To identify areas where shallow groundwater was most likely existed, a potentiometric surface was extrapolated from potentiometric contour map (Rawlinson & Begg, 2014) with the ArcGIS v10.2 *topo to raster* tool, the resulting raster subtracted from the DEM with the raster calculator, then reclassed to show only areas where the water table was less than 8 m from the surface. Although creating a potentiometric surface from 25 m potentiometric contours wasn't ideal, the map generated appeared to reasonably delineate the shallow aquifers extents. Considering most aquifers underlay the relatively flat plains of the Tararua GWMZ, the reliability of the potentiometric surface was validated by generating a series of slope maps from the Tararua GWMZ DEM (Figure 39). The resultant slope raster was reclassified by increments of 1° up to 5° and filtered to remove anomalous cells. These maps appeared to be in reasonable agreement with the potentiometric surface, and provided a reasonable guide in areas (e.g. the south eastern mudstone country) with scarce well data. Of the maps generated, a slope of < 3° appeared to the best fit of HRC wells to the extent of the potentiometric surface. The

simplified geological/soil map was clipped to the extent of the estimated water table < 8 m below ground level (bgl), then classified by main-rock and soil type. The polygons for each rock-soil class were exported as a shapefile and the areas calculated, then analysed in Microsoft Excel. Using the ArcGIS v10.2 *union* tool, the *QMap>main_rocks* field was combined with the *FSL soil-type* field. A new shapefile was produced that with appropriate symbology (*symbology>categories>unique values, many fields*), showed the range of main rock type and soil type combinations in the Tararua GWMZ. The area for each of the combinations were calculated and weighted according to area (Figure 38). The largest 20 combinations of main-rock and soil-type were selected and considered for sampling.

Data collected by Rivas et al. (2017) from 56 existing wells throughout the Tararua GWMZ provided an excellent opportunity to supplement the direct-push dataset. All key parameters (both laboratory analytes and field parameters) required to determine the nature of redox reactions and denitrification were analysed in both datasets. Lithology and well depths were compared and those that matched the direct-push dataset were included in the statistical analysis.

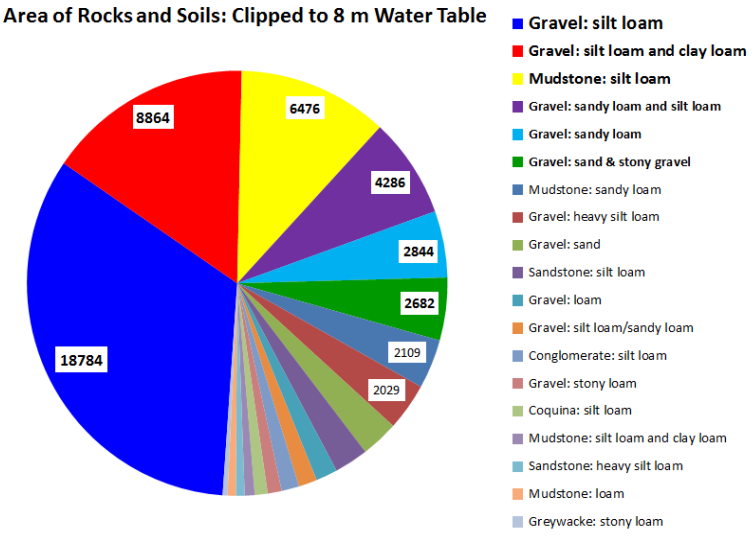

Figure 38: The area for each combination of main-rock and soil-type after being clipped to the extent of the water table < 8 m bgl (Labels indicate area in hectares). Although mudstone is the most prevalent lithology in the study area, gravels supersede this when aquifer extents and areas accessible to the direct-push/peristaltic pump system are considered (Data derived from Heron, 2014; Landcare Research, 2010b).

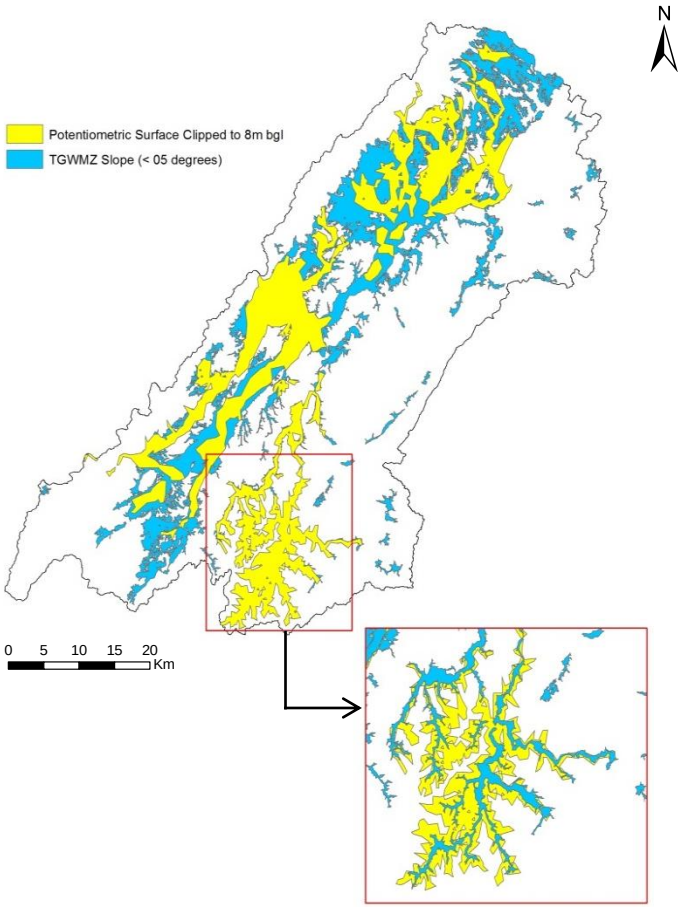

Figure 39: Comparison of slope and clipped potentiometric surface. The slope less than 5 degrees (blue) overlaid with the water table clipped to 8 m bgl (yellow). The 8 m bgl surface (yellow) was used in the following site selection process. Inset shows greater detail in the mudstone country, due to limited groundwater reserves in this lithology, the potentiometric surface is likely unreliable in these areas (Map generated in ArcGIS 10.2 using shapefiles and data derived from Landcare Research, 2010d; Rawlinson & Begg, 2014).

The number of shallow groundwater sites to be sampled per class of rock type and soil type were selected in proportion to the land area each class occupied in the Tararua GWMZ, i.e. larger the area, the more the sites selected. Multivariate statistical analyses such as ANNOVA require a minimum of three samples per sample category therefore each combination of rock and soil was planned to be sampled at least 3 times (Table 4). For example, for the gravel + silt loam class, 30 shallow groundwater samples were

required (i.e. 10 groups of 3 samples to be collected). To further determine the influence of rocks on the redox characteristics of shallow groundwater in the areas identified as gravel+ silt loam, the gravel + silt loam class was further subdivided according to the area occupied by the various sub- rock classes. Once the main rock + soil + subrock classes were determined, a simple unique identifier code was assigned to each site (Figure 40).

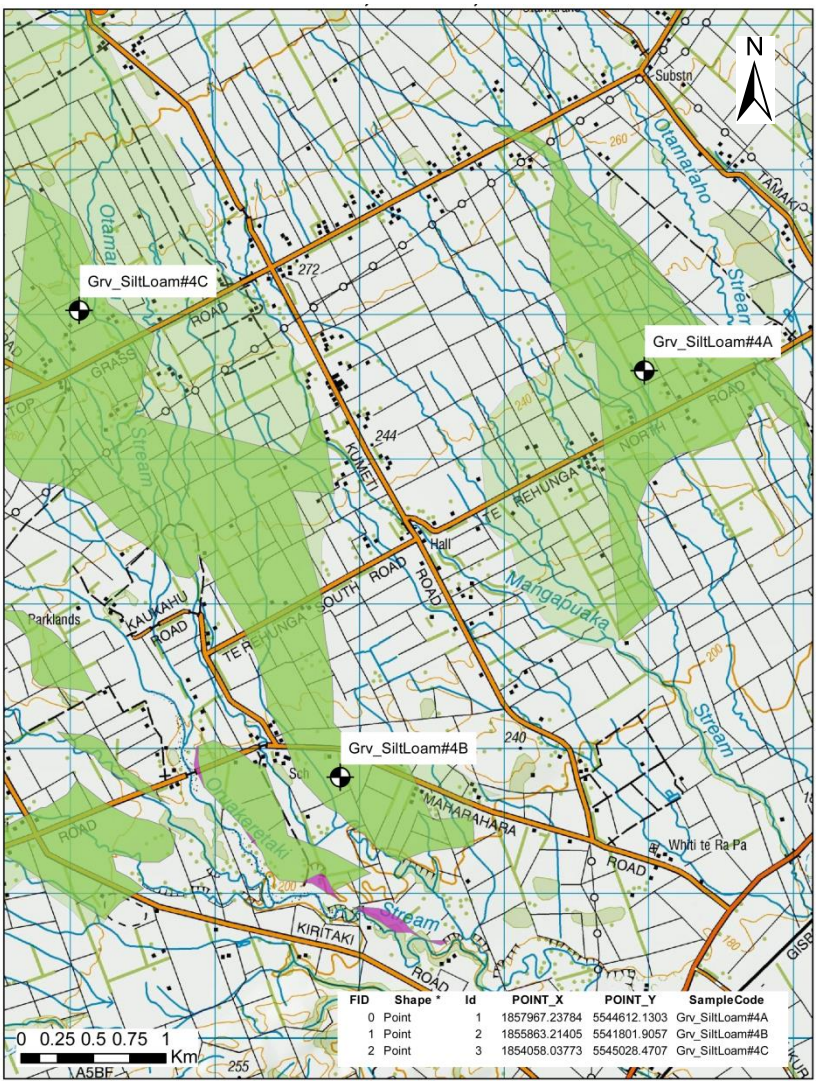

Figure 40: Typical site selection map. Site locations were selected according to the protocol described above. In this map the darker green polygons define Gravel + Silt Loam sites where the water table was inferred to lie < 8 m bgl; the lighter green surface is where the water table was inferred to lie < 10 m bgl (Map generated in ArcGIS 10.2 using shapefiles and data derived from Heron, 2014; Land Information New Zealand, 2011d; Rawlinson & Begg, 2014).

Table 4: Site selection classes for direct-push and existing well datasets used in this study.

Area Ranking	Rock Type	Soil Type	Wells Sampled	Direct-push Sampled	Wells + Direct-Push
1	Gravel	Silt Loam	19	16	35
2	Gravel	Silt Loam and Clay Loam	13	9	22
3	Mudstone	Silt Loam	-	1	1
4	Gravel	Sandy Loam and Silt Loam	9	2	11
5	Gravel	Sandy Loam	-	5	5
6	Gravel	Sand and Stony Gravel	2	3	5
7	Mudstone	Sandy Loam	-	-	-
8	Gravel	Heavy Silt Loam	2	1	3
9	Gravel	Sand	3	-	3
10	Sandstone	Silt Loam	3	-	3
11	Gravel	Loam	-	3	3
12	Gravel	Silt Loam, Sandy Loam	1	2	3
13	Conglomerate	Silt Loam	-	-	-
14	Gravel	Stony Loam	3	-	3
15	Coquina	Silt Loam	1	-	1
16	Mudstone	Silt Loam And Clay Loam	-	-	-
17	Sandstone	Heavy Silt Loam	-	-	-
18	Mudstone	Loam	-	-	-
n/a	Greywacke	Stony Loam	-	1	1
Total			**56**	**43**	**99**

Once the number of sites was determined, a suitable location for each site was identified by:

- Overlaying the relevant rock-soil-subrocks polygon over New Zealand imagery and New Zealand Topographic basemaps (ArcGIS *add data>add basemap*).
    - Local roads and access routes, landmarks, topography, waterways, ponds and potential groundwater areas were identified from various GIS layers.
    - Exporting the polygons as KML files, and importing them into Google Earth allowed 3D assessment of the factors describe above.

As each potential location was determined, a point was generated in ArcGIS v10.2 and saved with the appropriate SiteID and rock-soil-subrock class in the attribute table. When the optimal site locations were determined, Google Maps was used in tandem with the shape (point) files, Linz street address and property title boundaries shapefiles to establish the address and likely property owners to approach for access. The shapefiles were then combined into a single file and overlaid on the topographic basemap; clusters of sites were identified and the most efficient route to visit a series of sites and request access was established.

To ensure consistency in selecting sites, the following criteria were applied:

- Sites were located in the centre of polygons where possible.
- The largest polygons were preferred, and only if access or topography appeared challenging, smaller polygons were utilised.
- Sites were generally selected away from the existing wells that Rivas et al. (2017) had previously tested.
    - However, occasionally located sites were selected adjacent to them. particularly if oxic and anoxic wells were located close together, or if suboxic conditions were encountered.
- Sites were easily identified in the field by local landmarks such as shelter or fence lines, distinctive trees or buildings, road shape etc.
- In steeper topography sites were located on the flat, downhill margins of polygon to maximise the opportunity of successfully collecting a groundwater sample.

Maps of each set of sites were overlaid with topographic and aerial imagery basemaps that allowed the landowners to quickly identify their property and the proposed site location (Figure 41D; caption on following page). Landowners were then able to give their observations on field conditions, access to the site and Occupational Safety and

Health (OSH) requirements and safety concerns. Initially maps were printed with a resolution of 400 dpi, however, it was more convenient to present the maps to the farmers on a Microsoft Surface-Pro tablet which allowed panning-about, and zooming-in to features located in their property.

Figure 41: Locations of the sites were based on A) Topographic maps in ArcGIS; suitable polygons were able to be viewed and topography studied, geological and soil maps were easily referred to, and sites with potential identified. B) KML files (points and polygons) exported to Google Earth allowed 3D visualisation of surficial features for the proposed areas. C) Google Maps: street view was used to locate suitable access points, entrance ways, farm tracks and landmarks for ease and safety of access during sampling. D) Map used to discuss site with landowner showing: aerial basemap overlain with roads and road names (dashed red lines, black text over white labels), houses and road numbers (Red pentagon, red text over black labels), bore locations and depth to water table (cyan points, cyan text over black label), site location and unique identifier (black on white circle, black text on white label).

5.4 Direct-Push Shallow Groundwater Sampling Methodology

The portability and flexibility offered by direct-push technology to sample shallow groundwater at discrete locations not constrained by existing wells was of prime importance in this study. Direct-push involves using percussion hammer to drive a series of drill rods and a sacrificial tip into the substrate displacing sediments as they go. Tailings are not generated as with conventional drilling operations. When the desired depth is reached, the hammer is removed allowing a rigid pump-line and screen to be inserted. The rods are then lifted with a hydraulic jack and collect system, and the sacrificial tip is pushed out with the pump-line. The screen can be deployed at any desired depth and pumping can then proceed.

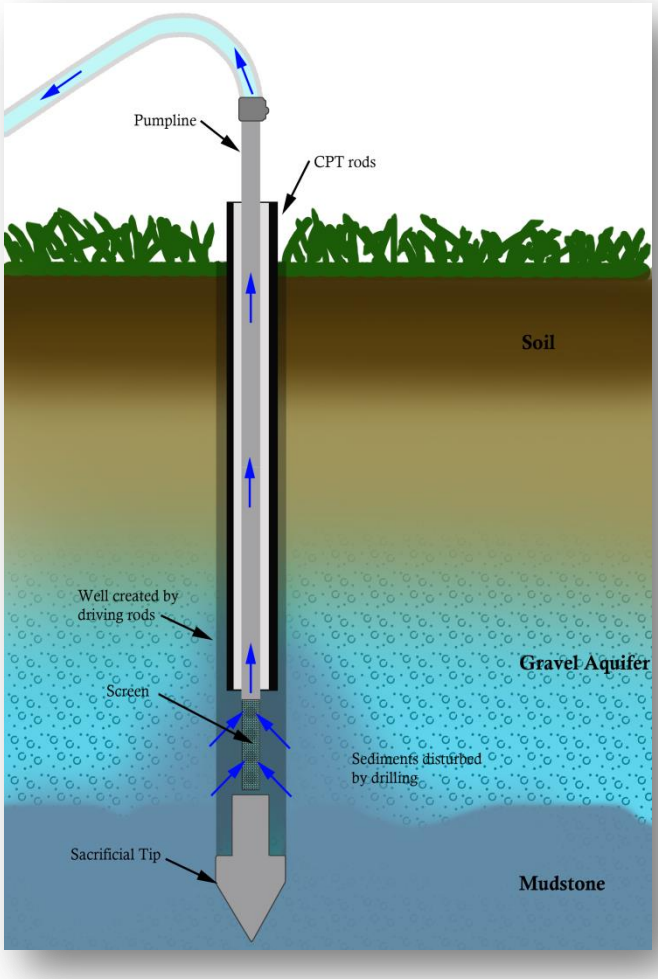

Figure 42: Schematic diagram of the direct-push system deployed in typical conditions found in gravel aquifers of the Tararua GWMZ not to scale). The 36 mm diameter sacrificial tip creates a hole slightly larger than the 32mm CPT rods. Once desired depth is reached the CPT rods are lifted and using the pump-line the tip is driven out hereby exposing the screen in the aquifer.

An Atlas Copco percussion hammer powered by a LP 9-20 P-F Hydraulic Power Pack was used to drive the drill rods. The LP 9-20 P-F also powered a collect-chuck type hydraulic lifter to raise or withdraw the rod string. Two separate rod types were utilised; 32 mm diameter (Ø) solid steel rods connected via 16 mm Ø solid threaded bar (referred hereafter to as spike rods), and 32 mm Ø hollow Cone Penetrometer Testing (CPT) drill rods connected via tapered threads. The CPT rods were kindly provided for the duration of the project by Perry Geotech Ltd., Tauranga. The drill rods were connected to the percussion-hammer bit via custom engineered fittings. A range of sampling head configurations were developed and tested, and a sacrificial tip system was selected as the most robust, practical, and economic.

Other researchers (Butler, Healey, McCall, Garnett, & Loheide, 2002; Hofmann, Darsow, Gröning, Aggarwal, & Suckow, 2010; McBeth et al., 2015; Schulmeister et al., 2003; Schulmeister, Healey, Butler, & McCall, 2004) had successfully employed direct-push to collect groundwater samples in a range of sands, tephras and other unconsolidated materials. We engineered a sampling head similar to the commercially available ones, but in the thick and often imbricated and moderately indurated gravel facies of the Tararua GWMZ, it was not robust enough to withstand repeated deployments.

The sacrificial tips deployed with the CPT rods were Computer Numerical Control (CNC) machined from 36 mm mild steel bar by Gordon Production Machining Ltd, Palmerston North. These tips performed relatively well but penetration may have been enhanced with a more elongate profile. The outer diameter of the tips were designed slightly larger than the spike rod (Figure 43) so the walls of the hole would hold the sacrificial tip in place and not allow it to drop down the hole if the CPT rods were driven down the (32 mm Ø) spiked hole. A wrap of insulation tape on the tip stem prior to inserting it into the hollow CPT rod served as further insurance that the tip would be remain in-situ during driving.

Figure 43: Left: CPT Rod, sampling head and sacrificial tip with dimensions. Right: Hydraulic lifter assembly, Green collet chuck clamps on the rods when jack (orange) is raised. Timber blocks stop the assembly from being forced into the ground when raising the drill rods in soft conditions.

A 12 mm Ø, 300 mm long, perforated stainless steel sampling head with a fine stainless steel mesh screen allowed sampling in a wide range of conditions encountered in the Tararua GWMZ. The sampling head was screwed to a string of hollow, 1 m long, 10 mm Ø stainless steel tubes (connected as required) by threaded stainless-steel hollow nipples; this assembly is hereafter referred to as the pump-line. The pump-line was inserted down the hollow CPT rods length by length until they contacted the sacrificial tip, the CPT rods were then raised (from 100 mm to several metres depending on conditions) while the pump-line was held in place to drive out the sacrificial tip. The pump-line then served as a tube through which to abstract the groundwater.

A Solinst 410 peristaltic pump was connected to the pump-line via 10 mm plastic tube and a smarTROLL multi parameter low flow cell installed downstream of the pump. Due to uncertainty of the volume of groundwater available, the abstracted water was directly collected into 2 x 2 L bottles which were filled alternately and emptied only

when the other bottle was completely filled (referred to as the 2-contaner system). The use of two containers ensured that should pumping fail at any point, as much water as possible was available for analysis. The bottles were housed in a bucket which collected any overflow and avoided creating a muddy work area (Figure 44a). Peristaltic pumps are theoretically are able to lift a column of water in a pump-line to 10.3 m, however, in field conditions it is unlikely a perfect vacuum can be generated.

Figure 44: Left: Pump setup. Peristaltic pump (A), smarTROLL low flow cell (B) and container unit (C). Red arrows indicate flow direction. The bucket collected overflow ensuring a clean, mud free work area. The 2 litre containers were filled alternately and reduced the risk of well failure resulting in no samples collected. Right: SmarTROLL low flow cell; essential for pumping at low rates in less permeable facies.

Pumping where the water table was around 8.5 to 9 m below ground level was the practical limit of our apparatus. To overcome this limitation, a foot valve may be installed at the base of the pump-line. Using this approach McBeth et al. (2015) were able to sample groundwater to depths up to 30 m. Although simply engineered, the

need to develop a foot valve for our system was not required as the water table in the designated sample areas is shallower than 9 m in most instances.

A smarTROLL Multi Parameter handheld instrument installed inline via the proprietary low-flow cell was used to analyse and record a range of water parameters and indicate when the sample was sufficiently stable to collect for lab analysis. Following sampling, water table depths were measured with a Solinst 102mi Water Level Meter, and the bore location and elevation determined by a Trimble R8 GPS. Post Processing Kinematic (PPK) mode was used to acquire accurate elevations and locations without the need to setup the Trimble Base Station over a Geodectic Mark. Once collected, groundwater samples were immediately placed on ice in an insulated cooler.

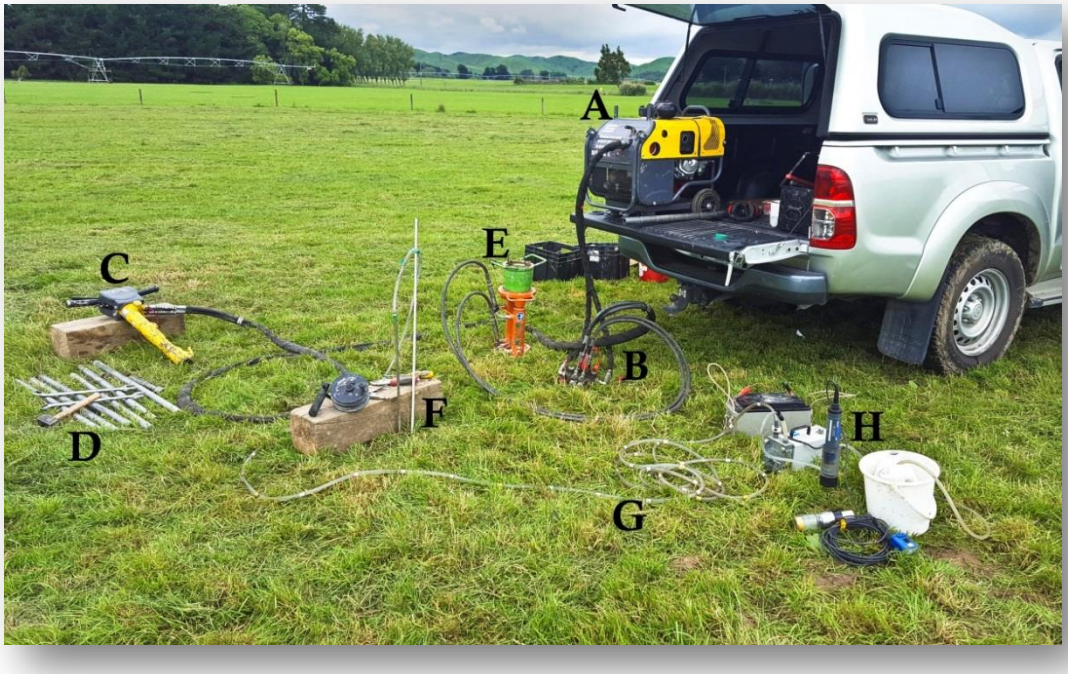

Figure 45: Direct-push setup. (A) hydraulic powerpack, (B) hydraulic control valves, (C) percussion hammer, (D) drill rods, (E) hydraulic lifter and collect clamp, (F) stainless-steel pump-line and well head, (G) plastic delivery tube, (H) peristaltic pump, smarTROLL sonde and low flow cell, and collection station.

5.4.1 Practical Observations of Direct-Push Groundwater Sampling

The hollow 32 mm Ø CPT drill rods and sacrificial tip were used exclusively at the start of the project. With experience, it became apparent that compared to the solid rods, they were slower and less effective at penetrating through the gravels. For example at site 50.8 (Bluff Road, Pahiatua) road cuttings and riverbanks show the soil/ alluvium is approx. 1m deep, and underlain by alluvial gravels, then mudstone. A hole was began with the CPT rods + sacrificial tip; during driving the CPT rods rapidly slowed until drilling was completely stopped at 5 m. The hole was abandoned and another started less than 1 m away. When driving the spike rods, a hard layer was struck at 6 m, but we were able to punch through it. Driving was stopped at 7 m as it was believed (due to operator experience and local observations of stream banks and road cuttings) the gravels had been penetrated and we were into underlying mudstone (Figure 46). The difference between CPT and spike rods is interpreted to be due to a less efficient tip design/profile than the spike rods, loss of energy due to increased vibration experienced when using these rods, or a combination of these factors.

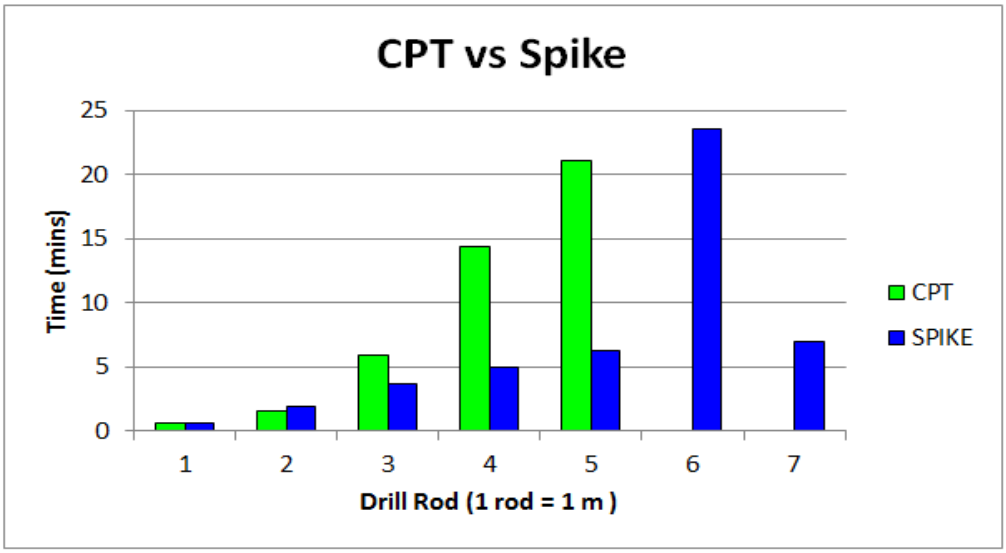

Figure 46: Comparison between drill rods. The two holes were located less than 1 m apart. Soil plus alluvium were approx. 1 m deep; underlain by alluvial gravels; then mudstone (*continued on following page).*

Figure 46 *continued*: The CPT rods rapidly slowed until drilling was completely stopped at 5 m. Spike rods struck a hard layer at 6 m but were able to punch through it. Drilling was stopped at 7 m as it was believed the gravels had been penetrated and we were into underlying mudstone.

Some failures were experienced with the CPT rods when they sheared off and sections of the rod string were lost down the holes during field operation. This was believed to be due to the rods extremely hard steel not being able to withstand the sustained percussion and vibration generated by the hydraulic hammer (T. Perry, personal communication, November 12, 2016). The stress on the CPT rods was alleviated to some degree by spiking with the solid rods prior to driving the CPT rods for shallow groundwater sampling.

Unlike drilling where the tailings give an indication of the type, nature, and thickness of units being drilled, with direct-push subtle changes to the rate of descent and feel of the hammer are the only indicator of the conditions being penetrated. Operator "feel" was developed with time and it was eventually possible to broadly discern whether alluvium, gravels or mudstone were encountered. In a moderately homogenous substrate, it was normal for the hammer to rotate slowly in a clockwise direction. In very soft colluvium, particularly when using the sacrificial tip and CPT rods the hammer would rotate clockwise a lot faster. If the operator could feel anticlockwise rotation of the hammer it was generally when the spike rod tip was becoming bound in mudstone. Gravels were often indicated by erratic downward progress. At times the rate of penetration would fluctuate significantly and it was impossible to identify whether matrix supported gravels or alternating hard and softer mudstone layers were the cause. When striking something hard, it was necessary to measure the rate of downward movement to decide whether to proceed or not. It was difficult to determine whether progress was halted due to a large gravel clast that might eventually fracture, or whether it was a layer unable to be penetrated such as well-indurated mudstone or sandstone. As a rule of thumb, drilling was generally suspended if it took over 18 minutes to drive one metre.

Figure 47: Beginning a well with the direct-push method (left). At times it was necessary to add more mass to the hammer to break through a difficult layer. When progress was arrested, it was difficult to determine whether a large gravel clast was the cause or well indurated mudstone as illustrated in the right hand image (Manawatu River, Kumeroa 40°20'34.5"S 175°58'59.9"E).

After spiking to the desired depth and having withdrawn the rods, the presence of water (if any) was determined with a Solinst water level meter. In many instances the pump-line was able to be inserted directly down the hole made by the spike rods. However, in gravels as the spike rods were withdrawn the hole would often collapse at the water table level, necessitating the CPT rods to be driven as a casing for the pump-line. If the CPT rods were used, the presence of water was quickly determined by felt resistance when blowing down the pump-line. The water table depth was measured after the pump-line was withdrawn.

This system was portable, robust and generally able to penetrate to over 8 m deep in a variety of substrate in around 30 to 40 minutes. Samples were obtained from a diverse range of locations including several from the mudstone country around Alfredton, where groundwater was generally considered limited.

5.5 Groundwater Sampling

Unlike conventional drilling, sludge that accumulated at the bottom of the hole during direct-push would not be removed and this generally created problems when pumping was initiated. Clogging of the screen by fine sediments (Figure 48) was often alleviated by driving the rods a metre or two below the contact between mudstone and the gravels, thereby creating a small reservoir below the screen for the sludge to accumulate. With experience it was then possible to locate the screen above the worst of the sludge. At times, agitation of the pump-line during the start of pumping would be necessary to clear the screen. McBeth et al. (2015) would introduce water down the hole to dilute the sludge and allow it to be pumped out. However, with experience we found this wasn't necessary, and preferred not to contaminate the system with any foreign water.

Figure 48: Clogged screen. Careful management of screen depth was required to avoid clogging by fine suspended sediments.

In some cases the hydraulic conductivity and/or intrinsic permeability was so low that pumping, even at low rates, exceeded recharge in the well. This was sometimes overcome by taping the screen (with insulation tape) to reduce its effective length. This reduced the pump rate and often allowed recharge to match the pump rate. Generally if the flow into the well was exceeded by pumping at the lowest rate with a taped screen, it was not worth persevering with. A well was left overnight in such conditions and although water did flow into it, insufficient had accumulated to collect for a sample. Furthermore as the water had been sitting in the well for a period of time, purging was required (Daughney, 2006) but unfeasible.

5.5.1 Sampling Procedure

National groundwater sampling protocols determined by Daughney (2006) state that at least three times the volume of standing water should be pumped from a well prior to sampling. In situations where wells were actively used and large volumes of water were regularly abstracted, sampling without purging was considered by Daughney et al. (2007) to be acceptable. As the direct-push rods penetrate directly into the aquifer and standing water is not encountered, chemical stabilisation (according to criteria presented in Table 5) of the groundwater was generally fairly rapid, it was deemed appropriate for direct-push abstraction also forgo purging prior to sampling.

The initial appearance of the groundwater generally ranged from turbid to extremely turbid and varied in colour depending on the type of rocks drilled into (Figure 49). The rate at which the groundwater cleared (if at all) depended on the amount of fine sediments present in the aquifer matrix, the hydraulic conductivity and the volume of groundwater present. Wells driven into productive gravel aquifers often cleared with five to eight minutes of pumping, however, wells installed in areas dominated by a larger fraction of silt or mudstone sometimes exhibited little improvement.

Consequently, the turbidity of the sample could vary from relatively clear to very turbid despite being assessed chemically stable.

Figure 49: A range of different coloured water collected soon after pumping initiated. The appearance of the groundwater indicated of the nature of substrate the well was drilled into. Generally the water had cleared by the time physical parameters had stabilised enough for sampling to proceed.

If the stabilised groundwater was relatively clear, sterile 50 ml Terumo syringes equipped with 0.45 µm Superpure NY filters were used in the field to filter the groundwater into labelled, sterile 60 ml screw cap PET containers prior to storage and transport in a chilly-bin with icepacks. Relatively turbid samples were collected into labelled, sterile 2 litre screw top containers, placed on ice, and transported to the laboratory where they were filtered that day with a vacuum flask system using 0.45 µm membrane filters and stored in labelled 60 ml screw cap PET containers. In extreme cases, the very turbid samples were centrifuged for 8 minutes @ 5400 rpm to remove the larger particulate matter, and filtered using the vacuum flask system prior to storage in labelled 60 ml screw cap PET containers.

The filtered samples intended for analysis of metals such as Fe and Mn were stabilised with nitric acid to pH < 3.0 prior to storage in a chiller. Samples intended to be analysed for alkalinity were unfiltered and analysed within 24 hours of collection. The rest of the filtered samples were frozen so that all the samples could be sent concurrently to the laboratory for chemical analysis.

Table 5: Parameters automatically recorded by smarTROLL MP instrument. Key parameters for assessment of chemical stability of groundwater during pumping are in bold text.

Parameter	Units	Stability Criteria
Temp	**°C**	**± 0.2**
Dissolved oxygen	**mg L^{-1}**	**± 0.3**
Specific conductivity	**µS cm^{-1}**	**± 3%**
		± 5% if SPC<100
pH	**pH**	**± 1.0**
ORP	mV	
Dissolved oxygen saturation	%	
Salinity	psu	
Total dissolved solids	ppt	
Barometric pressure	mbar	
Actual conductivity	µS cm^{-1}	
Depth	m	
Air temp	°C	
Line pressure	psi	

*Temperature was rejected as a stability criterion due to sunlight often heating water in the 10 mm clear plastic tube connecting the pump-line and the pump.

**Parameters were recorded automatically at 10 second intervals with the smarTROLL; however, such frequent recordings belied the assessment of stability. Rather, once a reasonable degree of stability was attained, key characteristics were recorded every 3 minutes.

Temp = Temperature; ORP = oxidation-reduction potential

mV = milli Volt psu = Practical Salinity Unit

ppt = parts per million µS cm^{-1} = micro Siemens per centimetre

psi = pounds per square inch

5.6 Laboratory Analysis of Groundwater

The levels of cations, anions, elements and nutrients were determined by a variety of methods. The oxidation-reduction potential (ORP) values measured with the smarTROLL (silver/silver chloride reference electrode) required conversion to *Eh* (standard hydrogen electrode) by adding 200 mV to the readings (Rice et al., 2012).

Acid titration using Massey University's TitraLab 865 instrument determined the pH, and titrant volume, from which total alkalinity milliequivalents per litre (meq L^{-1}), total alkalinity as mg $CaCO_3$, and Bicarbonate (HCO_3^- mg L^{-1}) were calculated. All other cations, anions, nutrients, and elements (Table 6) were analysed by Eurofins Limited, Wellington. The sampling methodology and detection limits are presented in Appendix C: Groundwater Quality Analysis Methods and their Detection Limits.

Table 6: Cations, anions, nutrients and metals and others analysed by Eurofins Limited, Wellington.

Cation	Anion	Nutrient	Metal	Other
K^+	Br^-	NO_2^- -N	Fe^{2+}	DOC
Ca^{2+}	Cl^-	NO_3^- -N	Mn^{2+}	DIC
Mg^{2+}	F^-	NH_4^+ -N	Br^-	IN
Na^+		SO_4^{2-}	As^{3+}	pH
SiO_2		TON		
		TDP		
		DRP		

As^{3+} = dissolved arsenic (mg L^{-1})
Br^- = dissolved bromide (mg L^{-1})
Ca^{2+} = dissolved calcium(mg L^{-1})
Cl^- = dissolved chloride (mg L^{-1})
DIC = dissolved inorganic carbon (mg L^{-1})
DOC = dissolved organic carbon (mg L^{-1})
DRP = dissolved reactive phosphorus (mg L^{-1})
Fe^{2+} = dissolved iron (mg L^{-1})
IN = inorganic nitrogen (mg L^{-1})
K^+ = dissolved potassium (mg L^{-1})
Mg^{2+} = dissolved magnesium(mg L^{-1})
Mn^{2+} = dissolved manganese (mg L^{-1})
Na^+ = dissolved sodium(mg L^{-1})
NH_4^+ -N = ammoniacal nitrogen (mg L^{-1})
NO_2^- -N = nitrite nitrogen (mg L^{-1})
NO_3^- -N = nitrate nitrogen (mg L^{-1})
SiO_2 = dissolved silica (mg L^{-1})
SO_4^{2-} = sulphate (mg L^{-1})
TDP = total dissolved phosphorus(mg L^{-1})
TON = total oxidised nitrogen (mg L^{-1})

5.7 Data Processing and Analysis Methods

Although 45 samples were recovered by the direct-push system and submitted for laboratory analysis, only 43 were considered for statistical analysis as two sites were sampled twice. Site 31.1 was sampled twice to distinguish if the groundwater chemistry changed greatly during pumping; and site 50.2, an unusual shallow unconfined aquifer in mudstone country was sampled twice for indications of chemical stratification. This

analysis showed little change in groundwater chemistry once the parameters recorded with the smarTROLL had stabilised and that little stratification was evident.

An opportunity to increase the spatial resolution of the study was taken by supplementing the dataset with a further 56 samples collected from conventional wells in the Tararua GWMZ by Massey University PhD student Aldrin Rivas (Rivas et al., 2017). Therefore, the data analysis was based on 99 samples comprised of 43 samples (+ 2 duplicates) collected by the direct-push and 56 samples from existing wells; the summary statistics are presented for both datasets individually and also collectively. Some analytes tested in the direct-push samples were not tested in the Rivas's dataset, for example fluoride, dissolved reactive phosphorus and arsenic, hence the missing summaries for these parameters in the existing wells and the combined summary statistics.

5.7.1 Censored Values

Censored values in groundwater analysis are those missing values or those that fall outside the detection limits for the particular analytical method; such variables are considered ineligible for multivariate statistical analysis (Güler, Thyne, McCray, & Turner, 2002). Farnham, Singh, Stetzenbach, and Johannesson (2002) and Güler et al. (2002) report techniques to replace censored values that include substitution of values under the detection limit with 0.75 x the lower detection limit, and for those over the detection limit by $\frac{4}{3} \cdot the\ upper\ detection\ limit$ (VanTrump & Miesch, 1977). Sanford, Pierson, and Crovelli (1993) support the use of 0.55 times the lower detection limit and 1.7 times upper detection limit for values below and above the detection limit, respectively. If the frequency of censored values exceed 10% of the sample number, Sanford et al. (1993) suggest calculating the mean of the normal distribution with a maximum likelihood estimation method, and deriving a replacement value from this

estimated mean. However, censored values in Rivas's (supplementary) data had already been treated by substituting $\frac{1}{\sqrt{2}} \cdot (the\ detection\ limit)$ (Helsel, 2009) and for consistency this method was adopted in the direct-push dataset. When examined, the direct-push dataset revealed missing fluoride values for sites 2.1, 8.3, 50.6, and 50.9, and several analytes had a number of values under the detection limit (Table 7). These values were all treated similarly by substituting $\frac{1}{\sqrt{2}} \cdot (the\ detection\ limit)$.

Table 7: Groundwater analysis values under the detection limit. (Combined datasets, n = 99)

Characteristic	Detection Limit (mg	Count under	% under DL (%)
NO_3^- -N	0.002	24	52.17
NH_4^+ -N	0.01	3	6.52
TDP	0.005	14	30.43
DRP	0.005	24	52.17
As	0.001	29	63.04

DL = Detection limit, NO_3^- -N = nitrate nitrogen, NH_4^+ -N = ammoniacal nitrogen, TRP = total reactive phosphorus, DRP = dissolved reactive phosphorus, As = arsenic. n = 99.

5.7.2 Charge Balance Error

Systematic errors in water analysis do occur (Fritz, 1994), therefore the validity of the lab analysis was assessed by calculating the percentage charge balance error (CBE) for each of the samples (Equation 9).

% Charge Balance Error

(Güler et al., 2002, p. 460)

$$\frac{\sum z \cdot m_c - \sum z \cdot m_a}{\sum z \cdot m_c + \sum z \cdot m_a} \cdot 100 \qquad \text{Equation 9}$$

where:

z = absolute value of the ionic valence

m_c = molarity of the cationic species

m_a = molarity of the anionic species.

The percentage charge balance error is an accepted method of evaluating the reliability of water analysis, where the net ionic charge of groundwater should be close to zero (Freeze & Cherry, 1979). Researchers accept varying tolerances depending on the nature of the study and aquifer conditions. Freeze and Cherry (1979) consider less than 5% deviation of the CBE from zero is acceptable. Fritz (1994) noted the average CBE from over 1000 published datasets was up to ± 9.34%, and around 60% of the CBE's were negative. Fritz (1994) and also Güler et al. (2002) assert the CBE of samples with low ionic concentrations often exceed 10%, and Tidswell, Conwell, and Milne (2012) concurred suggesting that in local conditions, a CBE of up to ± 15% in groundwater analysis is acceptable.

5.7.3 Data Screening, Transformation, and Standardization

An assumption of many of the anticipated statistical analyses is the data must display a normal distribution. In both the direct-push and existing well datasets (Rivas et al., 2017), a general trend of positive skewness and kurtosis was evident upon examination of histograms and normal Q-Q plots and therefore required transformation to the normal distribution; two examples are presented in Figure 50.

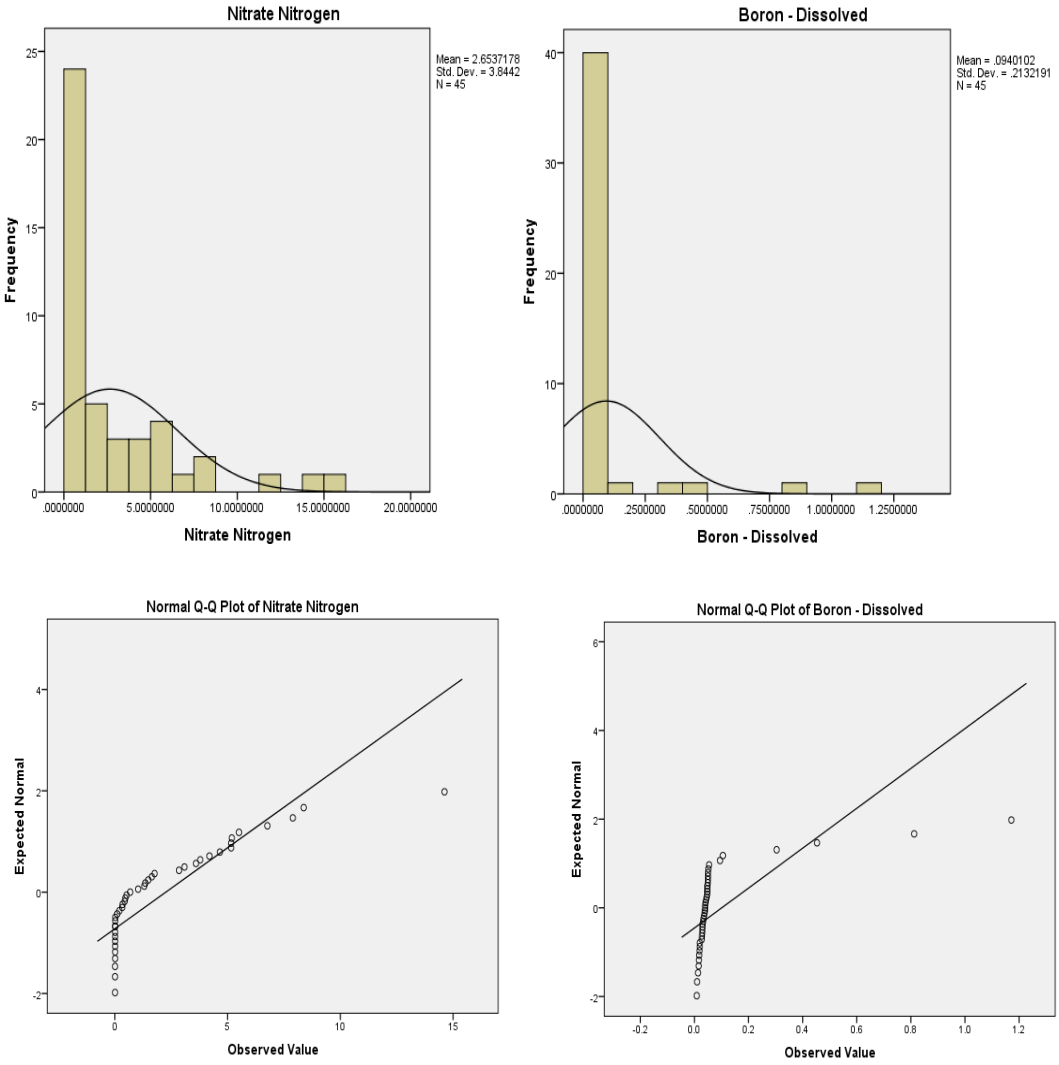

Figure 50: Histograms of nitrate-nitrogen (previous page left) and boron (previous page right) are typical for the data and indicate positive skewness (a lack of symmetry with trend to the right). The Normal Q-Q plots (bottom left and right) indicate positive kurtosis i.e. "r" shaped distribution in the Q-Q plot, which equates to a narrow peak on the histogram when compared to the normal distribution.

The data were also assessed for normality by evaluating the skewness and kurtosis Z value where

$$z(Skewness) = \frac{Skewness}{Standard\ error\ (Skewness)}\ and\ z(Kurtosis) = \frac{Kurtosis}{Std.Error(Kurtosis)}$$

At the statistical significance level of 0.01, a normal distribution equates to a z value of 0 ±2.58. Most of the data tended to violate the assumption of normality; confirmed by the

Shapiro-Wilk and Kolmogorov-Smirnov tests of normality where z > |2.58| (the absolute value of 2.58). The data was transformed using both a square root transformation commonly used for moderately skewed data, and a logarithmic transformation commonly applied to strongly positively skewed data (Figure 51). Results appeared inconsistent (Figure 51) when compared with the two-step approach endorsed by Templeton (2011). The two step approach involves using IBM SPSS or Microsoft Excel to transform the variable into a percentile rank, prior to applying an Inverse Distribution Function (*IDF.normal*) transformation to the ranked cases. This method creates a dataset of normally distributed z-scores (Templeton, 2011) and generally assimilates outliers. Note, it is necessary to examine the dataset following the rank-cases transformation step and replace the single value of "1" generated for each variable with the calculated value of 1-(1/n) where n= number of samples (Templeton, 2011). Following the two-step transformation procedure, normality was again assessed by the Shapiro-Wilk and Kolmogorov-Smirnov tests and the z scores were less than |2.58| which indicated a normal distribution. To confirm the validity of the two-step method, a Principal Component Analysis (PCA) with data transformed with the more conventional logarithmic and square root methods was compared to a PCA with data transformed with the two step approach and the results were statistically identical. However, for consistency, the two step approach was used exclusively in this study.

5.7.4 Outliers

Outliers, i.e. observations that lie a disproportionate distance from other values in a random sample of a population, are commonly encountered in environmental data (Gibbons, Bhaumik, & Aryal, 2009). Outliers may disproportionately influence results, and approaches to deal with them vary from ignoring them, deleting them, or assigning the variable an arbitrary value. Following transformation of the data, boxplots of the

data were examined for the presence of outliers; the two-step method used to transform the data tended to reduce the occurrence of significant outliers, consequently no further action was taken.

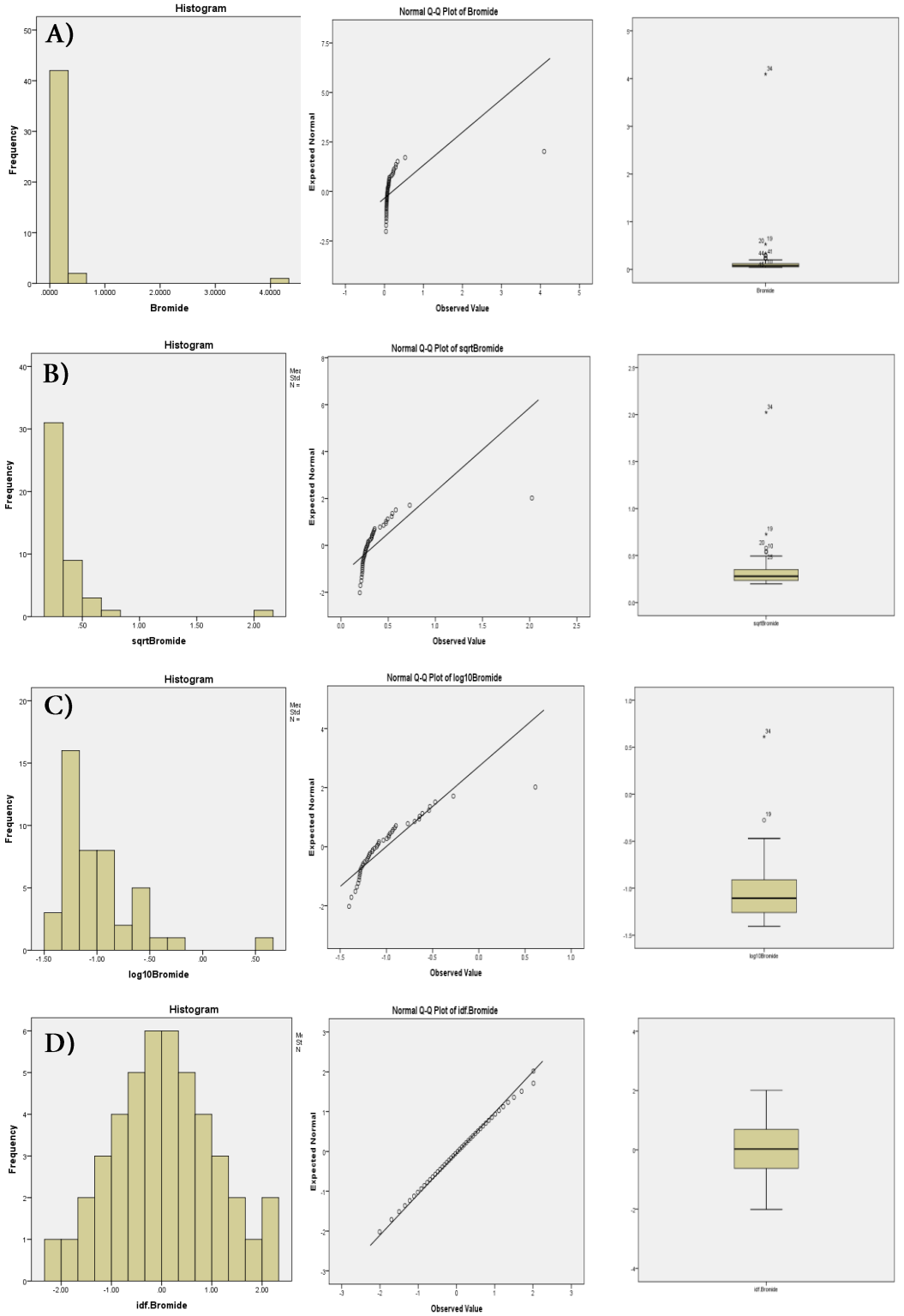

Figure 51: Comparison of transformation methods for the bromide dataset. An extreme example of skewness and kurtosis, these data well illustrate the advantages of the two step transformation compared to more traditional transformations (*continued on following page).*

Figure 51 *continued*: The raw data A) exhibits extremely strong skewness and kurtosis, with many outliers (evident in the boxplot). The square root transformation B) commonly applied to moderately positively skewed data slightly improves the distribution, kurtosis and frequency of outliers. The logarithmic transformation C) applied to strongly positively skewed data creates a closer to normal distribution but skewness and outliers are still problematic. The two-step transformation (D) transforms the data extremely well and allows inclusion of records that under the other transformations would be considered outliers and excluded from the analysis. The assumption of normality for this bromide analysis was satisfied by only the two-step method as assessed by the Shapiro-Wilk test of normality (sig. = .987, p> .05).

5.7.5 Water Type Classification

To characterise hydrogeological systems, graphical and statistical methods are regularly used to partition the chemistry of groundwater samples into homogenous groups (Güler et al., 2002). Graphical methods include Schoeller plots, Collins bar, Stiff pattern, pie, and Piper diagrams, while statistical methods include hierarchical cluster analysis (HCA), principal components analysis (PCA), K-means clustering, and fuzzy K-means clustering.

Güler et al. (2002) maintained although statistical clustering methods were most efficient (particularly for large datasets) they were unable to provide information on the chemical composition of the clusters they derived. While diagrams may identify groundwater of different sources and flowpaths, alone they are unable to objectively discriminate between groups or test the degree of similarity between the groups. Therefore, a combination of graphical and statistical methods are often used to provide consistent and objective classification of groundwater chemistry (Güler et al., 2002).

For larger datasets Güler et al. (2002) recommended HCA in conjunction with Piper plots to identify commonalities in groundwater chemistry. The water types in this study were determined with HCA in SPSS, the SiteID and cluster number were recorded in Microsoft Excel, and the mean for each analyte for each cluster calculated and analysed

for commonalities, prior to being exported into Geochemists Workbench v11.0 software to generate draw piper diagrams. Using the mean values of each cluster, a piper diagram was generated and the relevant water type for each sample was recorded in Microsoft Excel. The resulting spreadsheet was imported to ArcGIS v10.2 as a table, which was then joined to a shapefile of site locations via the SiteID field. The appended attributes table was exported as a new shapefile which allowed spatial analysis of the water type.

5.7.5.1 Piper Diagrams

The Piper diagram initially plots the percentage values of the cations Ca^{2+}, Mg^{2+}, K^{+}, Na^{+}, and the anions Cl^{-}, HCO^{-}_{3}, CO_3^{2-}, and SO_4^{2-} in separate ternary diagrams which are then projected onto a rhomb. The type of groundwater facies are identified by their relative location on the rhomboidal plot (Figure 52).

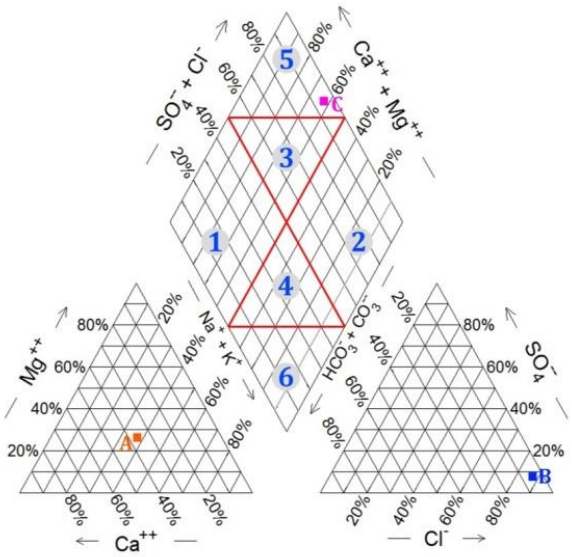

Water Type:

1 = $Ca\text{-}HCO_3$ type.

2 = Na-Cl Type.

3 = Mixed Ca-Mg-Cl type.

4 = $Na\text{-}K\text{-}HCO_3$ type.

5 = Ca-Cl type.

6 = Mixed $Na\text{-}HCO_3$ type.

Figure 52: Piper Diagram; cations are plotted on the lower left ternary diagram, anions on the right. The data is then plotted on the central rhomboid. Numbers indicate zones used to determine differing hydrochemical facies. Example for site 52.1, A) Cations = (Mg^{2+}= 25.88%, Na^{+}+K^{+}=38.56%, Ca^{2+}=35.56%); B) Anions = (SO_4^{2-}=7.39%, HCO_3^{-} + CO_3^{2-}=4.73% Cl^{-}=87.88%); C) Combined = (SO_4^{2-} +Cl^{-} = 95.27% Ca^{2+} + Mg^{2+} = 61.44%). Water = CaCl type. Classification from A. Singh and Kumar (2015, p. 100).

The actual thresholds for classification of groundwater into specific types with piper diagrams vary widely (for example Back, 1966; Cloutier, Lefebvre, Savard, Bourque, & Therrien, 2006; McPhillips, Creamer, Rahm, & Walter, 2014; Pehlivan, Emre, & Key, 2012; Sadashivaiah, Ramakrishnaiah, & Ranganna, 2008; A. Singh & Kumar, 2015). Sadashivaiah et al. (2008) suggested the modified piper diagram (Back, 1966) with domains of 0 to 10% and 90 to 100% on the central rhomboid instead of the traditional 25% increments was the most useful for their work. However, these thresholds are far from standardised and are often adapted to the researcher's specific requirements such as isolating the effects of saltwater intrusion or anthropogenic pollution. This study followed the framework of A. Singh and Kumar (2015) as presented in Figure 51 above.

5.7.7 Hierarchical Cluster Analysis

Hierarchical Cluster Analysis (HCA) is used to identify groups of (relatively) homogenous cases based on predetermined characteristics (Güler et al., 2002). Using an algorithm in SPSS, the procedure begins with each case, identifies similar cases and groups them together in a hierarchical basis, continuing until only a final cluster remains. This form of analysis has a number of similarity/dissimilarity measurements and linkage methods which produce a range of results when deriving the clusters (Güler et al., 2002). Most of the possible combinations were trialled, then evaluated with Microsoft Excel and Geochemists Workbench ver. 11.0, before concluding as did Güler et al. (2002) and Daughney and Reeves (2005), that the Squared Euclidean Distance combined with Wards Linkage method produced the most homogenous, and hydrochemically distinct clusters.. Güler et al. (2002) observes groundwater characteristics when analysed with Ward's linkage and Euclidian distance methodology generate clusters more of similar characteristics that were notably different to those in

other clusters. However, when running HCA in SPSS, a dialog is generated stating when Wards linkage is used, the Euclidian distance is invalid and the Squared Euclidian distance must be used. Raiber et al. (2012) verify the squared Euclidian distance is appropriate as a measure of similarity for variables such as Ca^{2+}, Mg^{2+}, Na^{+}, K^{+}, HCO_3^{-}, Cl^{-}, SO_4^{2-}, NO_3^{-} -N, NH_4^{+} -N, Mn^{2+}, Fe^{2+}, SPC and pH in groundwater. The analyses in this study exclusively applied Wards linkage combined with Squared Euclidian method.

The key output of this analysis is the dendrogram which allows visual interpretation of how the variables are related. A (HCA) dendrogram (Figure 53) was coloured to better illustrate the clades, leaves, and the associations of the variables. The large red clade indicates the characteristics of the right hand leaf are distinct from those on the left. For more detailed analysis the next level of clades may then be assessed i.e. the pink clade; ultimately it can be seen that clusters 9 and 10 are more closely associated than 11, 12, and 13.

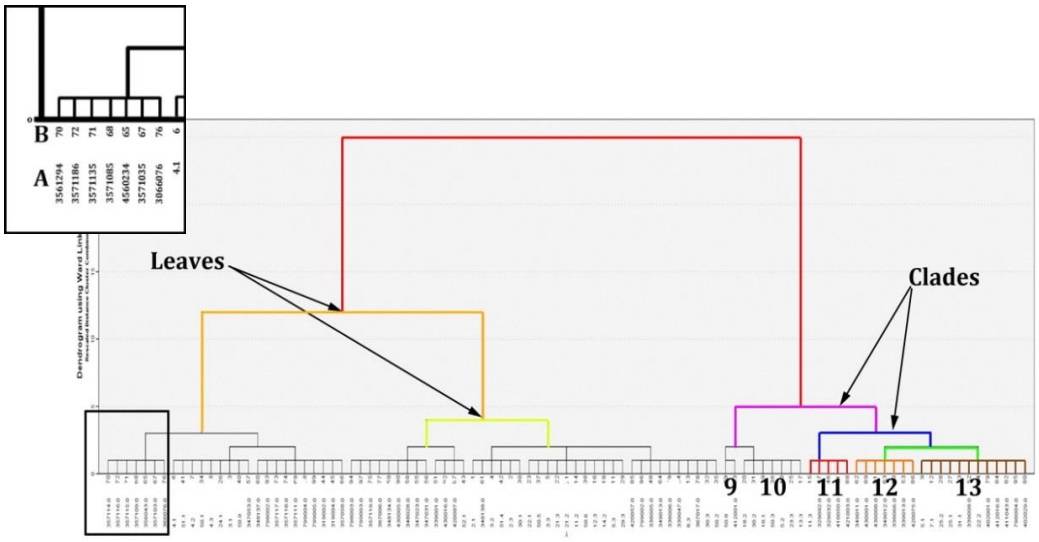

Figure 53: Components of a dendrogram. A clade links two groups together; the terminal ends of a clade are known as leaves. Each cluster is comprised of samples with similar characteristics; the clusters may then be linked by the different levels of clades to show broader associations.

5.7.8 Pearson's Product-Moment Correlation Analysis

The strength and direction of associations between water type and redox related parameters such as anions and cations, *Eh*, nutrients, and depth were analysed using Pearson's product moment correlation performed in SPSS. The transformed dataset (n = 99) satisfy the assumption (verified visually with scatterplots in SPSS) that a linear relationship exists between the pairs of variables (Figure 54). No significant outliers were observed using scatter plots and box and whisker plots in SPSS. The normal distribution was confirmed with Shapiro-Wilk and Kolmogorov-Smirnov tests in SPSS (Laerd Statistics, 2015d).

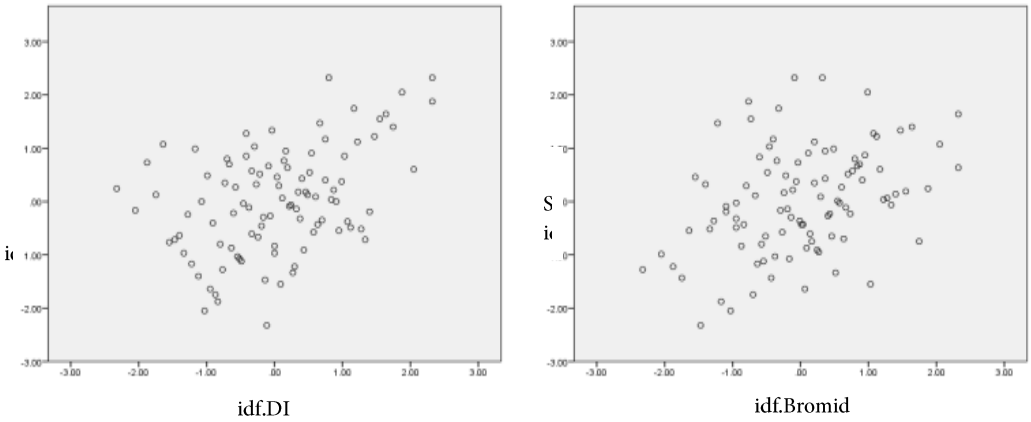

Figure 54: Scatter plots of transformed DIC and potassium (left), and bromide and silica (right). Both plots exhibit a fairly loose linear relationship that is acceptable for analysis with Pearson's Correlation.

The correlation coefficient "*r*" generated by the Pearson's analysis represents the direction and strength of a linear relationship between two samples of interest. An r value of 0 indicates no association between variables, an r value of 1 indicates a strong positive association, and an r value of -1 indicates a strong negative association. Table 8 identifies how the magnitude of the Pearson correlation coefficient may be interpreted. As an assumption of this method is the data must follow a normal distribution, the transformed data were used in this analysis.

Table 8: Explanation of the Pearson Coefficient associations (Laerd Statistics, 2015d).

Coefficient value	Nature of Association
r = -1.0	Perfect negative correlation
-0.99 < r <-0.50	Strong negative correlation
-0.49 < r < -0.30	Moderate negative correlation
0.10 < r < - 0.29	Weak negative correlation
r = 0	No correlation
0.01 < r < 0.29	Weak positive correlation
0.30 < r < 0.49	Moderate negative correlation
0.50 < r < 0.99	Strong negative correlation
r = 1	Perfect positive correlation

The analysis was performed via Bivariate Correlations from the Analyse > Correlate menu; two-tailed test of significance, missing values excluded pairwise and Pearson Correlation Coefficient where selected. Spearman's rank-order correlation coefficient (r_s) is determined and interpreted in a similar manner to Pearson's correlation coefficient but was used when ordinal and/or non-parametric factors such as main-rock or soil-type classes were analysed in conjunction with continuous variables such as anions, cations, *Eh*, nutrients, and depth .

5.7.9 Principal Component Analysis

PCA was used to reveal the dominant patterns within the groundwater's chemical and physical attributes. PCA emphasizes variation and identifies strong commonalities by identifying as few components as possible that account for the greatest variance within the original variables (Laerd Statistics, 2015e). PCA analyses of groundwater are used to

identify processes which have an effect on the water's chemistry by revealing which variables are highly correlated to a certain component (Matiatos, Alexopoulos, & Godelitsas, 2014). Although the actual process is not identified from the analysis, it may be inferred by the nature of variables loaded onto the components. For example, should the variables known to be associated with denitrification such as DO, DIC, Mn^{2+}, Fe^{2+}, SO_4^{2-} and NO_3^- be cleanly loaded on a particular component, then that component may be considered to represent denitrification processes (Rivas et al., 2017). Furthermore, scatterplots of two principal components, with symbology classified to hydrogeological characteristics such as rock type, soil texture etc. are able to depict the relationship between the components and the characteristics of interest (Rivas et al., 2017).

The approach used in this study to determine which components to retain was to consider the eigenvalue-one criteria in conjunction with a scree plot, the proportion of total variance, and the interpretability criteria (Laerd Statistics, 2015e). The interpretation of PCA output in SPSS is complex, and a detailed explanation exceeds the scope of this thesis, readers are directed to Laerd Statistics (2015e) for more information. Assumptions for this analysis to be reliable, as defined by Laerd Statistics (2015e) are multiple, continuous variables with a linear relationship existing between all variables (tested visually in SPSS by scatterplots of randomly selected cases). Sample sizes need to be large enough to ensure sampling adequacy, e.g. five to ten cases per variable is considered a minimum requirement (tested by Kaiser-Meyer-Olkin (KMO) measure of sampling adequacy in SPSS). There must be a reasonable correlation between variables (tested by Bartlett's test of sphericity within SPSS) so that they may be reduced to a smaller number of components and finally, there should be no significant outliers in the dataset (identified in SPSS as components scores more than 3 standard deviations (STDEV) from the mean).

The analysis was run in SPSS from Analyse> Dimension Reduction> Factor, and as with HCA, there are a range of methods that significantly affect the nature of the output, particularly the rotation and extraction methods; many combinations of which

were trialled and evaluated in Microsoft Excel. This study applies the Varimax rotation (options applied are presented in Figure 55) which is commonly applied in groundwater analysis (e.g. Donath, Daughney, Morgenstern, Cameron, & Toews, 2015; Garba, Ekanem, Garba, & Mustapha, 2016; Helena et al., 2000; Meraat, Jafari, & Qishlaqi, 2017; Rivas et al., 2017). The key outputs to interpret are presented in Appendix D: Statistical Analysis Tables.

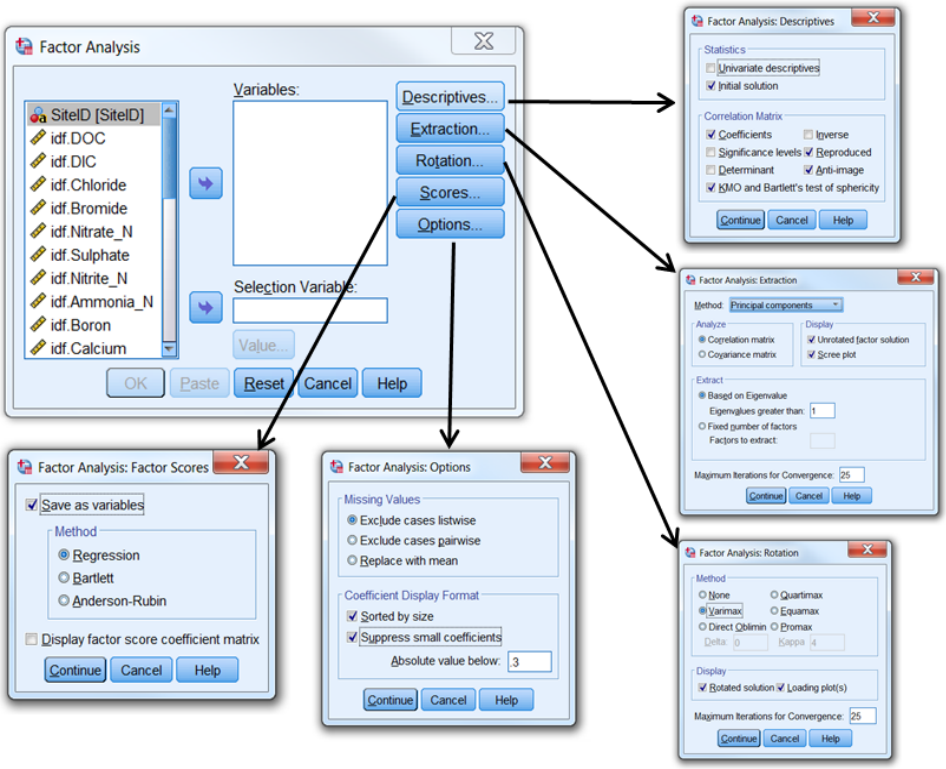

Figure 55: Parameters used in SPSS for initial Principal Component Analysis.

5.7.10 ANOVA and Independent-Samples T-Test

These parametric tests where assumptions are made of the population parameter are used to determine whether a statistically significant difference exists between sample groups (Laerd Statistics, 2015a, 2015c). The T-test is useful for comparing samples where the dependent variable is measured at the continuous level, and the independent

variable has only two factors e.g. nitrate levels vs shallow or deep wells. Analysis of variance (ANOVA) is used to analyse datasets with continuous dependent variables and more than two independent variables e.g. .g. nitrate levels vs wells of shallow, moderate or deep depths (Laerd Statistics, 2015b, 2015c). Key assumptions are normally distributed data, randomly sampled data, homogeneity of variance, independence of observations, and measurement of the dependent variable on the ratio or interval level. The process in SPSS is multifaceted and different approaches are required depending on preliminary test results. The method used in this study first tested the assumption of homogeneity of variance with Levene's test of equality of variances, where significance values (p values) greater than 0.05 indicate the assumption of heterogeneity has not been violated; the ANOVA and Tukey post hoc test may be then interpreted without further analysis (Laerd Statistics, 2015c). Should Levene's test be statistically significant, where $p < 0.05$, equal variances do not exist. In this case Welch's ANOVA (located in the robust tests of equality of means table) must be consulted; where $p < 0.05$ is statistically significant, and at least one of the groups means may be inferred to be different to one or more of the others (Laerd Statistics, 2015c). The Games-Howell post hoc test is then examined to determine where differences in group means lie. At times non parametric tests such as the Mann-Whitney U test were used in the analysis to compare differences between groups measured on a continuous scale with a ordinal variable e.g. nitrate levels from samples collected under diary pasture or sheep and beef pasture. The non-parametric tests facilitated use of non-transformed data which in turn allowed appraisal of the actual medians or means.

Chapter 6: Results and Discussion

6.1 Introduction

This chapter investigates the characteristics of groundwater recovered from a wide range of geological settings throughput the Tararua GWMZ. The suite of statistical analyses described in the previous chapter were applied to the groundwater sample's laboratory and field observations. Combining the direct-push dataset with that of Rivas et al. (2017) provided some discussion as whether they could indeed be compared in this study. Investigations were performed to verify whether statistically significant differences existed between the datasets with regard to well depth, chemical parameters and physical characteristics. Figure 56 shows the location of major catchments referred to during the analysis, the location of all sample sites are presented in Figure 57. Note: the catchment boundaries were somewhat difficult to delineate and to facilitate comparisons; boundaries were kept the same as used in Rivas et.al. (2017) and Elwan et al. (2016).

- In the following analyses, six digit site names refer to existing well samples collected by Rivas et al. (2017) from February March 2014, while three digit site names refer to direct-push samples collected in this study from October 2017 to May 2018.
- In the Results and Discussion chapter SiteID's are followed by a range of codes. The codes represent in the following order:
    - main rocks; soil texture; FSL carbon class = CC; FSL drainage class = DC; FSL pH class = pHC; and WT = water type where 1 = $CaCo_3$ type, 2 = mixed CaMgCl type and 3 = $NaHCO_3$ and 4 = NaCL. The relevant FSL classes are presented in Appendix E: FSL Class Definitions.

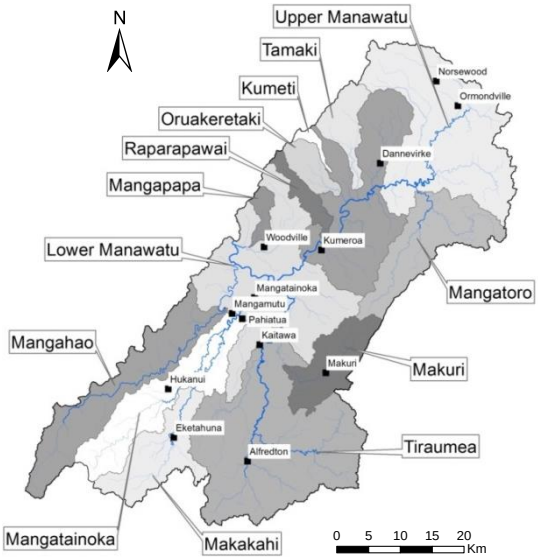

Figure 56: Location of main Tararua GWMZ catchments. It should be recognised that for the purpose of this study the smaller streams such as the Makakahi are considered separate entities, but at times may also be considered as part of larger catchments such as the Mangatainoka River. Both of which ultimately are tributaries of the Manawatu River.

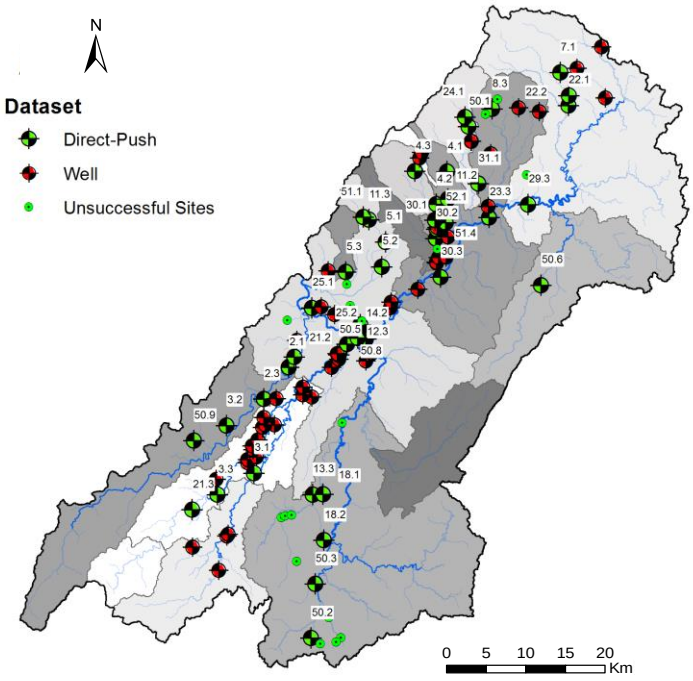

Figure 57: Groundwater sampling site locations. 43 successful direct-push sites (labelled with SiteID) are represented by the green drillhole icon, and 51 existing wells sampled by Rivas et al. (2017) are represented by pink drillhole icons. The solid black symbols indicate the sites where the direct-push method was unsuccessful in obtaining a groundwater sample at that location either due to groundwater being non-existent e.g. in many areas of the mudstone country, or where the water table was too deep to intercept to with the equipment at hand e.g. where limestone exceeded 10 m thickness. them (Map generated in ArcGIS 10.2 using shapefiles from Heron, 2014; Land Information New Zealand, 2011b).

Although the direct-push and existing well data were obtained from the Tararua GWMZ, well depths contrasted significantly between datasets (Figure 58). As the direct-push wells sampled only shallow aquifers while some existing wells sampled deeper water (or a combination of deeper and shallower water depending on local lithology and/or well construction) it was necessary to assess whether it was statistically valid to combine the direct-push dataset with the existing well dataset.

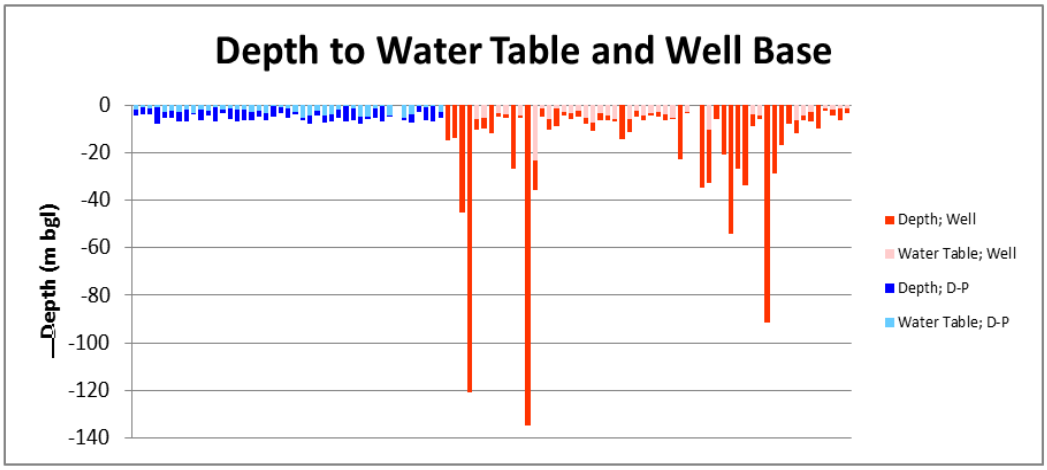

Figure 58: Depth to water table: blue series are direct-push, red are existing wells. Lighter coloured bars (for each series) illustrate the depth from ground level to the watertable. The darker coloured sections of the bars indicate the depth of the groundwater i.e. from the watertable to the bottom of the well.

Some of the existing-well data series have only dark shading. This indicates it wasn't possible to measure the water level as the well-head construction did not include a portal through which to deploy a water level meter (well depth was obtained from HRC records), (A. Rivas, personal communication, March 12, 2017). All direct-push samples were taken from less than 10 m deep, while those from existing wells were generally less than 20 m deep; 14 wells were deeper than 20 m.

6.2 Groundwater Chemistry from Existing and Direct-Push Wells of Different Depths

To determine whether a statistically significant difference existed between the means of the direct-push and existing well datasets, an independent-samples t-test was used to validate the null hypothesis H_0: $\mu_1 = \mu_2 = \mu_3$. The t-test identified sufficient statistically significant differences in the means of 12 analytes Appendix F: Laboratory Analysis Results to reject the null hypothesis and consider the alternative hypothesis H_0: $\mu_1 \neq \mu_2 \neq \mu_3$ (provided subsequent analyses supported the independent-samples t-test results). This test reported statistically significant differences existed for NH_4^+ -N, Ca^{2+}, DOC, *Eh*, HCO_3^-, Fe^{2+}, Mg^+, Mn^{2+}, NO_3^- -N, NO_2^- -N, K^+, and SPC; therefore further analysis was considered necessary.

Hierarchal cluster analysis was performed to identify the distribution of deeper wells throughout the clusters. Cluster analysis using Ward's linkage and the Squared Euclidian method revealed a distinct distribution with no deeper wells in the right hand clades of the dendrogram (Figure 59).

The HCA supported the independent-samples t-test that differences existed between the chemistry of the deeper groundwater and shallower groundwater. The physical and chemical characteristics of the deepest wells such as depth, cluster membership, and rock/soil class were scrutinised for differences or associations (with little success) and an ANOVA, being non-subjective, was then required.

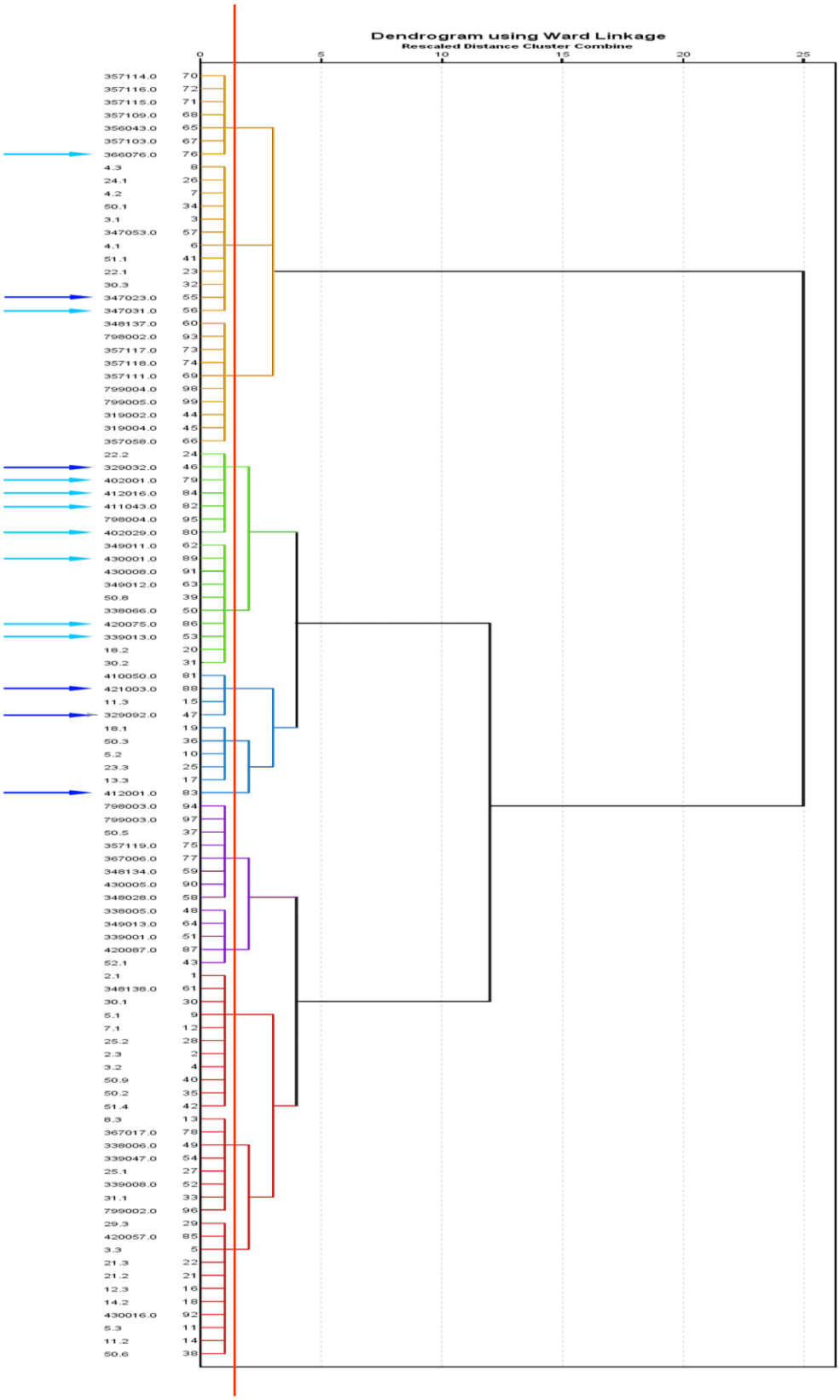

Figure 59: HCA dendrogram of all sites from both datasets combined (n=99). Dark blue arrows below dendrogram indicate wells deeper than 40 m bgl, light blue arrows indicate wells from 20 m to 40 m bgl; all other wells are less than 20 m bgl. The red line extending beyond chart boundary is the phenom-line; a data simplification technique Note: This. is not the dendrogram used for water type analysis which used the n= 94 dataset.

A one-way ANOVA was applied to the transformed datasets to determine whether groundwater chemistry was statistically different based on the depth of abstraction. Bore construction records showed that deeper wells were screened at lower levels, therefore in these wells it can be assumed shallow aquifer water was generally not drawn down into the deeper aquifer. In order to perform the analysis, the following nominal variables for well depth were created:

- Class 1 where well depth = 0 – 20 m (n = 85)
- Class 2 where well depth = 20 – 40 m (n = 9)
- Class 3 where well depth = > 40 m (n = 5)

The initial step in the analysis was to assess homogeneity of variances with Levene's test; if $p > 0.05$ the assumption of homogeneity of variance is accepted, a one-way ANOVA is appropriate. However, if $p < 0.05$, the assumption of homogeneity is violated therefore Welch's ANOVA must be used instead. Most parameters met the assumption of homogeneity of variances test; except Ca^{2+} and Fe^{2+} which were analysed with Welch's ANOVA. The one-way ANOVA only determines whether or not differences exist between the means of the analytes based on the three depth classes. Consequently, post hoc analysis was required to identify which of the depth classes highlighted by the ANOVA were statistically different from each other. Post hoc tests are used to provide statistical significance levels (the p value) for pairwise comparisons and confidence intervals (at 95% level in this study) for the mean difference of the comparisons (Laerd Statistics, 2015). The Tukey-Kramer post hoc test (Table 10) was used as the well depth classes didn't have an equal number of cases (equal numbers of cases use Tukey test). The Games-Howell post hoc test was applied to parameters which violated the assumption of homogeneity.

In the output-table generated with ANOVA, $p < 0.05$ indicated that statistically significant differences existed between the means of NH_4^+ -N, DIC, Fe^{2+}, HCO_3^-, NO_3^- -

N, pH, SiO_2, Na^+, SPC for the 3 different depth classes. (All sample sites, n = 99, were included in this phase of the analysis).

Inspection of the deeper wells locations showed they are situated in a range of geology and soils and a comparison was then sought to compare the chemistry of groundwater between wells located in common geological settings. However, as a minimum of three cases per depth class are able to be analysed with ANOVA, the following analysis was performed only on the gravel + silt loam geological setting.

The Levene's test validated the assumption of homogeneity of variance for all analytes except DO. The results of the ANOVA (Table 9) performed on wells located in gravel + silt loam polygons (n = 35) showed no statistically significant differences between the means for 16 of the 20 chemical parameters. Of the remaining analytes (DIC, NO_3^- -N, Na^+, pH, and SiO_2) it was not unexpected that SiO_2 levels increased from shallow to deeper depths due to longer residence time increasing opportunity for weathering of silicate minerals (Khan & Umar, 2010). Similarly, Nitrate-N levels were also expected to decrease with depth due to greater opportunity for denitrification to occur with increased residence time, lower connectivity with the atmosphere, and corresponding lower inputs of O_2, and total organic nitrogen from the soil zone (Beyer et al., 2016a). Variations in pH, Na, and DIC might be also explained by longer residence times and increased dissolution of aquifer minerals (Morgenstern, Brown, Begg, Daughney, & Davidson, 2009), yet if that is the case, at least some of the other analytes such as Ca^{2+} and Mg^{2+} might be expected to follow a similar trend. However, determining the cause of these variations exceeds the scope of this thesis.

Table 9: One-way ANOVA for sites with gravel + silt loam. Groundwater chemical parameters compared to the sampling-well depth in the Tararua GWMZ.

Parameter	Conclusion where p > 0.05	F-Value
	Means not statistically significantly different	
NH_4^+ -N		F(2, 32) = 0.117, p = 0.890
Br^{--}	"	F(2, 32) = 0.763, p = 0.475
Ca^{2+}	"	F(2, 32) = 0.929, p = 0.405
Cl^-	"	F(2, 32) = 0.870, p = 0.429
DOC	"	F(2, 32) = 1.412, p = 0.258
DO	"	Welch's F(2, 2.605) = 2.496, p = 0.248
Eh	"	F(2, 32) = 0.643, p = 0.533
HCO_3^-	"	F(2, 32) = 1.723, p = 0.195
Fe^{2+}	"	F(2, 32) = 0.362, p = 0.699
Mg^{2+}	"	F(2, 32) = 2.179, p = 0.130
Mn^{2+}	"	F(2, 32) = 0.678, p = 0.515
NO_2^- -N	"	F(2, 32) = 0.387, p = 0.682
K^+	"	F(2, 32) = 1.319, p = 0.281
SPC	"	F(2, 32) = 0.141, p = 0.869
SO_4^{2-}	"	F(2, 32) = 2.063, p = 0.144
	Means are statistically significantly different	
DIC	"	F(2, 32) = 4.918, p = 0.014
NO_3^- -N	"	F(2, 32) = 4.914, p = 0.014
pH	"	F(2, 32) = 3.834, p = 0.032
SiO_2	"	F(2, 32) = 5.955, p = 0.006
Na^+	"	F(2, 32) = 4.449, p = 0.020

All data was transformed to a normal distribution prior to analysis with ANOVA

ANNOVA; F(A.B) = C, p = D

where:

F indicates comparison to F distribution

A = Between groups degrees of freedom

B = Within groups [error] degrees of

C = Obtained F-value

D = Probability of obtaining C, if the null hypothesis is true

Welch's ANOVA; from "robust tests of equality of means table" F(A,B) = C, p = D

where:

F indicates comparison to F distribution

A = Between groups degrees of freedom

B = Within groups [error] degrees of freedom

C = Obtained F-value

D = Probability of obtaining C, if the null hypothesis is true

Br^- = dissolved bromide (mg L^{-1})

Ca^{2+} = dissolved calcium(mg L^{-1})

Cl^- = dissolved chloride (mg L^{-1})

DIC = dissolved inorganic carbon (mg L^{-1})

DO = dissolved oxygen (mg L^{-1})

DOC = dissolved organic carbon (mg L^{-1})

Eh = reduction potential (mV)

Fe^{2+}= dissolved iron (mg L^{-1})

HCO_3^- = bicarbonate (mg L^{-1})

K^+ = dissolved potassium(mg L^{-1})

Mg^{2+} = dissolved magnesium(mg L^{-1})

Mn^{2+}= dissolved manganese (mg L^{-1})

Na^+ = dissolved sodium(mg L^{-1})

NH_4^+ -N = ammoniacal nitrogen (mg L^{-1})

NO_2^- -N = nitrite nitrogen (mg L^{-1})

NO_3^- -N= nitrate nitrogen (mg L^{-1})

SiO_2 = dissolved silica (mg L^{-1})

SO_4^{2-}= sulphate (mg L^{-1})

SPC = specific conductivity (µScm^{-1})

Tukey-Kramer and Games-Howell post hoc tests (Table 10) were then used to provide significance levels (p values) for pairwise comparisons of the sampling-well depth classes with the mean-difference of the comparisons (Laerd Statistics, 2015c). There were conflicting results from these analyses, the ANOVA identified the means of DIC, NO_3^- -N, pH, SiO_2, and Na^+ from the different well depth classes to be statistically different, while the post hoc analysis only identified the means of DIC, NO_3^- -N and Na^+ to be significantly different. It is not uncommon where a statistically significant result is determined by the ANOVA, but not by the post hoc test or vice versa (Laerd Statistics, 2015c). The cause of this effect varies, but fundamentally it is due to the way differences in the distributions are used in the one-way ANOVA and Tukey post hoc test (see Hsu, 1996).

Table 10: Turkey post hoc analysis of wells located in gravel + silt loam settings

Parameter	Depth	20 m < compared to	Sig.	Statistical Significance
DIC		**20 to 40 m**	**0.023**	**significant difference between DIC from shallow and moderately deep wells**
		> 40 m	0.206	
NO_3^- -N		20 to 40 m	0.207	**significant difference between NO_3^- -N from shallow and deep wells**
		> 40 m	**0.023**	
Na^+		20 to 40 m	0.216	**significant difference in Na^+ from shallow and deep wells**
		> 40 m	**0.035**	

The means were not reported as the data were transformed prior to analysis with ANOVA.

Statistically significant difference exits between shallow groundwater and the class in bold text.

DIC = dissolved inorganic carbon

$NO3^-$ -N = nitrate nitrogen

Na^+ = sodium

6.2.1 Validity of Comparing Shallow and Deeper Wells

As 25% of the groundwater quality parameters of the deepest wells were shown to have statistically significant differences when compared to the shallower wells, the null hypothesis was rejected in favour of the alternative hypothesis H_0: $\mu_1 = \mu_2 \neq \mu_3$. As this study is focussed on shallow groundwater of the Tararua GWMZ, it was deemed prudent to remove the five deepest wells from the existing wells dataset prior to any further analysis. Determining which wells to remove from the dataset was a compromise between removing the wells most likely to influence analysis results and retaining the largest dataset possible. Therefore, results of the following analyses are based on the combined direct-push and existing well datasets (depth < 40 m; n= 94).

6.3 Groundwater Chemical Analysis

6.3.1 Charge Balance Analysis

The charge balance exercise highlighted chemical analysis inaccuracies in the direct-push groundwater dataset, while all CBE in the existing well data were less than |15%|. The direct-push data were inconsistent; eight CBE's were greater than the acceptable limit of ± 15% (Figure 60). The high negative CBE indicated an over subscription of anions which is likely to have arisen from systematic errors in acid titration for total alkalinity. These errors affected the titrant volume from which the total alkalinity was derived and which subsequently affected $CaCO_3$ and HCO_3 values. Upon systematic review of the ACID-titration procedure, it is believed the errors probably originated when the instrument was left idle and a faulty valve allowed acid to back-flow from the precision syringe via a delivery tube to the acid reservoir. Unfortunately this wasn't detected until very late in the fieldwork campaign. Consequently, calculations relying

on bicarbonate data (from sites 2.1, 5.1, 11.2, 11.3, 22.2, 25.1, 50.6, 50.8) should, and are, treated with caution in further analysis. Charge balances that violated the 15% tolerance are presented in Appendix G: Charge Balance Analysis.

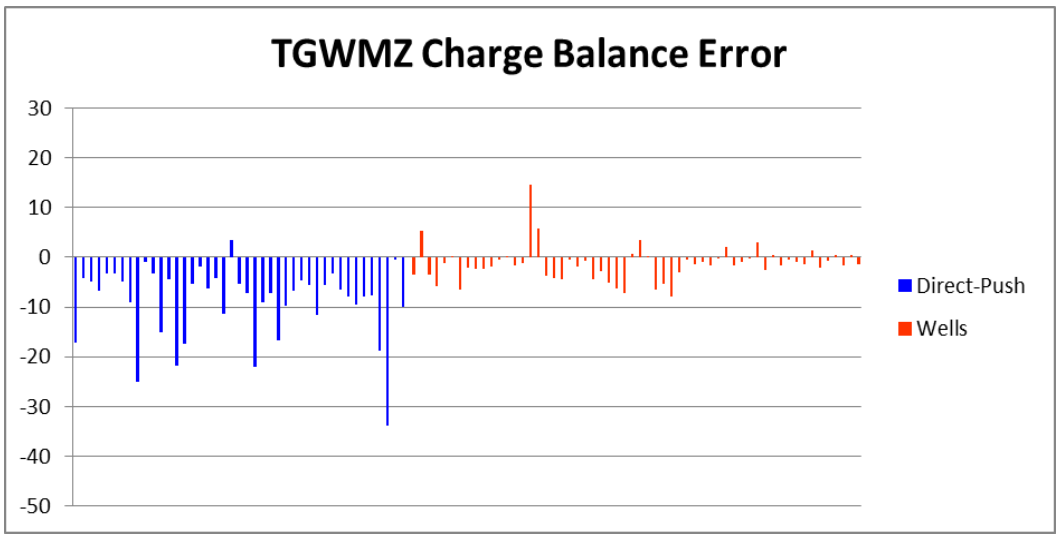

Figure 60: Charge balance error for both existing wells (Feb – Mar 2014) and direct-push groundwater (Oct 2017 – May 2018) datasets collected in the Tararua GWMZ. The majority of cases have negative values indicating higher levels of anions vs cations. The overall lower CBE from Rivas et al. (2017) data (right of centre) indicates more reliable analysis. The relatively high errors in charge balance for the direct-push groundwater dataset are suspected to arise from analytes derived from total alkalinity values from acid titration with the TitraLab 865 at the Massey Soils Laboratory.

The values for HCO_3 were analysed in SPSS with box and whisker plots, outliers were determined and compared with the samples that showed high CBE's, although not all of those with a CBE > 15% were classed as outliers by SPSS (relevant tables and charts presented in Appendix G: Charge Balance Analysis). The samples with a CBE > 15% were then plotted in a piper diagram against HCO_3^- with levels calculated in Microsoft Excel to bring the CBE down to below 15%. Although the plots determined a slight shift in the data points, the change was minimal and did not change the water type classification (Figure 61). Therefore, it was decided to use the HCO_3^- data without modification. The other data were within acceptable limits and considered valid for further analysis.

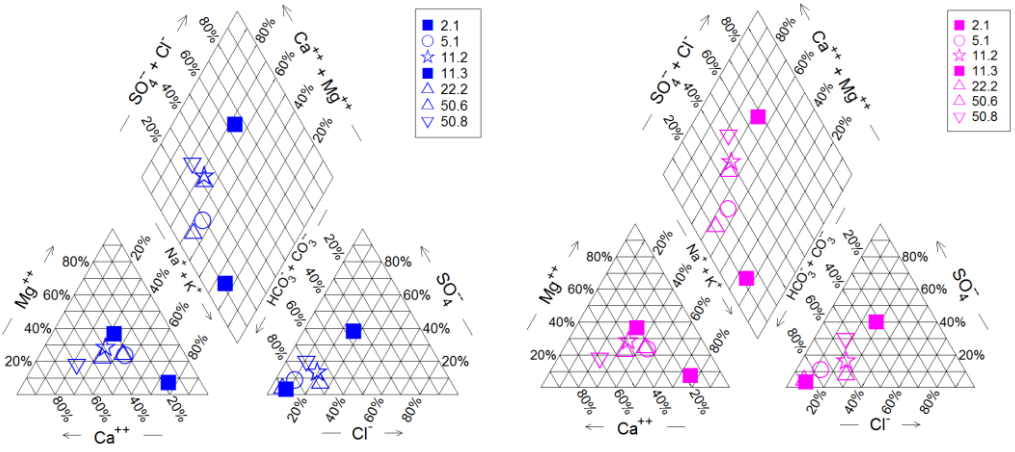

Figure 61: Comparison between original bicarbonate (HCO_3^-) values (left), and adjusted values that exhibited a CBE > 15% (right). The adjusted HCO_3^- values were manipulated to produce a CBE for that sample of just less than 15%. Although there is a little movement of the markers in the adjusted plot (right), there is no change to the overall water type classification therefore the original HCO_3^- data was considered adequate for further analysis.

6.3.2 Groundwater Analytes Exceeding Maximum Acceptable Values and Guideline Values

Maximum acceptable values (MAV) define the level of a particular analyte in water considered suitable for human consumption (Ministry of Health, 2000). Guideline values (GV) define a threshold value for a particular water analyte above which effects may be aesthetically unacceptable (such as taste or staining) but not necessarily unsafe for human consumption (Ministry of Health, 2000). Figure 63 shows the locations of sites which exceeded either the MAV or GV overlaid on the main geological units, while summary statistics are presented in Appendix H: Analytes Exceeding MAV.

Arsenic levels were only tested in the direct-push dataset and 29 (n = 43) were below the detection limit. The highest arsenic value (0.57 mg L^{-1}) was found at site 30.2 (gravel; loam; CC 3; DC 3; pHC 3; WT 2) located 2.5 km SW of the disused abattoir south of Dannevirke; it is unclear whether the high values are related to natural or anthropological factors such as leachate from a redundant sheep dip. Boron was also

only tested for in the direct-push dataset, the highest value (1.170 mg L^{-1}) was found at site 18.1 (mudstone; silt loam; CC 4; Dc 4; phC 3; WT 3), a swampy site at Tane Road located in Neogene mudstone. The association between redox status and iron and manganese levels is evident throughout the Tararua GWMZ where values above their respective GV's exhibited common distribution. Coincidentally, sites with nitrate-N levels above the MAV were all found within a 14 km radius of Dannevirke; however, any association between the urban area and the sites where high NO_3^- -N levels are recorded is virtually impossible as shallow groundwater flow paths (at the regional scale) is broadly south to southwest and geological and topographic barriers prevent any connection of shallow groundwater between these sites and the township.

The high nitrate value of 11.6203 mg L^{-1} at site 430016 (gravel; heavy silt loam; CC 3; DC 5; pHC 3; WT 1; Figure 62) is less than 150 m from a very low NO3- -N value of 0.0031 mg L-1 at site 430001 (gravel; heavy silt loam; CC 3; DC 5; pHC 3; WT 2; Figure 62). Both sites are existing wells and are situated in similar soils and geology. The disparity of NO_3^- -N levels in two wells so close together is likely due to depth (430001 = 12 m and 430001 = 28.8 m). But may also indicate localised denitrification, point source contamination at site 430016, or perhaps a subterranean geological barrier exists between the sites separating groundwater of two distinct types.

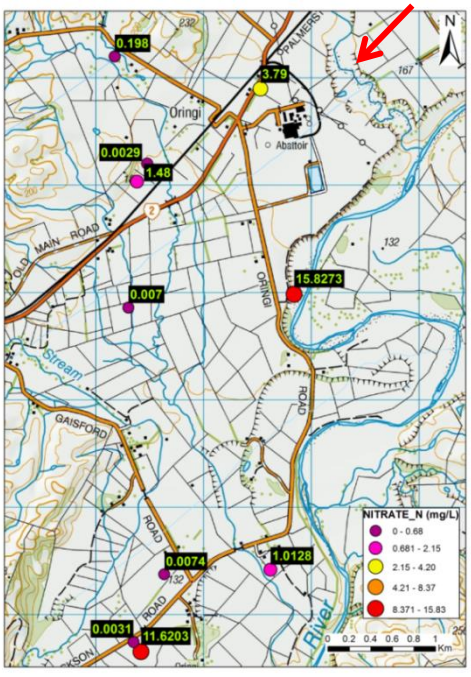

Figure 62: NO_3^- -N levels recorded adjacent to the (now decommissioned) Oringi Abattoir (red arrow), 8km SW of Dannevirke (both datasets). Landuse in this area is predominantly dairy farming. The range of NO_3^- -N levels measured in this area indicate significant spatial diversity of redox characteristics; where strongly oxidising conditions are found close to the Manawatu River and the Oringi Abattoir, and strong reducing conditions are found less than 2 km away. Depth of the wells is the most likely explanation for the two strongly contrasting NO_3^- -N levels seen at the bottom left of the figure.

Sites 50.3 (gravel; silt loam and clay loam; CC 4; DC 2; pHC 3; WT 0) and 18.1 (mudstone; silt loam; CC 4; DC 4; pHC 3; WT 3) featured with sodium above guideline values. Bromide and chloride are not discussed as maximum acceptable values or guideline values for these species are provided as bromate and chlorate for which the data was unavailable.

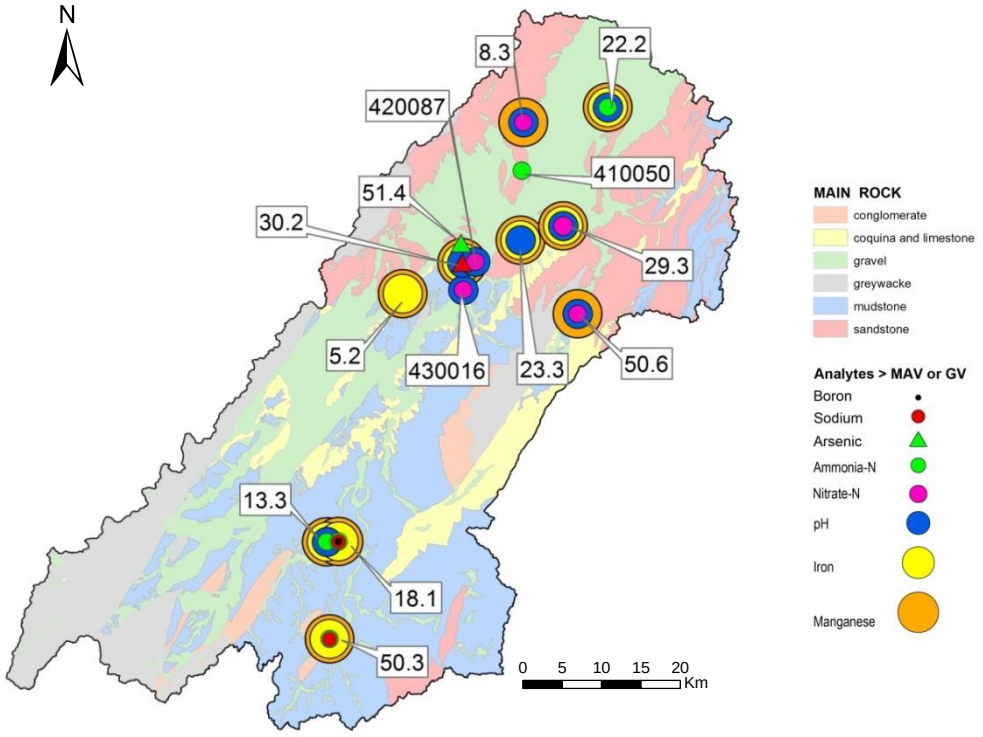

Figure 63: Groundwater analytes exceeding Maximum Acceptable Values and Guideline Values in the Tararua GWMZ. The sites which exceeded the MAV or GV tended to do so for a number of analytes and tended to be adjacent to mudstone (blue) or sandstone (pink). Sites in the main gravel aquifers tended to have more subdued water chemistry. Interestingly 11 of the 14 sites were collected with direct-push (three digit SiteID Labels). This might be explained as production wells are generally being drilled in areas where the water quality is known to be high, while the direct-push sites were determined on the basis of geology alone. The symbology of this map was designed to allow sites with a several analytes over the MAV/GV to be assessed concurrently. (Map generated in ArcGIS 10.2 using shapefiles from Heron, 2014).

6.4 Groundwater Characteristics

An appraisal of the data presented in Table 11 reveals a wide variation in all chemical parameters, indicative of the spatial diversity of groundwater chemistry across the Tararua GWMZ. Table 11 is formatted to show physical characteristics in the top panel, anions and cations in the centre, and redox specific characteristics below. There is potential for some overlap within these categories e.g. iron, manganese, and bicarbonate could be considered in either of the two lower categories, however, association with redox characteristics takes precedence in this study.

6.4.1 Physical Attributes

The shallow nature of the groundwater in the Tararua GWMZ is reflected in a mean well depth of 8.76 m bgl with 90% of wells less than 20 m deep. Values of zero in the existing-well dataset indicate physical characteristics of the well's headworks hampered attempts to insert a water level meter and therefore no depths were recorded. A single depth value of zero in the direct-push series indicates this sample was collected from an artesian spring outcropping at site 50.5 (gravel; silt loam and clay loam; CC 4; DC 2; pHC 3; WT 1). Although most wells were located in gravels, the deepest wells tended to be adjacent to sandstone and limestone lithologies.

The groundwater pH's ranged from 5.0 to 8.0, with a trend of lower pH (~5.0 to 6.0) evident west of Eketahuna, increasing to pH 6.0 towards Pahiatua, pH 7.0 towards Dannevirke, and (generally) over pH 7.0 east and north of Dannevirke. Of the 94 samples, 87 had a pH below 7.0. The lowest pH's tend to be located in the Mangatainoka and Mangahao catchments which originate in the greywacke of the axial ranges and flow through Late Pleistocene and Holocene river deposits, flanked (to the east) by Pliocene mudstones and Late Pliocene coquina. Sites located in the heart of the

mudstone country to the east of Eketahuna generally displayed pH's much higher than those to the west. The shift from low pH appears to coincide with proximity to larger areas of limestone and coquina and/or mudstones.

As expected, (groundwater) specific conductivity (SPC) displays similar trend and varies from 63.9 µS cm^{-1} to 2587.4 µS cm^{-1} with the lowest values being associated with catchments originating in the basement rocks of the Ruahine and Tararua Ranges. Most SPC values were below 830 µS cm^{-1} (95^{th} percentile = 699 µS cm^{-1}) except for two samples abstracted from sites 18.1 (1443 µS cm^{-1}) and 50.3 (2587.4 µS cm^{-1}) in mudstone near Alfredton. However, mudstone should not automatically associated with very high SPC, as samples taken from nearby mudstone sites 13.3 and 50.2 displayed considerably lower SPC values (697.6 µS cm^{-1} and 252 µS cm^{-1} respectively).

Table 11: Summary of chemical analysis of groundwater from combined direct-push (Oct 2017 – May 2018) and existing wells datasets (Feb – Mar 2014) collected from the Tararua GWMZ (n = 94).

Parameter	Unit	Mean	Std. Dev	Min	Max	Range	Median	Mode	Skewness	Kurtosis
Depth	m	8.76	7.48	0.0	36.0	36.00	6.40	7.000	2.374	5.182
Temp	°C	15.74	2.12	10.9	23.8	12.90	15.41	14.500	1.203	2.932
pH	pH	6.08	0.60	5.0	8.0	2.92	5.97	6.020	1.009	1.318
SPC	µS cm^{-1}	270.71	309.10	63.9	2587.4	2523.50	204.75	73.50[a]	5.330	35.743
Br-	mg L^{-1}	0.15	0.42	0.0	4.09	4.07	0.09	0.052	9.156	86.792
Cl-	mg L^{-1}	28.54	61.93	5.7	590.0	584.31	16.03	10.40[a]	8.252	74.493
Ca^{2+}	mg L^{-1}	17.07	14.63	1.9	85.1	83.15	13.28	11.10[a]	2.488	7.542
K^{+}	mg L^{-1}	2.89	1.93	0.5	13.8	13.34	2.42	1.37[a]	2.407	10.065
Mg^{2+}	mg L^{-1}	5.44	3.78	0.8	21.9	21.06	4.62	6.75[a]	1.573	3.515
Na^{+}	mg L^{-1}	25.97	50.49	4.9	418.0	413.15	14.15	13.40[a]	6.149	43.029
SiO_2	mg L^{-1}	13.90	15.46	6.5	81.3	74.82	19.20	15.70	1.472	2.024
DO	mg L^{-1}	2.94	2.85	0.03	9.1	9.02	1.89	0.210	0.649	-0.929
DIC	mg L^{-1}	17.50	17.07	1.5	113.0	111.50	11.59	8.20a	2.620	10.311
DOC	mg L^{-1}	1.80	2.65	0.1	17.9	17.79	1.07	0.300	3.702	16.619
Eh	mV	235.22	151.12	-198	554.3	752.30	237.50	-198.0	-0.267	-0.120
Fe^{2+}	mg L^{-1}	1.71	3.42	0.0	16.8	16.80	0.20	0.004	2.579	6.325
HCO_3^{-}	mg L^{-1}	101.24	124.19	6.1	666.9	660.84	61.22	9.760	2.554	6.981

Mn^{2+}	mg L^{-1}	0.31	0.44	0.0	2.6	2.58	0.15	0.004	2.493	8.164
NH_4^+ -N	mg L^{-1}	0.27	0.71	0.0	4.1	4.05	0.03	0.007	3.917	16.524
NO_2^- -N	mg L^{-1}	0.00	0.01	0.0	0.1	0.06	0.00	0.001	5.110	34.540
NO_3^- -N	mg L^{-1}	2.26	3.47	0.0	15.8	15.83	0.47	0.001	2.217	5.206
SO_4^{2-}	mg L^{-1}	13.90	14.61	0.0	101.0	101.0	10.16	0.004	3.066	13.718

[a] multiple modes exist, the lowest mode is shown.

Parameters grouped into: panel 1 - physical characteristics; 2 - anions and cations; and 3 - key denitrification characteristics.

Br^- = dissolved bromide (mg L^{-1})
Ca^{2+} = dissolved calcium(mg L^{-1})
Cl^- = dissolved chloride (mg L^{-1})
DIC = dissolved inorganic carbon (mg L^{-1})
DO = dissolved oxygen (mg L^{-1})
DOC = dissolved organic carbon (mg L^{-1})
Eh = reduction potential (mV)
Fe^{2+}= dissolved iron (mg L^{-1})
HCO_3^- = bicarbonate (mg L^{-1})
K^+ = dissolved potassium(mg L^{-1})
Mg^{2+} = dissolved magnesium(mg L^{-1})
Mn^{2+}= dissolved manganese (mg L^{-1})
Na^+ = dissolved sodium(mg L^{-1})
NH_4^+ -N = ammoniacal nitrogen (mg L^{-1})
NO_2^- -N = nitrite nitrogen (mg L^{-1})
NO_3^- -N= nitrate nitrogen (mg L^{-1})
SiO_2 = dissolved silica (mg L^{-1})
SO_4^{2-}= sulphate (mg L^{-1})
SPC = specific conductivity (µScm^{-1})

6.4.2 Anions and Cations

Although groundwater analyte levels from the main gravel aquifers are generally more homogenous, the spatial variation in groundwater chemistry throughout the Tararua GWMZ is still significant (Table 11; Table 12). The samples obtained from the mudstone sites in particular 50.3, 18.2, 18.1, and 13.3 featured regularly in the analysis; analyte values from these samples were often many times higher than the median values of the dataset (Table 12).

Table 12: Examples of high analyte levels collected from sites located in mudstone in the Tararua GWMZ

	Site ID				
Parameter (mg L^{-1})	**13.3**	**18.1**	**18.2**	**50.3**	**median value***
B	0.304	1.170	0.041	0.812	0.036
Br^-	0.170	0.530	0.338	4.090	0.093
Cl^-	31.500	89.800	30.900	590.000	16.025
DIC	62.700	113.000	43.600	65.600	11.59

F^-	0.397	0.403	0.142	0.360	0.083
Na^+	95.700	248.000	24.700	418.000	14.150
Mg^{2+}	11.700	6.310	12.300	15.700	4.620
SPC	697.6	1443	388.7	2587.4	204.750

*median values calculated from combined direct-push and existing well datasets (n = 94)

B = dissolved boron (mg L^{-1})

Br^- = dissolved bromide (mg L^{-1})

Cl^- = dissolved chloride (mg L^{-1})

DIC = dissolved inorganic carbon (mg L^{-1})

F^- = dissolved fluoride (mg L^{-1})

Na^+ =dissolved sodium(mg L^{-1})

Mg^{2+} = dissolved magnesium(mg L^{-1})

SPC = specific conductivity(µScm^{-1})

The mean value (0.15 mg L^{-1}) for bromide was skewed by a single reading of 4.09 mg L^{-1} acquired from site 50.3. The high bromide levels at this site were also accompanied by the highest sodium and chloride levels, and very high levels of DOC, DIC, NH_4^+ -N, Boron, Mg^{2+}, K^+, Na^+, SPC, and HCO_3^-. Bromide was strongly correlated with sodium ($r = .767$, $p < .0005$) but not as strongly with potassium ($r = .477$, $p < .0005$) suggesting perhaps at some point bromide existed as sodium bromate ($NaBrO_3$). See Appendix D.3 Pearson Correlation Table.

There was little correlation between most cations and anions and depth e.g. Br^- (Spearman's rho $r_s = .099$, $p = .343$); Cl^- ($r_s = .094$, $p = 367$); Ca ($r_s = .114$, $p = .274$) however, there was a moderate correlation between depth and silica ($r_s = .317$, $p = .002$). This relationship was interpreted as a loose association between depth and groundwater age by Rivas et al. (2017) although in this dataset, increases in silica levels appear more strongly correlated to higher pH ($r = .524$, $p < .0005$) ; the higher pH may reflect equilibrium with limestone. Increasing pH also showed moderate correlation with the cations Na^+ ($r_s = .500$, $p < .0005$), Ca^{2+} ($r_s = .455$, $p < .0005$), and Mg^{2+} ($r_s = .432$ $p < .0005$) but not K^+ ($r_s = .079$, $p = .007$); pH was less strongly correlated to Br^- and Cl^- ($r_s = .179$, $p = .084$ and $r_s = .236$, $p = .022$ respectively).

6.4.4 Redox Sensitive Parameters

The chemical parameters associated with redox reactions in groundwater (shown in the lower panel of (Table 11) are briefly discussed in the following section; high and low values, trends and sites of interest, and statistical correlations with other redox sensitive species are presented.

Dissolved oxygen levels tend to be low along the Manawatu River, in the mudstone sites, and north of Dannevirke. On the other hand, DO levels tend to be high in catchments which originate in the axial ranges such as the Mangatainoka River and the smaller Tamaki, Kumeti and Oruakeretaki catchments situated west of Dannevirke (Figure 64). Interestingly, sites along the Mangahao River reveal low DO levels, while the sites along the (adjacent and parallel flowing) Mangatainoka River are high in DO. The two highest DO values site 319002, 9.05mg L^{-1} (gravel; stony loam; CC 3; DC 5; pHC 3; WT 1) and site 319004, 8.82 mg L^{-1} (gravel; stony loam; CC 3; DC 5; pHC 3; WT 1) are recorded from wells less than 100 m from relatively small, fast flowing, gravel based streams near the Ruahine Ranges in the Kumeti Catchment. High groundwater DO values of around 8 to 9 mg L^{-1} suggest very high connectivity with surficial water; e.g. 9.5 mg L^{-1} of dissolved oxygen was recorded in the Otamaraho Stream near site 4.1 Te Rehunga Road, West of Dannevirke. The location of site 319004 (DO = 9.05 mg L^{-1}) less than 40 m from the Mangapuaka Stream, and site 319002 (DO = 8.82 mg L^{-1}) less than 120 m from the Otamarahu Stream, where abundant gravels are encountered above and below the stream level support a high degree on connectivity between these sites and the nearby streams. Dissolved oxygen was less than 1.0 mg L^{-1} at 37 sites with six sites having less than 0.1 mg DO L^{-1}. The lowest DO value was encountered at site 11.3 (gravel; silt loam and clay loam; CC 4; DC 2; pHC 3; WT 2), located on an 800 m by 600 m alluvial terrace only a metre or two higher than Coppermine Creek (230 m NE), and less than 1.0 km from the base of the Ruahine Ranges. This site is interesting, as the analysis results were expected to be oxic with low SPC and dissolved ions similar

to site 51.1 (gravel; sandy loam; CC 3; DC 3; pHC 3; WT 1) only 750 m upstream (also in Late Pleistocene river gravels 220 m SW of Coppermine Creek). Instead, the site 11.3 produced very high SPC, pH, DIC, Cl^-, Br^-, and Na^+ levels similar to those found in the mudstone country. It is conceivable a lens of silt or clay embedded in the gravels at site 11.3 isolated a small a body of water from the main aquifer. Another possibility is the drill rods could have been driven down past the gravels into the underlying mudstone and intersected connate water trapped in the mudstone.

Exhibiting moderately-strong negative correlation with DO are DIC ($r = -.606$, $p < .0005$), HCO_3^- ($r = -.702$, $p < .0005$), NH_4^+ -N ($r = -.716$, $p < .0005$), Fe^{2+}($r = -.566$, $p < .0005$) and Mn^{2+} ($r = -.631$, $p < .0005$) and moderate negative correlation DOC ($r = -.408$, $p < .0005$). These parameters are associated with reduction processes and as such, their levels increase as dissolved oxygen levels decrease. This is reinforced by positive correlations of DO with NO_3^- -N ($r = .508$, $p < .0005$) and *Eh* ($r = .631$, $p < .0005$) which mark the association between oxic waters and low denitrification potential. The analysis suggested no significant correlation exists between DO and depth ($r_s = -.141$, $p = .177$).

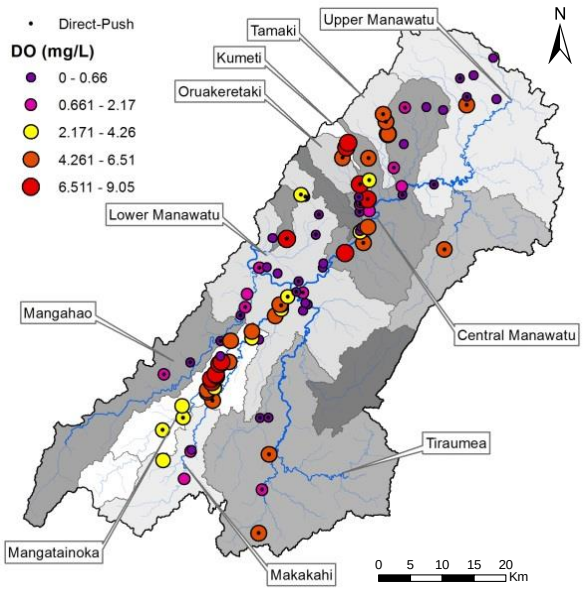

Figure 64: Dissolved oxygen levels measured in the Tararua GWMZ. High DO levels are recorded throughout the central plain. Low levels in the northern regions are thought to be due to microbial consumption during denitrification processes. Samples collected with direct-push are marked with black central dot.

Nitrate-nitrogen values <0.5 mg L^{-1} (i.e. the redox threshold used to identify redox processes were found at 48 sites, and these of 89 samples were under the MAV of 11.3 mg L^{-1}. The correlation with DO ($r = .508$, $p < .0005$) results in a similar spatial pattern where nitrate levels are higher in the Mangatainoka, and the Tamaki, Kumeti and

Oruakeretaki catchments near the axial ranges (Figure 65). Five samples exceeded the MAV of 11.3 mg L^{-1} NO_3^- -N, the highest of which was 15.82 mg L^{-1} was recorded at the site 420087 (gravel; sand; CC 4; DC 5; pHC 4; WT 1) near the Manawatu River and about 1 km downstream of the disused abattoir at the corner of State Highway 2 and Oringi Road (Figure 62). Located in Holocene river deposits, it is unclear whether contamination from (recent or historic) industrial activities such as the Oringi Abattoir or discharge or leachate from the Dannevirke domestic sewerage are implicated in these elevated NO_3^- levels. The 4th highest NO_3^- -N (11.62 mg L^{-1} at site 430016 (gravel; heavy silt loam; CC 3; DC 5; pHC 3; WT 1) level was also located in Late Pleistocene river deposits near the abattoir (3.6 km SSE of site 420087). The high NO_3^- -N values (> 11 mg L^{-1}) found in this area may substantiate point source contamination rather than landuse effects, as the eight surrounding sites revealed much lower NO_3^- -N values (< 0.003 mg L^{-1}) The second highest NO_3^- -N value (15.3 mg L^{-1}) was found in Holocene river deposits at site 50.6 adjacent to the Mangatoro stream, Waitahora Road. The next highest record of 14.6 mg L^{-1} NO_3^- -N was found in Late Pleistocene river deposits at site 29.3 (gravel; heavy silt loam; CC 3; DC 5; pHC 3; WT 2)on the uppermost of a suite of alluvial terraces on the true left of the Manawatu River 5km SE of Dannevirke. Both these sites are proximal to extensive limestone deposits and no obvious point source of nitrate contamination was noted. The other NO_3^- -N value that exceeded the MAV was located at the site 8.3 Te Kakapo road (gravel; heavy silt loam; CC 3; DC 5; pHC 3; WT 2), in Early Pleistocene river, lake, and shoreline deposits around 1 km from the base of the Ruahine Ranges; situated upslope of several dwellings, it was difficult to determine the provenance of the nitrates in this setting. These three sites are associated with sheep and beef farming, and the two sites near the Oringi abattoir are associated with dairy farming.

The lowest NO_3^- -N values (0.16 mg L^{-1} < NO_3^--N) were found in the areas of Upper Manawatu, where relatively close potentiometric contours signal higher hydraulic gradients, and south along the Manawatu River to the gorge where the potentiometric contours are spaced much farther apart and indicate relatively low hydraulic gradients. This indicates the groundwater in the Upper Manawatu may be moving faster within the aquifers than the more southern areas but significant denitrification occurs due to abundant DOC present in the voluminous peat and lignite deposits. Conversely, slower movement in the more southern areas allows greater residence time and therefore more opportunity for redox reactions to occur.

Strong to moderate negative correlations existed between the NO_3^- -N values with NH_4^+ -N ($r = -.528$, $p < .0005$), HCO_3^- ($r = -.467$, $p < .0005$), DIC ($r = -.470$, $p < .0005$), Fe^{2+} ($r = -.353$, $p = .001$), Mn^{2+} ($r = -.434$, $p < .0005$) which indicate the association between denitrification and by-products produced as the redox reactions proceed along the TEAP series. Nitrate levels were weakly negatively correlated to well depth ($r_s = -.295$, $p = .004$), which indicate a slight tendency for more denitrification to occur in slightly deeper environments. Nitrite (NO_2^- -N) levels were low throughout the study area with 50 (n = 94) below the detection limits of 0.002 mg L^{-1}. Site 50.6 Waitahora Road (gravel; silt loam; CC 3; DC 4; pHC 4; WT 1) that had the 2nd highest NO_3^- -N value also recorded the highest NO_2^- -N value. A trend of higher NO_2^- values is evident in the area north of Dannevirke which reflects production of NO_2^- as

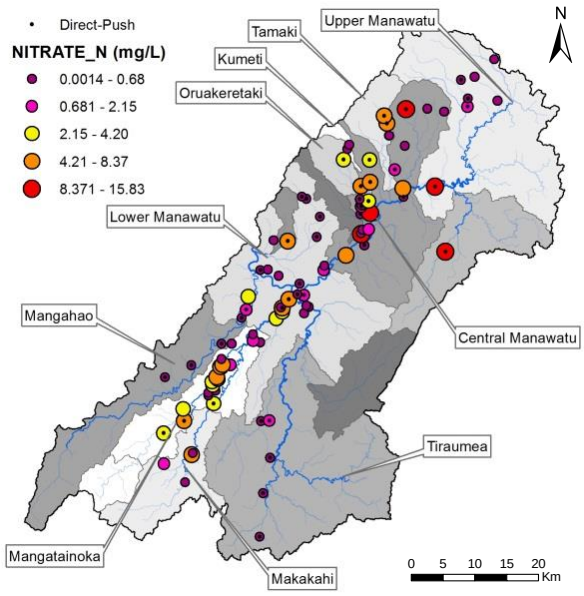

Figure 65: NO_3^- -N levels measured in the Tararua GWMZ. Highest levels are recorded throughout the central plains and low levels in the northern regions. The correlation between DO and NO_3^- -N levels reflect the association between levels of these analytes and denitrification processes in the subsurface environment.

an intermediate product of incomplete denitrification (Wrage, Velthof, Van Beusichem, & Oenema, 2001).

Manganese in excess of the MAV of 0.5 mg L^{-1} was detected in 20 of the 94 sites. The higher values tend to follow the spatial distribution of low DO, and NO_3^- -N and vice versa. Two of the highest values are recorded in the mudstone areas at sites 18.2 2.58 mg L^{-1}; (gravel; silt loam; CC 3; DC 5; pHC 3; WT 2) and 13.3, 1.66 mg L^{-1}; (gravel; silt loam and clay loam; CC 43; DC 2; pHC 3; WT 2), while the third highest value is recorded in heavily reduced (methanogenic) groundwater at site 30.2 (gravel; loam; CC 3; DC 35; pHC 3; WT 2) south of Dannevirke (Figure 66). Mn values are positively correlated to NH_4^+ -N, SiO_2 and Fe^{2+} and show little correlation to well depth (rs = .029 p = .54).

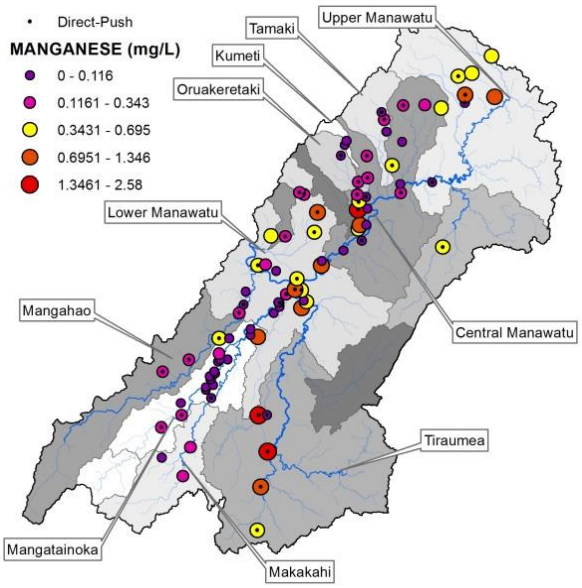

Figure 66: Manganese levels measured in the Tararua GWMZ. Mn^{2+} is the product of the latter stages of the TEAP and its presence indicates highly reduced conditions.

Bicarbonate may originate from dissolution of carbonate or silicate minerals or as a by-product rejected at each phase of the denitrification process (Rivett et al., 2008). It is difficult to discern which process is dominant in any given setting, although the moderate negative correlation between HCO_3^- and NO_3^- -N ($r = -.467$, $p < .0005$) would suggest HCO_3^- arising from denitrification processes would be dominant where lower NO_3^- -N levels prevail. Carbonate dissolution may be the dominant means of HCO_3^- production where higher NO_3^- -N levels are encountered. Bearing in mind anomalies identified by the charge balance analysis (discussed in Section 6.3.1), HCO_3^- results may be influenced by erroneous values from my titration. HCO_3^- levels vary from 6.1 mg L^{-1} to over 660 mg L^{-1}; 19 of the 20 lowest values (HCO_3^- < 25mg L^{-1}) are recorded in the

Mangatainoka, Tamaki, Kumeti and Oruakeretaki catchments (Figure 67). These catchments are associated with oxic conditions and higher NO_3^--N, and the low HCO_3^- levels reaffirm mineral dissolution or denitrification occurs at low levels in the catchments of this nature. Three of the five highest HCO_3^- values (HCO_3^- > 400 mg L^{-1}) are recorded from strongly anoxic conditions (NO_3^-/CH_4 reduction, or Fe(III)/SO_4^{2-} reduction) in the mudstone sites 50.3 (gravel; silt loam and clay loam; CC 4; DC 2; pHC 3; WT 0) , 18.1 (mudstone; silt loam; CC 4; DC 4; pHC 3; WT 3) and 13.3 (gravel; silt loam and clay loam; CC 4; DC 2; pHC 3; WT 2). However, it is difficult to conclude despite the strongly reduced conditions, whether the high HCO_3^- at these sites originates from denitrification processes. The fine grained sediments, low volumes of groundwater, and intensive shallow drainage systems in these areas suggest most NO_3^- -N rich leachate will be discharged directly to the streams rather than percolating deeper into groundwater zones. Thorstenson, Fisher, and Croft (1979) identify carbon dioxide derived from lignitic carbon reacts with, and dissolves, carbonate or silicate minerals. In the Fox Hills-Basal Hell Creek Aquifer in south-western North Dakota and north-western South Dakota pH was seen to rise to pH 8.1 and was coupled with significant rises in Cl^-. Therefore considering the high pH and levels of other chemical species e.g. DIC, Na^+, Cl^- ,B, Br^-, and Mg^{2+} at these sites, it may be more likely mineral dissolution is the prime factor associated with the high HCO_3^- levels.

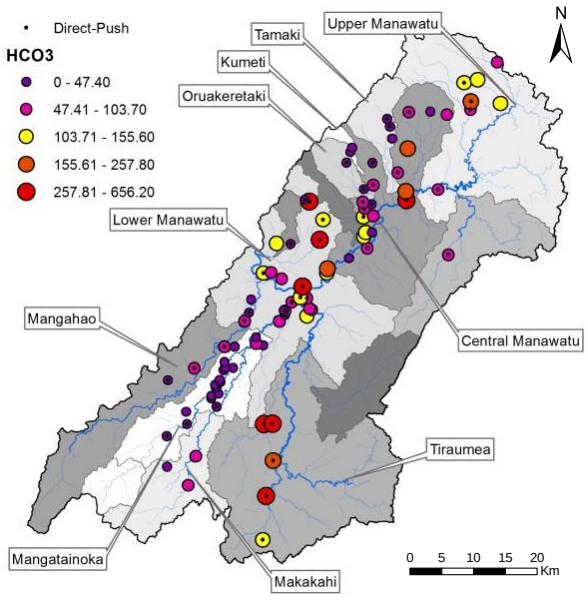

Figure 67: HCO_3^- levels measured in the Tararua GWMZ. High levels in the Tiraumea catchment seem to be related to dissolution of carbonate minerals while those in the Upper Manawatu are probably linked to denitrification processes.

The third highest HCO_3^- value (440.09 mg L^{-1} HCO_3^-) was obtained from an entirely different setting; i.e. site 50.8 (gravel; sand and stony gravel; CC 4;

DC 3; pHC 4; WT 2) from what appeared to be a productive aquifer in Holocene river deposits around 600 m from the Mangatainoka River. The soil texture is sand and stony gravel, FSL soil drainage class is 3 (imperfect) and FSL soil carbon class is 4 (very low). The sample site was situated in pasture surrounded by intensive dairying in what appeared to be a paleochannel bisecting a low alluvial terrace 500 m from the Mangatainoka River. This highly reduced site (Fe(III)/SO_4^{2-} reduction) exhibits very low NO_3^- -N levels and although it may be reasonable to expect the HCO_3^- detected is the product of denitrification processes; dissolution of carbonaceous facies in the Neogene sedimentary rocks 1 km to the north and east of the site may also be implicated.

Nearly a third of NH_4^+ -N values are under the detection limit of 0.01 mg L^{-1} and 87 are below 1 mg L^{-1} (Figure 68). The existence of NH_4^+ may be explained by dissimilatory nitrate reduction to ammonia (DNRA) which becomes dominant over denitrification in strongly reducing settings (Rütting, Boeckx, Müller, & Klemedtsson, 2011). This is supported by the strong negative correlations with DO (r = -.648, p <.0005) and *Eh* (r =-.730, p < .0005). The presence of NH_4^+ -N may also be attributed to mineralization of sediments rich in organic matter (White, 1957). Notably the highest five Ammonia-N levels showed characteristics (NH_4^+ -N > 0.15 mg L^{-1} + DOC/NO_3^- > 12) where dissimilatory nitrate reduction to ammonium (DNRA) could potentially occur (Rütting et al., 2011). Excluding the mudstone sites, the highest NH_4^+ -N values tend to be found in (or within < 1 km of) Pliocene sandstone and siltstone

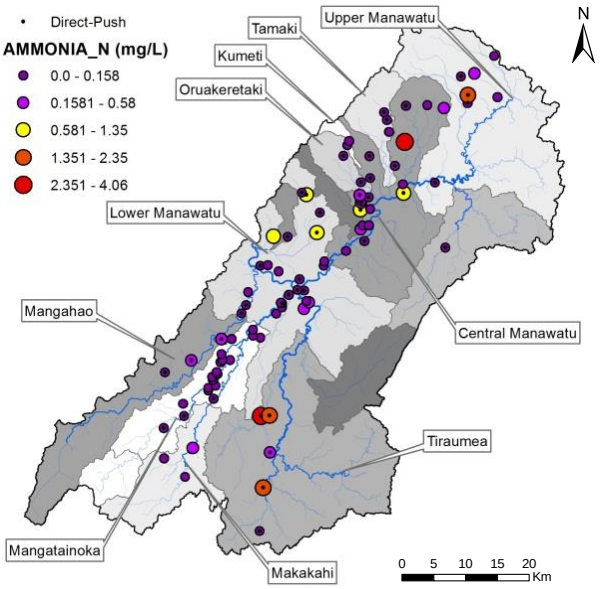

Figure 68: NH_4^+ -N levels measured in the Tararua GWMZ. The highest levels are found in conditions that DNRA could occur and tend to be located adjacent to Pliocene sandstone and siltstone units.

units. Furthermore NH_4^+ -N levels are strongly correlated to boron ($r = .635$, $p < .0005$) and bromide ($r = .529$, $p < .0005$), Cl^- ($r = .545$, $p < .0005$) and Ca^{2+} ($r = .509$, $p < .0005$) indicating that ammonia in these settings may originate from dissolution of minerals within buried marine sediments (White, 1957). High NH_4^+ -N levels were recorded at site 41005. This sample was from a production well situated directly alongside a small pond on Glangarry Road west of Dannevirke with characteristics of main rock, sandstone; soil texture, silt loam; soil carbon, medium; soil drainage, poor. The well appeared to be strongly connected to the pond, and decomposition of organic matter in anaerobic conditions may explain the high NH_4^+ -N levels in this situation (Mastrocicco, Giambastiani, & Colombani, 2013; Rütting et al., 2011). There appears to be no correlation between NH_4^+ -N and well depth ($r_s = .024$, $p = .819$).

Sulphate levels range from five samples below the detection limit (0.005 mg L^{-1}), to 101 mg L^{-1}, with 89 of 94 records below the 95th percentile (<42.45 mg L^-). Highest values tend to be located in the upper Mangatainoka catchment, the Oringi area south of Dannevirke, and central Tararua GWMZ where potentiometric contours indicate pooling of groundwater prior to exiting the Manawatu Gorge (Figure 69). The mudstone sites test very low for sulphates, as did the central Mangatainoka, Tamaki, Kumeti and Oruakeretaki catchments. That low sulphate levels are found in catchments with both poor hydraulic conductivity (mudstone) and also high hydraulic conductivity (gravel) is interesting. This may be explained by little dissolved sulphate being present in the connate water of the mudstone, while in the gravel aquifers sulphates (particularly those arising from fertilizer inputs) may be diluted by large volumes of groundwater and dissipated by relatively rapid groundwater flow in the Mangatainoka, Tamaki, Kumeti, and Oruakeretaki (inferred from groundwater pumping rates during sampling). There was no correlation between well depth and SO_4^{2-} levels (rs = -.025, p = 810).

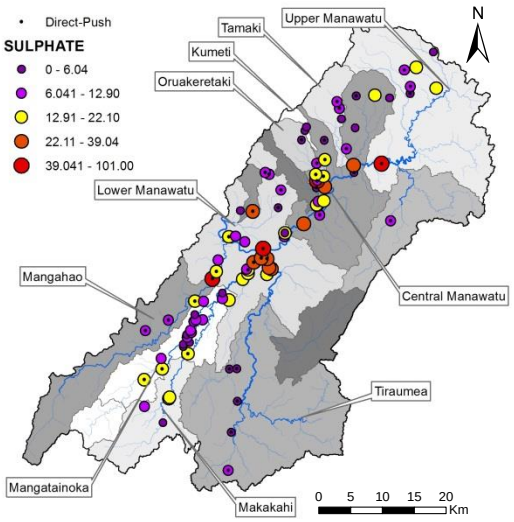

Figure 69: SO_4^{2-} levels measured in the Tararua GWMZ. SO_4^{2-} may be a product of advanced reduction processes or perhaps leachate from fertilizer inputs. The higher levels recorded throughout the central plains may indicate the latter.

Electron donors fundamental to redox reactions are dissolved organic carbon (DOC) and ferrous iron (Fe^{2+}); availability of these species are considered key limiting factors of denitrification (Korom, 1992). DOC is found in significantly higher levels in the mudstone sites (site 18.2 17.9 mg L^{-1}, site 50.3 11.2 mg L^{-1}) than those measured in gravels (DOC < 4.5 mg L^{-1}). This may be attributed to the high prevalence of swampy areas rich in decomposing organic matter adjacent to the sample sites.

Within the recognised aquifers, higher DOC levels tend to be recorded in the area north of Dannevirke where an abundance of carbon rich substrates such as peat and lignite are observed (Figure 70). Furthermore, a trend of higher DOC levels in the Mangahao catchment compared to the Mangatainoka catchment is observed. Ferrous iron levels below the detection limit (0.005 mg L^{-1}) are also evident in the Mangatainoka and the catchments west of Dannevirke, suggesting that the low denitrification potential in these areas may be due to limited availability of suitable electron donors. The availability of DOC as an electron donor arising from abundant peat and lignite deposits in the Upper Manawatu may also be augmented by glauconite as an alternative electron donor (Rissmann, 2011) which is observed overlying the Late Cretaceous - Paleogene Whangai Shale in the north-eastern regions of the Tararua GWMZ.

Although DOC levels appear low in the Upper Manawatu, the abundance of peat and lignite results in sufficient levels of DOC to facilitate high levels of reduction. Although the Mangahao Catchment is adjacent to the greywacke ranges it is interesting that DOC

and DIC levels appear higher than the Mangatainoka. This may result in higher levels of denitrification and the reason why NO3- -N and DO levels are low in the Mangahao.

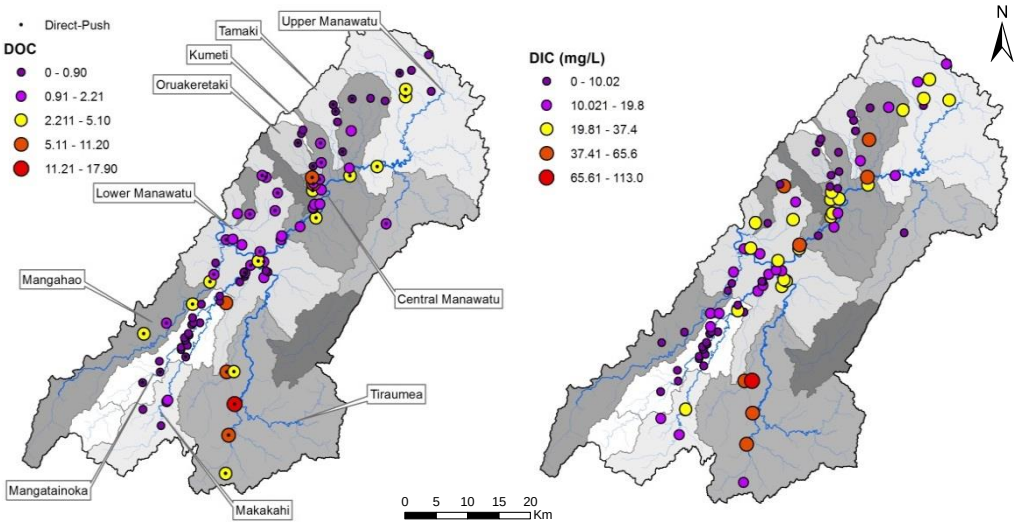

Figure 70: Dissolved organic carbon (left) and dissolved inorganic carbon levels (right) measured in the Tararua GWMZ. DOC levels were seen to vary widely throughout the Tararua GWMZ. Highest DOC levels are recorded in the mudstone country east of Eketahuna and lowest levels in the Mangatainoka and north-eastern catchments associated with greywacke steep-lands and thin soils Map generated in ArcGIS 10.2 using shapefiles from Heron (2014); Land Information New Zealand (2011b).

The oxidation reduction potential (ORP) results recorded with the smarTROLL rather than the *Eh* (ORP + 200mV) are presented in Figure 71. The negative values of ORP (which may indicate reducing conditions) provide a quick and simple means of assessing the redox potential *Eh* parameter. Negative values are found in the Upper and Lower Manawatu, as well as the Tiraumea and the Mangahao catchments. The lowest *Eh* value (-198.00 mV) is recorded at site 30.2 (gravel; loam; CC 3; DC 3; pHC 3; WT 2). Site characteristics are rock, gravel; soil texture, loam; soil carbon, medium; soil drainage, imperfect. DO and NO_3^- -N levels are 0.65 mg L^{-1} and 0.007 mg L^{-1}. Interestingly, this site is only a few kilometres from the highest DO (9.050 mg L^{-1}) recording at site 319002 (gravel; stony loam; CC 3; DC 5; pHC 3; WT 1) near Oringi Abattoir, Dannevirke, and two of the five highest NO_3^- -N readings (site 420087 gravel; sand; CC 4; DC 5; pHC 4; WT 1, and site 430016 gravel; gravel; heavy silt loam; CC 3;

DC 5; pHC 3; WT 1). This highlights the spatial variability of redox processes in the subsurface environment. The mudstone sites east of Eketahuna also exhibit negative ORP values and this may be due to poor hydraulic conductivity of the sediments and similarly poor connectivity and recharge with O_2 rich groundwater.

The five highest ORP values (>269 mV), suggesting strongly oxidising conditions where little denitrification might occur, are located in the Mangatainoka Catchment.

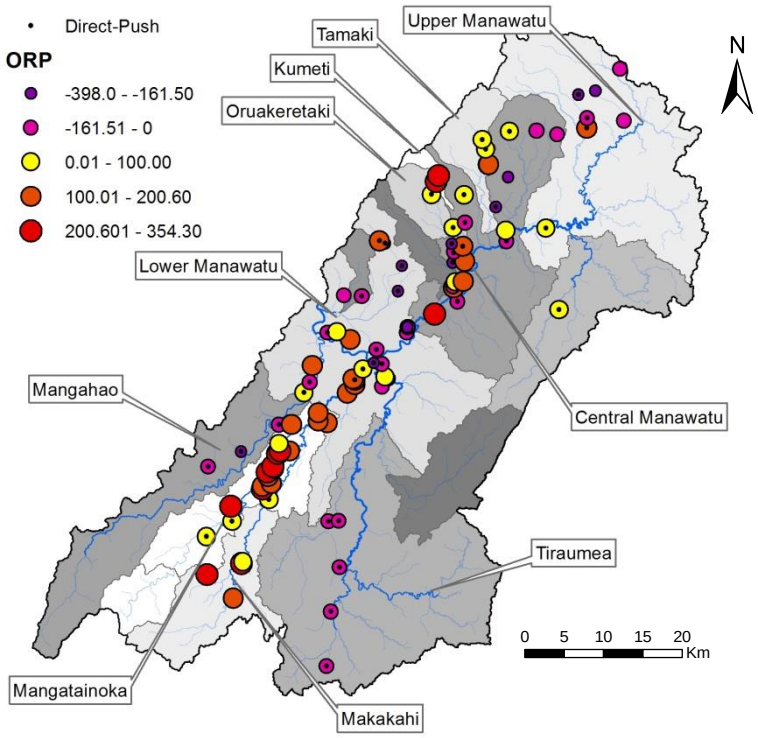

Figure 71: ORP values measured in the Tararua GWMZ. Strongly negative values (< -200 mV) indicate reducing conditions prevail and high positive values (>200 mV) indicate oxic conditions. Although not completely reliable ORP levels can provide a simple indication of the nature of the redox conditions. Reducing conditions are fairly consistent in the Upper and Lower Manawatu, and oxic conditions are prevalent in the catchments adjacent to the ranges and also the Central Manawatu and Mangatainoka Catchments. Map generated in ArcGIS 10.2 using shapefiles from Heron (2014); Land Information New Zealand (2011b).

6.4.5 Redox Classification

The redox sensitive parameters were further used to classify the redox status and the nature of the incumbent redox processes (Table 14) using Jurgens, McMahon, Chapelle, and Eberts (2009) workbook with thresholds defined in the method section (Table 1). Anoxic samples were identified at 28.5% of the sites, mixed anoxic at 10%, oxic at 32.5%, and mixed oxic at 28% of sites; 1% were defined as suboxic. As expected and forming a similar distribution with regard to dissolved oxygen levels, oxic water was encountered in the Mangatainoka, Tamaki, Kumeti and Oruakeretaki catchments (Figure 72). However, oxic sites also included a string of five wells in Late Pleistocene river deposits adjacent to the Manawatu River between Dannevirke and Woodville. From examination of the well depth, geology and geomorphology and the potentiometric map the oxic water found in sites 420087 (5.92 m deep; < 100m from the Manawatu River; gravel; sand; low soil carbon; well drained) and 339001 (4.7 m deep; < 350 m from the Manawatu River; gravel; sandy loam and silt loam; low soil carbon, well drained) may be linked to aquifer recharge originating from Manawatu River water. While site 430005 (17 m deep; 16 m from stream; gravel; sandy loam and silt loam; low carbon; well drained) is likely to be recharged from an unnamed tributary of the Manawatu River. The other two sites 4420057 (depth 34 m, gravel; silt loam; medium soil carbon; well drained) and 430016 (12 m deep; gravel; heavy silt loam; medium soil carbon; well drained) are situated on terraces well above the Manawatu River and recharge sources are not reliably inferred.

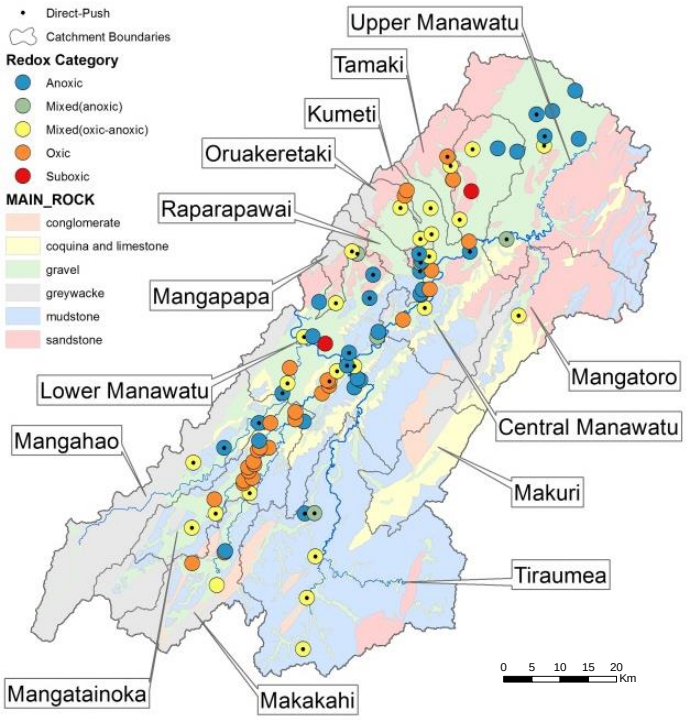

Figure 72: Redox categories measured in the Tararua GWMZ. As determined by DO and NO_3^- -N levels, anoxic conditions are found in the Upper and Central Manawatu, the Mangahao and the mudstone country. Oxic conditions occur particularly in the mid reaches of the Mangatainoka, Tamaki, Kumeti and Oruakeretaki Catchments. The potentiometric map (right) helps explain some of the distribution patterns of redox conditions with shallower water table and lower hydraulic gradient adjacent to the Manawatu Gorge. (Map generated in ArcGIS 10.2 using shapefiles from Heron (2014); Land Information New Zealand (2011b)).

Further examination of groundwater redox processes (Table 14) reveals occurrence of methanogenesis (highly reduced conditions with near complete reduction of nitrates, manganese). It is interesting that such heavily reducing conditions existed at site 30.2 (gravel; loam; CC 3; DC 3; pHC 3; WT 2) while site 420087 (gravel; sand; CC 4; DC 5; pHC 4; WT 1), only 1.5 km to the east, is assessed as oxic and exhibits the highest nitrate levels of the study. Greater proximity and connection of site 420087 to the Manawatu River, compared to site 30.2 may result in aquifer recharge with oxygen rich water from the Manawatu River. However, site 23.3 (gravel; sandy loam; CC 4; DC 3; pHC 3; WT 2) around 6km upstream is a similar distance from the Manawatu River yet is also classified as methanogenic (Table 13).

Table 13: Characteristics of wells in the Tararua GWMZ determined to be methanogenic.

SiteID	Depth (m)	Rock	FSL Soil Texture	FSLCarbon	FSLDrainage	water type
13.3	6.4	gravel	silt loam	3	5	2
338006	12	gravel	silt loam & clay loam	4	2	2
5.2	6.5	gravel	sandy loam	4	3	2
30.2	6.3	gravel	loam	3	3	2
23.3	7.7	gravel	sandy loam & silt loam	4	5	1

for class thresholds see Appendix E: FSL Class Definitions

Subsurface lithology and chemistry combined with the rate and direction of groundwater movement in these locations are likely to be the key factors influencing this wide variation of redox conditions. To firmly establish this, the profile of the contact between the underlying mudstone and the overlying gravels also needs to be mapped to model the flow through the unconfined aquifers constrained by mudstone aquitards. Although more work is required to identify why these sites exhibit such contrasting characteristics, this example clearly illustrates the spatial diversity of subsurface redox processes occurring in the Tararua GWMZ.

Table 14: Redox Classification and water type cluster membership (determined with HCA) in the Tararua GWMZ.

Redox Status	Redox Process	Cluster	Number of Sites	Sampling Method
Anoxic	CH4gen	3	2	1 Direct-push 1 Well
		4	3	3 Direct-push
	$Fe(III)/SO_4^{2-}$	2	4	1 Direct-push 3 Wells
		3	12	4 Direct-push 8 Wells
		4	1	1 Direct-push
	$Fe(III)/SO_4^{2-}$	3	4	4 Wells
	$Fe(III)/SO_4^{2-}$	2	1	1 Well

Mixed (anoxic)	Fe(III)-SO_4^{2-}	4		1	1 Direct-push
	NO3-CH4gen	5		1	1 Direct-push
	NO3-Fe(III)/SO_4^{2-}	2		2	2 Wells
		3		4	4 Direct-push
				1	1 Well
Mixed(oxic-anoxic)	O2-CH4gen	6		1	1 Direct-push
	O2-Fe(III)	2		1	1 Direct-push
		3		1	1 Well
	O2-Fe(III)/SO4	2		10	9 Direct-push
					1 Well
		3		8	8 Direct-push
	O_2-Mn(IV)	2		2	2 Direct-push
		3	2		2 Direct-push
	O_2-SO_4^{2-}	3	1		1 Direct-push
Oxic	O_2	1	19		19 Wells
		2	11		2 Direct-push
					9 Wells
		3	1		1 Well
Suboxic	Suboxic	3	1		1 Well

CH4gen = methanogenesis
SO_4^{2-} = sulphate
Mn(IV) =manganese
Fe(III) = ferric iron
NO_3^- = nitrate
O_2 = oxygen;

Curiously, site 50.3 (gravel; silt loam and clay loam; CC 4; DC 2; pHC 3; WT 0) displays both oxic and methanogenic characteristics; this site necessitated a very low pumping rate which reflected the low hydraulic conductivity of the fine grained alluvium derived from surrounding and upstream mudstone. Chemical parameters (determined with Jurgens et al., 2009 workbook) suggest that the groundwater sampled consists of both methanogenic and oxic characteristics. This unusual situation of extremely reducing water combined with high levels of DO may indicate only a thin body of methanogenic groundwater lies along the contact between the alluvium; and oxic groundwater overlies it. When pumping has abstracted the methanogenic groundwater, oxic groundwater is then drawn into the well. It is possible that air may have been mixed

with the groundwater as the cone of depression developed during pumping; but no evidence of air bubbles were noted at the time. There appears to be no clear spatial distribution of mixed-oxic water samples in the study area. However, mixed oxic-anoxic samples are disproportionally represented in the datasets i.e. 25 from 26 samples were collected with the direct-push (Figure 73). This is interesting and that mixed redox processes originate from merging of groundwater of different flow paths may not completely explain the tendency particularly for mixed oxic-anoxic water to be collected by the direct-push.

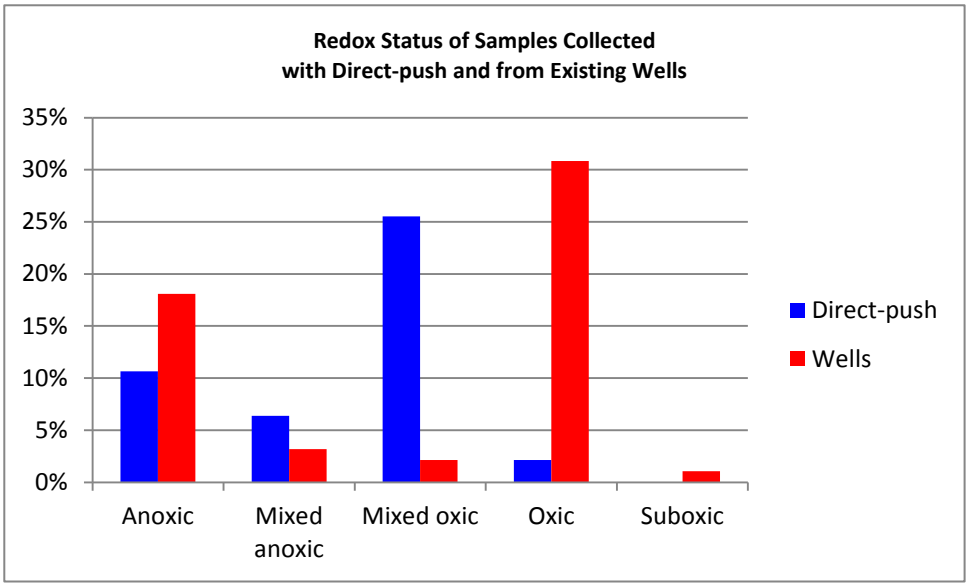

Figure 73: Redox status of groundwater samples collected with the two methods in the Tararua GWMZ. Groundwater collected from existing wells tends to be classified as either anoxic or oxic, while samples collected by direct-push appear to be more frequently mixed anoxic or oxic. The mechanisms that drive this phenomenon are unclear but may due to regular pumping affecting flowpaths, aquifer materials, or groundwater geochemistry which in turn controls redox reactions, or it may be due to the direct-push method itself.

6.4.6 Groundwater Type Classification

The groundwater type classification began with PCA of all groundwater parameters to determine the associations, if any, between the physical and chemical parameters. The PCA correlation matrix identified the rocks, soils, and subrocks were not significant factors (correlation scores < 0.3) of influence on groundwater hydrochemistry so were not considered in the subsequent HCA. The PCA was rerun and as the Kaiser-Meyer-Olkin measure of sampling adequacy score of 0.846 determined the analysis to be meritorious, an HCA was justifiably performed. Hierarchal cluster analysis (dataset n = 94) with SPSS identified three major clusters and three minor clusters (Figure 74). The three major clusters 1, 2, and 3 (numbered from the left of dendrogram) consisted of 19, 31 and 37 groundwater samples respectively, while the minor clusters 4, 5 and 6 had only 5, 1, and 1 groundwater samples respectively. Interestingly, Cluster 1 (CL1) was exclusively populated by existing well data, while clusters 4, 5 and 6 were populated entirely by direct-push data, the remaining clusters were relatively evenly subscribed to by both datasets. Over 70% of samples were allocated to either cluster 2 (CL2) or cluster 3 (CL3).

A trend of increasing DOC, DIC, major cations (except K^+) and anions, and decreasing NO_3^-, DO, and *Eh* suggested redox potential increased as cluster membership moved from left to right across the dendrogram. Not surprisingly the distinctive sites 18.1 and 50.3 (that featured regularly in the summary analysis above), were allocated unique clusters (CL5 and CL6 respectively), while other sites with notably high analyte levels (5.2, 11.3, 13.3, 23.3, and 50.8) were also clustered together in Cluster 4. The Stiff diagrams plotted below the dendrogram in Figure 74 reveal the trend of increasing anion and cation levels culminating in Cluster 6 (site 50.3).

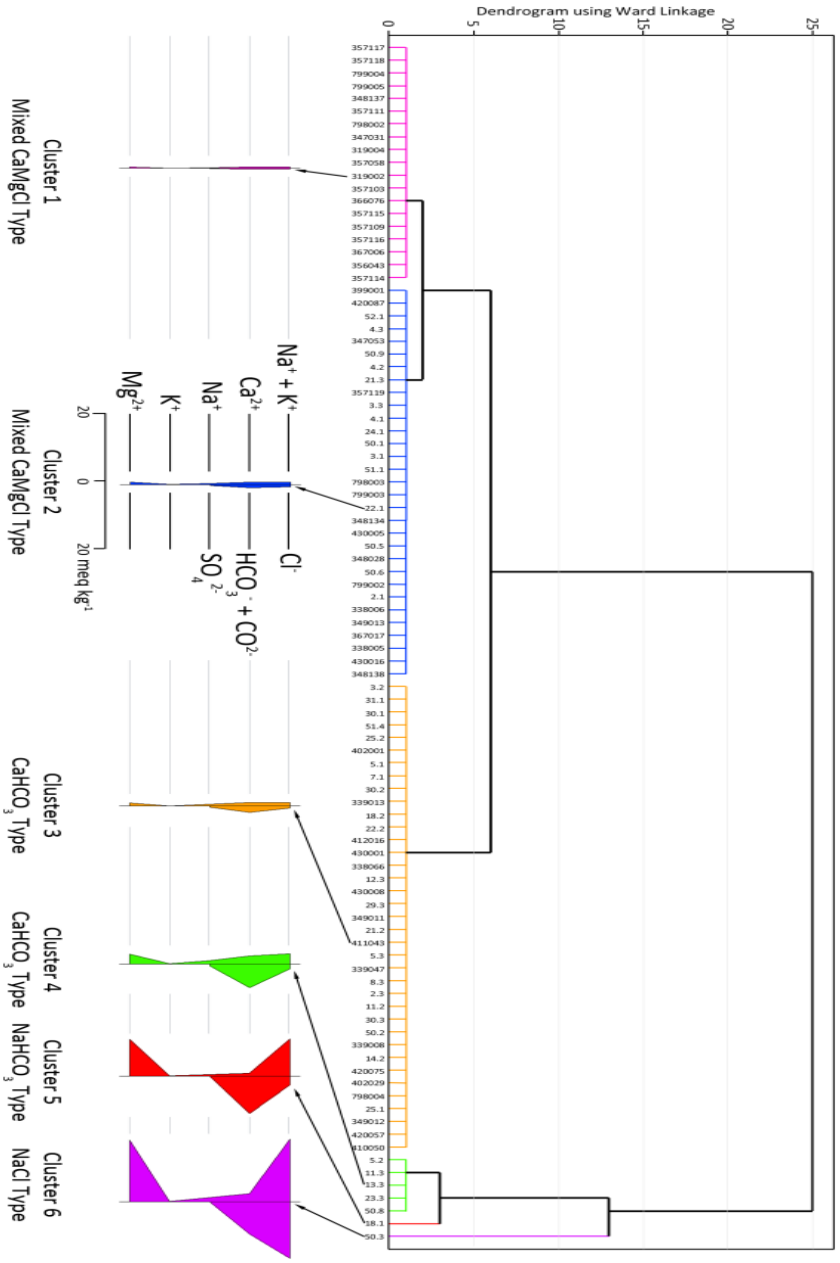

Figure 74: HCA Water type classification dendrogram of all groundwater samples (n=94) in the Tararua GWMZ 72% of groundwater samples are accounted for in the first three clusters. The other clusters show increasingly evolved hydrochemistry. The colours of the Stiff diagrams relate to the appropriate cluster in the dendrogram, while the shape is determined by the levels of cations (left of the vertical centre) and anions (right of centre) according to the scale shown on cluster 2 (2nd from left).

When analysed with ArcGIS v10.2 (Figure 75), it became evident that Cluster 1 (mixed Ca-Mg-Cl type, n = 19) represented sites in the upper Mangatainoka, Tamaki, Kumeti, and Oruakeretaki catchments, all of which exhibited DO levels > 1 mg L^{-1} and low levels of ionic species. This cluster shows characteristics typical of relatively young groundwater in steep terrain where the hydrochemistry in those catchments remains poorly evolved today-due to a combination of faster movement through the catchment, contact with thinner soils and relatively inert rock type (Beyer et al., 2016b).

Sites within Cluster 2 (n = 31) are distributed mainly in the lower reaches of the same catchments as Cluster 1 and extended to the lower Manawatu River. This cluster represents a mix of 19 anoxic/mixed anoxic, 11 oxic and 1 suboxic sites; all with slightly increased ion levels compared to Cluster 1. Overall, the hydrochemical facies of this cluster is similar to Cluster 1 and is reflected in a similar water type of mixed Ca-Mg-Cl.

Cluster 3 (n = 37) bracket slightly more evolved groundwater than the previous clusters, generally from sites along the central reaches of the Manawatu and Mangahao Rivers, and the areas north of Dannevirke. This cluster also includes two mudstone sites with more moderately evolved hydrochemistry (18.2 and 50.2), where more extensive groundwater reserves were encountered than the other mudstone sites. Samples from this cluster tend towards more anoxic water with 23 (n = 37) sites anoxic or mixed anoxic and increasing bicarbonate is recognised in a change in classification to Ca-HCO_3^- type.

Cluster 4 (n = 5) marked the first of the more chemically distinctive sites; all of which were sampled with the direct-push method. Only site 13.3 was located in the mudstone country; the others were located in gravel aquifers. These sites exhibited strong hydrochemical signatures which may indicate the groundwater at the sampling depth is poorly coupled to the unconfined gravel aquifers. Another possibility is the drill rods driven through the gravels and into the underlying mudstone, may have disturbed salt present in connate water within the sediments. Any salts present could be rapidly

dissolved into the surrounding groundwater and subsequently recovered along with the groundwater sample. Sites in Cluster 4 are all anoxic and compared to the previous clusters, increasingly chemically evolved, however although having a stronger chemical signature than Cluster 3; the water type for Cluster 4 remains Ca-HCO_3^-.

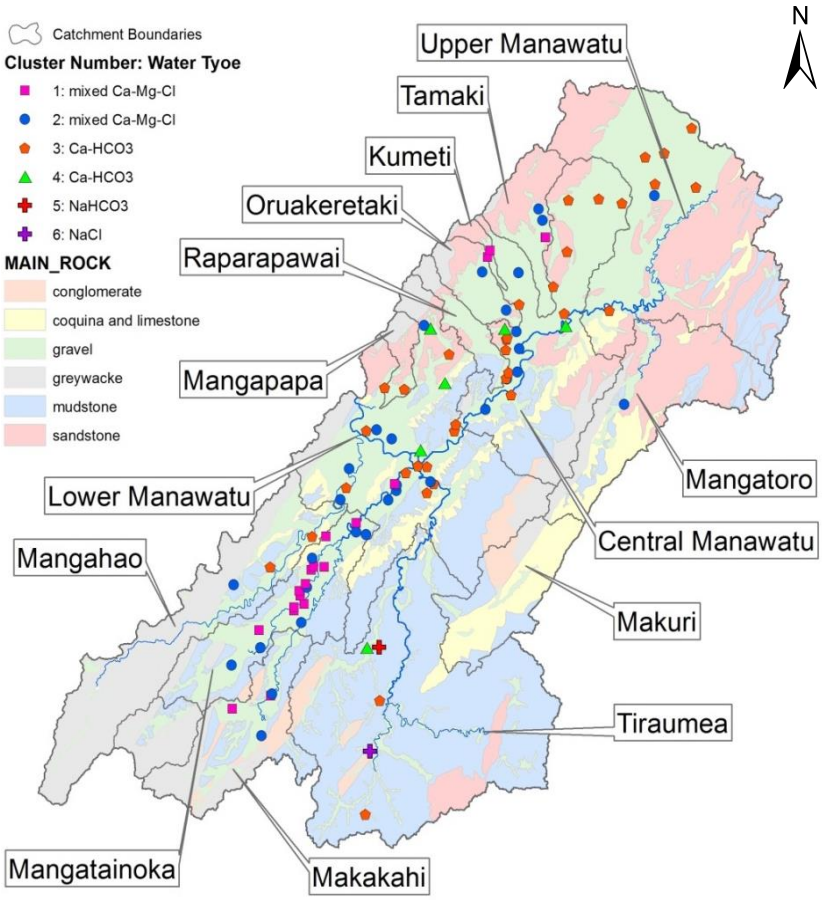

Figure 75: Groundwater clusters and water type in the Tararua GWMZ. Groundwater sites have been grouped according to the HCA output and laid over main rock groups. Clusters 1 and 2 the least evolved chemistry are generally found in the Mangatainoka and Manawatu and also the smaller Tamaki and Kumeti catchments near the ranges. Cluster 3 is represented by sites along Upper and Central Manawatu and tended to be associated with higher states of reduction. Cluster 4 has quite significant levels of anions and cations, the product of either extreme reducing conditions or significant mineral dissolution. Clusters 5 and 6 from the mudstone country exhibited extremely evolved groundwater chemistry and is believed to be the product of mineral dissolution and little dilution. Map generated in ArcGIS 10.2 using shapefiles from Heron (2014); Land Information New Zealand (2011b).

Cluster 5 consists of a single sample collected from site 18.1 (mudstone; silt loam; CC 4; DC 4; pHC 3; WT 3) in the mudstone country. Located at the foot of a small drainage

basin truncated by Pa Valley Road, the groundwater collected at this site had the highest DIC, B, SiO_2, pH, and HCO_3^- and second highest DIC, Cl^-, Br^-, NH_4^+ -N, Na^+, and SPC levels. This cluster also featured the lowest SO_4^{2-} which may indicate strongly reducing conditions. The boundaries of this small drainage basin are well defined and the influences on the water quality are likely to have come only from the soils and rocks within this small catchment. However, contribution to the groundwater by via fractures in the mudstone should not be discounted as the Pa Valley Fault strikes NE – SW along the Pa Valley (0.5 km away) and quite different lithologies are observed outcropping on opposing sides of Estcourt Road. The water type for this site is categorised as $NaHCO_3$ type.

Cluster 6 also consists a single sample (50.3; gravel; silt loam and clay loam; CC 4; DC 2; pHC 3; WT 4) collected in the mudstone east of Eketahuna. Previously discussed, the hydrochemical characteristics of this sample are extreme and resulted in a classification of NaCl water type.

6.5 Principal Component Analysis

Principal component analysis (PCA) was used to determine the groundwater chemical parameters that exerted the most significant influence on the variance within the datasets. Trials with different combinations of sites and parameters showed considerable variation in the PCA results, and it was difficult to conclude whether sites from Clusters 4, 5, and 6 should be considered outliers, or valid representatives of the diversity of the Tararua GWMZ's hydrochemistry. After careful consideration, the complete set of parameters from the entire direct-push and existing wells datasets (n = 94 sites) were analysed, and supplementary analysis from the dataset comprised of Cluster 1, 2, and 3 (n = 87 sites) are presented if significant differences between the n = 94 and n = 87 datasets were observed.

6.5.1 Principal Components

A principal component analysis was run on both n = 94 and n = 87 datasets. The transformed data satisfied the method's initial assumptions, and Bartlett's test of sphericity was statistically significant ($p < 0.0005$) which confirmed the data was suitable to be analysed by PCA. Examination of the correlation matrix revealed most variables except NO_2^- -N and SO_4^{2-} had at least one correlation coefficient greater than the acceptable limit of 0.3. As it is recommended to remove variables with correlation coefficients greater than 0.3 from the analysis (Laerd Statistics, 2015e), a PCA was performed without NO_2^- -N and SO_4^{2-}. However, the correlation matrices of both PCA's were virtually identical and as these analytes elements associate with redox processes, they were retained in further analysis. The Kaiser-Meyer-Olkin measure of adequacy (KMO) for the dataset was 0.842, and individual KMO scores were greater than 0.805 for all parameters (except NO_2^- -N and SO_4^{2-}); scores over 0.8 are regarded as "meritorious" by Kaiser (1974). The number of significant components to retain (the PCA generates as many components as variables, of which many have little influence on the variance) was determined initially based on the eigenvalues greater than one, and subsequently refined by visual scree plot analysis and the "total variance explained" falling between 60% and 70% (Laerd Statistics, 2015e). The PCA (n = 94) generated five components with eigenvalues exceeding one, which explained 48.9%, 12.8%, 8.4%, 6.3%, and 5.3% of the total variance, respectively. As three components explained over 70% of the total variance, and having inspected the scree plot and factor loadings, these three components were considered significant, while the remaining components are likely to represent noise within the data or insignificant processes (Nolan, 1999). Rotations are mathematical procedures that affect the loadings of each factor on the principal component(Bryant & Yarnold, 1995). Therefore rotations may be employed with the objective of deriving a simple structure, and aid interpretability (Yaremko, Harari, Harrison, & Lynn, 2013). As discussed in Section 5.7.9 the Varimax Orthogonal

Rotation is often used for groundwater analysis (e.g. Daughney, 2010; Donath et al., 2015; Helena et al., 2000; Meraat et al., 2017; Raiber et al., 2012; Rivas et al., 2017) and for consistency is used exclusively in this analysis.

A limitation of the PCA is that no explanation is given as to the commonalities of factors in each component, and therefore it must be inferred as to what each component may represent. Component 1 (Table 15; left) rotated component matrix for the n = 94 dataset) accounted for 48.6% of the sample's variance and displayed strong loadings (> 0.75) of Cl^-, Br^-, Na^+, and SPC and moderate loadings (0.50 to 0.75) of Mg^{2+}, K^+, and Ca^{2+}. These loadings are very similar to those identified by Rivas et al. (2017) with the analysis of existing 56 wells only. Although Rivas et al. (2017) were unable to positively identify the factors involved, they suggested either anthropogenic activities, volcanic materials, weathering and dissolution of greywacke rocks, or deposition of seaborne salts may be the key influences on Component 1 (Cmp1). Bearing in mind Clusters 5 and 6 are each represented by a single a sample; the chemistry of these clusters is very distinctive. Given the major ion levels found in Clusters 5 and 6, the vast deposits of marine sediments in the region, and that the chemistry of groundwater proximal to the greywacke ranges tended to be poorly evolved; interaction with marine derived salts and/or sediments may be a reasonable explanation for factors linked to Component 1. Component 2 (Cmp2) accounted for 12.8% of the variance, factors such as Fe^{2+}, Mn^{2+}, NH_4^+ -N, DO, and *Eh* were strongly loaded (> 0.75), and DOC, DO, HCO_3^-, and NO_3^- -N moderately loaded (0.50 to 0.75) onto this component; indicating that Cmp2 could be reasonably associated with redox related processes. This assumption is supported by positive loadings of Fe^{2+} and Mn^{2+}, and negative loadings of DO, *Eh*, and NO_3^- -N. By overlaying the redox status of their 56 wells over a raster layer generated with Cmp2 scores Rivas et al. (2017) were able to show that positive Cmp2 scores represent anoxic conditions. Component 3 (Cmp3) accounted for 8.4% of variance and exhibited strong positive loadings of pH, DIC, and HCO_3^-. Rivas et al. (2017) also encountered similar loadings and suggest these factors may be associated

with dissolution of carbonate minerals, which aligns with conclusions from previous analyses in this study.

A PCA was then performed using the n = 84 dataset (Table 15; right). With Clusters 4, 5, and 6 removed from the analysis, redox related parameters became strongly loaded onto Cmp1 and accounted for 41.6% of the variance, while Cmp2 (14.6%) was loaded with similar factors to Component 1 in the previous analysis where n = 94. Cmp3 displayed strong loadings of SO_4^{2-}, DOC, and strong negative loadings of DIC. Displaying 10.4% of the variance, this is a reasonably significant component but it is difficult to ascertain what processes this actually represents. Considering the "total variances explained" from the PCA's, the shift of Cmp2 from 12.8% in the first analysis, to 41.6% as Cmp1 in the second analysis, represents a significant change in the variances. The factors and their percentage weighting within each component appear to be relatively similar in both analyses. Except for SPC which changes from 11.25% of Cmp1 to 5.32% of Cmp2, K (9.26% to 5.63%) and SiO_2 (5.5% up to 11.25%) (n = 94 and n = 87 respectively); the significance or effect of this component on the analysis is not clear. The reversal of Cmp1 with Cmp2, when the samples with strong signatures are removed, suggest that across the greater Tararua GWMZ, the primary influence on groundwater chemistry may be interaction with mudstones and mineral dissolution. However, more work is required to conclude whether interaction with mudstones and mineral dissolution are the dominant influences on groundwater chemistry or to what degree groundwater chemistry is also influenced by redox reactions. Within the shallow gravel aquifers, redox processes are inferred to be the dominant factors that influence groundwater chemistry.

Table 15: PCA rotated component matrices (n=94, left) and (n=87, right) of groundwater samples measured in the Tararua GWMZ.

Rotated Component Matrix (n=94)

	Component				
Factor	1	2	3	4	5
idf.Cl^-	**0.916**	*0.162*	*0.097*	*-0.137*	*0.054*
idf.Br^-	**0.885**	*0.088*	*0.075*	*-0.190*	*-0.143*
idf.Na^+	**0.830**	*0.282*	**0.356**	*-0.052*	*-0.051*
idf.SPC	**0.823**	**0.321**	*0.281*	*0.046*	*0.132*
idf.Mg^{2+}	**0.705**	**0.369**	*0.266*	*0.021*	*0.260*
idf.K^+	**0.678**	*0.172*	*0.020*	**0.360**	*0.090*
idf.Ca^{2+}	**0.656**	*0.155*	**0.429**	*0.142*	**0.357**
idf.Fe^{2+}	*0.226*	**0.898**	*0.037*	*0.069*	*0.030*
idf.Mn^{2+}	*0.244*	**0.813**	*0.230*	*0.041*	*0.011*
idf.NH_4^+-N	*0.282*	**0.782**	***0.351***	*-0.002*	*-0.204*
idf.Eh	*-0.085*	**-0.727**	**-0.500**	*-0.088*	*-0.047*
idf.DOC	**0.489**	**0.583**	*-0.045*	*0.217*	*0.065*
idf.DO	*-0.193*	**-0.580**	**-0.475**	*0.108*	**-0.351**
idf.SiO_2	**0.402**	**0.527**	**0.411**	*-0.137*	*-0.103*
idf.pH	*0.126*	*0.239*	**0.867**	*0.163*	*-0.136*
idf.DIC	**0.490**	*0.147*	**0.752**	*-0.063*	*-0.130*
idf.HCO_3^-	**0.445**	**0.448**	**0.706**	*0.116*	*0.031*
idf.NO_2^--N	*-0.099*	*0.168*	*0.185*	**0.876**	*0.042*
idf.NO_3^--N	*0.105*	**-0.488**	**-0.498**	**0.567**	*0.131*
idf.SO_4^{2-}	*0.095*	*-0.043*	*-0.168*	*0.081*	**0.931**

Extraction Method: Principal Component Analysis.
Rotation Method: Varimax with Kaiser Normalization.
Rotation converged in 7 iterations.
idf.* = inverse df normalised dataset
Blue font = inferred redox related factor
Bold font = components > 0.3
Italic font = components < 0.3

Rotated Component Matrix (n=87)

	Component			
Factor	1	2	3	4
idf.Cl^-	0.105	**0.916**	0.077	-0.164
idf.Br^-	0.052	**0.841**	-0.012	-0.275
idf.Na^+	0.299	**0.840**	0.164	0.079
idf.SPC	-0.135	**0.403**	**0.441**	**0.395**
idf.Mg^{2+}	**0.377**	**0.752**	0.119	0.140
idf.K^+	**0.678**	**0.427**	-0.220	0.000
idf.Ca^{2+}	0.220	**0.739**	0.021	**0.337**
idf.Fe^{2+}	**0.779**	0.084	**0.451**	-0.030
idf.Mn^{2+}	**0.827**	0.235	0.159	0.050
idf.NH_4^+-N	**0.876**	0.157	0.131	-0.093
idf.Eh	**-0.863**	-0.076	-0.086	-0.179
idf.DOC	**0.417**	**0.353**	**0.567**	0.102
idf.DO	**-0.707**	-0.272	-0.009	-0.163
idf.SiO_2	**0.345**	**0.852**	-0.073	-0.036
idf.pH	-0.001	**0.505**	**0.319**	**0.395**
idf.DIC	**0.464**	**0.513**	**-0.527**	0.180
idf.HCO_3^-	**0.727**	**0.431**	-0.197	**0.308**
idf.NO_2^--N	0.165	-0.146	0.071	**0.813**
idf.NO_3^--N	**-0.679**	0.050	**0.367**	**0.405**
idf.SO_4^{2-}	0.096	-0.002	**0.678**	0.080

Extraction Method: Principal Component Analysis.
Rotation Method: Varimax with Kaiser Normalization.
Rotation converged in 8 iterations.
idf.* = inverse df normalised dataset
Blue font = inferred redox related factor
Bold font = components > 0.3
Italic font = components < 0.3

Br^- = dissolved bromide (mg L^{-1})
Cl^- = dissolved chloride (mg L^{-1})
DO = dissolved oxygen (mg L^{-1})
Eh = reduction potential (mV)
HCO_3^- = bicarbonate (mg L^{-1})
Mg^{2+} = dissolved magnesium(mg L^{-1})
Na^+ = dissolved sodium(mg L^{-1})
NO_2^- -N = nitrite nitrogen (mg L^{-1})
SiO_2 = dissolved silica (mg L^{-1})
SPC = specific conductivity (µScm^{-1})
Ca^{2+} = dissolved calcium(mg L^{-1})
DIC = dissolved inorganic carbon (mg L^{-1})
DOC = dissolved organic carbon (mg L^{-1})
Fe^{2+}= dissolved iron (mg L^{-1})
K^+ = dissolved potassium(mg L^{-1})
Mn^{2+}= dissolved manganese (mg L^{-1})
NH_4^+ -N = ammoniacal nitrogen (mg L^{-1})
NO_3^- -N= nitrate nitrogen (mg L^{-1})
SO_4^{2-}= sulphate (mg L^{-1})

A scatter-plot was generated with the redox related component on the horizontal axis and the other most significant component on the vertical axis. When the symbology of the scatter plot was coloured to the physical factor of interest, it provided a convenient means of assessing the influence of physical factors on the entire suite of redox characteristics. With the data points coloured to reflect their redox status (Figure 77),

the reduced groundwater samples (positive values) are plotted to the right of the vertical line (x axis origin 0) and oxic (negative values) to the left. Therefore, the centroids of each factor around 1.0 (x axis) may be considered reducing and those around -1.0, oxic, while centroids around zero may represent mixed oxic/anoxic conditions. The redox status centroids may be compared to the centroid of a physical factor of interest (e.g. Landuse or soil type) and conclusions drawn as to the nature of any associations between them.

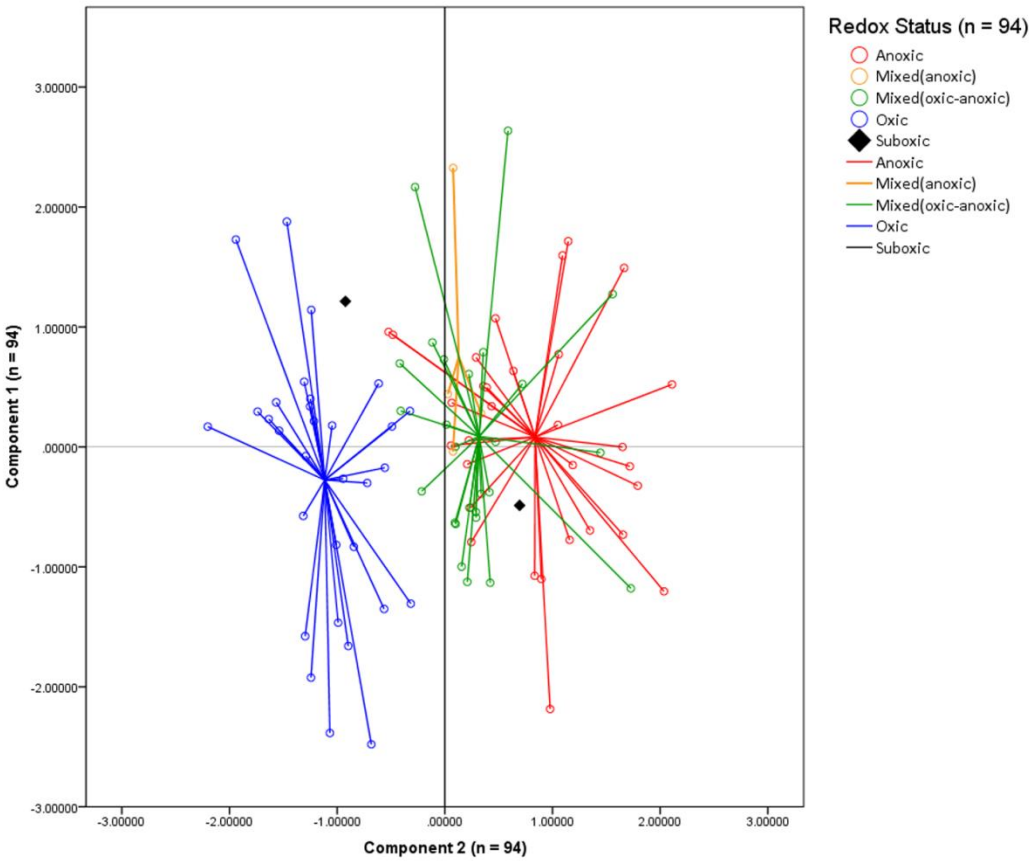

Figure 76: Scatter-plot of redox status plotted against Cmp1 vs Cmp2 scores for all samples n = 94. This scatterplot is compared with a similar chart generated with the n = 87 dataset and is discussed in the caption of Figure 77 *(continued on following page).*

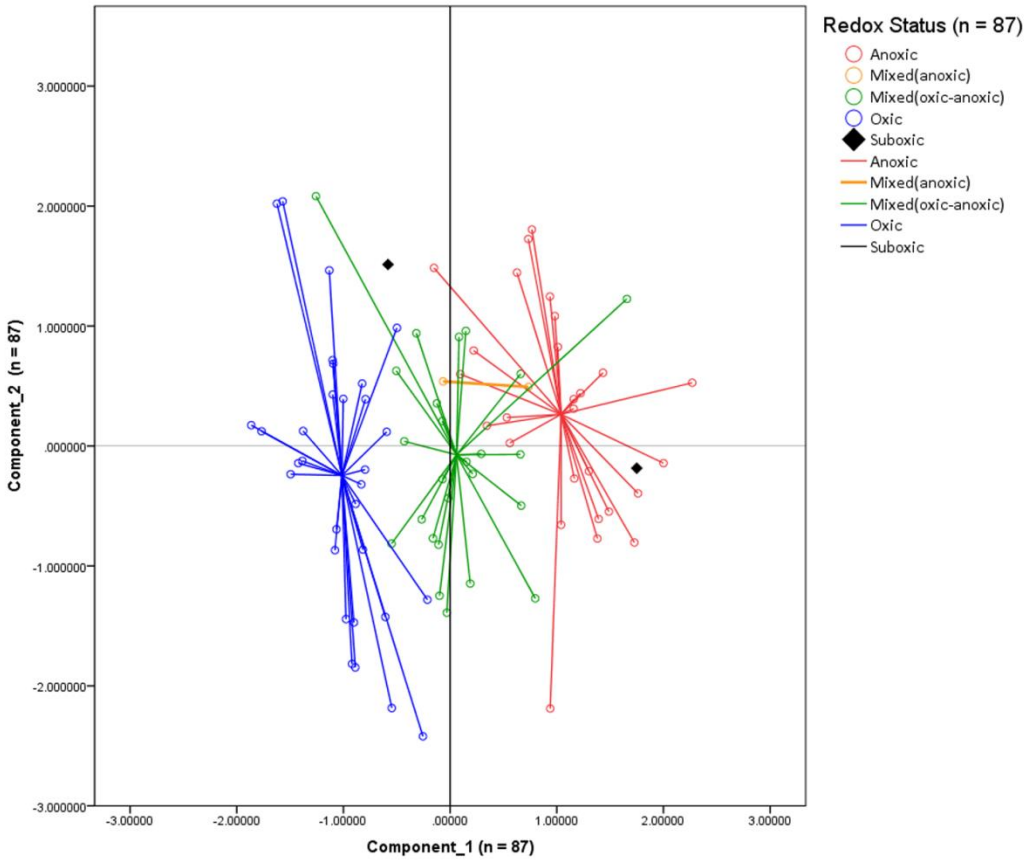

Figure 77 *continued*: Scatter-plot of redox status plotted against Cmp1 vs Cmp2 scores for all samples n = 87 (only clusters 1, 2, and 3). The component associated with redox conditions is plotted on the x axis. Red symbols indicate groundwaters with anoxic status; orange mixed anoxic; green, mixed oxic/anoxic; and blue oxic. Suboxic samples are plotted as black symbols without the spikes. The centroid of each redox status is clearly visible and further plots which seek to identify a variety of factors that influence groundwater quality may be referred to these plots and in order to identify their effect on the samples redox status. The effect of removing Clusters 4, 5, and 6 results in a slight change in distribution and clearer separation of the mixed oxic-anoxic group, but little other effects are apparent.

To further substantiate Cmp2 as a valid means to assess groundwater redox conditions, the ArcGIS v10.2 *spline tool with barriers* was used to interpolate a raster surface from Cmp2 data points using the minimum curvature spline technique (Figure 78). The resulting image when overlaid with the redox category shapefile reaffirmed the positive Cmp2 values > 1.0 (blue) align well with the sites classified as anoxic, and the negative Cmp2 values < -1.0 (red) align well with the oxic sites.

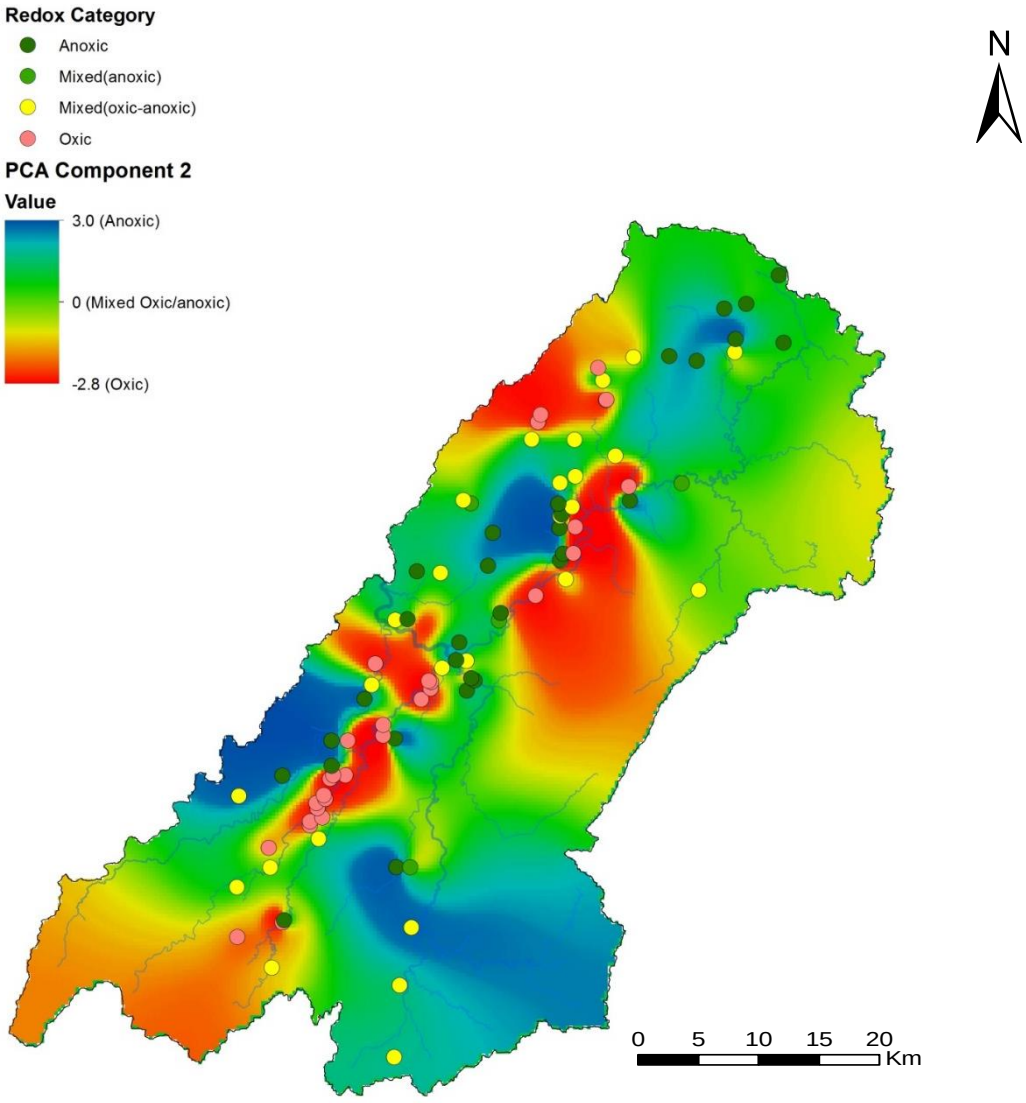

Figure 78: Spatial distribution of oxic and reducing conditions across the Tararua GWMZ. The base surface was generated from principal component 2; assessed to be associated with redox conditions. Earlier analysis suggested positive component values could be considered reducing and negative values oxidising. That the blue zones are strongly reducing and red zones are strongly oxic is confirmed by overlaying the redox category shapefile. The oxic (pink) wells align with the oxic red zones as do the green anoxic wells with the blue anoxic zones. The data was extrapolated to the eastern and south western margins of the Tararua GWMZ but it is unlikely the data is reliable in these areas and needs further investigations (Map generated in ArcGIS 10.2 using shapefiles from Heron (2014); Land Information New Zealand (2011b)).

6.5.2 Influences of Physical Factors on Redox Status

The analyses of preceding sections illustrate the variability of groundwater chemistry throughout the Tararua GWMZ. Inputs to the aquifers originate as dilute NaCl meteoric water, and although the influence of connate water is noticeable at some sites, poor connection between these (probably) minor and localised water bodies, results in their effect being masked by the sheer volume of meteoric water flowing through the system. The meteoric water undergoes a degree of modification (in some instances quite significant modification) during movement through the aquifers toward its eventual discharge via the Manawatu River. The redox conditions identified in this study range from extremely reducing methanogenic groundwater to oxic water similar in redox chemistry to that found in streams and rivers. That the water passes though different soils and lithologies, under different landuse regimes, at different rates, and resides for different durations, and mixes with other water types is evidenced by the range of hydrochemical facies encountered in this study.

A scatter plot (Figure 79) has been shaded to identify zones where principal components associated with oxic conditions (blue), mixed oxic/anoxic (green) and anoxic (pink) are located. Analyses of redox characteristics in this chapter will refer to these zones and appreciation of this figure will aid interpretation of other analyses using various physical parameters such as landuse, rock type and soil characteristics. By integrating a range of techniques, the following section attempts to identify the most significant physical factors that impose their influence on the redox chemistry of the groundwater. The physical factors are evaluated with a top-down approach, i.e. landuse is considered first followed by soil characteristics, rocks and subrock characteristics. Note, in the following section a number of analyses such as soil texture and QMap key-name are strongly influenced by small sample populations, but are presented nevertheless. This is done in order to offer a complete analysis where negative or null

results are considered valid outcomes of the research, and as such may be of significant value to future researchers (Knight, 2003)

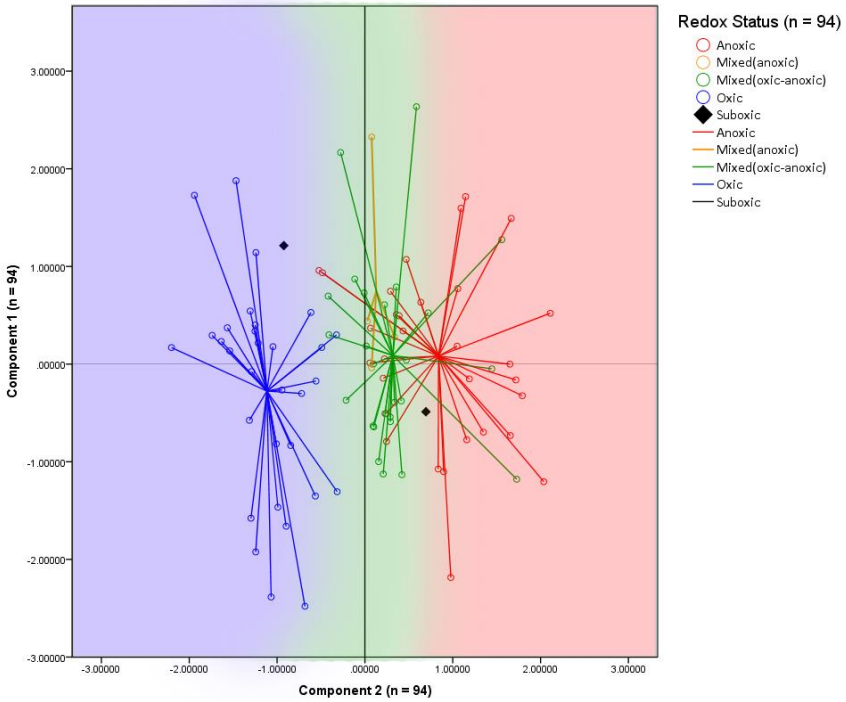

Figure 79: Cmp1 vs Cmp2 Redox status. This scatter plot has been shaded to identify zones where principal components associated with oxic conditions (blue), mixed oxic/anoxic (green) and anoxic conditions (pink). Appreciation of this distribution of these characteristics will aid interpretation of other analyses using a range of physical parameters.

6.5.2.1 Landuse

An objective of this analysis was to identify natural factors that influence the capacity of the subsurface environment to attenuate nitrate rich leachate, and establish whether the level of denitrification might be dependent or independent on the nature of the overlying landuse. To this end, a non-parametric Mann-Whitney (U) test was applied to the non-transformed groundwater chemistry samples, to test whether differences existed in the actual medians (rather than the medians of the transformed dataset) of groundwater redox related parameters between the main landuse classes of dairy and sheep/beef. An initial visual assessment of scatter plots confirmed the distributions of

groundwater redox parameters from both landuse classes were similar; which established the validity of the Mann-Whitney test for these data. The test determined that statistically significant differences did not exist between the medians of any of the redox parameters (except SO_4^{2-}) when considered in relation to dairy or sheep/beef farming; minimum U > 875, p > .083 when an exact sampling distribution for U was applied (Dineen & Blakesley, 1973). The test was repeated for the n = 87 dataset with similar results. That statistically significant differences were identified between the sulphate levels in groundwater under dairy and sheep/beef farming is interesting. However, more research is required to establish whether the differences in sulphate levels in the shallow groundwater is solely related to fertilizer inputs or perhaps due to dissolution or weathering of minerals e.g. pyrite-derived sulphate (Moncaster, Bottrell, Tellam, Lloyd, & Konhauser, 2000)

To complement the Mann-Whitney test, a scatter-plot was generated using the two main principal components (Cmp1 and Cmp2) with symbology that reflected the appropriate landuse for each sample (Figure 80). The distribution of this plot also indicates landuse has little association with the processes identified in either Cmp1 or Cmp2 (n = 94). There was slightly more separation between Cmp1 and Cmp2 in the n = 87 dataset but as with the larger dataset, no significant associations between landuse and the principal components were observed (Ledgard et al., 1999).

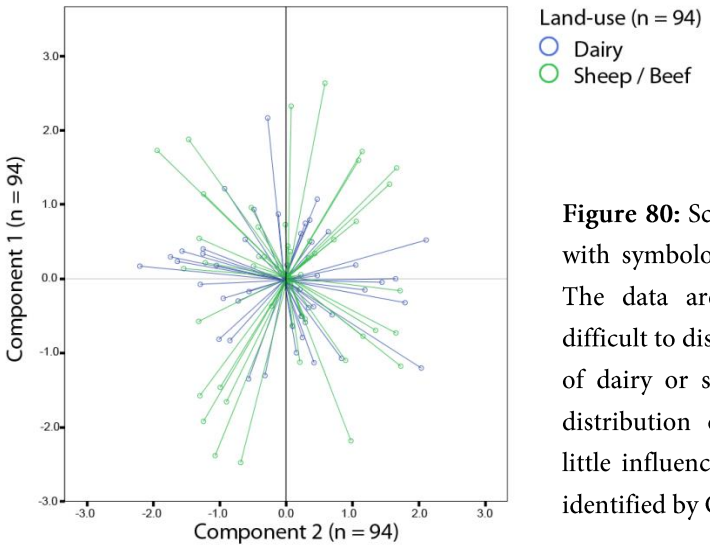

Figure 80: Scatter-plot of Cmp1 and Cmp2 with symbology related to main land uses. The data are well distributed and it is difficult to distinguish between the centroids of dairy or sheep/beef land-use. The even distribution of land use classes indicates little influence of landuse on the processes identified by Cmp1 and Cmp2.

In the study area, many dairy farms had designated effluent disposal areas. Some sites sampled with the direct-push method were adjacent to these areas and it was considered prudent to examine NO_3^- -N levels recorded at these sites. However, upon closer examination, it was established that aside from the effluent disposal areas, effluent settling ponds were often located quite near the cowsheds, as were the farm's water wells. Although determining the influence on groundwater quality from nitrate rich leachate (if any) from these sources may be an important factor in quantifying the effect of landuse on redox characteristics of shallow groundwater, the complexities of this analysis exceeded the scope of this thesis, and is not investigated further.

6.5.2.2 Soils

The influence of soils may be the strongest factor controlling the redox related chemical signatures of shallow groundwater (Beyer et al., 2016a). However, strong spatial variability in the distribution of soils, and interaction with other hydrological elements can mask the soil's effects on groundwater chemistry (Beyer et al., 2016a). To evaluate the influence (or association) of a range of soil classes and physical properties on groundwater quality, the relevant symbology was combined with scatterplots of Cmp1 vs Cmp2. In this series of scatter-plots large numbers of classes often cluttered the charts and made interpretation difficult (in these cases the centroid of the appropriate class was presented rather than the data points). The soil texture was initially investigated, followed by analysis of soil drainage, carbon, and soil pH to gain an appreciation of their effect on the groundwater's redox status. Note, in some of the following analyses it is likely the number of sites represented by each class influenced the results. For example Figure 81 illustrates this effect for soil texture, where the classes with the small sample sizes plot furthest from the vertical axis (x = 0). Therefore

parameters were combined whenever possible to increase the sample population, e.g. Figure 84 combines FSL soil textures into three texture classes.

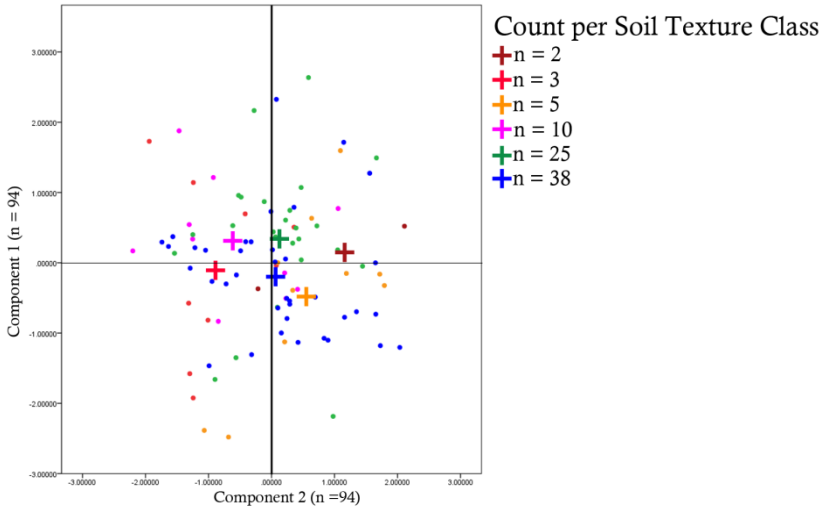

Figure 81: Scatter plot of Cmp1 and Cmp2 sample size vs soil type. When considering Component 2 (redox characteristics), the centroid markers for classes with 10 or fewer samples plotted (on the x axis) at either extent of the range, while the two larger classes (25 and 38 samples) plotted near the zero on the axis; possibly indicating the sample size is influencing the plots. However, when considering Component 1, the effect of sample size is not nearly so apparent. This is interesting and greater sampling density may be required to establish whether the centroids for the smaller samples are valid representatives of the sample population.

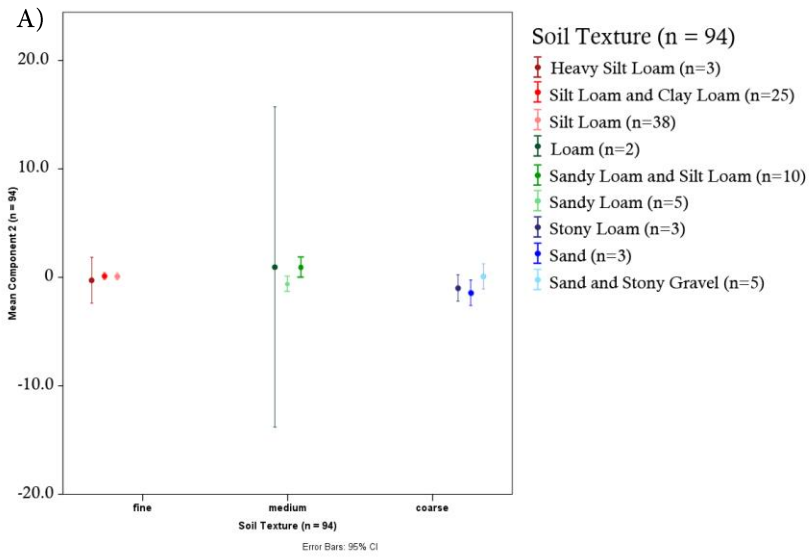

Figure 82: Error bar charts for soil texture and the mean of Component 2. *(continued on following page).*

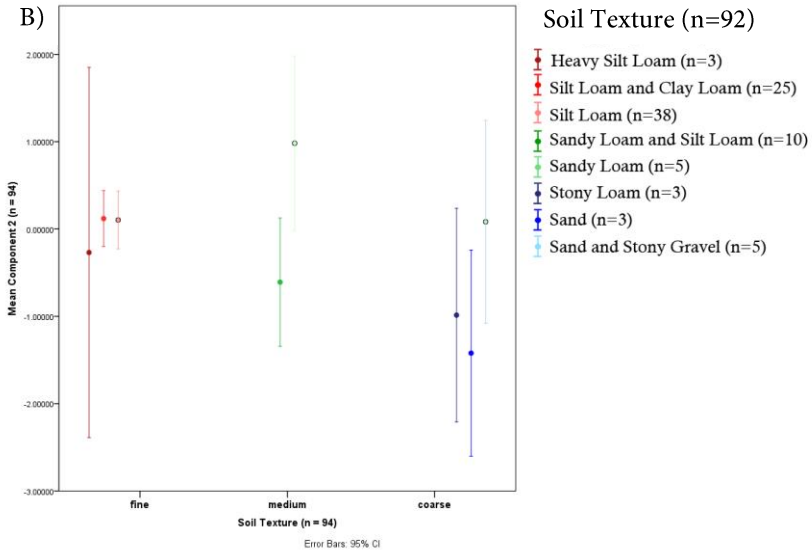

Figure 82 *continued:* Error bar charts for soil texture and the mean of Component 2. The extents of the vertical bars indicate where the mean of Component 2 for each soil texture might lie for 95% of samples. The Loam class n = 2 (green error bars in centre of chart a) has such a large effect on the means confidence limits that the y axis scale was -20.0 to 10.0, but by removing loam from the analysis the vertical axis scale decreased to 3 to -3. Therefore the benefit of analysing larger sample sizes i.e. silt loam, and silt loam and clay loam is obvious (chart B).

6.5.2.3 FSL Soil Texture

The FSL soil-class determined from the New Zealand Soil Classification Subgroups shapefile produced 21 distinct soil classes with small sample populations therefore was not considered further. The soil-texture classification also resulted in fewer relatively small sample populations (four classes less than n = 3) therefore further analysed. When the principal components were plotted with soil-type, the centroid for each soil-type class indicated reducing conditions are encountered in loam, and sandy loam, while oxic conditions are detected in sand, stony loam, and "sandy loam and silt loam". It could also be inferred that mixed oxic/anoxic conditions are found in sand and stony gravel, silt loam and heavy silt loam. As the soil-texture classes are ordered (in the legend) from finest to coarsest (A. Palmer, personal communication, September 27, 2017) similar coloured symbols might be expected to plot near to each other. The finer

textured soils might be expected to plot in the anoxic zone (x axis = ~1.0), medium in the mixed zone (x = ~0), and coarse in the oxic zone (x = ~-1.0). However, the finest soil textures plotted in the mixed zone while the medium textured soils plotted in the anoxic zone. The coarse textured soils such as sand and stony loam were strongly associated with oxic conditions, although what was interpreted as the coarsest soil type (Sand and Stony Gravel) plotted in the mixed oxic zone.

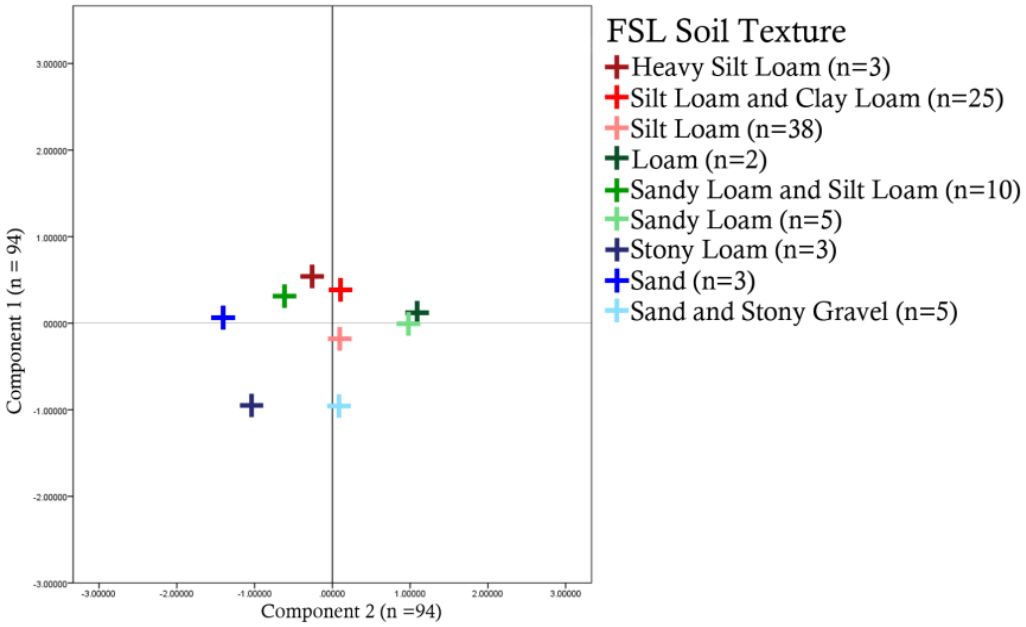

Figure 83: Relationship between FSL soil texture and redox characteristics of Cmp2 in the Tararua GWMZ. There appears to be an association between coarse soil texture and oxic conditions. There also appears to be a relatively strong association between sample size and the redox characteristics. The soil texture classes were simplified in the following analysis to further investigate this.

These inconsistencies may reflect either the soil texture classification was not correct; the legacy of the large scale soil maps where localised variations in soil-type may not be accounted for, or that soil textures have a degree of influence on groundwater chemistry but other hydrogeological factors also contribute. Therefore, soil texture is could be considered too broad to be applied in this manner. More research is required

with larger sample populations to clearly define which factor may have the most influence on the analysis. Additional research to define the soil-texture at the sample location may provide a clearer understanding of the key factors involved. The effect of sample size on soil-class was nullified to a degree (in a similar manner to Rivas et al., 2017) by simplifying the soil-type to three classes of soil-texture according to criteria presented in Table 16.

Table 16: Soil texture classification where FSL soil texture is simplified to only three groups.

FSL Soil Texture	Sample Size	Soil Texture	Texture Code	Sample Size
heavy silt loam	3	Fine	1	66
silt loam	38			
silt loam and clay loam	25			
loam	2	Medium	2	17
sandy loam	5			
sandy loam and silt loam	10			
sand	3	Coarse	3	11
sand & stony gravel	5			
stony loam	3			

Although sample sizes per class increased and the centroid of the coarsest texture plotted in the oxic zone, it was still a smaller sample population than the other two texture classes. It is difficult to predict whether the centroid for coarse textures lying in the oxic zone (where x values < -0.5) would shift should the analysis include more coarse texture samples. Careful interpretation of Figure 84 shows the spikes (i.e. lines radiating from the centroid to each data point the hollow circles) show little horizontal separation. That is the spread of coarse texture data points (blue) lie within the spread of fine (red) and/or medium textures (green). It is the vertical separation (component 1; inferred to be associated with mineral dissolution) of the centroids that gives the impression that the coarse texture class lies some distance away from the others.

The coarse textured soils might be expected to be associated with oxic groundwater due to higher hydraulic conductivity and higher rates of movement, and lower residence times possible in this type of medium. Why the converse does not hold for the finer soil textures is not immediately obvious. This example highlights the complexity of attempting to isolate the effects of any single physical factor on groundwater chemistry, when the chemistry is a product of many different interactions that occur from the time precipitation begins to fall, to its arrival at the sample location. As Figure 84 is a summary of variables based on Component 2 and may not completely reflect the weighting of individual variables. Therefore, a series of box plots of key redox parameters based on the three soil texture classes (Figure 85) were generated to supplement the scatter plots in Figure 84 and Figure 83.

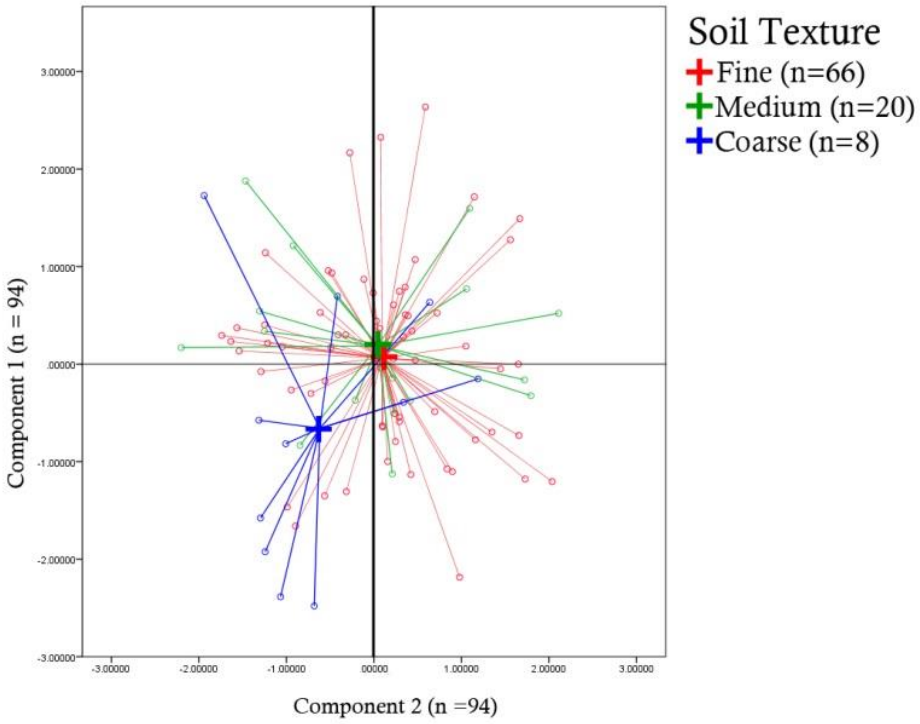

Figure 84: Scatterplot of soil textures. Results are similar to those recorded by Rivas et al. (2017) where coarse soil texture was associated with oxic conditions.

Fine soil textures tended to have higher DOC (Figure 85a), Fe^{2+} (D), and Mn^{2+} (F), and lower DO (B), and *Eh* (C) which indicate reducing conditions, while coarse textures

tended to indicate more oxic conditions (Figure 82). Note: The large number of outliers in the original datasets made visual analysis of boxplots virtually impossible, therefore the idf transformed datasets were used in this analysis. With the apparent association between fine soil textures and reducing conditions, nitrate nitrogen levels (Figure 85e) might have been expected to increase with coarsening soil texture, but this was not the case. It is possible that NO_3^- -N exceeding 10 mg L^{-1} at sites 420087, 50.6, 29.3, 430016, and 8.3 may have influenced the results, as some of these sites may be implicated with point source contamination rather than agricultural leachate; however following this analysis the n = 87 dataset where sites 420087, 50.6, 29.3, 430016, and 8.3 are removed was plotted but exhibited very similar results.

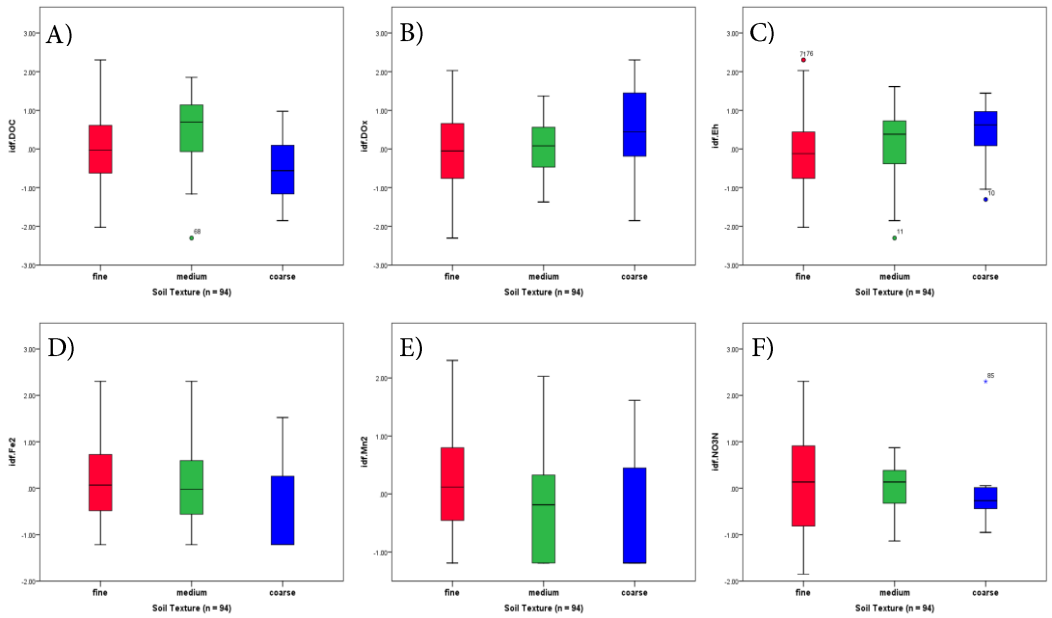

Figure 85: Box plots of key redox parameters plotted in relation to soil texture (A = DOC; B = DO; C = Eh; D = Fe^{2+}; E = Mn^{2+}; F = NO_3^- -N. Red = fine texture; green = medium and blue = coarse) in the Tararua GWMZ. Transformed data was used in this series as due to the occurrence of outliers it was more easily interpreted than non-transformed data. All parameters except NO_3^- -N (f) indicate coarse soil texture is associated with oxic groundwater and fine texture with anoxic groundwater. The trend for nitrates to decline as soil texture coarsens is interesting and difficult to explain.

6.5.2.4 FSL Soil Drainage

Soil drainage may be considered synonymous with soil texture (Rodway et al., 2016), however, a comparison between these classes reveals (in this dataset) the soil texture has a more subdued effect on the shallow groundwater's redox characteristics (Figure 86; Figure 87). To reduce the effect of small sample sizes, the FSL soil drainage classes were simplified by combining the moderately-well-drained class (n = 4) with the well-drained class (n = 56). The effect of soil texture and soil drainage on shallow groundwater chemistry was assessed by comparing the (Spearman's) correlation between soil texture and key redox parameters with the correlation between soil drainage and key redox parameters. Soil drainage was weakly correlated to DO, $r_s(92)$ = .226, p = .028; weakly negatively correlated to DOC $r_s(92)$ = -.237, p = .021; and moderately correlated to *Eh*, $r_s(92)$ = .328, p =.001; and NO_3^- -N, $r_s(92)$ = .322, p = .002, while the only statistically significant correlation for soil texture was a weak negative correlation with Mn^{2+}, $r_s(92)$ = -.237, p = .021. The moderate correlations of Eh and NO_3^- -N to soil drainage may give an indication, but do not provide a reliable means of predicting the redox characteristics of shallow groundwater. Following this analysis the n = 87 dataset was plotted with practically identical results.

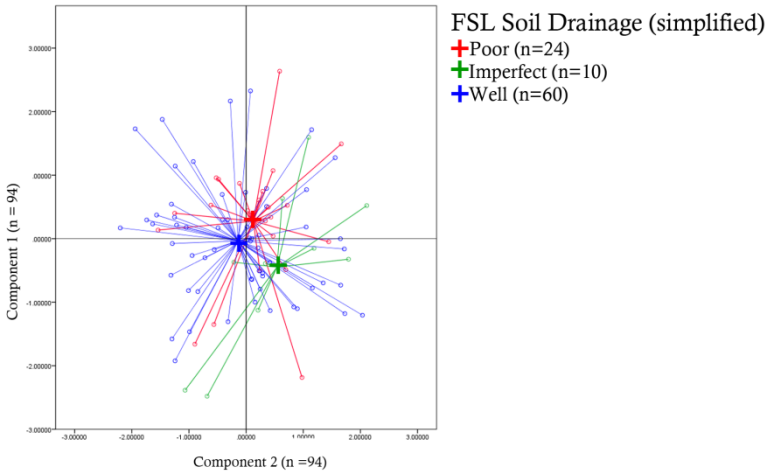

Figure 86: Scatterplot of soil drainage acquired from the Fundamental Soil Layer shapefile (Landcare Research, 2010c). The centroids indicate imperfectly drained soils tend to be associated with anoxic groundwater, although as in previous analyses, the sample size may be more significant than soil drainage.

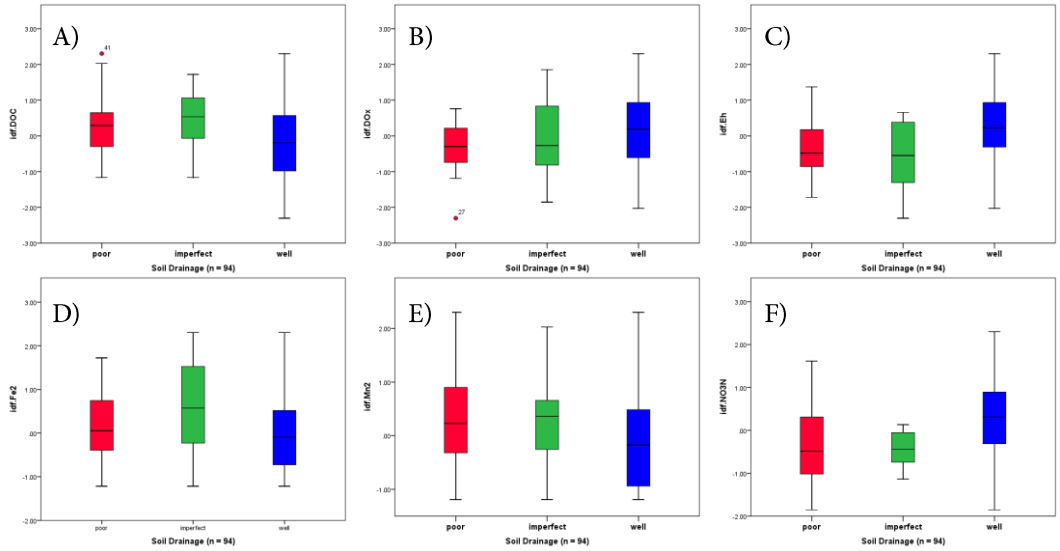

Figure 87: Boxplots of redox specific characteristics and soil drainage for transformed data (A = DOC; B = DO; C= Eh; D = Fe^{2+}; E = Mn^{2+}; F = NO_3^- -N). Well drained soils (blue) compared to poorly drained soils (red) appear to have higher DO, Eh , and NO_3^- -N levels, while DOC and Mn^{2+} levels appear to be lower in well drained soils. The Fe^{2+} levels presented in this boxplot appear higher in imperfectly drained soils and slightly lower in well drained soils. These charts support the assumption (when classified with the criteria used in this study) that poorly drained soil can be associated with anoxic conditions and well drained soils with oxic conditions.

Note Due to poor resolution in some charts generated with SPSS; please refer to the caption rather than figure labels.

6.5.2.5 FSL Soil Carbon

The soil carbon (organic matter content) in the FSL layers is an estimated weighted average for total carbon in the soil profile from 0 – 0.2 m depth (Landcare Research, 2010c). The influence of the soil carbon class was assessed by Spearman's correlation coefficient analysis to determine whether the level of soil carbon is correlated to the DOC found in the groundwater samples. The procedure determined a significant but weak correlation between the FSL soil carbon class and DOC of the groundwater samples $r_s(92) = .253$, $p = .014$; the other key redox related parameters were similarly analyzed but no further significant correlations were noted. The scatter plot of principal

components revealed the centroid of the high soil carbon class lay towards the anoxic zone (Figure 88), indicating the importance of available DOC for reduction to occur.

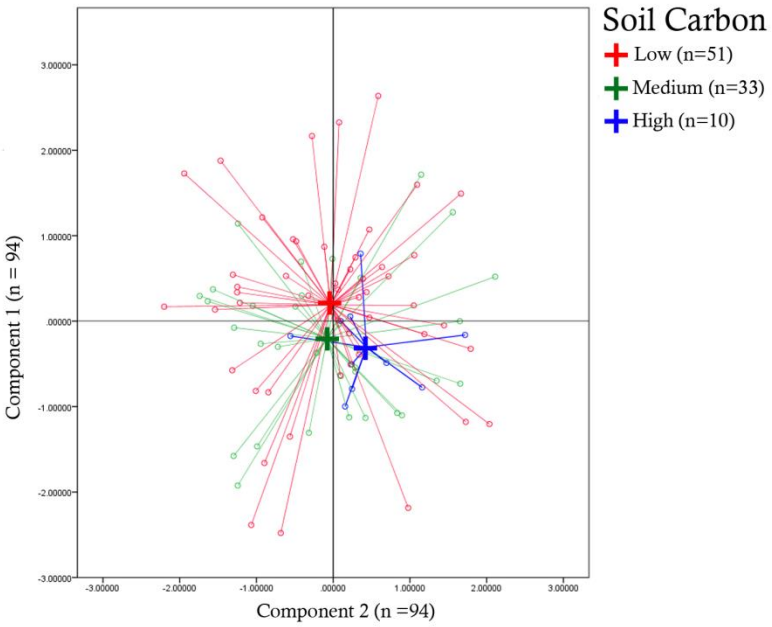

Figure 88: Scatterplot of FSL soil carbon classes. This plot shows high carbon levels may be associated with anoxic groundwater, but again this may be influenced by smaller sample numbers not reflecting the true population distribution.

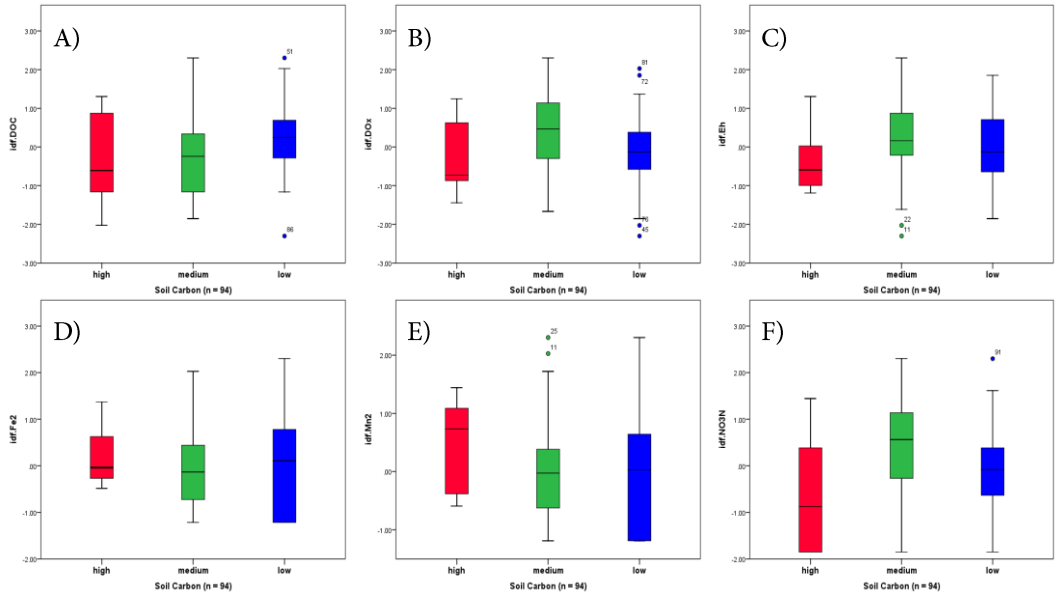

Figure 89: Boxplots of FSL soil carbon classes (A = DOC; B = DO; C = Eh; D = Fe^{2+}; E = Mn^{2+}; F = NO_3^- -N; Red = high; green = medium; blue = low). Low levels of DOC, DO, Eh, Fe^{2+}, NO_3^- -N, and higher Mn^{2+} were noted in high soil carbon classes, and indicates reducing conditions are associated with the FSL high soil carbon class.

The boxplot series for soil carbon reveals high soil carbon tended to have low DOC, DO, *Eh*, Fe^{2+}, NO_3^- -N, and higher Mn^{2+} (Figure 89). The distribution of Fe^{2+} levels between the soil carbon classes was difficult to compare; the minimum levels are highest in high soil carbon, but as the range was smallest, the median, and the firsts and third quartiles were lower than the low soil carbon class. Nevertheless the data supports stronger reducing conditions were associated with high soil carbon levels as determined from the FSL soil carbon data.

6.5.2.6 FSL Soil pH

As oxidation of water yields protons which may influence soil pH to a degree (Sparks, 2003), soil pH was investigated as a potential criterion for predicting redox status. For consistency the FSL soil pH class boundaries (Landcare Research, 2010b) were used despite being based on biological responses rather than physical characteristics. The scatterplot (Figure 90) reveals the centroid for moderately low pH lies within the oxic zone while the low and near neutral pH centroids lie towards the margins of the anoxic and mixed zones. This is an interesting trend but it is curious why in Figure 91 the low pH class plots to the right in the anoxic zone rather than to the left of the moderately low pH class in the oxic zone as one might expect the trend associated with lowering of pH to continue in the same direction.

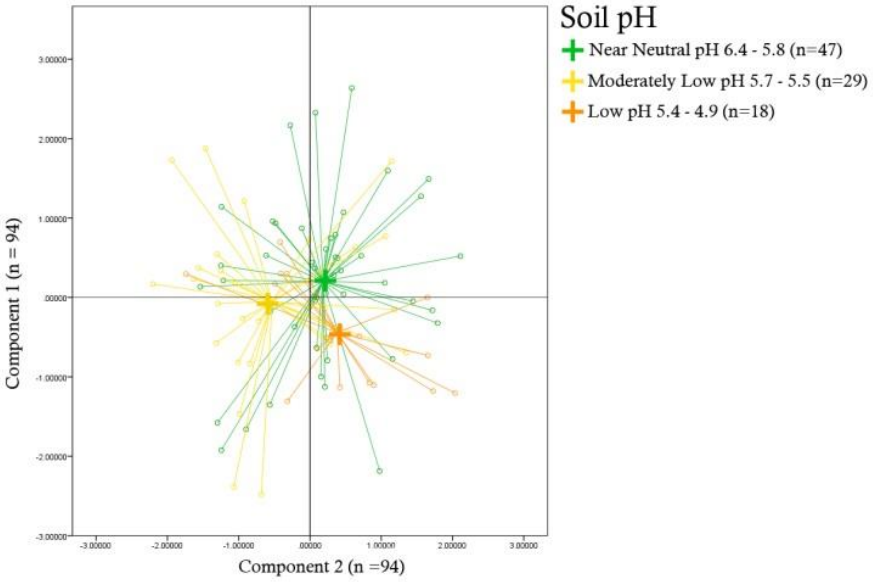

Figure 90: Scatterplot of FSL soil pH. This plot shows the near-neutral pH samples (green) tends to lie in the mixed oxic-anoxic zone, the moderately-low pH samples (yellow) in the oxic zone and the low pH samples (orange) in the anoxic zone.

Boxplots of soil pH (Figure 91) revealed the moderately low pH class exhibited low DOC, Fe^{2+}, and Mn^{2+} and high DO and *Eh* which supports Figure 90, where pH's between 5.5 and 5.79 may be associated with oxic conditions.

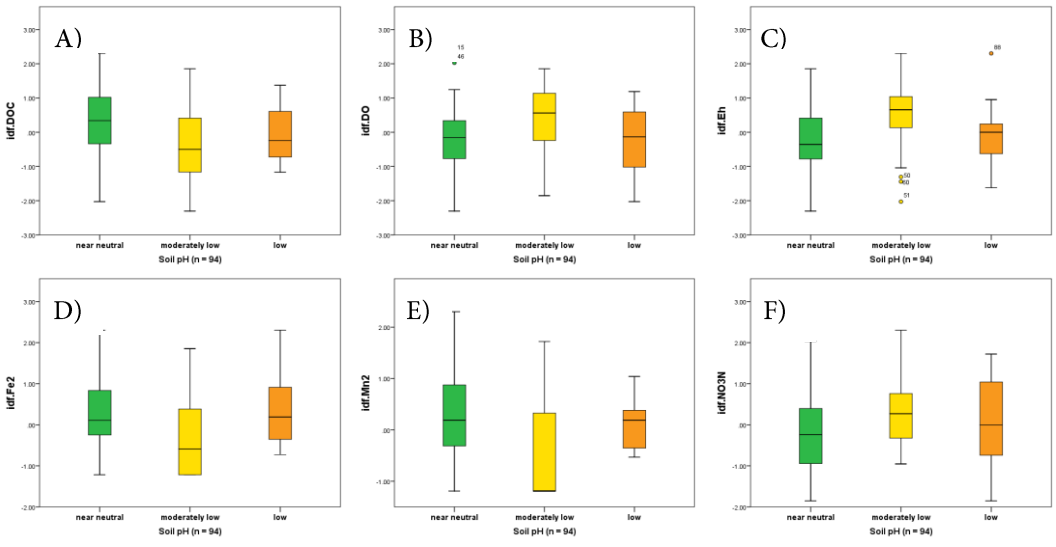

Figure 91: Boxplots of FSL soil pH (A = DOC; B = DO; C = Eh; D = Fe^{2+}; E = Mn^{2+}; F = NO_3^- -N. Green boxplot represents the near neutral class with a pH 5.8 to 6.49, yellow plots are moderately low pH (5.5 to 5.79), and orange plots are low pH (4.9 to 5.59). Other than indicating soil pH from 5.5 to 5.79 (yellow) is likely to be associated with oxic conditions, it is difficult to draw any other conclusions from these charts.

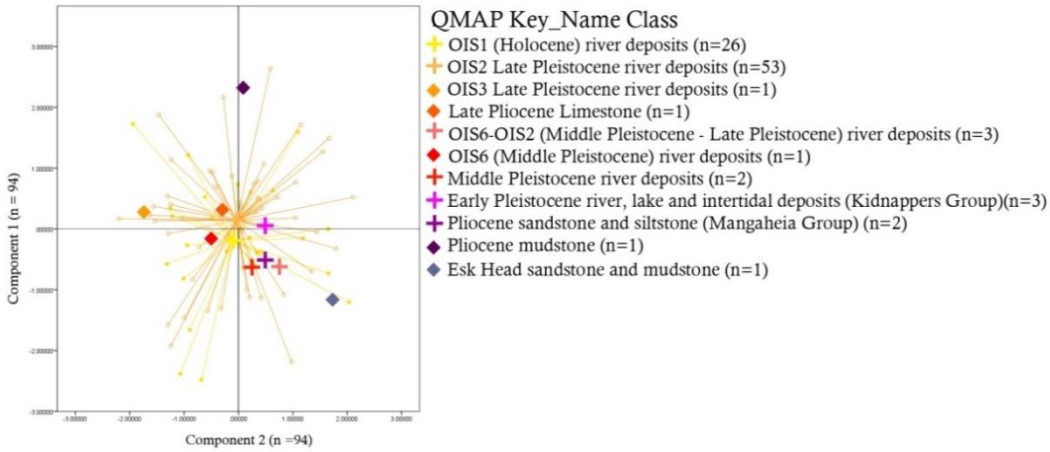

Figure 92: Scatter plot classified using QMap Key_Name criteria. Centroids are overlaid on the spikes for the two largest datasets (n = 26, n = 53) which allowed appreciation of the data distribution. The usefulness of increasing the number of classes was offset by influence of small sample sizes.

6.5.2.7 Lithological Characteristics

Although soils are attributed with having a significant effect on the redox potential (Rissmann et al., 2016), Rivas et al. (2017) identified a significant correlation between oxic conditions and gravel sedimentary units. QMap has several classes that categorise rock type at different grouping levels; at the highest grouping level an analysis using the QMap Main_Rock class was unlikely to provide any definitive results due to 89 of the 94 samples being located in the gravel main-rock class. Therefore, to provide robust analysis of the effect of rock type on redox characteristics of groundwater it was necessary to analyse the data with the classes defined in Appendix I: QMap Lithological Classes. The scatterplot of the two principal components plotted against Sim_Name (Figure 93) revealed Middle to Late Pleistocene river sediments and Early Pleistocene river lake and shoreline deposits plotted in the anoxic zone. This result aligned with the reduced groundwater generally encountered north of Dannevirke which was likely to be related to an abundance peat and lignite deposits observed in road cuttings, slips, river banks and stream beds throughout the area. The analysis with the Key_Name

classification (Figure 92) showed a wider distribution in centroids but it was difficult to determine whether this movement was due to the influence from samples where n ≤ 6.

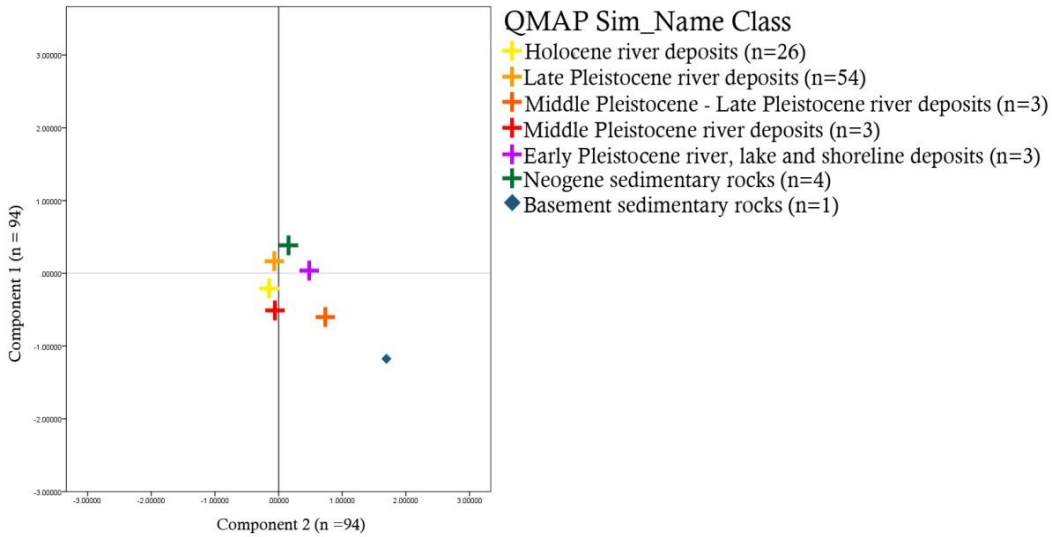

Figure 93: Scatter plot centroids for the QMap Sim_Name class. This chart reveals anoxic samples are collected from Middle – Late Pleistocene river sediments and Early Pleistocene river lake and shoreline deposits found in the northern areas of the Tararua GWMZ. Unable to be inferred from this figure, examination of QMap data reveals oxic samples are generally collected Holocene river deposits and Late Pleistocene river sediments with single samples from both Late Pliocene Limestone, and OIS6 (Middle Pleistocene) river deposits.

The single sample from the basement sedimentary rocks (grey rhomboid symbol) (collected from alluvium) at the base of the Tararua Ranges was also highly reduced. Site 50.9 (greywacke, silt loam; CC 4; DC 5; pHC 5; WT 1) lay 35 m east of a small fast flowing, gravel bedded tributary of the Wahaoteika Stream (Figure 94) and challenged the perception that groundwater adjacent to the greywacke ranges tended to be poorly evolved and generally oxic.

Although it was possible to simplify the QMap subrock class from eleven to eight classes, only two were larger than ten samples. As the properties of the larger classes were quite similar (sand, silt, clay and sand, loess, silt) further analysis of the subrock class was of little benefit. The main rock class was predominantly gravels and also little was gained from the analysis.

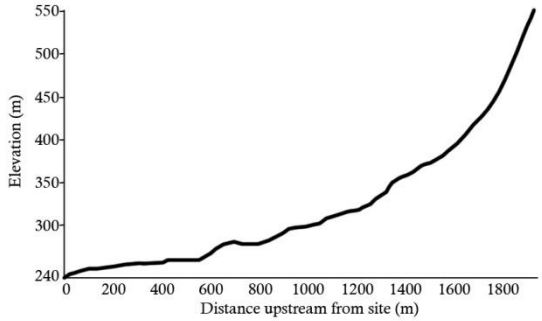

Figure 94: Elevation plot upstream of site 50.9. The streams rises in the very steep greywacke ranges and its origin is less than 2 km NW from the sample site. Although typically poorly evolved, groundwater close to the ranges may not always conform to this expectation, as illustrated by this site.

6.5.2.8 Water Type

The scatterplot of water type generated from the PCA components (Figure 95) reveal a distinct trend for mixed CaMgCl water type (derived from HCA clusters 1 and 2) to be associated with oxidising conditions, and $CaHCO_3$ water type (clusters 3 and 4) associated with reducing conditions. The $NaHCO_3$ water type (single sample from site 18.1) plots high in relation to the y-axis and close to zero on the x-axis and may be interpreted to reflect the influence of mineral dissolution on this sample's chemistry rather than redox influences. The high y-axis position of the NaCl water type and positive position on the x-axis suggests the chemistry of this (single) sample may be influenced by both mineral dissolution and by reducing conditions.

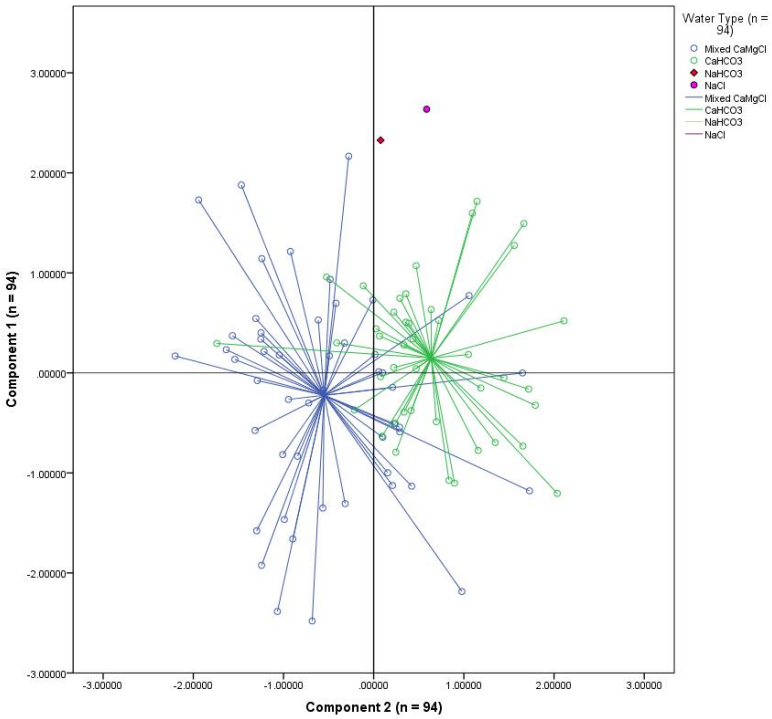

Figure 95: PCA component scatterplot of water type. Mixed CaMgCl (blue) water type was associated with predominantly oxidising conditions and derived from HCA clusters 1 and 2. The $CaHCO_3$ (green) water type derived from clusters 3 and 4 was clearly associated with reducing conditions. The high vertical position of $NaHCO_3$ and NaCl types (single rhomboidal symbols) reflect the influence of mineral dissolution on their chemistry rather than redox influences. The position of the NaCl water type relative to 0 on the x axis indicates it may be associated with reducing conditions.

When the redox category was assessed using Jurgens et al. (2009) workbook, a large number of samples were classed (particularly direct-push samples) as mixed oxic-anoxic which proved ambiguous to analyse. However, when the scatter plot of water type was scrutinized, it was interesting to note the relatively discrete plots and little overlap between Mixed CaMgCl and $CaHCO_3$ groups. Pearson's correlations (Table 17) indicate a strong association with water type and redox conditions where mixed Ca-Mg-Cl water displayed clear association with oxic conditions and $CaHCO_3^-$ type water with anoxic conditions. Of note is this water-type classification was determined using piper diagrams from only four cations (Ca^{2+}, Mg^{2+}, Na^+, K^+), three anions (HCO_3^-, SO_4^{2-}, Cl^-), and pH. This research analysed NO_3^- -N, NO_2^- -N, NH_4^+ -N, DO, Fe^{2+}, Mn^{2+}, and DOC to identify redox status of groundwater. Therefore using this method to classify

redox status with Ca-Mg-Cl and CaHCO3- type water may facilitate classification of groundwater redox characteristics from less comprehensive, and perhaps historic, analysis results.

Table 17: Pearson's moment correlation coefficients for water type and groundwater chemistry parameters measured in the Tararua GWMZ.

Parameter	Pearson's Correlation Coefficient	Strength
idf.Bromide	r(92) = 0.275, p < 0.0079	Weak
idf.Ca^{2+}	r(92) = 0.498, p < 0.0005	Moderate
idf.Cl^-	r(92) = 0.351, p < 0.0006	Moderate
idf.Depth	r(92) = 0.208, p < 0.0469	Weak
idf.DIC	r(92) = 0.545, p < 0.0005	Strong
idf.DOC	**r(92) = 0.412, p < 0.0005**	**Moderate**
idf.DO	**r(92) = -0.602, p < 0.0005**	**Strong (negative)**
idf.Eh	**r(92) = -0.792, p < 0.0005**	**Strong (negative)**
idf. Fe^{2+}	**r(92) = 0.603, p < 0.0005**	**Strong**
idf.HCO_3^-	**r(92) = 0.697, p < 0.0005**	**Strong**
idf.K^+	r(92) = 0.195, p < 0.0626	Weak
idf. Mg^{2+}	r(92) = 0.583, p < 0.0005	Strong
idf.Mn^{2+}	**r(92) = 0.667, p < 0.0005**	**Strong**
idf.Na^+	r(92) = 0.545, p < 0.0005	Strong
idf.NH_4^+ -N	**r(92) = 0.641, p < 0.0005**	**Strong**
idf.NO_2^- -N	**r(92) = 0.235, p = 0.0241**	**Weak**
idf.NO_3^- -N	**r(92) = -0.452, p < 0.0005**	**Moderate (negative)**
idf.pH	r(92) = 0.598, p < 0.0005	Strong
idf.SiO_2	r(92) = 0.613, p < 0.0005	Strong
idf.SO_4^{2-}	r(92) = 0.082, p = 0.4393	Weak
idf.SPC	r(92) = 0.508, p < 0.0005	Strong

note: the prefix idf indicates the use of inverse DF transformed data as explained in section

Br^- = dissolved bromide (mg L^{-1})
Ca^{2+} = dissolved calcium(mg L^{-1})
Cl^- = dissolved chloride (mg L^{-1})
DIC = dissolved inorganic carbon (mg L^{-1})
DO = dissolved oxygen (mg L^{-1})
DOC = dissolved organic carbon (mg L^{-1})
Eh = reduction potential (mV)
Fe^{2+}= dissolved iron (mg L^{-1})
HCO_3^- = bicarbonate (mg L^{-1})
K^+ = dissolved potassium(mg L^{-1})
Mg^{2+} = dissolved magnesium(mg L^{-1})
Mn^{2+}= dissolved manganese (mg L^{-1})
Na^+ = dissolved sodium(mg L^{-1})
NH_4^+ -N = ammoniacal nitrogen (mg L^{-1})

NO_2^- -N = nitrite nitrogen (mg L^{-1})

NO_3^- -N= nitrate nitrogen (mg L^{-1})

SiO_2 = dissolved silica (mg L^{-1})

SO_4^{2-}= sulphate (mg L^{-1})

SPC = specific conductivity (µScm^{-1})

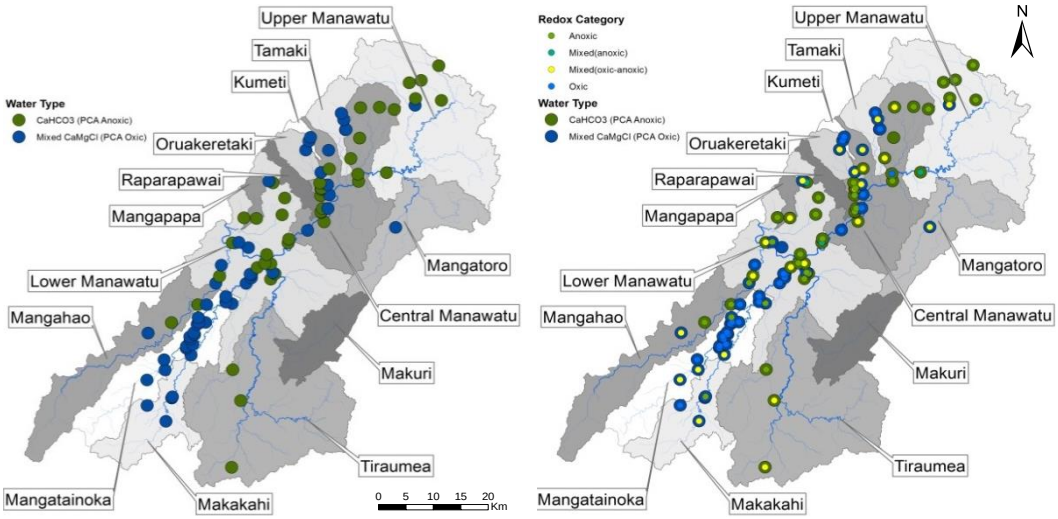

Figure 96: Redox category generated by two different methods. The clear differentiation between the oxic/anoxic water types determined with PCA analysis (left) may allow mixed oxic-anoxic water determined by Jurgen's workbook (right) to be further classified as either oxic or anoxic water. Smaller, yellow symbols (right) indicate mixed-oxic-anoxic water, the dominant redox category as determined by PCA are shown by the larger underlying symbols. The water type classification fits relatively well with spatial patterns of oxic/reducing conditions identified in this study Map generated in ArcGIS 10.2 using shapefiles from Heron (2014); Land Information New Zealand (2011b).

6.5.2.9 Nitrogen Attenuation Classes

The preceding analyses illustrate the complexity of predicting redox characteristics and that no single factor may fully explain the variability in groundwater redox conditions exists across the Tararua GWMZ. Furthermore, the influence of sample size is recognised in this study and that simplification of physical characteristics based on potential influence on redox characteristics is required. To this end methodology of R Singh et al. (2017) and (Elwan, 2015) was followed where physical characteristics such as soil texture, drainage, and carbon levels (determined at each site with ArcGIS

v10.2) were assigned a score of 1 to 3. Different groupings of these physical factors may then be combined, averaged to provide an attenuation factor (R Singh et al., 2017) that presented a simple reflection of the cumulative influence a range of factors may have on the level of nitrogen attenuation.

In this study an attenuation score of 1 represents a high denitrification potential and a score of 3 a low denitrification potential. For example, soil characteristics as soil carbon, pH and drainage class were determined at each site by merging site location data and FSL soil maps with ArcGIS v10.2; while characteristics such as carbon availability was derived from rock type. Peat or lignite as sources of dissolved organic carbon were assessed to have high influence on redox (and therefore assigned a score of 1), limestone was assessed to have moderate carbon availability and therefore assigned a score of 2, and marine mudstones and greywacke were considered to have low carbon availability and assigned a score of 3. Characteristics such as rock porosity or drainage was assessed, but found difficult to quantify due to conflicting characteristics. For example gravels were considered to have rapid drainage that generally result in low attenuation, slow water movement within the subsurface was associated with greater opportunity for denitrification. However, marine mudstones with very low intrinsic permeability were generally considered aquitards where little available groundwater exists and consequently any attenuation is probably of little importance.

The average attenuation score generated from a wide variety of groupings of physical characteristics were then analysed in ArcGIS v10.2 and assessed visually with both maps and with scatterplots of principal components (Cmp1 vs Cmp2, n = 94) in SPSS (refer to section 6.5 Principal Component Analysis). The parameters and attenuation scores assigned in this analysis are presented in Appendix J: Attenuation Classes. The average of combined attenuation factors lay anywhere between 1 and 3, and to represent these values as three discrete classes required defining class limits (i.e. bins). Determining to which bins the attenuation factor should be allotted was difficult.

Bin limits could be arbitrary defined e.g. bin 1 = 1.5 to 2.0; bin 2 = 2.01 to 2.5; and bin 3 = 2.51 to 3.0, or the bin limits could be defined as bin 1 = 1.0 to 1.75; bin 2 =1.76 to 2.25; and bin 3 = 2.26 to 3.0; but different arbitrary bin limits significantly influenced the nature of groupings. In order to provide an unbiased assessment of the combined nitrogen attenuation scores, bin limits groups were classified using Jenks natural breaks. This was undertaken by importing the average attenuation factor for each site into ArcGIS v10.2 and classifying them using *properties>symbology>classify>Jenks Natural Breaks (3 classes) system* to provide unbiased bin limits.

Despite assessing nearly all possible combinations of physical characteristics with this method Appendix J: Attenuation Classes, few outputs bore any clear similarity to Figure 77 (scatterplot of redox status plotted against Cmp1 vs Cmp2, n= 94). Although the scatter plot centroids were sometimes similar to those generated in Figure 77, none of the combinations of characteristics completely matched it. Of all the scatter plots, combination_3, i.e. FSL soil gravel class + FSL soil pH + FSL soil drainage + FSL soil carbon + FSL soil texture + QMap subrock carbon content was considered (arguably) the best fit to the redox characteristics scatterplot (Figure 97).

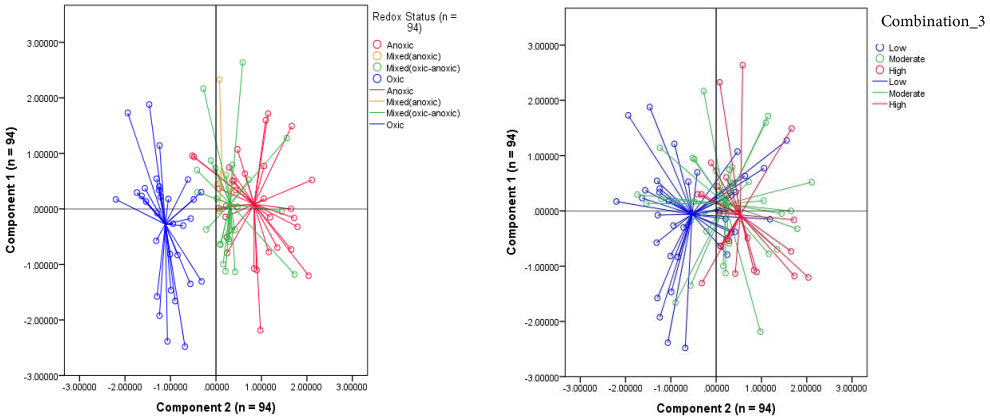

Figure 97: Redox category and attenuation class comparison. Left: Cmp1 (Y-axis) vs Cmp2 (x-axis) shaded to reveal redox category (blue, oxic; green, mixed oxic-anoxic; orange, mixed anoxic; red, anoxic). Note the distinct separation of oxic from mixed and anoxic samples and relatively little overlap between the mixed categories. Right: attenuation class_3 generated from FSL soil gravel class, pH, drainage, carbon, soil texture and carbon content of subrocks. One of the better matches to the redox status chart, attenuation class_3 is still far from a precise match.

Vector maps were created from each of these parameters in combination_3, and then combined to produce a map with three attenuation classes, i.e. low, medium, and high capacity to attenuate nitrogen. The results from this analysis were disappointing. As can been seen from Figure 98 the attenuation classes fit very poorly with the redox category determined at each site. Close et al. (2016); Rivas et al. (2017); and R Singh et al. (2017) successfully demonstrated similar strategies could be applied to model redox conditions from similar parameters but identifying the key factors and assigning an accurate attenuation factor that could be applied across the Tararua GWMZ was complex and required lengthy analysis which exceeded the time frame of this thesis.

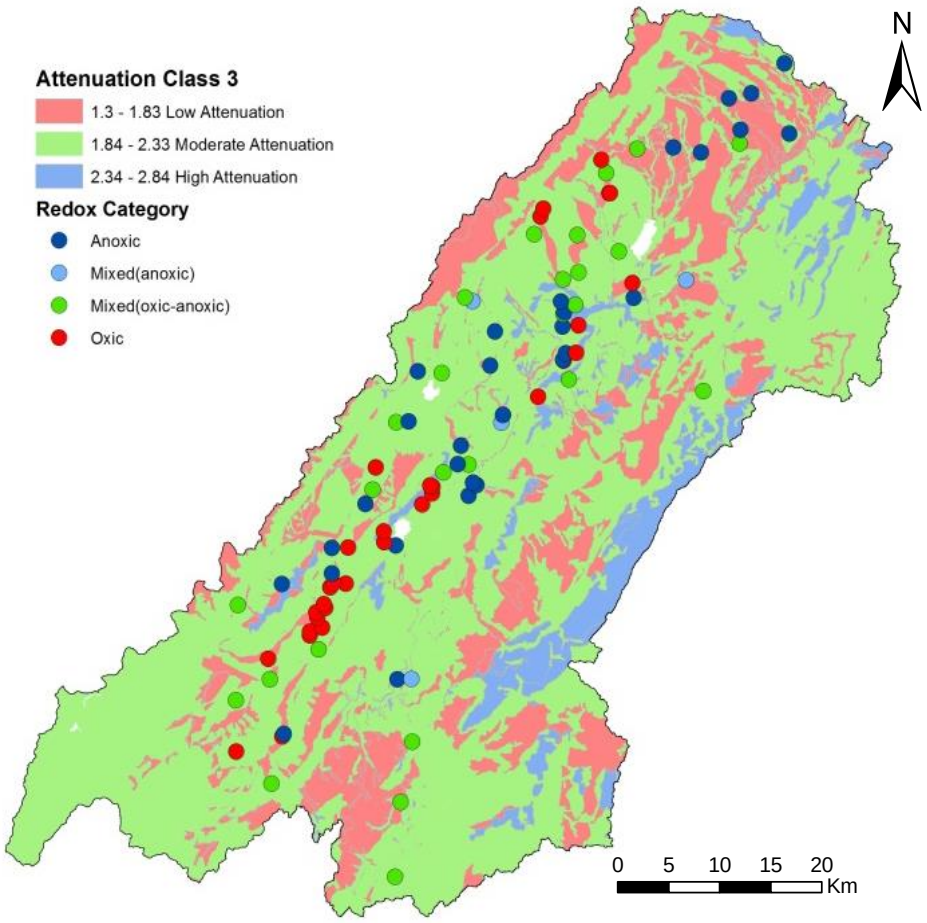

Figure 98: Spatial representation of Nitrogen attenuation classes. The attenuation classes derived from FSL soil gravel class, pH, drainage, carbon, soil texture, and carbon content of subrocks do not match the actual redox characteristics measured at the wells sampled. Other researchers have had success with this method and with further refinement it is likely similar success could be achieved. (Map generated in ArcGIS 10.2 using shapefiles from Heron (2014); Land Information New Zealand (2011b)).

Although this series of maps did not fit the distribution of redox conditions in the Tararua GWMZ particularly well, the surface developed with the spline tool (Figure 99) appears to be an effective means of predicting redox at a given location in the Tararua GWMZ.

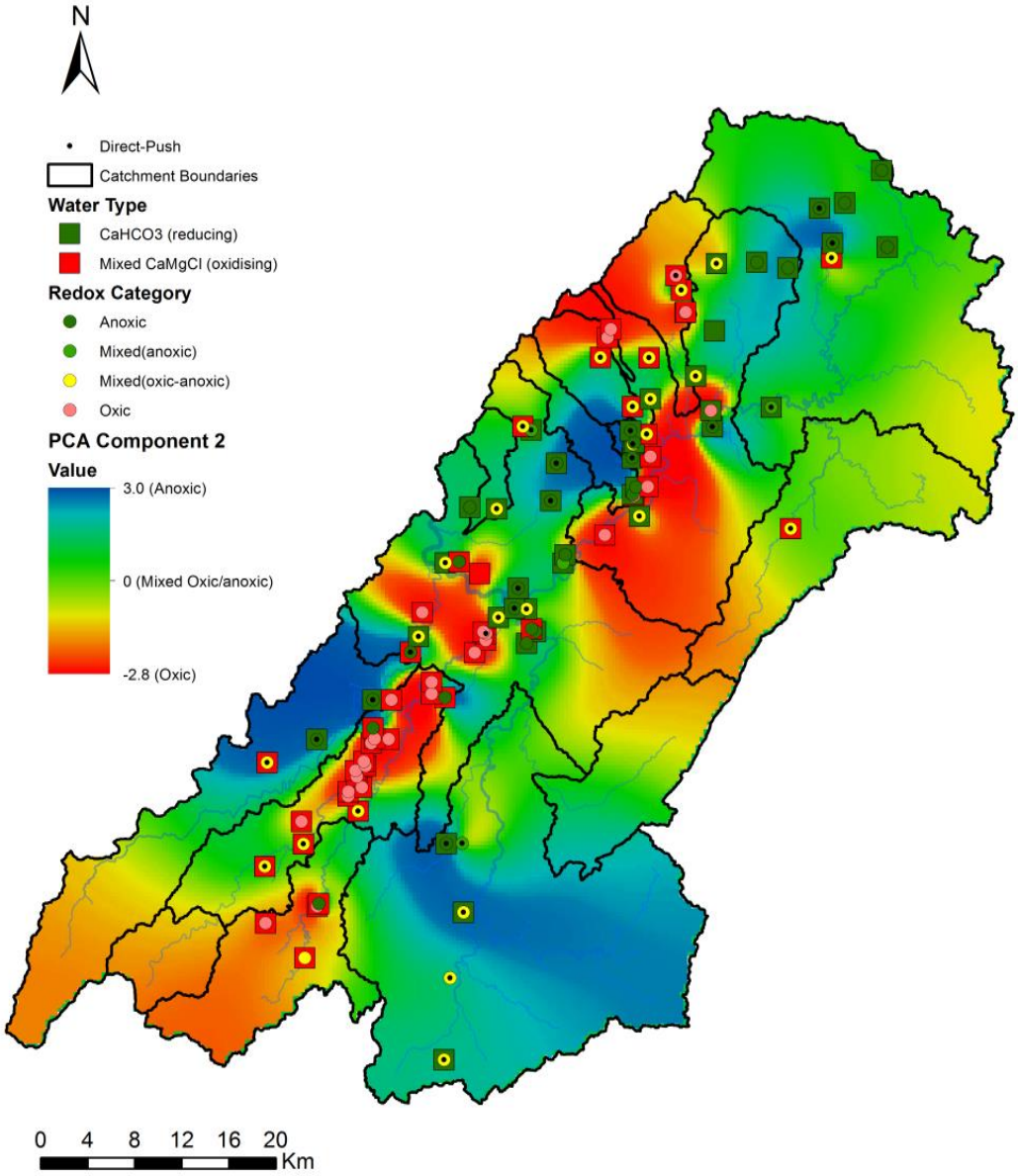

Figure 99: Spatial distribution of oxic and reducing conditions across the Tararua GWMZ. Catchment boundaries outlined in black. The base surface is generated from principal component 2 associated with redox conditions. Wells determined from hydrochemistry to be oxic (pink) wells align with the oxic red zones, and the green anoxic wells with the green to blue anoxic zones. $CaHO_3$ water types align with reducing areas, and Mixed CaMgCl type with oxic areas. (Map generated in ArcGIS 10.2 using shapefiles from Heron (2014); Land Information New Zealand (2011b)).

The complexity of predicting redox conditions revolves around the huge variations between catchment characteristics through which infiltrated precipitation travels is illustrated by Figure 100 (mid-west Tararua GWMZ). This map was generated in ArcGIS v10.2 by using the *Fill Tool* (*Spatial Analyst Tools>Hydrology>Fill)* to remove small imperfections in the DEM, then creating a Flow Direction Model (*Spatial Analyst Tools>Hydrology>Flow direction*), and snapping a pour-point (*Spatial Analyst Tools> Hydrology>Snap Pour Point)* to the watercourse nearest to the sample location. The catchment extent upstream of the pour point was then delineated using the *Watershed* Tool (*Spatial Analyst Tools> Hydrology>Watershed).* To show the variability of the geology between the catchments the symbology of the catchment shapefile was classified to the subrocks category and overlaid on the Tararua GWMZ DEM. From this map (Figure 100) it is possible to appreciate the differences in orientation, size, and geology of basins in the Tararua GWMZ through which infiltrated precipitation must move to reach the sample point. Furthermore, the complexity of catchment characteristics are compounded when considering that precipitation may have fallen anywhere within the boundary of the basin. Although precipitation may infiltrate and flow through the same catchment, the length of time, distance, and substrate the precipitation flows through will also vary and will exert varying degrees of influence on the groundwater chemistry. Figure 100 serves to illustrate the difficulty in predicting or assessing redox characteristics from a single or a group of characteristics at a given location. Not only are the size, aspect and slope of catchments unique, but the subrocks, soils, groundwater and flowpaths and hydraulic gradients are extremely variable.

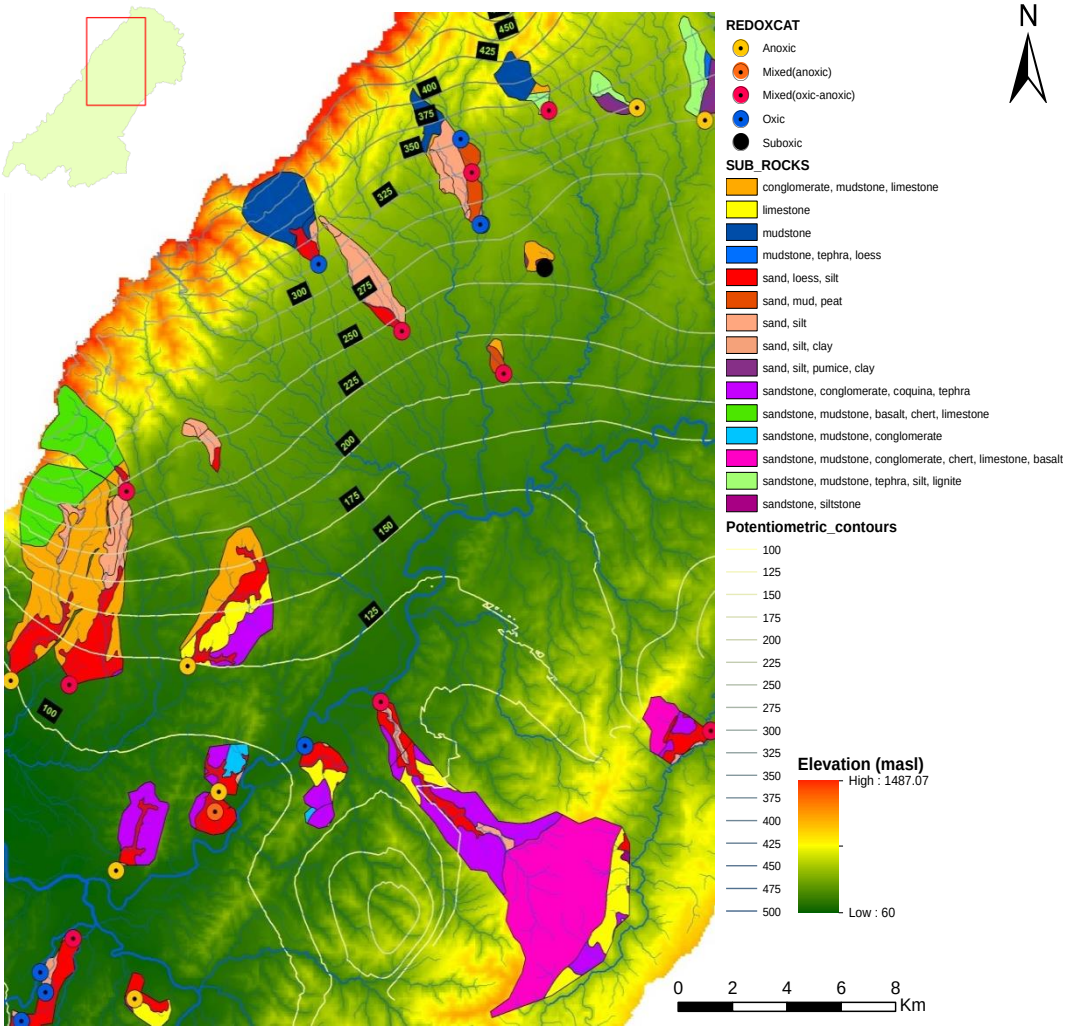

Figure 100: Catchment characteristics. The diversity in size, topography, and lithology of catchments and groundwater flowpaths upstream of groundwater sample points are presented in this map. The brightly coloured polygons are the delineated catchments up-flow of the sample site. The colours indicate the range of lithologies present in each catchment. It is possible to estimate the size, orientation of a basin through which infiltrated precipitation must move to reach the sample point. This serves to illustrate the difficulty in predicting or assessing redox characteristics from a single or a group of characteristics at a given location. Map generated in ArcGIS 10.2 using shapefiles from Heron (2014); Land Information New Zealand (2011b).

6.6 Comparison of Direct-Push and Existing Wells

Inconsistencies between the chemical and redox characteristics of groundwater collected from existing wells and the direct-push system were recognised. This raised

the question whether the regular pumping of an aquifer had in some way affected the characteristics of the groundwater or the aquifer materials, whether the differences were due to inherent but unidentified flaws in the direct-push system, or due to the groundwater being abstracted from different depths. Although a comprehensive investigation exceeds the scope of this thesis, a brief analysis was undertaken to quantify whether further investigation is warranted. It should be noted that samples collected using the two different methods were acquired in different years which may be responsible for the discrepancies.

Sites 5.2, 11.3, 13.3, 23.3, 50.8; 18.1; 50.3 (assigned to clusters 4, 5, and 6) previously identified by HCA to have strong chemical signatures not representative of water from the main gravel aquifers in the Tararua GWMZ were removed from this analysis. To better visualise potential differences between sampling methods, box and whisker plots were generated for both transformed data and the original data. Analysis of the boxplots (Figure 101) revealed the major anion and cation levels in both datasets to be somewhat similar and the interquartile range for the direct-push method was generally smaller for the existing wells. Furthermore DOC, Fe^{2+} (and possibly Mn^{2+}) levels seemed to be higher and *Eh* lower in the direct-push dataset.

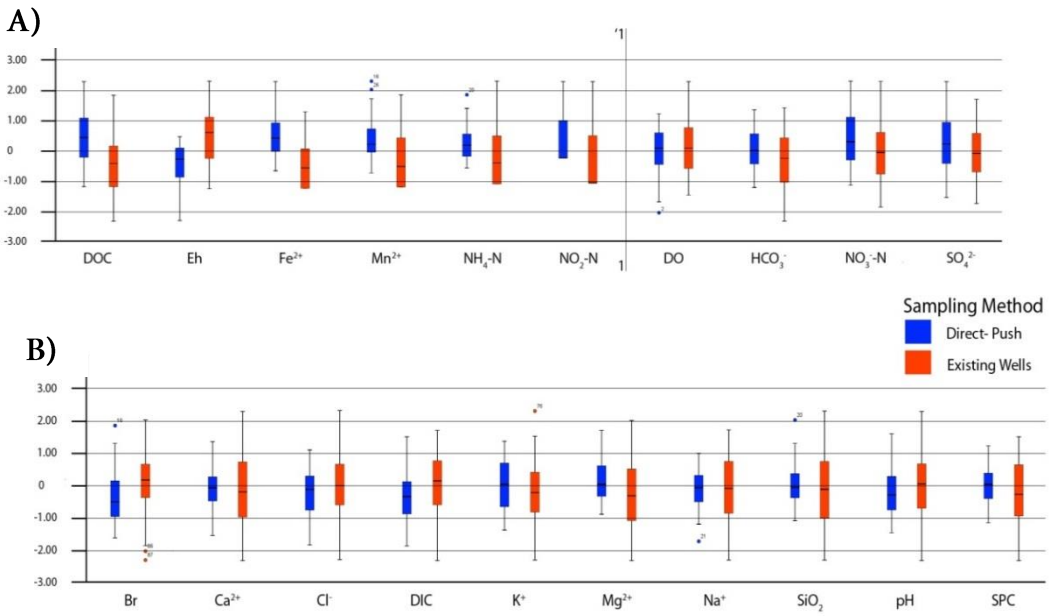

Figure 101: Box and whisker plot of A) redox related parameters and B) all other parameters. *(continued on the following page).*

Figure 102 *continued:* Box and whisker plot of A) redox related parameters and B) all other parameters. Means of the redox related parameters left of the vertical bar (1-‘1 in chart A) were identified to be statistically significant different when collected by direct-push compared to that collected by existing wells. The redox characteristics right of the line were not assessed to be different. The shape of the boxplots also indicates the direct-push method tends to have smaller interquartile ranges (less variation in the data). Low Cohen’s d values suggested a small effect size for these parameters but the boxplots suggest the differences may be more significant and perhaps more in depth analysis is required.

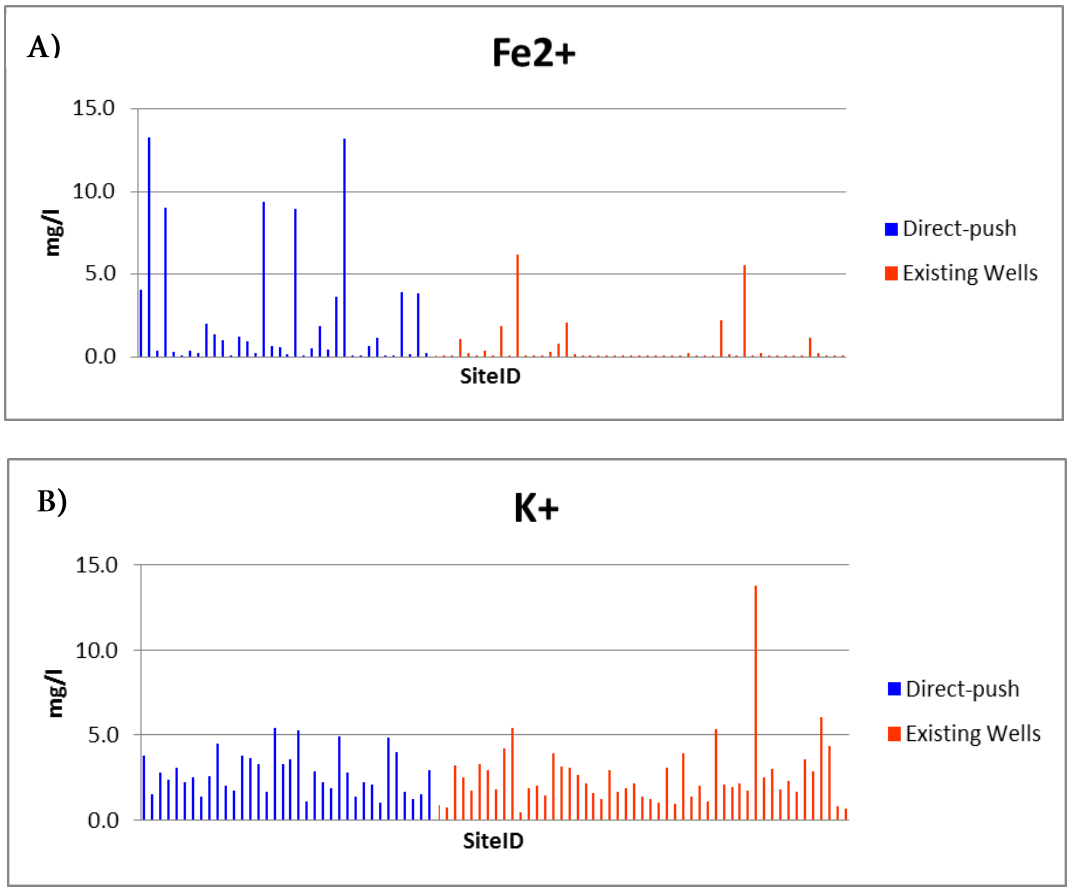

Figure 102: Bar plots of dissolved iron A) and potassium B). These bar graphs confirm the levels of analytes such as Fe^{2+} to be different when collected by direct-push or from existing wells. In particular the redox related parameters appeared to be quite different while graphs of the major ions such as K^{+} showed relative homogeneity between the methods.

Greater resolution provided by bar graphs (Figure 102) revealed noticeable differences between redox related parameters (i.e. Fe^{2+}) of water collected by the different methods; this trend was not obvious with non-redox related parameters (i.e. K^{+}). Subjective analysis of both plots tended to substantiate the hypothesis that the chemical

characteristics of groundwater collected by the two methods were different, but only for the redox related parameters in particular those shown in the left hand panel of Figure 101a.

An independent-samples t-test was conducted to objectively evaluate the data. The test revealed significant differences (at 95% confidence intervals) between the major redox related parameters collected by the two methods (Table 18), but not for the non-redox related parameters. In order to determine the effect-size of the independent-samples t-test, Cohen's d was calculated for those parameters assessed to have a statistically significant difference. As a Cohen's d effect-size less than 0.2 is considered small, and most results (except NO_2^- -N) were below this level, it appears from a statistical standpoint differences between the two datasets do exist but were fairly weak.

Table 18: Independent-samples t-test results for main redox related parameters between samples abstracted from existing wells and the direct-push method.

Parameter	T-test value	Cohen's d	Statistically Significant Differences
DO	t(85) = -0.896 p = 0.373	n/a	No
DOC	t(85) = 4.665 p < 0.0005	0.054	Yes
Eh	t(85) = -4.972 p < 0.0005	-0.042	Yes
Fe^{2+}	t(85) = 6.198 p < 0.0005	0.100	Yes
HCO_3^-	t(84.912) = 2.201 p = 0.030	n/a	No[1]
Mn^{2+}	t(83.77) = 3.301 p < 0.0005	0.122	Yes[1]
NH_4^+ -N	t(84.925) = 3.097 p = 0.003	-0.056	Yes[1]
NO_2^- -N	t(81.819) = 3.371 p = 0.001	0.226	Yes[1]
NO_3^- -N	t(85) = 2.294 p = 0.024	n/a	No
SO_4^{2-}	t(85) = 1.533 p = 0.129	n/a	No

[1] Unequal variances are assumed for this parameter

Difference between 2 groups is statistically significant if sig p < .05

Cohens d effect size: 0.2 to 0.5 small, 0.5 to .8 moderate, > 0.8 strong

DO = dissolved oxygen (mg L^{-1})

DOC = dissolved organic carbon (mg L^{-1})

Eh = reduction potential (mV)

Fe^{2+}= dissolved iron (mg L^{-1})

HCO_3^- = bicarbonate (mg L^{-1})

Mn^{2+}=(mg L^{-1})

NH_4^+ -N = ammoniacal nitrogen (mg L^{-1})

NO_2^- -N =nitrate nitrogen (mg L^{-1})

NO_3^- -N= nitrate nitrogen (mg L^{-1})

SO_4^{2-}=sulphate (mg L^{-1})

As recognised in the summary statistics and confirmed by higher Fe^{2+}, Mn^{2+}, and *Eh* values, box and whisker plots, bar graphs, different redox classifications, and independent-samples t-tests, differences in the hydrochemistry of specific redox related parameters exist between the two datasets; perhaps more so than the Cohen's d effect-size calculation suggests. The cause of these differences is unclear, but may be related to:

- wells tending to be installed in areas where higher quality and volumes of groundwater are likely to be encountered,
- wells may be installed in areas where flow paths are more distinct,
- pumping over time might develop or enhance groundwater flow paths,
- regular pumping may alter the nature of the groundwater proximal to the bore, perhaps by scrubbing the aquifer gravels of materials pivotal for redox reactions to occur such as DOC.

It is possible that the direct-push method is influencing the groundwater quality, for example it may be possible that air was unknowingly drawn into the pump-line, or perhaps the direct-push holes act as low volume, unscreened wells that draw of different chemistry and sources from throughout the water column. The validity of either of these scenarios seems unlikely; that air may be drawn into the pump-line can be refuted by the fact that 29 oxic samples were collected from existing wells and only 2 from the direct-push. If drawing air into the pump-line was the problem, then more oxic samples should have been collected by the direct-push system. Furthermore, increased air alone would not account for the changes observed in redox related analyte levels. It is possible that the direct-push method acts as an unscreened well, where aquifer water of different characteristics flow into the well and due to relatively low well

volume and short pumping durations, influence the chemical composition of the sample. However, if this was the case then it would be reasonable to assume that the levels of other non-redox related analytes would also vary in some way or another; which they don't. The evidence presented above appears to support the notion that an inherent difference might exist between the redox characteristics of aquifer water proximal to a production well and that of "virgin" aquifer water distal from the wellhead. Notwithstanding the actual causal factor or factors, more research is required before the null hypothesis that no statistically significant differences exist between water collected by the different methods can be confirmed or rejected.

6.7 Unsuccessful Direct-Push Sites

Although groundwater was abstracted successfully from 43 sites, 20 attempts were unsuccessful either due to groundwater not being present or the direct-push method being unable to penetrate deep enough to intersect the aquifer (Figure 103). Discussions with farmers revealed that large parts of flat land throughout the Tararua GWMZ are subsurface drained, which may impact on the volume of infiltration reaching the aquifers. Subsurface drains are seen to discharge into local waterways throughout the Tararua GWMZ. Particularly in the mudstone country, drains are observed to flow rapidly in response to precipitation, indicating water that accumulated in the soil zone is efficiently removed by these shallow drainage systems before infiltrating to deeper strata. This raises the question whether groundwater reserves existed in the mudstone areas. Further discussions indicate little groundwater is available east of Eketahuna; water for stock and human consumption is piped to the district from the Pori Aquifer (some kilometres away in the Puketoi Ranges) via a reticulation system. However, a number of saline springs outcropped within the region are reported to flow continuously regardless of season (P. Marden, personal

communication, October 14, 2016). Although interesting, determining the chemistry, nature and origin of these saline springs exceeded the scope of this study.

Following sampling efforts with the direct-push system in the mudstone country, it became apparent that groundwater didn't exist in many areas due to the low intrinsic permeability of fine grained sediments which restricted infiltration of precipitation any deeper than the uppermost (drained) zones. Drilled in mudstone to 7 – 8 m deep, sites 16.1, 16.2, 32.1 were completely dry, and at sites 16.3 and 34.1 only around 50 mm of damp sediments were encountered. Holes at sites 19.3 and 34.2 were drilled up to 8.5 m deep within metres of adjacent streams, yet following drilling only a small amount (< 25 mm) of wet sludge was detected. The gear was left in place at site 34.2 overnight and rechecked 16 hours later; less than 200 mm of water had accumulated at the base of the hole. It was unclear whether this water had accumulated due to overnight precipitation flowing down the outside of the drill rods, or whether the small amount of water had percolated into the hole from the surround sediments. A soil core taken at site 18.1 exhibited a strongly gleyed upper profile which supported the assumption that in these fine grained sediments, water is more likely to sit in the upper profile and not percolate very deeply. In the plains from Pahiatua to Dannevirke, sites drilled in gravels but near to limestone, coquina and sandstone were generally unsuccessful; this is perhaps that in these porous sediments the water table lay too deep for the direct-push system unless underlain by mudstone facies less than 10 m bgl. Furthermore, what is presumed to be impervious iron rich layers pans, well-indurated mudstones, or large gravel clasts occasionally stopped drilling prior to reaching the water table.

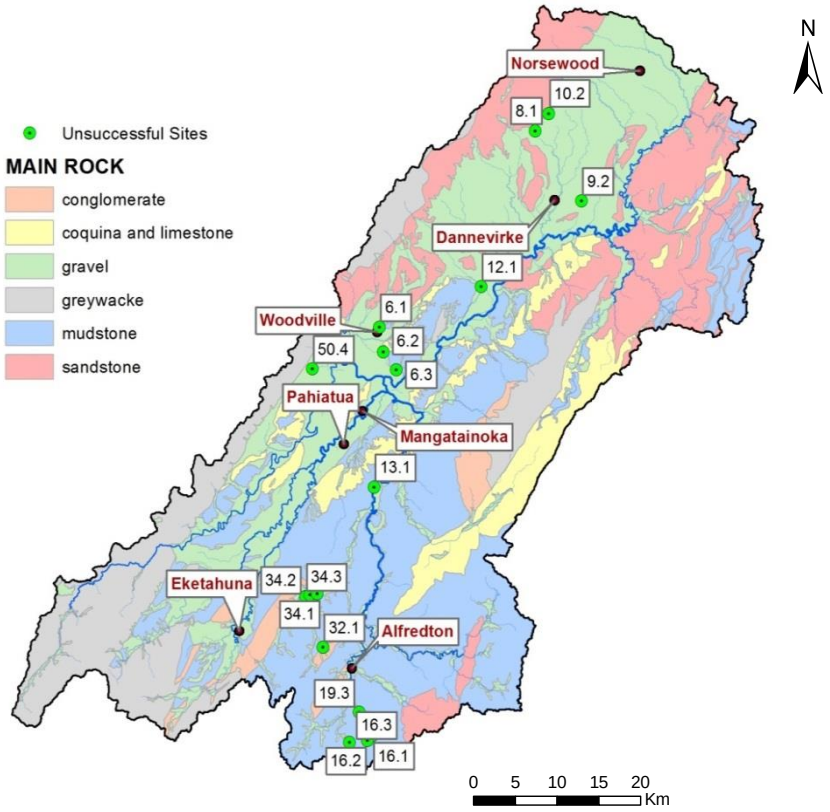

Figure 103: Unsuccessful sites. Sites in the southeast were in mudstone and it is unlikely groundwater existed in these areas. The central unsuccessful sites tended to be adjacent to mudstone or sandstone units where existing wells tended to be sited very close to streams, which indicated the gravels were very localised. In the northern regions unsuccessful sites probably were due to the water table being too deep. (Map generated in ArcGIS 10.2 using shapefiles from Heron (2014); Land Information New Zealand (2011b)).

6.8 Additional observations

The majority of groundwater samples were collected from settings typical of the Tararua GWMZ that include expansive grassed plains, underlain by silt loam, and gravel, then mudstone facies. Gravels varied in nature depending on spatial relationship to paleochannels and floodplains. The thickness of the gravel facies observed in river banks, road cuttings and slips also varied throughout the Tararua GWMZ from less than a metre, to units tens of metres thick. The aquifers appear to be generally

unconfined and relatively well connected to surficial water bodies, as evidenced by short mean residence times determined by Morgenstern et al. (2014). Although located in gravels and within the plains of the Tararua GWMZ, the anomalous hydrochemistry of clusters 4 to 6 suggest a different provenance may exist for these samples compared to those subscribed to Clusters 1-3 (Section 6.4.4; Figure 74). However, being unable to examine drill tailings with the direct-push method, it was impossible to determine whether the groundwater was abstracted either from poorly connected sediments below the gravels, from a poorly connected or confined aquifer, or whether it was connate water trapped in pockets within the mudstone.

Figure 104: Onoke group sediments in a road cutting (Alfredton Road, Eketahuna 40°39'59.0"S 175°47'22.8"E) 7 km West of site 50.3. It is difficult to determine the provenance of water recovered from site 50.3 but it may be water trapped in the fractured mudstone or the slightly more permeable sediments directly on top of the contact between the overlying layer.

The two sites that exhibited very high levels of analytes were located in quite different topography. Site 50.3 (mudstone-gravel; silt loam and clay loam; CC 4; DC 2; pHC 3; WT 0) lay in a small (approx. 200 m x 600 m) river terrace surrounded by moderately steep pasture along Alfredton Road, Eketahuna. Neogene mudstone of the Onoke group are visible in a nearby road cutting, with a prominent two to three metre fractured layer evident below the contact with the overlying colluvium (Figure 104).

The effective pump rate at this site was relatively low, which may indicate the fracture porosity great enough to hold and transmit the small amount of water we abstracted. On the other hand, it is also possible that water is being transmitted through a more permeable unit situated anywhere between the ground surface and the base of the drillhole.

Site 18.1 (mudstone; silt loam; CC 4; DC 4; pHC 3; WT 3) was situated in a swampy area at the intersection of two larger catchments (1.5 km x 1 km to the south and 2.5 km x 1 km to the east of the site) on Tane Road, while site 13.3 (1.5 km west, on Mangaone Valley Road) was located in a significant broad river valley. Site 18.2 (gravel; silt loam; CC 3; DC 5; pHC 3; WT 2) was sited in a wet swampy area upstream of Pa Valley Road at the base of a distinct 400 m x 300 m drainage basin. Although most of these sites were located in areas mapped as gravels in the QMap the gravels observed tended to be of mudstone origin rather than the greywacke and sandstone derived gravels of the central Tararua GWMZ. These sites were surrounded by blue grey Onoke mudstone sediments but the contact between the overlying alluvium/colluvium was not fractured. A 200 mm band of medium-brown, sandy material overlying the massive mudstone unit was observed to be transmitting water. The high levels of analytes encountered in the mudstone lithologies could be a product of dissolution of carbonate minerals coupled with slow water movement or perhaps arise from the influence of connate water; however, more work is required to determine the factors responsible. These unusual sites are described in detail as they regularly feature in the following analysis of the groundwater's chemical characteristics.

Figure 105: High DOC levels were recorded in mudstone areas. Soils on the hill slopes were thin and underlain by massive mudstone units resulting in precipitation rapidly flowing downslope and pooling in flat, low lying areas valleys such as pictured. Consequently groundwater was scarce and generally found only where the alluvium/colluvium was permeable enough to allow water to move deeper into the subsurface zones.

Site 11.3 (gravel; silt loam and clay loam; CC 4; DC 2; pHC 3; WT 2) displayed low DO and high HCO_3^-, however, unlike the mudstone sites 50.3, 18.1 and 13.3 it was located in Late Pleistocene river deposits close to the Ruahine Ranges and was expected to exhibit high-DO and low levels of ions similar to those detected in the Tamaki, Kumeti and Oruakeretaki catchments. It is likely the drill rods were driven through the gravel aquifer and into the underlying mudstone where sufficient water was encountered to collect. The nature of this water is difficult to quantify but may have been a body of water within the mudstone poorly connected to the aquifer.

Chapter 7: Summary and Conclusions

7.1 Introduction

This chapter presents the study summary and conclusions with regard to the study objectives, i.e. to develop a direct push method capable of collecting shallow groundwater samples from the Tararua GWMZ, analyse and study the groundwater chemistry, determine the groundwater redox characteristics, and attempt to determine the influence of geological factors on the groundwater redox characteristics distribution.

Specifically the aims of this research were to (i) develop a direct-push method able to effectively sample groundwater from a wide range of geological settings; (ii) analyse chemical and physical characteristics of groundwater and determine their redox characteristics and distribution; and (iii) identify the influence catchment characteristics such as soil texture and drainage, and rock types have on groundwater chemistry and its redox characteristics across the Tararua GWMZ.

The shallow groundwater of the Tararua GWMZ was widely explored in this thesis. A total of 45 (including two duplicates) groundwater samples were collected with the direct-push system; some from geological settings where groundwater was considered scarce or non-existent, and consequently the chemistry has never previously been investigated. This new groundwater data set was combined with an existing groundwater dataset (Rivas et al., 2017) obtained from sampling and laboratory analysis of 56 existing wells in the Tararua GWMZ. The groundwater chemistry was broadly analysed initially, then in more detail to determine the nature of groundwater redox processes and denitrification occurring throughout the study area. A summary of the direct-push system, outcomes of the chemical analysis are discussed, before key points pertaining to groundwater redox conditions of the Tararua GWMZ are

considered. The difficulties of predicting redox characteristics are discussed and finally opportunities for further work arising from findings of this study are presented.

7.2 Direct-Push

The direct-push system developed in this study was used to sample shallow groundwater at discrete locations not constrained by existing wells. A percussion hammer was used to drive a series of hollow drill rods and sacrificial tip into the substrate which then act as a temporary well casing.. Once the rods are driven into the aquifer the percussion hammer is removed and a rigid stainless steel pump-line and screen are inserted into the well. The rods are then lifted with a hydraulic jack and collect system, and using the rigid pump-line, the sacrificial tip is pushed out. The screen can be deployed at any desired depth and pumping can then proceed.

With conventional drilling rates running between $200 and $300 per metre, the sacrificial tip, direct-push system proved to be economical, portable and relatively reliable. The ability to sample groundwater where desired with the direct-push system, rather than be constrained by existing wells (which tend to be located in areas where the highest quality would be encountered) provided interesting contrasts to the supplementary dataset of Rivas et al., (2017).

Using the direct-push system a total of 45 groundwater samples including two duplicates were successfully collected (twenty sites were drilled but unsuccessful) from a wide range of geological settings across the Tararua GWMZ. Gravels of differing sizes and densities underlain by marine mudstones are the most commonly encountered lithology in the area. With a little perseverance, direct-push system drilled into these facies generally successfully; provided large clasts were not struck deeper in the hole. Additional weight on the percussion hammer was often instrumental in breaking

through to deeper levels. Spiking first with solid rods and then driving the CPT rods to form a well casing evolved as the preferred method. An 8 m hole could take from 30 minutes to several hours depending on the substrate. Driving a hole around a meter or so deeper than required would create a sump into which the sediments disturbed by drilling could settle, thereby allowing more efficient pumping. Limestone and coquina proved difficult for two reasons, firstly the watertable tended to be deeper than the direct-push system was able to drill (or pump) and secondly this rock was hard and very difficult to penetrate (and equally difficult to withdraw the rods from). Mudstone, particularly older, more consolidated facies could be difficult to penetrate and groundwater reserves are often very limited. The stainless steel pump-line and screen worked particularly well and could be relied upon to knock out the sacrificial tip, and agitate the pump-line to clear the screen. The effective screen size could be reduced by taping when pumping was required at low rates. By filling alternate sterile two litre containers, the simple twin container system (described in chapter 5, figure 6) facilitated collection of samples in conditions where for a variety of reasons, pumping might fail at any time. The Trimble GPS in PPK mode was a simple and efficient means of accurately surveying the elevation and locations of the sites.

Two limitations of the direct-push system became apparent. Firstly due to the lack of tailings it was very difficult to know what lithology was being drilled through and when it was appropriate to stop. The use of a flexible sewer camera to inspect the walls of the hole as the drill rods were withdrawn might prove useful in determining lithologies drilled through. Secondly, although the peristaltic pumps practical depth limit of around 8 m was generally not an issue in this study, it could be problematic in other regions. This could be overcome by the use of a foot-valve or a bailer depending on the situation. The material the 32 mm CPT rods are made from was not suited to the rotational stress and percussion generated by the percussion hammer; it is likely conventional drill rods may be more durable. The portability of this system was highly valued and a single worker could be set up ready to drill in less than 10 minutes. All

things considered, the direct-push system developed for this project was very successful, which is supported by the diversity of settings the groundwater water samples were collected from.

7.3 Groundwater Chemistry of the Tararua GWMZ

The diversity and variability of groundwater hydrochemistry established in this study bears testimony that a range of biogeochemical processes have modified the chemistry of water from that of the original precipitation. In the Tararua GWMZ, groundwater range from poorly-evolved mixed calcium-magnesium-chloride type with low levels of dissolved ions, to highly-evolved sodium chloride type with extremely high levels of dissolved ions and high pH. The spatial distribution of the water types is fairly consistent, with mixed Ca-Mg-Cl generally associated with steep topography, thin soils, and inert rock types. The slightly more evolved calcium-bicarbonate water type is found associated with areas where conditions facilitated redox reactions to occur. Mineral dissolution is determined to have the strongest influence on groundwater samples collected from mudstone areas which were analysed to be highly evolved sodium bicarbonate and sodium chloride types.

Several groundwater samples did not conform to these generalisations e.g. site 50.9 (greywacke, silt loam; CC 4; DC 5; pHC 5; WT 1) which although located less than 300 m from the Tararua Ranges was highly reducing, and site 11.3 (gravel; silt loam and clay loam; CC 4; DC 2; pHC 3; WT 2) located under a kilometre from the Ruahine ranges, was very saline with high levels of dissolved ions and high pH. As both sites were close to the ranges, where thin soils, steep topography and relatively chemically inert greywacke gravels dominate, both the groundwater samples were anticipated to be poorly evolved with low dissolved ions. Furthermore, the samples collected from the mudstone country feature strongly in the analysis where many analytes such as B, Br^-,

DIC, F^-, Na^+, and Mg^{2+} are the highest recorded and often exceeded MAV or guideline values. Of particular interest in this study are nitrate levels which are similarly diverse, and despite higher inputs associated with dairy farming, showed poor correlation to landuse. The highest nitrate levels are inferred to be the result of point source contamination rather than diffuse leachate arising from farming practices. The levels of nitrogen tends to follow the water type, where oxic poorly-evolved mixed Ca-Mg-Cl water tends to have high levels of NO_3^- -N while lower levels of NO_3^- -N in the Ca-HCO_3^- water type which is generally associated with reducing groundwater conditions.

7.4 Redox Processes and Characteristics

This research identifies a wide range of redox processes throughout the Tararua GWMZ. The size and physical characteristics of catchments for each of the sample sites was seen to be extremely variable and provide considerable challenges to determine key factors that influence the redox characteristics of shallow groundwater.

Oxic conditions are encountered at 32.5% of the sites and mixed oxic/anoxic at 28%. Anoxic conditions including purely anoxic (32.5%) and mixed anoxic (10%) are found at 42.5% of the sample sites. The spatial distribution of redox characteristics tend to follow that recognised in the water type and chemical parameters analyses. Two distinct areas where oxic water generally is associated were identified i.e. steep topography with, thin soils and chemically inert material in catchments close to the ranges such as the Tamaki, Kumeti and Oruakeretaki rivers; and productive aquifers well connected to surficial water typically found in coarse gravels overlain by free draining soils such as the major catchments of the Mangatainoka River.

Notable in both these areas are low levels of dissolved organic carbon, a key limiting factor in the level of groundwater reduction processes in subsurface environment.

The anoxic sites also are able to be grouped into two distinct categories, i.e. areas north of Dannevirke where prolific carbon rich deposits such as peat and lignite provide high levels of DOC essential for groundwater redox reactions; and areas east of the head of the Manawatu Gorge where lower hydraulic gradients result in some degree of ponding, longer groundwater residence times and consequently greater opportunity for groundwater redox reactions.

Exceptions to these findings are found throughout the study area (e.g. sites 5.2 and 11.3). From careful observations of local geology, in particular the thickness of overlying gravel units in road cuttings, farm tracks, escarpments, and stream banks, compared with direct-push well depths, it is likely that water samples from these sites were collected after the direct-push rods penetrated mudstone facies lying below the gravel . Whether the water collected in these settings was connate, bound in a lens of more permeable material within the mudstone, or poorly connected to the overlying aquifer was not able to be determined. Suboxic conditions were found at 2 sites where insufficient evidence was available to classify the samples.

The level of reduction (represented by the redox process) is generally advanced, with the majority of reducing sites classified as iron/sulphate (28/36 sites) or methanogenic (4/36) reduction, where nitrate levels are considered to have been reduced to levels where bacteria find it more efficient to reduce these lower energy yielding species.

The use of principal component analysis provided a convenient and effective means to assess the association of various factors to a group of groundwater redox related parameters. Although limitations due to the groundwater sample population size were observed, soil drainage, texture and carbon are assessed to have a significant influence on the redox potential at a given site. Other factors such as ground surface slope, carbon availability from the adjacent rocks, and the physical properties of gravels including drainage are also deemed to have some influence on the redox characteristics of shallow groundwater.

From the analyses it is apparent that no single factor has an overriding influence on the redox characteristics of shallow groundwater in the Tararua GWMZ. Rather, a complex suite of physical factors that include topography, local rock type, aquifer rock type and physical properties, soil texture, and drainage, flow paths and rates combine to influence the redox characteristics. Of these factors, the availability of suitable electron donors, typically lignite and peat (and possibly glauconite) and factors that controlled the rate of water movement with the subsurface environments are confirmed to be significant. Attempts to combine these factors into nitrogen attenuation classes to map redox potential throughout the study area provided disappointing results. However, with improved allocation of scores for parameters such as rock-carbon availability, rock drainage etc. it is possible that the factors identified in this research could produce acceptable results. By using the ArcGIS v10.2 *spline interpolation* tool based on the principal component associated with redox characteristics developed by Rivas et al., (2017), a raster surface was created, (and extended to the entire district), that provided a reasonable means of predicting the redox conditions throughput the Tararua GWMZ.

Another interesting outcome of this research was from the water type classification. Mixed Ca-Mg-Cl water was clearly associated with oxic conditions, and $CaHCO_3^-$ type water was clearly associated with anoxic conditions. This was determined using piper diagrams to create a water type classification using only four cations (Ca^{2+}, Mg^{2+}, Na^+, K^+), three anions (HCO_3^-, SO_4^{2-}, Cl^-) and pH. As this research analysed parameters (e.g. NO_3^- -N, NO_2^-N, DO, Fe^{2+}, Mn^{2+}, and DOC) specifically targeted to identify redox status of groundwater, using the method to classify Ca-Mg-Cl and $CaHCO_3^-$ type water may also allow classification of groundwater redox characteristics from less comprehensive, or historic, analysis results.

Although more work is required to confirm whether this holds true for other locations, this method may prove useful to estimate the redox characteristics of shallow groundwater from groundwater analysis not specifically targeted towards redox characteristics.

7.5 Direct-push vs Existing Wells

As all except one mixed oxic/anoxic sample was collected using the direct-push system, and only two (of 31) oxic samples were collected with the direct-push system, analysis of differences in groundwater hydrochemistry between the direct-push and existing well datasets was deemed necessary. Statistically significant differences were noted for groundwater redox related parameters (e.g. DOC, *Eh*, Fe^{2+}, Mn^{2+}, NH_4^+-N, NO_3^--N) between the respective datasets, while levels of most other anions and cations were quite similar. Causes for the apparent differences between the two methods were difficult to identify but may be related to systemic fundamental shortcomings of the direct-push system; installation of production wells naturally being targeted to high quality water; well depth; or the pumping affecting aquifer materials or flow paths. However, should the level of denitrification around existing wells be proven to be affected by pumping, assessments based exclusively on data from these wells may significantly underestimate the occurrence and distribution of redox processes in groundwater systems.

7.6 Further Work

This research has identified several opportunities for further work that include opportunities to extend the knowledge of groundwater in the Tararua GWMZ, identify redox characteristics in virgin aquifers vs production wells, use of the direct-push method, and possibility that water type analysis from routinely monitored parameters may allow estimation of the redox characteristics of shallow groundwater..

Knowledge of shallow groundwater in the Tararua GWMZ might be increased by:

- Utilising the portability, efficiency and economy of the direct-push method to facilitate transect or grid groundwater sampling regimes across entire aquifers.
- Mapping the extent and thickness of gravel aquifers including the contact between gravels and mudstones to model the flow paths in shallow gravel aquifers constrained by impervious mudstones. This will allow the rate and direction of groundwater movement and catchment dimensions in the Tararua GWMZ to be more accurately defined.
- Identify the physical and chemical characteristics of soil at each sample site to refine and validate the large scale FSL soil maps. Soil properties have been shown to fundamentally influence groundwater redox characteristics and increasing the accuracy and spatial resolution of these maps should increase the accuracy of inferences based on them.
- Investigate groundwater redox conditions adjacent to the axial ranges. Highly reducing conditions were found at some sites which challenged the assumption that these areas should be oxidising. Furthermore, determining whether logging-slash and charcoal originating from historic deforestation practices enhance DOC levels and subsequently denitrification in the steep, thin soils adjacent to the axial ranges.
- Investigate statistically significant differences recognized in this study between sulphate levels and landuse. Higher SO_4^{2-} levels were associated with dairy farming and the potential effects on aquifer and surficial water quality warrants further research.

The redox properties of virgin aquifers vs production wells.

- Use direct-push methodology to compare and contrast chemistry of virgin groundwater and that under irrigation systems, or adjacent to existing wells.
- Identify whether long term and/or large volume abstraction regimes from production wells influences the aquifer characteristics and groundwater

chemistry of redox related parameters; and whether this results in under or over estimation of the level of redox processes occurring at the local or regional scale.

- Exploiting the impermeable nature of fine grained sediments and soils
- Determine whether denitrification can be significantly increased in mudstone country. This research identified in mudstone country little precipitation infiltrated deeper than the subsurface drainage systems. This water may dissolve and transport nitrogen rich leachate and discharge it directly into waterways. Further research is required to identify how best to utilise the low permeability of substrates in areas farmed in mudstone country. This study identified that little groundwater percolates downwards in these geological settings. It may be possible to exploit this geological characteristic and more easily reroute subsurface drainage systems directly into denitrifying bioreactors than in more freely draining substrates.

Specifically the aims of this research were to (i) develop a direct-push method able to effectively sample groundwater from a wide range of geological settings; (ii) analyse chemical and physical characteristics of groundwater and determine their redox characteristics and distribution; and (iii) identify the influence catchment characteristics such as soil texture and drainage, and rock types have on groundwater chemistry and its redox characteristics across the Tararua GWMZ. These objectives were addressed systematically and this research has provided insight into the redox characteristics of shallow groundwater in the Tararua GWMZ.

References:

Aksever, F., Davraz, A., & Karagüzel, R. (2015). Relations of hydrogeologic factors and temporal variations of nitrate contents in groundwater, Sandıklı basin, Turkey. *Environmental Earth Sciences, 73*(5), 2179-2196.

Anastasiadis, S., Kerr, S., Nauleau, M. L., Cox, T., & Rutherford, K. (2014). Does complex hydrology require complex water quality policy? *Australian Journal of Agricultural and Resource Economics, 58*(1), 130-145.

Aravena, R., & Robertson, W. D. (1998). Use of multiple isotope tracers to evaluate denitrification in ground water: study of nitrate from a large-flux septic system plume. *Ground Water, 36*(6), 975-982.

Baalousha, H. (2010). Assessment of a groundwater quality monitoring network using vulnerability mapping and geostatistics: A case study from Heretaunga Plains, New Zealand. *Agricultural Water Management, 97*(2), 240-246.

Baber, H. L., & Wilson, A. T. (1972). Nitrate pollution of groundwater in the Waikato region. *Chemistry in New Zealand, 36*, 179-183.

Back, W. (1966). *Hydrochemical facies and ground-water flow patterns in northern part of Atlantic Coastal Plain*: US Government Printing Office.

Banchuen, T. (2002). *A microcosm-based investigation into oxidized nitrogen removal in the hypolimnetic waters of the Occoquan Reservoir of Northern Virginia.* Virginia Polytechnic Institute and State University.

Bardon, C., Poly, F., Piola, F., Pancton, M., Comte, G., Meiffren, G., & el Zahar Haichar, F. (2016). Mechanism of biological denitrification inhibition: procyanidins induce an allosteric transition of the membrane-bound nitrate reductase through membrane alteration. *FEMS Microbiology Ecology, 92*(5).

Barkle, G., Clough, T., & Stenger, R. (2007). Denitrification capacity in the vadose zone at three sites in the Lake Taupo catchment, New Zealand. *Soil Research, 45*(2), 91-99.

Barkle, G., Stenger, R., Wöhling, T., Moorhead, B., Wall, A., & Clague, J. (2013). Fate of a dairy cow urine pulse in a layered volcanic vadose zone. In: *Accurate and efficient use of nutrients on farms.* (Eds L.D. Currie and C L. Christensen). http://flrc.massey.ac.nz/publications.html. Occasional Report No. 26. Fertilizer and Lime Research Centre, Massey University, Palmerston North, New Zealand. 15 pages.

Beauchamp, E., Gale, C., & Yeomans, J. C. (1980). Organic matter availability for denitrification in soils of different textures and drainage classes. *Communications in Soil Science and Plant Analysis, 11*(12), 1221-1233.

Begg, J., & Johnston, M. (2000). *Geology of the Wellington area. Institute of GeologicaI & Nuclear Sciences I :250 000 geological map 10. I sheet+ 64p. Lower Hutt, New Zealand: Institute of GeologicaI & Nuclear Sciences Limited.*

Begg, J., Palmer, A., & Gyopari, M. (2005). *Geological synopsis of the Manawatu-Horowhenua area for a review of the region's hydrogeology*: Institute of Geological & Nuclear Sciences Limited.

Beyer, M., Rissmann, C., Rodway, E., Killick, M., Pearson, L., Marapara, T., & Hodgetts, J. (2016a). *Physiographics of Southland part 1: Delineation of key drivers of regional hydrochemistry: Technical Chapter 6: Influence of Soil and Geological Composition over Redox conditions for Southland groundwater and surface waters.* Environment Southland publication.

Beyer, M., Rissmann, C., Rodway, E., Killick, M., Pearson, L., Marapara, T., & Hodgetts, J. (2016b). Physiographics of Southland Part 1:Delineation of key drivers of regional hydrochemistry and water quality *Technical Chapter 6: Influence of Soil and Geological Composition over Redox conditions for Southland groundwater and surface waters* (pp. 45): Environment Southland.

Bishop, P., & Manning, M. (2010). Urea volatilisation: the risk management and mitigation strategies. In: *Adding to the knowledge base for the nutrient manager.* Eds Currie, L.D.; Christiensen, C.L. http://flrc.massey.ac.nz/publications.html. Occasional Report No. 24. Fertilizer and Lime Research Cente, Massey University, Palmerston North, New Zealand. 13 pages.

Black, P. E. (1996). *Watershed hydrology* (2nd ed.). Chelsea, Michigan: Ann Arbor Press.

Böhlke, J., & Denver, J. (1995). Combined use of groundwater dating, chemical, and isotopic analyses to resolve the history and fate of nitrate contamination in two agricultural watersheds, Atlantic coastal plain, Maryland. *Water Resources Research, 31*(9), 2319-2339.

Bothe, H., Ferguson, S. J., & Newton, W. E. (Eds.). (2007). *Biology of the nitrogen cycle* (1st ed ed.). Amsterdam ; Oxford: Elsevier.

Bowman, S., & Conway, P. (2013). China's recent growth and its impact on the New Zealand economy *New Zealand Treasury Working Paper 13/15.* Wellington, N.Z.: The Treasury.

Bryant, F. B., & Yarnold, P. R. (1995). Principal-components analysis and exploratory and confirmatory factor analysis. In L. G. Grimm & P. R. Yarnold (Eds.), *Reading and understanding multivariate statistics* (pp. 99 –136). Washington, DC: American Psychological Association.

Burkitt, L., Bretherton, M., & Singh, R. (2015). Monitoring stream sediment, nitrogen and phosphorus concentrations in grazed hill country in the Manawatu Region. In: *Moving farm systems to improved attenuation.* (Eds L.D. Currie and L.L Burkitt). http://flrc.massey.ac.nz/publications.html. Occasional Report No. 28. Fertilizer and Lime Research Centre, Massey University, Palmerston North, New Zealand. 10 pages.

Butler, J. J., Healey, J. M., McCall, G., Garnett, E. J., & Loheide, S. P. (2002). Hydraulic tests with direct-push equipment. *Ground Water, 40*(1), 25-36.

Carlyle, G., & Hill, A. (2001). Groundwater phosphate dynamics in a river riparian zone: effects of hydrologic flowpaths, lithology and redox chemistry. *Journal of Hydrology, 247*(3), 151-168.

Carrick, S., Fraser, P., Dennis, S., Knight, T., & Tabley, F. (2013). Challenges for leachate monitoring from alluvial sedimentary soils. In: *Accurate and efficient use of nutrients on farms. (Eds L.D. Currie and C L. Christensen).* http://flrc.massey.ac.nz/publications.html. Occasional Report No. 25. Fertilizer and Lime Research Centre, Massey University, Palmerston North, New Zealand. 8 pages.

Carrick, S., Palmer, D., Webb, T., Scott, J., & Lilburne, L. (2013). Stony soils are a major challenge for nutrient management under irrigation development. In: *Accurate and efficient use of nutrients on farms.* (Eds L.D. Currie and C L. Christensen). http://flrc.massey.ac.nz/publications.html. Occasional Report No. 25. Fertilizer and Lime Research Centre, Massey University, Palmerston North, New Zealand. 8 pages.

Chapelle, F. H., Bradley, P. M., Thomas, M. A., & McMahon, P. B. (2009). Distinguishing Iron-Reducing from Sulfate-Reducing Conditions. *Ground Water, 47*(2), 300-305.

Chapelle, F. H., Haack, S. K., Adriaens, P., Henry, M. A., & Bradley, P. M. (1996). Comparison of Eh and H_2 Measurements for Delineating Redox Processes in a Contaminated Aquifer. *Environmental science & technology, 30*(12), 3565-3569.

Chapelle, F. H., McMahon, P. B., Dubrovsky, N. M., Fujii, R. F., Oaksford, E. T., & Vroblesky, D. A. (1995). Deducing the distribution of terminal electron-accepting processes in hydrologically diverse groundwater systems. *Water Resources Research, 31*(2), 359-371.

Chappell, P. R. (2015). *The climate and weather of Manawatu-Wanganui* (NIWA science and technology series number 66). Auckland, New Zealand: NIWA.

Charlton, R. (2007). *Fundamentals of fluvial geomorphology.* Abingdon, Oxon ; New York, NY: Routledge.

Christensen, T. H., Bjerg, P. L., Banwart, S. A., Jakobsen, R., Heron, G., & Albrechtsen, H.-J. (2000). Review article: Characterization of redox conditions in groundwater contaminant plumes. *Journal of Contaminant Hydrology, 45*, 165-241.

Clague, J. (2013). *Denitrification in the shallow groundwater system of two agricultural catchments in the Waikato, New Zealand.* (Unpublished doctoral dissertation) Lincoln University, Christchurch, New Zealand.

Clague, J., Stenger, R., & Clough, T. (2015). Evaluation of the stable isotope signatures of nitrate to detect denitrification in a shallow groundwater system in New Zealand. *Agriculture, ecosystems & environment, 202*, 188-197.

Clark, J. (2013). An introduction to redox equilibria and electrode potentials. Retrieved from http://www.chemguide.co.uk/physical/redoxeqia/introduction.html#top

Close, M. E., Abraham, P., Humphries, B., Lilburne, L., Cuthill, T., & Wilson, S. (2016). Predicting groundwater redox status on a regional scale using linear discriminant analysis. *Journal of Contaminant Hydrology, 191*, 19-32.

Cloutier, V., Lefebvre, R., Savard, M. M., Bourque, É., & Therrien, R. (2006). Hydrogeochemistry and groundwater origin of the Basses-Laurentides sedimentary rock aquifer system, St. Lawrence Lowlands, Québec, Canada. *Hydrogeology Journal, 14*(4), 573-590.

Cole, J. W., & Lewis, K. B. (1981). Evolution of the Taupo-Hikurangi subduction system. *Tectonophysics, 71*, 1-21.

Collins, S. B. (2015). *Investigating the transport and fate of nitrogen from farms to river in the lower Rangitikei Catchment.* (Unpublished Masters Thesis), Massey University, Palmerston North, New Zealand.

Collins, S. B., Singh, R., Rivas, A., Palmer, A., Horne, D., Roygard, J., & Matthews, A. (2016). Assessment of nitrogen flow pathways and its potential attenuation in shallow groundwaters in the lower Rangitikei Catchment. In: *Integrated nutrient and water management for sustainable farming.* (Eds L. D. Currie and R. Singh). http://flrc.massey.ac.nz/publications.html. Occasional Report No. 29.

Fertilizer and Lime Research Centre, Massey University, Palmerston North, New Zealand. 14 pages.

Cooke, J. G., & Cooper, A. B. (1988). Sources and sinks of nutrients in a New Zealand hill pasture catchment III. *Hydrological Processes, 2*(2), 135-149.

Daughney, C. J. (2006). *A national protocol for state of the environment groundwater sampling in New Zealand*: Ministry for the Environment.

Daughney, C. J. (2008). *Multivariate statistical methods for assessment of groundwater chemistry in the Waiareka and Deborah Aquifers, Otago.* Lower Hutt, New Zealand: GNS Science.

Daughney, C. J. (2010). *Hydrochemical classification of groundwater and river state of the environment monitoring sites in the Greater Wellington Region* (Vol. 2009/68). Lower Hutt, New Zealand: GNS Science.

Daughney, C. J., Baker, T., Jones, A., Hanson, C., Davidson, P., Thompson, M., . . . Zemansky, G. (2007). Comparison of groundwater sampling methods for State of the Environment monitoring in New Zealand. *Journal of Hydrology (New Zealand), 46*(1), 19.

Daughney, C. J., Guggenmos, M., McAlister, D., Begg, J. G., & Jackson, B. (2009). *Assessment of groundwater and surface water chemistry in the upper and lower Wairarapa Valley*. Taupo, New Zealand: GNS Science.

Daughney, C. J., Meilhac, C., & Zarour, H. (2009). Spatial and temporal trends in groundwaterquality in the Manawatu-Wanaganui region. GNS Science Report 2009/02, GNS Science, Lower Hutt (2009), p. 137.

Daughney, C. J., & Reeves, R. R. (2005). Definition of Hydrochemical Facies in the New Zealand National Groundwater Monitoring Programme. *Journal of Hydrology (New Zealand), 44*(2), 105.

Dineen, L., & Blakesley, B. (1973). Algorithm AS 62: Generator for the sampling distribution of the Mann-Whitney U statistic. *Applied Statistics, 22, 269-273.*

Donath, F. M., Daughney, C. J., Morgenstern, U., Cameron, S. G., & Toews, M. W. (2015). Hydrochemical interpretation of groundwater-surface water interactions at catchment and local scales, Lake Rotorua catchment, New Zealand. *Journal of Hydrology, 54*(1), 11.

Dravid, P. N., & Brown, L. J. (1997). *Heretaunga Plains Groundwater Study : Volume 1-Findings.* Napier, New Zealand: Hawke's Bay Regional Council.

Elwan, A. (2015). Spatial nitrogen reduction capacity and its relationships with hydrogeological characteristics in the Manawatu River catchment. *WISPAS (Online)*.

Elwan, A., Singh, R., Horne, D., Roygard, J., Clothier, B., & Jones, G. (2016). *Influence of catchment characteristics on soluble inorganic nitrogen in the Manawatu River*. Paper presented at the New Zealand Society of Soil Science and Soil Science Australia, Queenstown, New Zealand.

Elwan, A., Singh, R., Horne, D., Roygard, J., & Clothier, B. E. (2015). Nitrogen attenuation factor: Can it tell a story about the journey of nutrients in different subsurface environments?. *In: Moving farm systems to improved attenuation.* (Eds L.D. Currie and L.L Burkitt). http://flrc.massey.ac.nz/publications.html. Occasional Report No. 28. Fertilizer and Lime Research Centre, Massey University, Palmerston North, New Zealand. 25 pages.

Espanto, P. (2015). *Assessment of the transport and transformation of nitrogen in the unsaturated and saturated zones under two dairy farms in the Manawatu River catchment.* (Unpublished Masters Thesis), Massey University, Palmerston North, New Zealand.

Etheridge, Z., & Scott, M. (2015). *Predicting consequences of future Scenarios in the Waitaki Catchment: Upper Waitaki Groundwater quality* (Report No. R15/61). Christchurch, New Zealand: Environment Canterbury Regional Council.

Farnham, I. M., Singh, A. K., Stetzenbach, K. J., & Johannesson, K. H. (2002). Treatment of nondetects in multivariate analysis of groundwater geochemistry data. *Chemometrics and Intelligent Laboratory Systems, 60*(1), 265-281.

Forster, P., Ramaswamy, V., Artaxo, P., Berntsen, T., Betts, R., Fahey, D. W., . . . Myhre, G. (2007). Changes in atmospheric constituents and in radiative forcing. Chapter 2 *Climate Change 2007. The Physical Science Basis.*

Fowler, D., Steadman, C. E., Stevenson, D., Coyle, M., Rees, R. M., Skiba, U. M., . . . Galloway, J. N. (2015). Effects of global change during the 21st century on the nitrogen cycle. *Atmospheric Chemistry And Physics*, 13849.

Freeze, R. A., & Cherry, J. A. (1979). Groundwater, 604 pp: Prentice-Hall, Englewood Cliffs, NJ.

Fritz, S. J. (1994). A survey of charge-balance errors on published analyses of potable ground and surface waters. *Groundwater, 32*(4), 539-546.

Gao, S., Tanji, K., Scardaci, S., & Chow, A. (2002). Comparison of redox indicators in a paddy soil during rice-growing season. *Soil Science Society of America Journal, 66*(3), 805-817.

Garba, A., Ekanem, E., Garba, I., & Mustapha, A. (2016). Multivariate Statistical Analysis of Groundwater Chemistry Data from Hadejia Local Government Area of Jigawa State, Nigeria. *Glob. J. Adv. Res, 3*, 713-722.

Gibbons, R. D., Bhaumik, D. K., & Aryal, S. (2009). *Statistical methods for groundwater monitoring* (Vol. 59): John Wiley & Sons.

GNS Science (Cartographer). (2012). 1:250 000 Geological Map of New Zealand (QMAP)

Graham, I. J. (2008). *A continent on the move: New Zealand geoscience into the 21st century*: Geological Society of New Zealand.

Groffman, P. M., & Tiedje, J. M. (1989). Denitrification in north temperate forest soils: relationships between denitrification and environmental factors at the landscape scale. *Soil Biology and Biochemistry, 21*(5), 621-626.

Gruber, N., & Galloway, J. N. (2008). An Earth-system perspective of the global nitrogen cycle. *Nature, 451*(7176), 293-296.

Güler, C., Thyne, G. D., McCray, J. E., & Turner, K. A. (2002). Evaluation of graphical and multivariate statistical methods for classification of water chemistry data. *Hydrogeology Journal, 10*(4), 455-474.

Gyopari, M. (2014). *Lower Hutt aquifer model revision (HAM3): Sustainable management of the Waiwhetu Aquifer.* Wellington, New Zealand: Greater Wellington Regional Council. 224 pages

Hadfield, J., & Gibbs, M. (2007). *Field investigation of nitrogen attenuation in Lake Taupo catchment groundwater.* Paper presented at the Proceedings of the New Zealand Hydrological Society Conference, Rotorua, New Zealand.

Hansen, R. J., & Kamp, P. J. (2008). *New insights into the condensed nature and stratigraphic significance of the Late Neogene Ariki Formation, Taranaki Basin.* Paper presented at the 2008 New Zealand Petroleum Conference, Auckland, New Zealand.

Helena, B., Pardo, R., Vega, M., Barrado, E., Fernandez, J. M., & Fernandez, L. (2000). Temporal evolution of groundwater composition in an alluvial aquifer (Pisuerga River, Spain) by principal component analysis. *Water research, 34*(3), 807-816.

Helsel, D. (2009). Much ado about next to nothing: incorporating nondetects in science. *Annals of occupational hygiene, 54*(3), 257-262.

Heron, D. (2014). Geological Map of New Zealand 1:250 000. GNS Science Geological Map 1. Lower Hutt, New Zealand. GNS Science.

Hiscock, K., Lloyd, J., & Lerner, D. (1991). Review of natural and artificial denitrification of groundwater. *Water research, 25*(9), 1099-1111.

Hofmann, T., Darsow, A., Gröning, M., Aggarwal, P., & Suckow, A. (2010). Direct-push profiling of isotopic and hydrochemical vertical gradients. *Journal of Hydrology, 385*(1), 84-94.

Horizons Regional Council. (2016). Tararua Groundwater Management Zone. Retrieved from http://www.lawa.org.nz/explore-data/manawatu-wanganui-region/water-quantity/groundwater-zones/tararua-groundwater-mz/

Howarth, R. W., & Marino, R. (2006). Nitrogen as the limiting nutrient for eutrophication in coastal marine ecosystems: evolving views over three decades. *Limnology and Oceanography, 51*(1), 364-376.

Jha, N., Sagger, S., Deslippe, J., Tillman, R., Giltrap, D., & Bowatte, S. (2013). Measuring bacterial denitrifier genes distribution and abundance in New Zealand dairy-grazed pasture soils. In: *Accurate and efficient use of nutrients on farms.* (Eds L.D. Currie and C L. Christensen).. http://flrc.massey.ac.nz/publications.html. Occasional Report No. 26. Fertilizer and Lime Research Centre, Massey University, Palmerston North, New Zealand. 21 pages.

Jha, N., Sagger, S., Tillman, R., & Giltrap, D. (2011). Preliminary studies to measure denitrification enzyme activity and denitrification rate in New Zealand pasture soils. In: Adding to the knowledge base for the nutrient manager. (Eds L.D. Currie and C L. Christensen). http://flrc.massey.ac.nz/publications.html. Occasional Report No. 24. Fertilizer and Lime Research Centre, Massey University, Palmerston North, New Zealand. 8 pages.

Jurgens, B. C., McMahon, P. B., Chapelle, F. H., & Eberts, S. M. (2009). *An Excel® workbook for identifying redox processes in ground water.* US Geological Survey Open-File Report 2009-1004 (pp. 8).

Kaiser, H. F. (1974). An index of factorial simplicity. *Psychometrika, 39*(1), 31-36.

Kamp, P. J., Vonk, A. J., Bland, K. J., Hansen, R. J., Hendy, A. J., McIntyre, A. P., . . . Nelson, C. S. (2004). Neogene stratigraphic architecture and tectonic evolution of Wanganui, King Country, and eastern Taranaki Basins, New Zealand. *New Zealand Journal of Geology and Geophysics, 47*(4), 625-644.

Kensington, C., Richards, K., Murray, D., & Peake, B. (2003). Nitrogen Species Distribution in the Taieri Plain Aquifer, New Zealand.

Khan, M. M. A., & Umar, R. (2010). Significance of silica analysis in groundwater in parts of Central Ganga Plain, Uttar Pradesh, India. *Current Science*, 1237-1240.

Killick, M., Rissmann, C., & Stenger, R. (2014). *Estimating soil zone denitrification potential for Southland* (Technical Report 2016-01). Invercargill, New Zealand. Environment Southland. 32 pages.

Killpack, S., & Buchholz, D. (2008). *Nitrogen in the environment: What is nitrogen. Report project supported by the United States Department of Agriculture. Extension Service (*Under special project number 89-EWQI-1-9203; 2008).

Klingbeil, R., Kleineidam, S., Asprion, U., Aigner, T., & Teutsch, G. (1999). Relating lithofacies to hydrofacies: outcrop-based hydrogeological characterisation of Quaternary gravel deposits. *Sedimentary Geology, 129*(3-4), 299-310.

Knight, J. (2003). Negative results: Null and void. *Nature, 422(6932)*, 345-347.

Korom, S. F. (1992). Natural denitrification in the saturated zone: a review. *Water Resources Research, 28*(6), 1657-1668.

Krieger, F. W. (1992). *Sedimentology and paleoenvironmental analysis of Castlecliffian strata in the Dannevirke Basin.* (Unpublished Masters Thesis), Massey University, Palmerston North, New Zealand.

Laerd Statistics. (2015a). Independent-samples t-test using SPSS Statistics. Retrieved from https://statistics.laerd.com/

Laerd Statistics. (2015b). Independent-samples t-test using SPSS Statistics: statistical tutorials and software guides. Retrieved from https://statistics.laerd.com/

Laerd Statistics. (2015c). One-way ANOVA using SPSS Statistics.: statistical tutorials and software guides. Retrieved from https://statistics.laerd.com/

Laerd Statistics. (2015d). Pearson's product-moment correlation using SPSS Statistics. Statistical tutorials and software guides. Retrieved from https://statistics.laerd.com/

Laerd Statistics. (2015e). Principal components analysis (PCA) using SPSS Statistics: Statistical tutorials and software guides. Retrieved from https://statistics.laerd.com/

Lalisse-Grundmann, G., Brunel, B., & Chalamet, A. (1988). Denitrification in a cultivated soil: optimal glucose and nitrate concentrations. *Soil Biology and Biochemistry, 20*(6), 839-844.

Land Information New Zealand. (2011a, 15 Apr 2017). NZ Property Titles. Retrieved from https://data.linz.govt.nz/layer/804-nz-property-titles/

Land Information New Zealand. (2011b, 13 Feb 2017). NZ River Centrelines (Topo, 1:250k)

Retrieved from https://data.linz.govt.nz/layer/182-nz-river-centrelines-topo-1250k/

Land Information New Zealand. (2011c, 13 Feb 2017). NZ Road Centrelines (Topo, 1:250k). Retrieved from https://data.linz.govt.nz/layer/184-nz-road-centrelines-topo-1250k/

Land Information New Zealand. (2011d, 07 Apr 2017). NZ Topo50 Maps. Retrieved from https://data.linz.govt.nz/layer/767-nz-topo50-maps/

Land Information New Zealand. (2013, 31 Aug 2016). NZ Place Names. Retrieved from https://data.linz.govt.nz/layer/1681-nz-place-names-nzgb/

Landcare Research. (2010a). FSL carbon class. Retrieved from https://lris.scinfo.org.nz/layer/48098-fsl-soil-carbon/

Landcare Research. (2010b). FSL New Zealand soil classification. Retrieved from https://lris.scinfo.org.nz/layer/79-fsl-new-zealand-soil-classification/

Landcare Research. (2010c). FSL Soil Drainage Class. Retrieved from https://lris.scinfo.org.nz/layer/104-fsl-soil-drainage-class/

Landcare Research. (2010d). NZDEM North Island 25 metre. Retrieved from https://lris.scinfo.org.nz/layer/131-nzdem-north-island-25-metre/

Landcare Research. (2010e, March 10, 2016). NZLRI Land Use Capability. Retrieved from https://lris.scinfo.org.nz/layer/76-nzlri-land-use-capability/

Landcare Research. (2015, 16 Jul 2015). LCDB v4.1 - Land Cover Database version 4.1, Mainland New Zealand. Retrieved from https://lris.scinfo.org.nz/layer/423-lcdb-v41-land-cover-database-version-41-mainland-new-zealand/

Landcare Research. (2018). Soil data and maps. Retrieved from https://soils.landcareresearch.co.nz/index.php/soil-data/fundamental-soil-layers/

Ledgard, S., Penno, J., & Sprosen, M. (1999). Nitrogen inputs and losses from clover/grass pastures grazed by dairy cows, as affected by nitrogen fertilizer application. *The Journal of Agricultural Science, 132*(02), 215-225.

Lee, J., & Begg, J. G. (2002). Geology of the Wairarapa area. Institute of Geological & Nuclear Sciences 1:250 000 geological map 11. 1 sheet + 66 p. Lower Hutt, New Zealand. GNS Science.

Lee, J., Bland, K., Townsend, D., & Kamp, P. (2011). *Geology of the Hawke's Bay area. Institute of Geological & Nuclear Sciences 1:250 000 geological map 8.* Lower Hutt, New Zealand: Institute of Geological and Nuclear Sciences. 1 folded sheet + 93 pages.

Lilburne, L., Hewitt, A., & Webb, T. (2012). Soil and informatics science combine to develop S-map: A new generation soil information system for New Zealand. *Geoderma, 170*, 232-238.

Lillie, A. R. (1953). *The geology of the Dannevirke Subdivision. New Zealand Geological survey Bulletin.*: New Zealand Geological survey Bulletin. RE Owen, Govt. printer.

Liotta, M., D'Alessandro, W., Bellomo, S., & Brusca, L. (2016). Volcanic plume fingerprint in the groundwater of a persistently degassing basaltic volcano: Mt. Etna. *Chemical Geology, 433*, 68-80. doi:10.1016/j.chemgeo.2016.03.032

Lovley, D. R. (1993). Dissimilatory metal reduction. *Annual Reviews in Microbiology, 47*(1), 263-290.

Luo, J. (1996). *Nitrogen loss through denitrification in soil under pasture in New Zealand* (Unpublished doctoral dissertation). Massey University, Palmerston North, New Zealand.

Luo, J., Tillman, R., & Ball, P. (1999). Factors regulating denitrification in a soil under pasture. *Soil Biology and Biochemistry, 31*(6), 913-927.

Luo, J., Tillman, R., & Ball, P. (2000). Nitrogen loss through denitrification in a soil under pasture in New Zealand. *Soil Biology and Biochemistry, 32*(4), 497-509.

Luo, J., Tillman, R., White, R., & Ball, P. (1998). Variation in denitrification activity with soil depth under pasture. *Soil Biology and Biochemistry, 30*(7), 897-903.

Magesan, G. (1992). A Study of the Leaching of Non-reactive Solutes and Nitrates under Laboratory and Field Conditions. *Massey University, Turitea Campus, Palmerston North.*

Mastrocicco, M., Giambastiani, B., & Colombani, N. (2013). Ammonium occurrence in a salinized lowland coastal aquifer (Ferrara, Italy). *Hydrological Processes, 27*(24), 3495-3501.

Matiatos, I., Alexopoulos, A., & Godelitsas, A. (2014). Multivariate statistical analysis of the hydrogeochemical and isotopic composition of the groundwater resources in northeastern Peloponnesus (Greece). *Science of the total environment, 476*, 577-590.

McArthur, K., Roygard, J., Ausseil, O., & Clark, M. (2007). Development of water management zones in the Manawatu-Wanganui Region : Technical report to support policy development (pp. 131): Horizons Regional Council.

McBeth, K., Morgenstern, U., Toews, M. A., Feek, D., & Begg, J. G. (2015). Development of a Direct-Push Groundwater Probe to New Zealand Conditions. *GNS Science Internal Report* 2014/06. 25p.

McLaren, R., & Cameron, K. (1990). *Soil science : an introduction to the properties and management of New Zealand soils.* Auckland, New Zealand: Oxford University Press.

McLarin, W., Bekesi, G., Brown, L., & McConchie, J. (1999). Nitrate contamination of the unconfined aquifer, Manakau, Horowhenua, New Zealand. *Journal of hydrology. New Zealand, 38*(2), 211-235.

McMahon, P. B., & Chapelle, F. H. (2008). Redox processes and water quality of selected principal aquifer systems. *Ground Water, 46*(2), 259-271.

McPhillips, L. E., Creamer, A. E., Rahm, B. G., & Walter, M. T. (2014). Assessing dissolved methane patterns in central New York groundwater. *Journal of Hydrology: Regional Studies, 1*, 57-73.

Mendizabal, I., Stuyfzand, P. J., & Wiersma, A. P. (2011). Hydrochemical system analysis of public supply well fields, to reveal water-quality patterns and define groundwater bodies: The Netherlands. *Hydrogeology Journal, 19*(1), 83-100.

Meraat, M., Jafari, H., & Qishlaqi, A. (2017). Assessing the source of nitrate and heavy metals in groundwater resources of Abarkooh plain, central Iran.

Ministry of Health. (2000). *Drinking-water Standards for New Zealand.* Wellington: Ministry of Health.

Moir, J. L., Cameron, K. C., Di, H. J., & Fertsak, U. (2011). The spatial coverage of dairy cattle urine patches in an intensively grazed pasture system. *The Journal of Agricultural Science, 149*(04), 473-485.

Molloy, L. (1988). *Soils in the New Zealand landscape: the living mantle.* Wellington, New Zealand: Mallinson Rendell

Moncaster, S., Bottrell, S., Tellam, J., Lloyd, J., & Konhauser, K. (2000). Migration and attenuation of agrochemical pollutants: insights from isotopic analysis of groundwater sulphate. *Journal of Contaminant Hydrology, 43*(2), 147-163.

Morgenstern, U., Begg, J. G., Townsend, D. B., Martindale, H., Matthews, A., Roygard, J., & Clark, M. (2014). Groundwater lag times in the water discharges from the Whanganui, Rangitikei and Manawatu catchments, *GNS Science Report 2014/35*. 1-39.

Morgenstern, U., Brown, L., Begg, J., Daughney, C., & Davidson, P. (2009). Lin*kwater catchment groundwater residence time, flow pattern, and hydrochemistry trends.* (GNS Science report 2009/08). Lower Hutt, New Zealand. 47 pages

Mortimer, N. (1994). Origin of the Torlesse terrane and coeval rocks, North Island, New Zealand. *International geology review, 36*(10), 891-910.

Neall, V. E., & Hanson, J. (1995). *The Neotectonics of the Ruahine and Mohaka Faults, Between the Manawatu Gorge and Puketitiri*: Earthquake and War Damage Commission.

Newsome, P., Wilde, R., & Willoughby, E. (2008). *Land resource information system spatial data layers: data dictionary*: Landcare Research New Zealand.

NIWA. (2016). CLUES – Catchment land use for environmental sustainability model. Retrieved from https://www.niwa.co.nz/freshwater-and-estuaries/our-services/catchment-modelling/clues-%E2%80%93-catchment-land-use-for-environmental-sustainability-model

Nolan, B. T. (1999). Nitrate behavior in ground waters of the southeastern USA. *Journal of Environmental Quality, 28*(5), 1518-1527.

Palmer, A. (2009). Detailed soil mapping in the Tararua District. Dannevirke, NZ: Tararua District Council.

Parfitt, R., Schipper, L., Baisden, W., & Elliott, A. (2006). Nitrogen inputs and outputs for New Zealand in 2001 at national and regional scales. *Biogeochemistry, 80*(1), 71-88.

Parfitt, R., Stevenson, B. A., Dymond, J. R., Schipper, L. A., Baisden, W. T., & Ballantine, D. (2012). Nitrogen inputs and outputs for New Zealand from 1990 to 2010 at national and regional scales. *New Zealand Journal of Agricultural Research, 55*(3), 241-262.

Pedersen, J. K., Bjerg, P. L., & Christensen, T. H. (1991). Correlation of nitrate profiles with groundwater and sediment characteristics in a shallow sandy aquifer. *Journal of Hydrology, 124*(3-4), 263-277.

Pehlivan, R., Emre, H., & Key, D. (2012). Effect of Talus Deposit Excavations on Hydrogeochemical Characteristics of Kuvars Spring Water, Maltepe, Istanbul, Turkey. *Journal of Water Resource and Protection, 4*(5), 294.

Peterson, M., Curtin, D., Thomas, S., Clough, T., & Meenken, E. (2013). Denitrification in vadose zone material amended with dissolved organic matter from topsoil and subsoil. *Soil Biology and Biochemistry, 61*, 96-104.

Peyton, B. M., Mormile, M. R., & Petersen, J. N. (2001). Nitrate reduction with Halomonas campisalis: kinetics of denitrification at pH 9 and 12.5% NaCl. *Water research, 35*(17), 4237-4242.

Pfenning, K., & McMahon, P. (1997). Effect of nitrate, organic carbon, and temperature on potential denitrification rates in nitrate-rich riverbed sediments. *Journal of Hydrology, 187*(3), 283-295.

Puckett, L. (2004). Hydrogeologic controls on the transport and fate of nitrate in ground water beneath riparian buffer zones: results from thirteen studies across the United States. *Water Science & Technology, 49*(3), 47-53.

Raiber, M., White, P. A., Daughney, C. J., Tschritter, C., Davidson, P., & Bainbridge, S. E. (2012). Three-dimensional geological modelling and multivariate statistical analysis of water chemistry data to analyse and visualise aquifer structure and groundwater composition in the Wairau Plain, Marlborough District, New Zealand. *Journal of Hydrology, 436*, 13-34.

Ramesh Kumar, A., & Riyazuddin, P. (2012). Seasonal variation of redox species and redox potentials in shallow groundwater: A comparison of measured and calculated redox potentials. *Journal of Hydrology, 444-445*, 187-198. doi:10.1016/j.jhydrol.2012.04.018

Rawlinson, Z., & Begg, J. G. (2014). Hydrogeology of the Upper Manawatu and Mangatainoka Catchments, Tararua *GNS Science Consultancy Report* (Vol. 2104/127, pp. 48p).

Rice, E., Baird, R., Eaton, A., & Clesceri, L. (Eds.). (2012). *Standard Methods for the Examination of Water and Wastewater, twenty-second ed. American Public Health Association, American Water Works Association, Water Environment Federation.* .

Rissmann, C. (2011). *Regional mapping of groundwater denitrification potential and aquifer sensitivity* (Technical Report 2011-12). Invercargill, New Zealand: Southland Regional Council.

Rissmann, C., Rodway, E., Beyer, M., Marapara, T., Hodgetts, J., Pearson, L., & Killick, M. (2016). *Physiographics of Southland part 1: Delineation of key drivers of regional hydrochemistry: Technical Chapter 5: Comparison of Soil Water with Surface water and Groundwater Chemistry.* Environment Southland publication.

Rivas, A., Singh, R., Bishop, P., Horne, D., Roygard, J., & Hedley, M. J. (2014). Measuring denitrification in the subsurface environment of Manawatu River catchment. *In: Nutrient management for the farm, catchment and community.* (Eds L.D. Currie and C L. Christensen). http://flrc.massey.ac.nz/publications.html. Occasional Report No. 27. Fertilizer and Lime Research Centre, Massey University, Palmerston North, New Zealand. 13 pages.

Rivas, A., Singh, R., Horne, D., Roygard, J., Mathews, A., & Hedley, M. J. (2015). An assessment of the denitrification potential in shallow groundwaters of the Manawatu River catchment. *In: Moving farm systems to improved attenuation.* (Eds L.D. Currie and L.L Burkitt). http://flrc.massey.ac.nz/publications.html. Occasional Report No. 28. Fertilizer and Lime Research Centre, Massey University, Palmerston North, New Zealand. 15 pages.

Rivas, A., Singh, R., Horne, D., Roygard, J., Matthews, A., & Hedley, M. J. (2014). *Characterization of denitrification in the Subsurface Environment of the Manawatu River catchment, New Zealand.* Paper presented at the 21st Century Watershed Technology Conference and Workshop Improving Water Quality and the Environment Conference Proceedings, 3-6 November 2014, University of Waikato, New Zealand.

Rivas, A., Singh, R., Horne, D., Roygard, J., Matthews, A., & Hedley, M. J. (2017). Denitrification potential in the subsurface environment in the Manawatu River catchment, New Zealand: Indications from oxidation-reduction conditions, hydrogeological factors, and implications for nutrient management. *Journal of Environmental Management, 197*, 476-489.

Rivett, M. O., Buss, S. R., Morgan, P., Smith, J. W., & Bemment, C. D. (2008). Nitrate attenuation in groundwater: a review of biogeochemical controlling processes. *Water research, 42*(16), 4215-4232.

Rodway, E., Rissmann, C., Beyer, M., Wilson, K., Hughes, B., Millar, R., . . . Hodgetts, J. (2016). *Physiographic controls over southland's ground and surface water*

hydrochemistry and quality. Environment Southland publication number: 2016/13 ISBN: 978-0-909043-16-2 (online).

Rose, S., & Long, A. (1988). Monitoring dissolved oxygen in ground water: some basic considerations. *Groundwater Monitoring & Remediation, 8*(1), 93-97.

Rosen, M. R., & McNeill, W. J. (1996). Hydrogeology, water quality, and nitrate movement in the unconfined gravel aquifer beneath Maraekaho sheep feedlot, Hawke's Bay, New Zealand. *Journal of Hydrology, 35*(1), 28-48.

Rütting, T., Boeckx, P., Müller, C., & Klemedtsson, L. (2011). Assessment of the importance of dissimilatory nitrate reduction to ammonium for the terrestrial nitrogen cycle. *Biogeosciences, 8*(7), 1779-1791.

Sadashivaiah, C., Ramakrishnaiah, C., & Ranganna, G. (2008). Hydrochemical analysis and evaluation of groundwater quality in Tumkur Taluk, Karnataka State, India. *International journal of environmental research and public health, 5*(3), 158-164.

Saggar, S., Jha, N., Deslippe, J., Bolan, N., Luo, J., Giltrap, D., . . . Tillman, R. (2013). Denitrification and N2O: N2 production in temperate grasslands: processes, measurements, modelling and mitigating negative impacts. *Science of the total environment, 465*, 173-195.

Sanford, R. F., Pierson, C. T., & Crovelli, R. A. (1993). An objective replacement method for censored geochemical data. *Mathematical Geology, 25*(1), 59-80.

Schulmeister, M. K., Butler, J., Healey, J. M., Zheng, L., Wysocki, D., & McCall, G. (2003). Direct-Push Electrical Conductivity Logging for High-Resolution Hydrostratigraphic Characterization. *Groundwater Monitoring & Remediation, 23*(3), 52-62.

Schulmeister, M. K., Healey, J. M., Butler, J. J., & McCall, G. W. (2004). Direct-push geochemical profiling for assessment of inorganic chemical heterogeneity in aquifers. *Journal of Contaminant Hydrology, 69*(3), 215-232.

Schüring, J., Schulz, H. D., Fischer, W. R., Böttcher, J., & Duijnisveld, W. H. (2013). *Redox: fundamentals, processes and applications*: Springer Science & Business Media.

Singh, A., & Kumar, S. (2015). Quality assessment of groundwater for drinking and irrigation use in semi-urban area of Tripura, India. *Ecology, Environment and Conservation, 21(1)*, 97-108.

Singh, R., Elwan, A., Horne, D., Manderson, A., Patterson, M., & Roygard, J. (2017). Predicting land-based nitrogen loads and attenuation in the Rangitikei River

catchment–the model development. In: Science and Policy: Nutrient Management Challenges for the Next Generation. (Eds L.D. Currie and M. J. Hedley). http://flrc.massey.ac.nz/publications.html. Occasional Report No. 30. Fertilizer and Lime Research Centre, Massey University, Palmerston North, New Zealand. 13 pages.

Singh, R., Rivas, A., Espanto, P., Elwan, A., Horne, D., Roygard, J., . . . Clothier, B. E. (2014a). Assessment of transport and transformation of nitrogen in the subsurface environment of Manawatu River catchment – work in progress. *In: Nutrient management for the farm, catchment and community.* (Eds L.D. Currie and C L. Christensen). http://flrc.massey.ac.nz/publications.html. Occasional Report No. 27. Fertilizer and Lime Research Centre, Massey University, Palmerston North, New Zealand. 11 pages.

Singh, R., Rivas, A., Espanto, P., Elwan, A., Horne, D., Roygard, J., . . . Clothier, B. E. (2014b). Measuring denitrification in the subsurface environment of Manawatu River catchment. *In: Nutrient management for the farm, catchment and community.* (Eds L.D. Currie and C L. Christensen). http://flrc.massey.ac.nz/publications.html. Occasional Report No. 27. Fertilizer and Lime Research Centre, Massey University, Palmerston North, New Zealand. 11 pages.

Singh, R., Rivas, A., Espanto, P., Elwan, A., Horne, D., Roygard, J., . . . Clothier, B. E. (2014). Assessment of transport and transformation of nitrogen in the subsurface environment of Manawatu River catchment – work in progress. *In: Nutrient management for the farm, catchment and community.* (Eds L.D. Currie and C L. Christensen). http://flrc.massey.ac.nz/publications.html. Occasional Report No. 27. Fertilizer and Lime Research Centre, Massey University, Palmerston North, New Zealand. 11 pages.: Occasional Report.

Singleton, M., Esser, B., Moran, J., Hudson, G., McNab, W., & Harter, T. (2007). Saturated zone denitrification: potential for natural attenuation of nitrate contamination in shallow groundwater under dairy operations. *Environmental science & technology, 41*(3), 759-765.

Sirisena, K. A., Daughney, C. J., Moreau-Fournier, M., Ryan, K. G., & Chambers, G. K. (2013). National survey of molecular bacterial diversity of New Zealand groundwater: relationships between biodiversity, groundwater chemistry and aquifer characteristics. *FEMS Microbiology Ecology*(3), 490.

Smil, V. (1999). Detonator of the population explosion. *Nature, 400*(6743), 415.

Spalding, R. F., & Exner, M. E. (1993). Occurrence of nitrate in groundwater—a review. *Journal of Environmental Quality, 22*(3), 392-402.

Sparks, D. L. (2003). *Environmental soil chemistry.* London, UK: Academic press.

Spruill, T. (2004). Effectiveness of riparian buffers in controlling ground-water discharge of nitrate to streams in selected hydrogeologic settings of the North Carolina Coastal Plain. *Water Science & Technology, 49*(3), 63-70.

Statistics New Zealand. (2017). River water quality: nitrogen. Retrieved from http://archive.stats.govt.nz/browse_for_stats/environment/environmental-reporting-series/environmental-indicators/Home/Fresh%20water/river-water-quality-nitrogen.aspx.

Steele, K. W., Bonish, P., & Sarathchandra, S. (1984). Denitrification potentials and microbiological characteristics of some northern North Island soils. *New Zealand Journal of Agricultural Research, 27*(4), 525-530.

Stefánsson, A., Arnórsson, S., & Sveinbjörnsdóttir, Á. E. (2005). Redox reactions and potentials in natural waters at disequilibrium. *Chemical Geology, 221*, 289-311.

Stenger, R., Barkle, G., Bidwell, V., Burgess, C., Wall, A., Haas, M., & Mertens, J. (2005). From the paddock to the stream—Unravelling the nitrogen flowpaths in a New Zealand dairying catchment *Managing Watersheds for Human and Natural Impacts: Engineering, Ecological, and Economic Challenges* (pp. 1-10).

Stenger, R., Barkle, G., Burgess, C., Wall, A., & Clague, J. (2008). Low nitrate contamination of shallow groundwater in spite of intensive dairying: the effect of reducing conditions in the vadose zone-aquifer continuum. *Journal of Hydrology (New Zealand), 47*(1), 1.

Stenger, R., Clague, J., Woodward, S., Moorhead, B., Burbery, L., & Canard, H. (2012). Groundwater assimilative capacity -an untapped opportunity for catchment-scalenitrogen management? In: *Advanced Nutrient Management: Gains from the Past -Goals for the Future.* (Eds L.D. Currie and C L. Christensen). http://flrc.massey.ac.nz/publications.html.Occasional Report No. 25. Fertilizer and Lime Research Centre, Massey University, Palmerston North, New Zealand. 10 pages

Stenger, R., Clague, J., Woodward, S., Moorhead, B., Wilson, S., Shokri, A., . . . Canard, H. (2013). Denitrification – the key component of a groundwater system's assimilative capacity for nitrate. In: *Accurate and efficient use of nutrients on farms.* (Eds L.D. Currie and C L. Christensen). http://flrc.massey.ac.nz/publications.html. Occasional Report No. 26. Fertilizer and Lime Research Centre, Massey University, Palmerston North, New Zealand. 11 pages.

Stenger, R., Clague, J., Woodward, S., Moorhead, B., Wilson, S., Shokri, A., . . . Canard, H. (2013). Denitrification–The key component of a groundwater system‟ s assimilative capacity for nitrate. *Accurate and efficient use of nutrients on farms.(Eds LD Currie and C L. Christensen). Occasional Report*(26).

Stenger, R., Clague, J., Woodward, S., Morgenstern, U., & Clough, T. (2015). Multi-pronged approach to elucidate nitrate attenuation in shallow groundwater. *In: Moving farm systems to improved attenuation. (Eds L.D. Currie and L.L Burkitt).* http://flrc.massey.ac.nz/publications.html. Occasional Report No. 28. Fertilizer and Lime Research Centre, Massey University, Palmerston North, New Zealand. 7 pages.

Taylor, C., Trompetter, V., Brown, L., & Bekesi, G. (2001). The Manawatu aquifers, North Island, New Zealand: Clarification of hydrogeology using a multidisciplinary environmental tracer approach. *Hydrological Processes, 15*(17), 3269-3286.

Templeton, G. (2011). A two-step approach for transforming continuous variables to normal: implications and recommendations for IS research. *Communications of the Association for Information, 28(4)*, 41-58.

Tesoriero, A. J., Liebscher, H., & Cox, S. E. (2000). Mechanism and rate of denitrification in an agricultural watershed: Electron and mass balance along groundwater flow paths. *Water Resources Research, 36*(6), 1545-1559.

Thorstenson, D. C., Fisher, D. W., & Croft, M. G. (1979). The geochemistry of the fox hills-basal hell creek aquifer in southwestern North Dakota and northwestern South Dakota. *Water Resources Research, 15*(6), 1479-1498.

Tidswell, S., Conwell, C., & Milne, J. (2012). *Groundwater quality in the Wellington region: State and trends* (GW/EMI-T-12/140). Retrieved from http://www.gw.govt.nz/assets/Our-Environment/Environmental-monitoring/Environmental-Reporting/Groundwater-Quality-SoE-report.pdf

Trewick, S., & Bland, K. (2012). Fire and slice: palaeogeography for biogeography at New Zealand's North Island/South Island juncture. *Journal of the Royal Society of New Zealand, 42*(3), 153-183.

Vale, S., Fuller, I., Procter, J., Basher, L., & Smith, I. (2015). Application of a confluence-based sediment-fingerprinting approach to a dynamic sedimentary catchment, New Zealand. *Hydrological Processes, 30*, 812-829.

Van Den Heuvel, R., Van Der Biezen, E., Jetten, M., Hefting, M., & Kartal, B. (2010). Denitrification at pH 4 by a soil-derived Rhodanobacter-dominated community. *Environmental microbiology, 12*(12), 3264-3271.

VanTrump, G., & Miesch, A. (1977). The US Geological Survey RASS-STATPAC system for management and statistical reduction of geochemical data. *Computers & Geosciences, 3*(3), 475-488.

Verchot, L. V., Franklin, E. C., & Gilliam, J. W. (1998). Effects of agricultural runoff dispersion on nitrate reduction in forested filter zone soils. *Soil Science Society of America Journal, 62*(6), 1719-1724.

Vidon, P., & Hill, A. R. (2005). Denitrification and patterns of electron donors and acceptors in eight riparian zones with contrasting hydrogeology. *Biogeochemistry, 71*(2), 259-283.

Wang, Z., Bush, R. T., Sullivan, L. A., & Jianshe, L. (2013). Simultaneous Redox Conversion of Chromium(VI) and Arsenic(III) under Acidic Conditions. *Environmental science & technology, 47*(12), 6486-6492.

Webb, T., Claydon, J. J., & Harris, S. R. (2000). Quantifying variability of soil physical properties within soil series to address modern land-use issues on the Canterbury Plains, New Zealand. *Australian Journal of Soil Research*(6).

Webb, T., Hewitt, A., Lilburne, L., McLeod, M., & Close, M. (2010). Mapping of vulnerability of nitrate and phosphorus leaching, microbial bypass flow, and soil runoff potential for two areas of Canterbury. *Environment Canterbury Technical Report, 10*.

White, D. E. (1957). Magmatic, connate, and metamorphic waters. *Geological Society of America Bulletin, 68*(12), 1659-1682.

WHO, G. (2011). Guidelines for drinking-water quality. *World Health Organization, 216*, 303-304.

Woods, R., Elliott, S., Shankar, U., Bidwell, V., Harris, S., Wheeler, D., . . . Gibb, R. (2006). The CLUES project: predicting the effects of land-use on water quality–stage II. *NIWA client report MAF05502*.

Woods, R., Elliott, S., Shankar, U., Schmidt, J., Bidwell, V., Bright, J., . . . Gibb, R. (2004). The CLUES project: predicting the effects of land-use on water quality–stage I. *NIWA client report MAF04501*, 107.

Woodward, S., Stenger, R., & Bidwell, V. (2011). Using a simple 2D steady-state saturated flow and reactive transport model to elucidate denitrification patterns in a hillslope aquifer. 19th International Congress on Modelling and Simulation, Perth, Australia, 12-16 December 2011.

Woodward, S., Stenger, R., & Bidwell, V. (2013). Using stream flow and chemistry data to estimate catchment scale groundwater and nitrate flux. In: *Accurate and efficient use of nutrients on farms.* (Eds L.D. Currie and C L. Christensen). http://flrc.massey.ac.nz/publications.html. Occasional Report No. 26. Fertilizer and Lime Research Centre, Massey University, Palmerston North, New Zealand. 12 pages.

Wrage, N., Velthof, G., Van Beusichem, M., & Oenema, O. (2001). Role of nitrifier denitrification in the production of nitrous oxide. *Soil Biology and Biochemistry, 33*(12-13), 1723-1732.

Yaremko, R. M., Harari, H., Harrison, R. C., & Lynn, E. (2013). *Handbook of research and quantitative methods in psychology: For students and professionals*: Psychology Press.

Yeomans, J., Bremner, J., & McCarty, G. (1992). Denitrification capacity and denitrification potential of subsurface soils. *Communications in Soil Science & Plant Analysis, 23*(9-10), 919-927.

Younger, P. L. (2007). *Groundwater in the environment : an introduction*. Malden, MA: Blackwell Pub.

Zapata-Peñasco, I., Salazar-Coria, L., Saucedo-García, M., Villa-Tanaca, L., & Hernández-Rodríguez, C. (2016). Bisulfite reductase gene expression of thermophilic sulphate-reducing bacteria from saline connate water of oil reservoirs with high temperature. *International Biodeterioration & Biodegradation, 108*, 198-206.

Zemansky, G. M. (2007). *Kowhitirangi and Kokatahi plains groundwater assessment.* Taupo, N.Z.: GNS Science.

Appendices:

Appendix A: Geological History of the Tararua GWMZ

A.1 Introduction

Following the onset of rifting in the Tasman Sea during the Cretaceous, the eastward movement of the New Zealand continental block and subsequent cooling of the oceanic lithospheric plates resulted in a significant marine transgression. The oceanic transgression peaked in the late Oligocene when the entire country was virtually submerged (Graham, 2008). In the early Miocene, initiation of subduction to the east gradually exhumed most of what was to become the New Zealand landmass (Graham, 2008). However much of the southern North Island remained submerged right through to the early Pliocene, while parts of the Manawatu, Wairarapa and Wellington areas (Figure 109) were still inundated until the mid Quaternary (Kamp et al., 2004).

Since the Miocene epoch, tectonic deformation combined with fluctuation in eustatic sea level in New Zealand has resulted in periodic marine transgressions and deposition of a range of sediments throughout the Tararua GWMZ. These more recent stratigraphic units comprise the majority of the regions aquifer/aquitard systems and are of key importance to the hydrogeology of the Tararua GWMZ. The provenance of these sediments is fundamental to the understanding the hydrogeological properties of the various lithological units in the Tararua GWMZ and therefore a brief geological history from the Pliocene and Pleistocene is provided.

A.2 Tectonic Framework and Geological Structure of the Tararua GWMZ

The diverse topography of the Tararua GWMZ is indicative of a complex geological history fundamentally controlled by plate tectonics (Rawlinson & Begg, 2014). Figure 106 illustrates the current tectonic setting where at the Hikurangi Trough, the western margin of the Australian Plate is obliquely under thrust by the eastward moving Pacific

Plate (Begg & Johnston, 2000). Convergence along the entire subduction margin is variable (Cole & Lewis, 1981); however, Lee and Begg (2002) estimate convergence of around 40 mm per year offshore of the Tararua GWMZ at the Hikurangi trench. The compressional tectonic regime has resulted in a classic series of subduction associated landforms such as a frontal ridge and axial ranges, forearc basin, and accretionary prism associated with NE-SW trending folds and faults (Cole & Lewis, 1981; Lee et al., 2011).

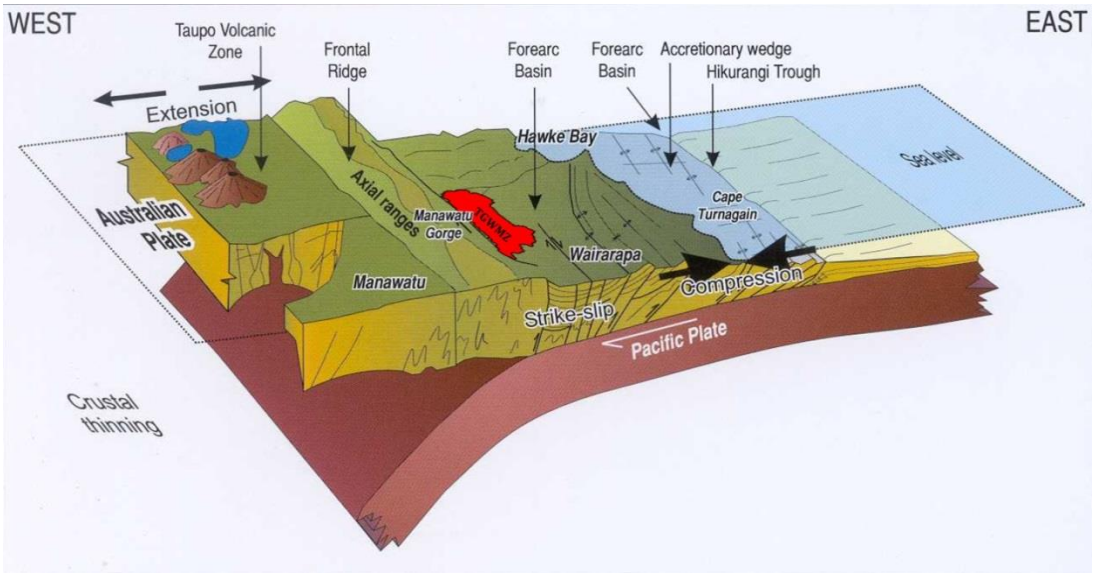

Figure 106: 3D conceptual diagram of the current tectonic setting for Southern Hawkes Bay – Northern Wairarapa; approximate location of the Tararua GWMZ overlaid in red. The Pacific Plate is converging with, and subducting below the Australian Plate at approx. 40 mm y^{-1}. Key aspects of the tectonic setting in relation to the hydrogeology of the Tararua GWMZ (red polygon) location include the forearc basin, axial ranges, and margin parallel fault and fold systems (adapted from Lee & Begg, 2002).

Within the Tararua GWMZ, compressional forces are expressed by a number of reverse and thrust faults that dip to the west and strike approximately parallel to the subduction margin (Figure 107). Many of the reverse faults initiated in the late Neogene to early Quaternary are currently considered inactive (Rawlinson & Begg, 2014). The active strike-slip faults such as the Wellington, Ruahine and Mohaka Faults are components of the North Island Fault System. These features are noteworthy for the

extensive level of vertical slip expressed in the elevations of the Tararua and Ruahine Ranges (Rawlinson & Begg, 2014). The Pahiatua and Alfredton Faults that lie in the centre and along the eastern margins of the Tararua GWMZ respectively are also active and are noted for their steep westerly dips (Rawlinson & Begg, 2014). Also conspicuous throughout the study area are a series of asymmetrical synclines and anticlines with (approximately) NE-SW striking axes, and eastern limbs that dip much steeper than the westward limbs (Krieger, 1992). Most folds in the area are inactive, with only the northerly plunging Pori, Tawhero, and Waipatiki synclines considered active (Heron, 2014).

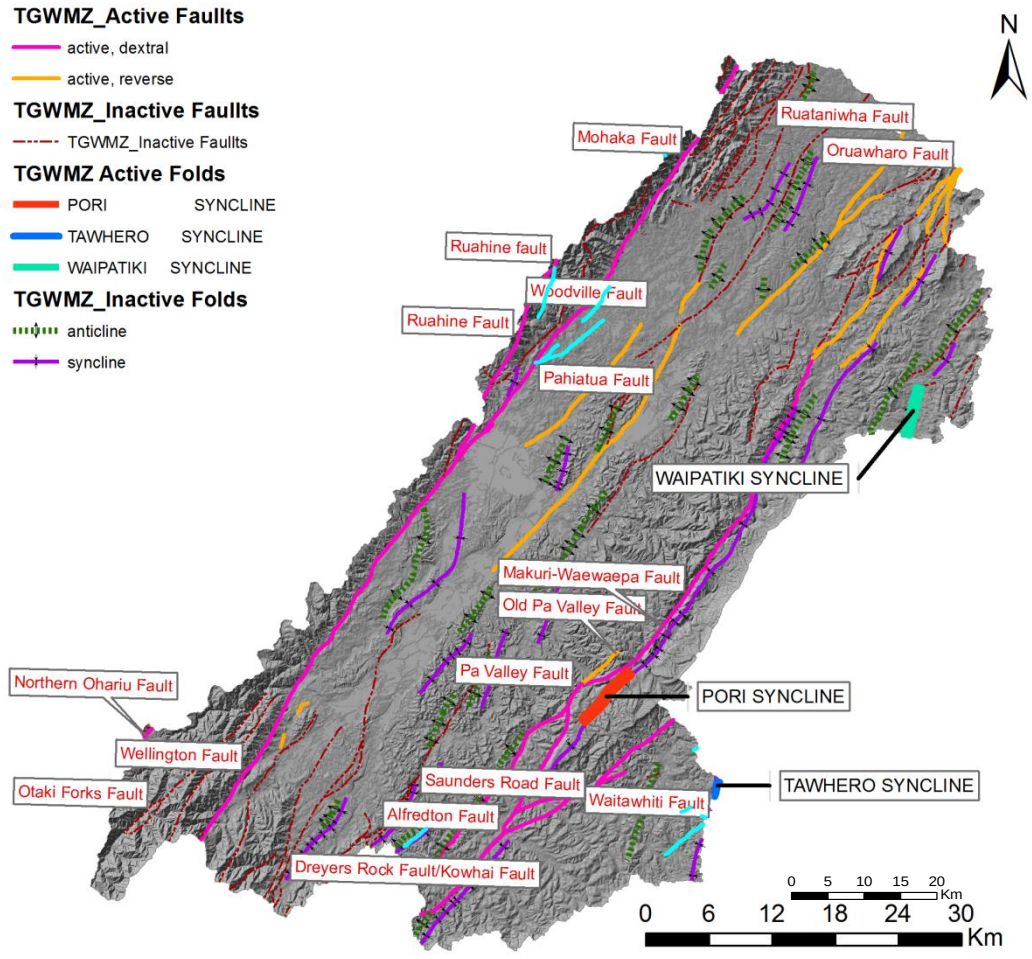

Figure 107: Faults and active folds in the Tararua GWMZ. The NE-SW strike of the faults and folds echo the strike of the Hikurangi Trench around 150 km to the east, at the subduction margin between the Pacific and Australian plates. Active features are labelled while only the traces of inactive faults and the axes of inactive folds are displayed. (Map generated in ArcGIS 10.2 using shapefiles from Heron (2014); Land Information New Zealand (2011b)).

A.3 Early Pliocene

Circa 4.7 Ma, the tectonically driven Tangahoe Pulldown (Hansen & Kamp, 2008) forced an intense period of subsidence in the Manawatu-Wanganui region which culminated in depths of the central Wanganui basin increasing to over 400 m (Trewick & Bland, 2012). East of the (present day) axial ranges and striking N-S, a sedimentary basin began to form with its western margin proximal to the (still submerged) ridge-crest of the axial ranges (Krieger, 1992). Trewick and Bland (2012) suggest in the late-early Pliocene, the Ruahine and Tararua Ranges were little more than a low lying finger of basement rocks, showing no evidence of a seaway where the Manawatu Gorge exists today. As uplift of the accretionary wedge continued, small islands and shoals appeared in Eastern Hawke's Bay and Northern Wairarapa (Trewick & Bland, 2012). The shallowing of the seas are reflected in a change in deposition from massive, homogenous, soft, fine grained sediments to calcareous sandstones, mudstones, and eventually limestones and coquina along the margins of the islands, shoals and proto-ranges (Figure 108).

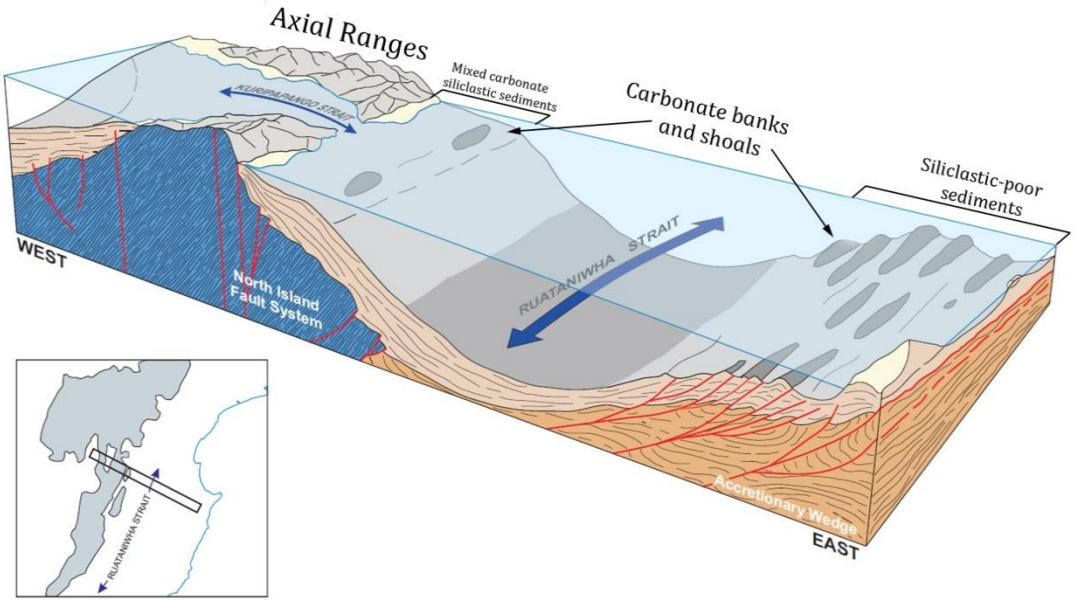

Figure 108: Conceptual diagram illustrating the nature of sediments deposited during the Pliocene in relation to diverse depositional conditions proximal to the Axial Ranges, within the Ruataniwha Straight and along the uplifted margins of the accretionary wedge (adapted from Lee, Bland, Townsend, & Kamp, 2011, p. 34).

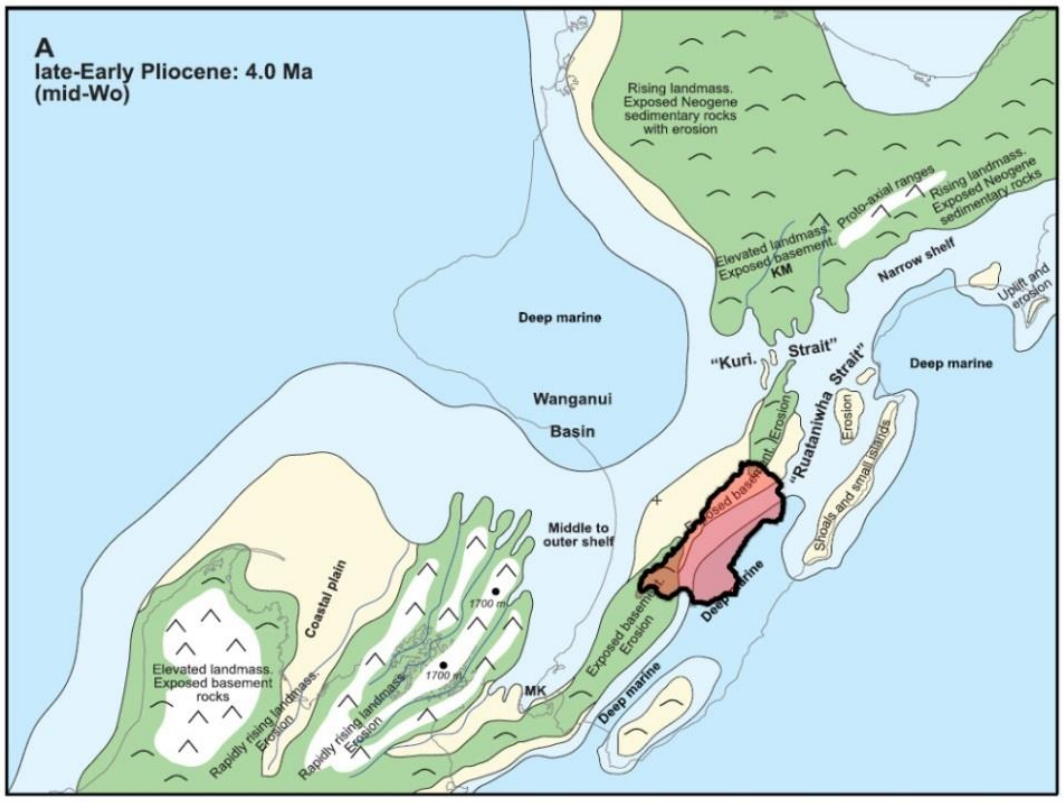

Figure 109: The extent of Central New Zealand's landmass around 4.0 Ma. At this time the Kuri Strait between Taihape and Napier was open, and further south an erosional surface which exposed the basement greywackes was evident. The provenance of sediments in the central margins of the Tararua GWMZ attest to inundation by shallow marine conditions while the eastern margins were covered by considerable deeper water. Note: Shading is the same for the following series of maps. Green shading indicates exhumed land, pale yellow = coastal plains, pale blue = shallow marine, and mid-blue indicates deep marine environments. The present day coastline is shown by the thin black line and the red shaded polygon is the relative location of the Tararua GWMZ (adapted from Trewick & Bland, 2012, p. 161).

A.4 Mid to Late Pliocene

During the mid Pliocene (Waipipian Stage 3 – 2.5 Ma) the Wanganui basin continued to subside due to faulting, the axial ranges ridge crest remained submerged and deposition of sand, mud, and gravel into the basin continued (Krieger, 1992). Depths in the Wanganui Basin were still around 400 m to 600 m but shallowed to 0 - 200 m in the Ruataniwha Strait. Continued uplift of the accretionary wedge saw the accumulation of

extensive shell banks around the shallowing shoals and developing archipelagos (Trewick & Bland, 2012). At this time, the modern-day Tararua Ranges were a low lying peninsula that terminated in a narrow seaway where the Manawatu Gorge now exists (Trewick & Bland, 2012).

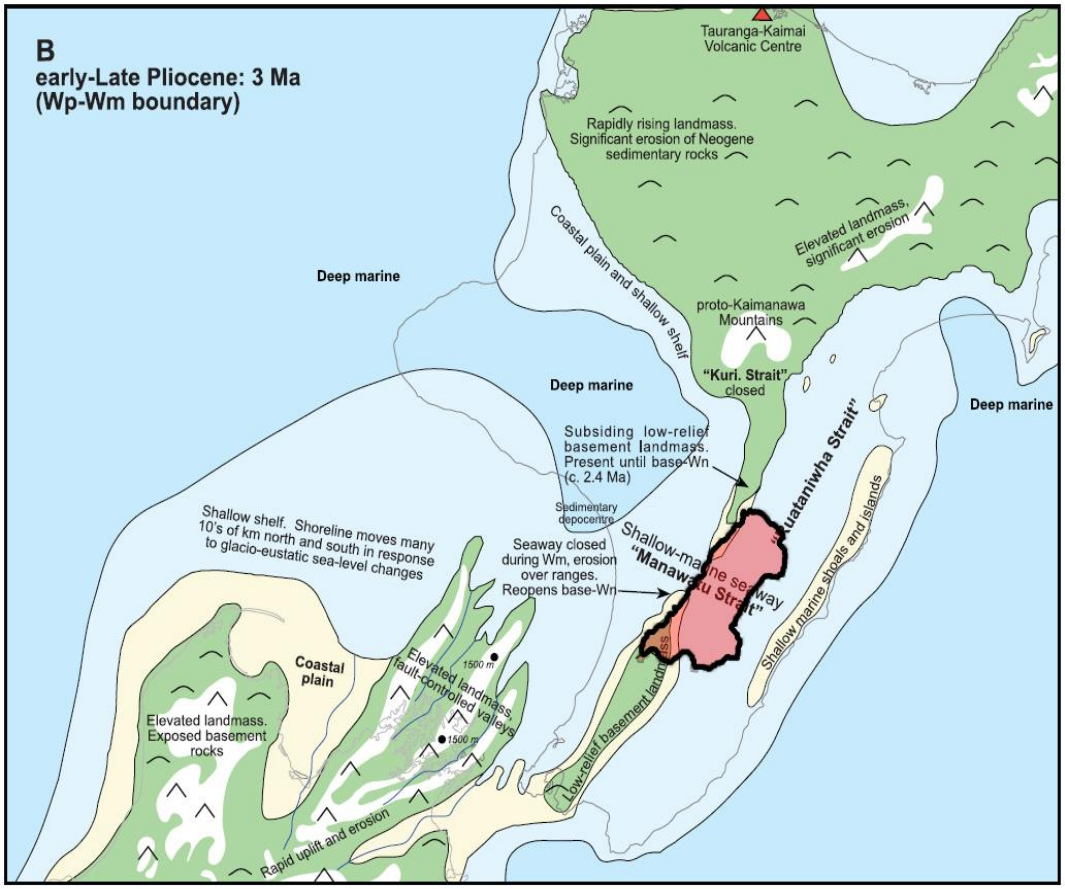

Figure 110: The extent of Central New Zealand's landmass around 3.0 Ma. Practically the entire Tararua GWMZ was occupied by a shallow marine environment comprised of the Manawatu and Ruataniwha Straits. The proto axial ranges were exposed north and south of the Manawatu Strait and at the time were actively subsiding, while the Waewaepa ranges merely consisted of shallow marine shoals and islands (adapted from Trewick & Bland, 2012, p. 161).

A.5 Early Pleistocene

At the early Quaternary (2.4 Ma; the Mangapanian- Nukumaruan New Zealand stage boundary) the Ruahines were still submerged and the Manawatu seaway had reached its greatest size, extending lengthways from the Wanganui Basin to Central and Southern Hawkes Bay and widthways from the (modern) southern Ruahines and northern Tararuas; depths at the time are estimated to be up to 100 m (Trewick & Bland, 2012). The Nukumaruan shallow-marine limestones of the area were accreting onto the now subaerial eroded and ravened flanks of the Ruahine ranges. Erosion of the axial ranges generated significant volumes of greywacke gravels that were deposited over the marine sediments in braided river systems and alluvial fans to the east of the ranges (Trewick & Bland, 2012).

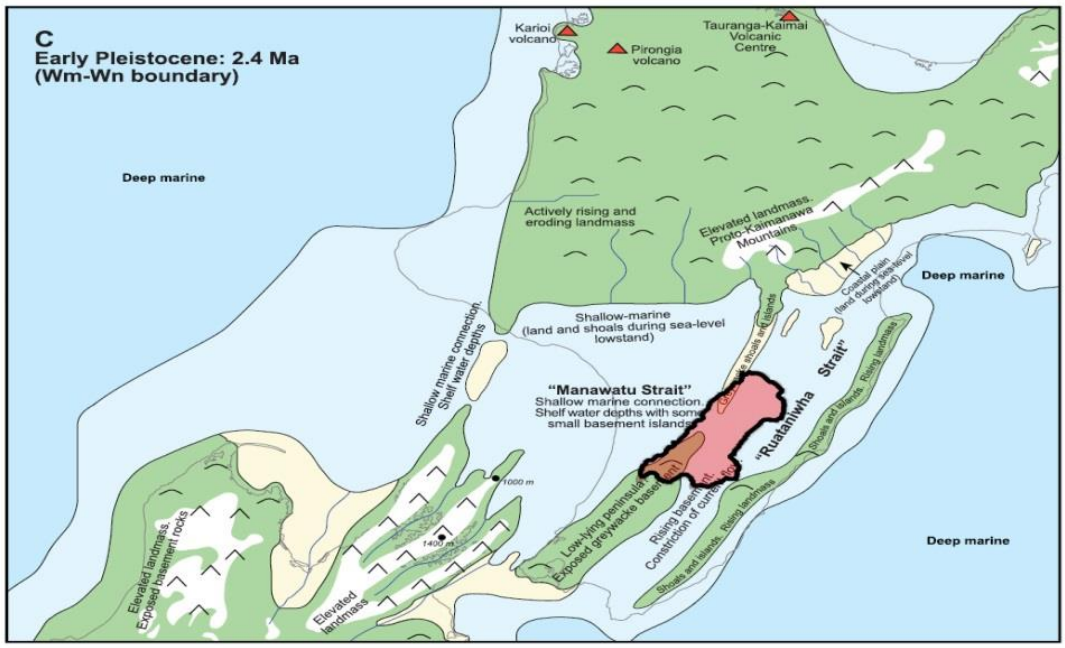

Figure 111: The extent of Central New Zealand's landmass around 2.4 Ma. Uplift was evidenced in the Tararua GWMZ by the shallowing of the marine environment and both eastern and western ranges becoming more pronounced. The Manawatu Strait still connected the Ruataniwha Strait with the Whanganui Basin but the rising basement and constriction of current flow was modifying the nature of sediments deposited (adapted from Trewick & Bland, 2012, p. 162).

A.6 Early to Mid Pleistocene

From the early to mid Pleistocene (2.0 to 1.26 Ma) despite continued basinal subsidence, uplift limited the deposition of marine sediments to west of what is now the Waewaepa Ranges. The Wairarapa Seaway gradually closed off in response to uplift of the Mount Bruce block and subsequently two discrete drainage basins developed; the Pahiatua Basin to the North and the Masterton basin to the south (Krieger, 1992; Trewick & Bland, 2012). At this time water depths in the Manawatu–Wanganui area were considered shelf to marginal marine (Trewick & Bland, 2012).

Uplift of the Ranges along the Wellington, Wairarapa and Ruahine Faults which had begun around 1.5 Ma rapidly accelerated by the mid Quaternary (around 1 Ma) due to significant vertical displacement that Trewick and Bland (2012) suggest was in response to increased convergence along the entire North Island fault system. The rapid uplift was signalled by the deposition of vast quantities of greywacke derived gravels into the basins lying east and west of both ranges. As uplift in the East continued, it forced a reversal in drainage of the Manawatu River from eastwards to westwards via what was to become the Manawatu Gorge. As down cutting of the river equalled or exceeded uplift, the Manawatu River was able to continue in its present day path through the steadily rising ranges.

A.7 Late Pleistocene to Holocene

During the Pleistocene through to the Holocene (late Quaternary c. 1 Ma) enormous volumes of rhyolitic pumiceous clasts and sands originating from the TVZ were eroded from unwelded ignimbrites and fluvially transported to be deposited within the basins. This period was also marked by a deposition of a repeating series of shallow water limestones, sandstones, and mudstones that were overlain by a sequence of estuarine

muds, silts and sands. These sediments indicate shallowing of the marine environment due to unrelenting tectonic exhumation of the landmass (Krieger, 1992) and oscillating eustatic sea levels (Lee et al., 2011).

Ultimately in the late Pleistocene and Holocene, and following the seaways retreat, vast amounts of gravels eroded from the Ruahine and Tararua Ranges were distributed widely across the plains by the meanderings of the local braided rivers and in places, covered by thick layers of loess during intensely cold and windy periods of glaciations. It is these coarse sediments that form the majority of aquifers in the region (Rawlinson & Begg, 2014).

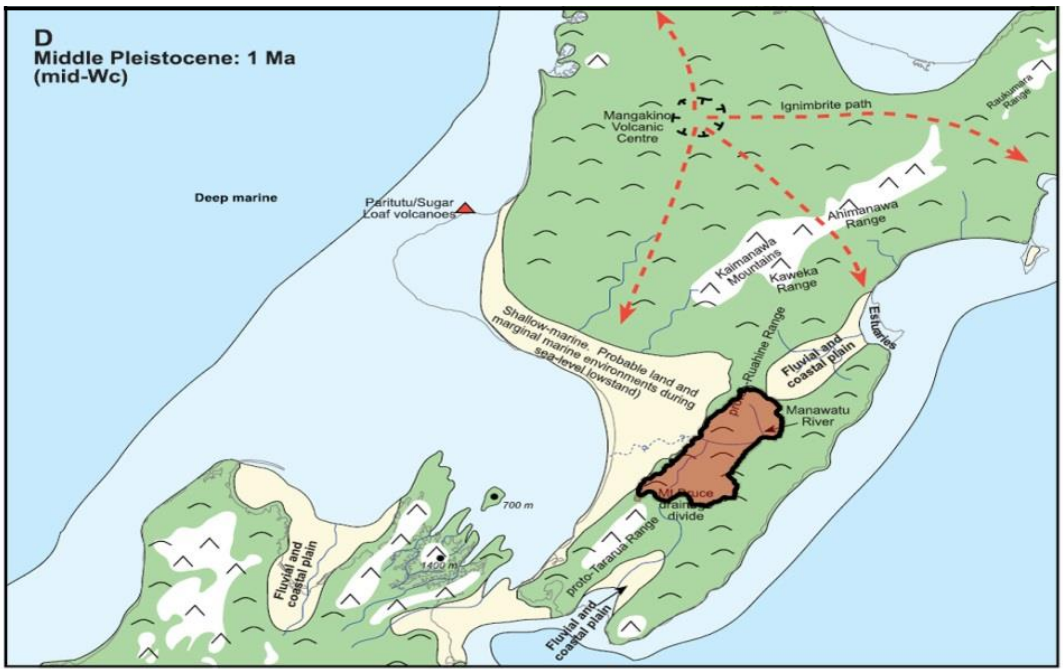

Figure 112: By 1 Ma the seaways had closed off and the sediments exposed. The uplift of Tararua and Ruahine ranges had only recently initiated. The vigorous volcanic activity of the TVZ during the late Quaternary deposited vast amount of ash, tephra and ignimbrites, across the North Island. Significant quantities of which were reworked and deposited within the Tararua GWMZ (adapted from Trewick & Bland, 2012, p. 162).

Appendix B: Digital Data Sources

B.1 Geographical and Hydrogeological Digital Data Sources

Table 19: A description and sources of geographical and hydrogeological digital data used in this study.

File	Description	Type	Scale	Source
QMap	Comprehensive geological map of New Zealand.	Vector: polygon	1:250,000	(Heron, 2014)
FSL	Fundamental Soil Map.	Vector: polygon	1:50,000	(Landcare Research, 2010b)
NZDEM	New Zealand: North Island, Digital Elevation Model (DEM).	Image: raster	1:50,000 (25m resolution)	(Landcare Research, 2010d)
Hill-shade	Hill shade Model.	Image: raster	1:250,000	(Heron, 2014)
Topographic	Georeferenced Topographic map with contours	Image: raster	1:250,000 (4.233m resolution)	(Land Information New Zealand, 2011d)
LCDB 4.1	Land Cover Database version 4.1.	Vector: polygon	1:50,000	(Landcare Research, 2015)
Potentiometric Contours	Potentiometric contours prepared for Horizons Regional Council.	Vector: linestring	n/a	(Rawlinson & Begg, 2014)
Drainage	FSL Soil drainage class.	Vector: polygon	1:50,000	(Landcare Research, 2010c)
Landuse	Land use capability.	Vector: polygon	1:50,000	(Landcare Research, 2010e)
Rivers centrelines	Centre lines of rivers of the district.	Vector: linestring	1:250,000	(Land Information New Zealand, 2011b)
Road Centrelines	Centre lines of the roads of the Tararua GWMZ.	Vector: linestring	1:250,000	(Land Information New Zealand, 2011c)
Property Titles	Property boundaries, titles & owners.	Vector:multipolygon	1:50,000	(Land Information New Zealand, 2011a)

Street Address	Street address information.	Vector: point	1:50,000	(Land Information New Zealand, 2011c)
Towns	Location of towns/cities.	Vector: point	1:50,000	(Land Information New Zealand, 2013)
WellData	Chemical analysis of bore water in the Tararua GWMZ.	Vector: point	n/a	(Rivas et al., 2017)
Horizons Bore Data	Spreadsheet of horizons well data imported into ArcGIS v10.2.	Excel spreadsheet	n/a	Horizons Regional Council

Appendix C: Groundwater Quality Analysis Methods and their Detection Limits.

C.1 Laboratory Analysis Method and Detection Limits

Table 20: A brief description of various laboratory analysis methods used for groundwater chemistry analysis of samples collected in this study.

Test	Methodology	Detection Limit	Uncertainty
Inorganic Nitrogen	By Calculation - NNN plus Ammonia	0.01 g/m^3	0.16 - 0.29
Dissolved (NP) Organic carbon	Dissolved Non-Purgeable Organic Carbon. APHA 22nd Edition 5310B,C, ASTM 02579, D4839	0.1 g/m^3	2.6 - 3.2
Dissolved inorganic carbon	APHA 22nd Edition 5310B,C, ASTM D2579, 04839	0.1 g/m^3	10.8 - 13.2
Fluoride	Ion Chromatography following IJSEPA 300.0 (modified)	0.005 g/m^3	0.061 - 0.075
Chloride	Ion Chromatography following IJSEPA 300.0 (modified)	0.005 g/m^3	11.2 - 12.4
Bromide	Ion Chromatography following IJSEPA 300.0 (modified)	0.005 g/m^3	0.041 - 0.051
Nitrate nitrogen	Ion Chromatography following IJSEPA 300.0 (modified)	0.002 g/m^3	0.009 - 0.011
Sulphate	Ion Chromatography following IJSEPA 300.0 (modified)	0.005 g/m^3	21.0 - 23.2
Nitrite-nitrogen	Ion Chromatography following IJSEPA 300.0 (modified)	0.002 g/m^3	0.002-0.003
Total oxidised nitrogen	By Calculation. Nitrite nitrogen + nitrate nitrogen. also known as nitrate-nitrite nitrogen	0.002 g/m^3	0.01 - 0.02
Ammonia nitrogen	Flow Injection Autoanalyser following APHA 22nd Edition Method 4500 NH3-H.	0.01 g/m^3	0.15 - 0.28
Boron - dissolved	ICP-OES following APHA 22nd Edition Method 3120 B (modified)	0.005 g/m^3	0.030 - 0.045
Calcium - dissolved	ICP-OES following APHA 22nd Edition Method 3120 B (modified).	0.01 g/m^3	18.6 - 22.7
Iron - dissolved	ICP-OES following APHA 22nd Edition Method 3120 B (modified).	0.005 g/m^3	12.0 - 14.6
Magnesium - dissolved	ICP-OES following APHA 22nd Edition Method 3120 B (modified).	0.01 g/m^3	3.53 - 4.31
Manganese - dissolved	ICP-OES following APHA 22nd Edition Method 3120 B (modified).	0.005 g/m^3	-
Potassium - dissolved	ICP-OES following APHA 22nd Edition Method 3120 B (modified).	0.01 g/m^3	1.33 - 1.63
Sodium - dissolved	ICP-OES following APHA 22nd Edition Method 3120 B (modified).	0.02 g/m^3	7.93 - 9.69
Silica - dissolved	ICP-OES following APHA 22nd Edition Method 3120 B (modified)	0.02 g/m^3	22.9 - 28.0
Total dissolved phosphorus	APHA 22nd Edition Method 4500-P G. Persulphate digestion follows APHA 21st Edition 4500-P	0.005 g/m^3	0.016 - 0.026
Dissolved reactive phosphorus	Flow Injection Autoanalyser following APHA 22nd Edition Method 4500-P G.	0.005 g/m^3	-0.004

Arsenic - dissolved	ICP-MS following APHA 22nd edition method 3125 (modified).	0.001 g/m^3	0.007 - 0.009
pH - onsite reading	Analysed on site by sampler	0.1 g/m^3	n/a

Appendix D: Statistical Analysis Tables

D.1 Key PCA Criteria

Table 21: Key criteria in PCA outputs generated by SPSS (Laerd Statistics, 2015e) for Data Collected Between February 2014 and May 2016.

Output	Criteria	Interpretation	Action
Correlation Matrix.	Variables < 0.03	Variables without at least one correlation score of > 0.3 throughout the matrix show little correlation to the other variables.	These values should be considered for removal from the analysis
KMO and Bartlett's Test Table and Anti-Image matrix.	Kaiser-Meyer-Olkin (KMO) measure of sampling adequacy KMO ≥ 9 Marvellous 0.8 ≤ KMO < 0.9 Meritorious 0.7 ≤ KMO < 0.8 Middling 0.6 ≤ KMO < 0.7 Mediocre 0.5 ≤ KMO < 0.6 Miserable KMO < 0.5 Unacceptable (Kaiser, 1974)	requirement for sampling adequacy > 0.5 to 0.6	Variables with KMO < 0.5 should be removed and PCA re-run
KMO and **Bartlett's** Test table	Bartlett's test of sphericity p < 0.05	Data suitable for PCA if Bartlett's test p < 0.05	Some latitude with Bartlett's test can be tolerated, PCA may still proceed with caution

D.2 Independent-Samples T-Test

Table 22: Independent-Samples T-Test Results for Data (n=99) Collected Between Feb 2014 and May 2016.

Parameter	Conclusion	t- value
Br^-	$p > 0.05$ no significant differences	$t(97) = -0.493$ $p = 0.623$
Cl^-	"	$t(97) = 0.64$ $p = 0.523$
DIC	"	$t(97) = -1.597$ $p = 0.114$
DO	"	$t(97) = -1.034$ $p = 0.303$
pH	"	$t(97) = -0.183$ $p = 0.855$
Na^+	"	$t(97) = 1.02$ $p = 0.31$
SO_4^{2-}	"	$t(97) = 0.63$ $p = 0.53$
SiO_2	"	$t(93.240) = 1.288$ $p = 0.201$[a]
NH_4^+-N	$p < 0.05$ statistically significant differences.	$t(96.957) = 3.301$ $p = 0.001$[a]
Ca^{2+}	"	$t(96.999) = 2.067$ $p = 0.041$[a]
DOC	"	$t(97) = 5.264$ $p = 0.000$
Eh	"	$t(97) = -5.239$ $p = 0.000$
HCO_3^-	"	$t(97) = 2.22$ $p = 0.029$
Fe^{2+}	"	$t(97) = 7.665$ $p = 0.000$
Mg^{2+}	"	$t(97) = 3.146$ $p = 0.002$
Mn^{2+}	"	$t(96.920) = 4.669$ $p = 0.000$[a]
NO_3^--N	"	$t(97) = 2.125$ $p = 0.036$
NO_2^--N	"	$t(96.966) = 2.96$ $p = 0.004$[a]

K^+	"	t(97) = 2.059 p = 0.042
SPC	"	t(97) = 2.335 p = 0.022

t test value t(A) = B, p =C; where t indicates comparison to t distribution, A = Between groups degrees of freedom, B = Obtained t-value, C = Probability of obtaining C, if the null hypothesis is true

[a] Unequal variances are assumed for this analyte; consequently the degrees of freedom and the t values are calculated differently to those reported where equal variances are assumed.

Mean values aren't reported as the means from transformed datasets have little relevance.

Br^- = dissolved bromide (mg L^{-1})
Ca^{2+} = dissolved calcium(mg L^{-1})
Cl^- = dissolved chloride (mg L^{-1})
DIC = dissolved inorganic carbon (mg L^{-1})
DO = dissolved oxygen (mg L^{-1})
DOC = dissolved organic carbon (mg L^{-1})
Eh = reduction potential (mV)
Fe^{2+}= dissolved iron (mg L^{-1})
HCO_3^- = bicarbonate (mg L^{-1})
K^+ = dissolved potassium(mg L^{-1})
Mg^{2+} = dissolved magnesium(mg L^{-1})
Mn^{2+}= dissolved manganese (mg L^{-1})
Na^+ = dissolved sodium(mg L^{-1})
NH_4^+ -N = ammoniacal nitrogen (mg L^{-1})
NO_2^- -N = nitrite nitrogen (mg L^{-1})
NO_3^- -N= nitrate nitrogen (mg L^{-1})
SiO_2 = dissolved silica (mg L^{-1})
SO_4^{2-}= sulphate (mg L^{-1})
SPC = specific conductivity (µScm^{-1})

D.3 Pearson Correlation Table

Parameter		idf.DOC	idf.DIC	idf.Cl^-	idf.Br^-	idf.$NO3^-$-N	idf.$SO4^{2+}$	NO_2^--N	idf.NH_4^--N	idf.Ca^{2+}	idf.Fe^{2+}	idf.Mg^{2+}	idf.Mn^{2+}
idf.DOC	Pearson Correlation	1											
	Sig. (2-tailed)												
	N	99											
idf.DIC	Pearson Correlation	.324**	1										
	Sig. (2-tailed)	0.001											
	N	99	99										
idf.Chloride	Pearson Correlation	.497**	.513**	1									
	Sig. (2-tailed)	0.000	0.000										
	N	99	99	99									
idf.Bromide	Pearson Correlation	.368**	.547**	.886**	1								
	Sig. (2-tailed)	0.000	0.000	0.000									
	N	99	99	99	99								
idf.Nitrate_N	Pearson Correlation	-0.161	-.448**	-0.137	-0.140	1							
	Sig. (2-tailed)	0.112	0.000	0.177	0.168								
	N	99	99	99	99	99							
idf.Sulphate	Pearson Correlation	0.105	-0.160	0.108	-0.047	.307**	1						
	Sig. (2-tailed)	0.299	0.113	0.286	0.644	0.002							
	N	99	99	99	99	99	99						
idf.Nitrite_N	Pearson Correlation	0.120	0.092	-0.086	-0.139	.240*	0.113	1					
	Sig. (2-tailed)	0.235	0.363	0.395	0.170	0.017	0.266						
	N	99	99	99	99	99	99	99					

**. Correlation is significant at the 0.01 level (2-tailed); *. Correlation is significant at the 0.05 level (2-tailed).

Parameter		idf.DOC	idf.DIC	idf.Cl^-	idf.Br^-	idf.$NO3^-$-N	idf.$SO4^{2+}$	NO_2^--N	idf.NH_4^--N	idf.Ca^{2+}	idf.Fe^{2+}	idf.Mg^{2+}	idf.Mn^{2+}
idf.Ammonia_N	Pearson Correlation	.570**	.561**	.430**	.389**	-.543**	-.216*	0.187	1				
	Sig. (2-tailed)	0.000	0.000	0.000	0.000	0.000	0.032	0.064					
	N	99	99	99	99	99	99	99	99				
idf.Calcium	Pearson Correlation	.400**	.483**	.587**	.502**	-0.027	.308**	.203*	.342**	1			
	Sig. (2-tailed)	0.000	0.000	0.000	0.000	0.789	0.002	0.044	0.001				
	N	99	99	99	99	99	99	99	99	99			
idf.Iron	Pearson Correlation	.562**	.212*	.325**	.266**	-.334**	-0.001	0.181	.653**	.355**	1		
	Sig. (2-tailed)	0.000	0.035	0.001	0.008	0.001	0.996	0.073	0.000	0.000			
	N	99	99	99	99	99	99	99	99	99	99		
idf.Magnesium	Pearson Correlation	.479**	.439**	.650**	.541**	-0.116	.238*	0.124	.493**	.819**	.462**	1	
	Sig. (2-tailed)	0.000	0.000	0.000	0.000	0.252	0.018	0.222	0.000	0.000	0.000		
	N	99	99	99	99	99	99	99	99	99	99	99	
idf.Manganese	Pearson Correlation	.479**	.340**	.280**	.283**	-.386**	-0.030	.226*	.644**	.451**	.763**	.617**	1
	Sig. (2-tailed)	0.000	0.001	0.005	0.005	0.000	0.767	0.024	0.000	0.000	0.000	0.000	
	N	99	99	99	99	99	99	99	99	99	99	99	99
idf.Potassium	Pearson Correlation	.535**	.423**	.544**	.476**	0.077	.214*	.243*	.403**	.423**	.252*	.440**	.202*
	Sig. (2-tailed)	0.000	0.000	0.000	0.000	0.449	0.034	0.015	0.000	0.000	0.012	0.000	0.045
	N	99	99	99	99	99	99	99	99	99	99	99	99
idf.Sodium	Pearson Correlation	.550**	.752**	.846**	.754**	-.281**	-0.015	0.022	.619**	.522**	.362**	.644**	.391**
	Sig. (2-tailed)	0.000	0.000	0.000	0.000	0.005	0.881	0.828	0.000	0.000	0.000	0.000	0.000
	N	99	99	99	99	99	99	99	99	99	99	99	99
idf.Silica	Pearson Correlation	.291**	.596**	.441**	.380**	-.455**	-0.108	0.090	.573**	.283**	.509**	.501**	.543**
	Sig. (2-tailed)	0.003	0.000	0.000	0.000	0.000	0.287	0.373	0.000	0.005	0.000	0.000	0.000
	N	99	99	99	99	99	99	99	99	99	99	99	99

**. Correlation is significant at the 0.01 level (2-tailed); *. Correlation is significant at the 0.05 level (2-tailed).

Parameter		idf.DOC	idf.DIC	idf.Cl^-	idf.Br^-	idf.$NO3^-$-N	idf.$SO4^{2+}$	NO_2^--N	idf.NH_4^--N	idf.Ca^{2+}	idf.Fe^{2+}	idf.Mg^{2+}	idf.Mn^{2+}
idf.pH	Pearson Correlation	.285**	.718**	.268**	.204*	-.499**	-.223*	.277**	.621**	.375**	.237*	.345**	.301**
	Sig. (2-tailed)	0.004	0.000	0.007	0.043	0.000	0.027	0.006	0.000	0.000	0.018	0.000	0.002
	N	99	99	99	99	99	99	99	99	99	99	99	99
idf.HCO3	Pearson Correlation	.554**	.841**	.525**	.444**	-.453**	-0.053	.236*	.727**	.602**	.466**	.596**	.515**
	Sig. (2-tailed)	0.000	0.000	0.000	0.000	0.000	0.605	0.019	0.000	0.000	0.000	0.000	0.000
	N	99	99	99	99	99	99	99	99	99	99	99	99
idf.DOmgL	Pearson Correlation	-.409**	-.556**	-.367**	-.260**	.514**	-0.130	-0.117	-.664**	-.380**	-.516**	-.399**	-.508**
	Sig. (2-tailed)	0.000	0.000	0.000	0.009	0.000	0.200	0.247	0.000	0.000	0.000	0.000	0.000
	N	99	99	99	99	99	99	99	99	99	99	99	99
idf.Eh	Pearson Correlation	-.436**	-.452**	-.253*	-0.163	.488**	0.088	-.206*	-.696**	-.333**	-.681**	-.455**	-.654**
	Sig. (2-tailed)	0.000	0.000	0.011	0.107	0.000	0.384	0.041	0.000	0.001	0.000	0.000	0.000
	N	99	99	99	99	99	99	99	99	99	99	99	99
idf.ORP	Pearson Correlation	-.436**	-.452**	-.253*	-0.163	.488**	0.088	-.206*	-.696**	-.333**	-.681**	-.455**	-.654**
	Sig. (2-tailed)	0.000	0.000	0.011	0.107	0.000	0.384	0.041	0.000	0.001	0.000	0.000	0.000
	N	99	99	99	99	99	99	99	99	99	99	99	99
idf.SpCond	Pearson Correlation	.561**	.655**	.806**	.716**	-0.179	0.095	0.090	.617**	.687**	.447**	.761**	.447**
	Sig. (2-tailed)	0.000	0.000	0.000	0.000	0.077	0.351	0.373	0.000	0.000	0.000	0.000	0.000
	N	99	99	99	99	99	99	99	99	99	99	99	99
idf.TA_CaCO3	Pearson Correlation	.554**	.841**	.525**	.444**	-.453**	-0.053	.236*	.727**	.602**	.466**	.596**	.515**
	Sig. (2-tailed)	0.000	0.000	0.000	0.000	0.000	0.605	0.019	0.000	0.000	0.000	0.000	0.000
	N	99	99	99	99	99	99	99	99	99	99	99	99

**. Correlation is significant at the 0.01 level (2-tailed); *. Correlation is significant at the 0.05 level (2-tailed).

Parameter		idf.K^+	idf.Na^+	idf.SiO2	idf.pH	idf.HCO_3^-	idf.DOmgL	idf.Eh	idf.ORP	idf.SpCond	idf.TA_CaCO3
idf.Sodium	Pearson Correlation	.608**	1								
	Sig. (2-tailed)	0.000									
	N	99	99								
idf.Silica	Pearson Correlation	.371**	.668**	1							
	Sig. (2-tailed)	0.000	0.000								
	N	99	99	99							
idf.pH	Pearson Correlation	.231*	.555**	.456**	1						
	Sig. (2-tailed)	0.021	0.000	0.000							
	N	99	99	99	99						
idf.HCO3	Pearson Correlation	.501**	.764**	.629**	.806**	1					
	Sig. (2-tailed)	0.000	0.000	0.000	0.000						
	N	99	99	99	99	99					
idf.DOmgL	Pearson Correlation	-.364**	-.500**	-.504**	-.474**	-.674**	1				
	Sig. (2-tailed)	0.000	0.000	0.000	0.000	0.000					
	N	99	99	99	99	99	99				
idf.Eh	Pearson Correlation	-.232*	-.452**	-.565**	-.621**	-.691**	.628**	1			
	Sig. (2-tailed)	0.021	0.000	0.000	0.000	0.000	0.000				
	N	99	99	99	99	99	99	99			
idf.ORP	Pearson Correlation	-.232*	-.452**	-.565**	-.621**	-.691**	.628**	1.000**	1		
	Sig. (2-tailed)	0.021	0.000	0.000	0.000	0.000	0.000	0.000			
	N	99	99	99	99	99	99	99	99		
idf.SpCond	Pearson Correlation	.637**	.867**	.531**	.475**	.743**	-.542**	-.451**	-.451**	1	
	Sig. (2-tailed)	0.000	0.000	0.000	0.000	0.000	0.000	0.000	0.000		
	N	99	99	99	99	99	99	99	99	99	
idf.TA_CaCO3	Pearson Correlation	.501**	.764**	.629**	.806**	1.000**	-.674**	-.691**	-.691**	.743**	1
	Sig. (2-tailed)	0.000	0.000	0.000	0.000	0.000	0.000	0.000	0.000	0.000	
	N	99	99	99	99	99	99	99	99	99	99

**. Correlation is significant at the 0.01 level (2-tailed); *. Correlation is significant at the 0.05 level (2-tailed).

Br^- = dissolved bromide (mg L^{-1})

Cl^- = dissolved chloride (mg L^{-1})

DO = dissolved oxygen (mg L^{-1})

Eh = reduction potential (mV)

HCO_3^- = bicarbonate (mg L^{-1})

Mg^{2+} = dissolved magnesium(mg L^{-1})

Na^+ = dissolved sodium(mg L^{-1})

NO_2^- -N = nitrite nitrogen (mg L^{-1})

SiO_2 = dissolved silica (mg L^{-1})

SPC = specific conductivity (µScm^{-1})

Ca^{2+} = dissolved calcium(mg L^{-1})

DIC = dissolved inorganic carbon (mg L^{-1})

DOC = dissolved organic carbon (mg L^{-1})

Fe^{2+}= dissolved iron (mg L^{-1})

K^+ = dissolved potassium(mg L^{-1})

Mn^{2+}= dissolved manganese (mg L^{-1})

NH_4^+ -N = ammoniacal nitrogen (mg L^{-1})

NO_3^- -N= nitrate nitrogen (mg L^{-1})

SO_4^{2-}= sulphate (mg L^{-1})

Appendix E: FSL Class Definitions

E.1 FSL Soil Carbon Classes

CARBON_ CLASS	*CARBON_ MIN (%)*	*CARBON_ MAX (%)*	*CARBON_ MOD (%)*	*Description*
1	20	60	Refer comment under 'Item values & Interpretation'	Very high
2	10	19.9		High
3	4	9.9		Medium
4	2	3.9		Low
5	0	1.9		Very low

(Newsome, Wilde, & Willoughby, 2008)

E.2 FSL Soil pH Classes

PH_ CLASS	*PH_ MIN*	*PH_ MAX*	*PH_ MOD*	*Description*	*Notes on plant growth relationships*
1	7.6	8.3	Refer comment under 'Item values & Interpretation'	High	May seriously retard plant growth.
2	6.5	7.5		Moderately high	May depress growth, possible deficiencies of some nutrients may be induced.
3	5.8	6.4		Near neutral	Satisfactory pH for many plants.
4	5.5	5.7		Moderately low	Earthworm numbers, microbial activity, and nutrient cycling may be restricted.
5	4.9	5.4		low	Al often toxic and probably limits growth.
6	4.5	4.8		Very low	Both Al and Mn are likely to be toxic.

(Newsome et al., 2008)

E.3 FSL Soil Drainage

DRAIN_CLASS	Description	Depth below A horizon (cm)	Depth from surface (cm)	Low chroma on ped or cut Surfaces (%)	High Chroma Redox mottles (%)
1	Very poor	1	≤10	≥50	
2	Poor	≤15	≤30	≥50	
3	Imperfect	≤15	≤30	≤50	and/or ≥2
		>15	30–90	≥50	
4	Moderately well		30–90		≥2
			60–90	≥50	
5	Well		<90		<2

(Newsome et al., 2008)

Appendix F: Laboratory Analysis Results

F.1 Laboratory Analysis Results for the Direct-push Dataset

Table 23: Laboratory Analysis Results for the direct-push dataset collected in the Tararua GWMZ from October 2016 to May 2017.

Qualarc	SiteID	Inorganic N	DOC	DIC	Fluoride	Chloride	Bromide	NO_3^--N	Sulphate
1008061	2.1	0.06	4.3	2.4	0.00354	27.1	0.058	0.012	52.7
1008062	2.3	0.23	2.9	12	0.068	11.8	0.046	0.01	22.1
1008063	3.1	3.09	0.6	2.6	0.038	10.7	0.063	3.09	15.4
1008064	3.2	0.92	1.1	8	0.066	16	0.074	0.338	11.5
1008065	3.3	5.21	0.9	5.6	0.067	17.3	0.109	5.18	14
1008066	4.1	2.86	1.6	8.3	0.071	9.86	0.052	2.84	6.04
1008067	4.2	5.53	0.8	5	0.08	9.54	0.052	5.5	10.6
1008068	4.3	3.61	0.3	3.3	0.044	9.98	0.052	3.6	2.64
1008069	5.1	0.17	1.2	14.5	0.226	10.8	0.061	0.102	12.2
1008070	5.2	1.37	2.2	37.1	0.169	88.4	0.289	0.013	0
1008071	5.3	6.79	1.4	4.5	0.055	24.3	0.127	6.76	24.9
1008072	7.1	0.46	0.8	19.3	0.095	9.29	0.042	0.321	12
1008073	8.3	11.6	0.3	8.6	0.00354	17.3	0.115	11.5	2.29
1008074	11.2	7.95	1.3	6.5	0.113	15.4	0.08	7.89	14
1008075	11.3	1	1.4	57.8	0.286	24.3	0.093	0.013	12.6
1008076	12.3	8.4	1.2	11.3	0.095	24.1	0.118	8.37	27.5
1008077	13.3	4.08	10	62.7	0.397	31.5	0.17	0.011	0
1008078	14.2	1.37	1.2	12.9	0.098	29.3	0.106	1.35	36.4
1008079	18.1	3.68	5	113	0.403	89.8	0.53	1.76	0.021
1008080	18.2	0.5	17.9	43.6	0.142	30.9	0.338	0.007	1.82
1008081	21.2	1.32	1.8	8.2	0.083	11.1	0.054	1.31	20.7
1008082	21.3	4.22	0.6	5.1	0.052	11.2	0.064	4.2	14.9
1008105	22.1	1.65	3.2	8.6	0.126	14.6	0.055	1.64	4
1008083	22.2	2.26	3.3	25.6	0.151	10.4	0.056	0.014	8.25
1008104	23.3	1.26	2.7	37.4	0.142	55.3	0.296	0.012	0
1008084	24.1	4.67	0.3	5.5	0.031	8.3	0.039	4.66	6.61
1008085	25.1	0.49	1.1	18.2	0.09	11.9	0.067	0.461	17.3
1008086	25.2	0.11	2.5	17.8	0.04	16.6	0.071	0.016	38.6
1008087	29.3	14.7	2.7	10.2	0.136	17	0.048	14.6	54.5
1008088	30.1	1.68	6.8	2.7	0.076	16.7	0.07	1.48	53.2
1008089	30.2	1	2.8	22	0.368	39.5	0.202	0.007	0.076
1008090	30.3	0.73	2.5	12	0.129	15.2	0.065	0.678	9.64
1008091	31.1	1.08	0.7	16.4	0.263	10.4	0.078	1.03	6.59
1008093	50.1	5.18	0.6	3.5	0.052	6.31	0.049	5.16	6.5
1008095	50.2	0.05	5.1	17.3	0.167	25.8	0.228	0.01	10
1008096	50.3	2.36	11.2	65.6	0.36	590	4.09	0.011	0.114
1008097	50.5	5.16	1.5	8.7	0.078	15.8	0.082	5.15	16.5
1008098	50.6	15.5	2.1	8.2	0.00354	20.8	0.083	15.3	7.69
1008099	50.8	0.1	1.1	22.7	0.04	40.8	0.123	0.009	101
1008100	50.9	0.12	2.4	2.9	0.00354	11.9	0.051	0.018	12.9
1008101	51.1	0.45	1	7.4	0.061	8.55	0.051	0.437	7.09
1008102	51.4	0.54	8.2	5.4	0.232	17.7	0.106	0.198	19.1
1008103	52.1	3.82	1.3	1.5	0.05	129	0.245	3.79	14.7
Detection Limits		0.01	0.1	0.1	0.005	0.005	0.005	0.002	0.005

Inorganic N = Inorganic nitrogen (mg L^{-1})
DOC = Dissolved organic carbon (mg L^{-1})
DIC = Dissolved inorganic carbon (mg L^{-1})
NO_3^--N = Nitrate nitrogen (mg L^{-1})

SiteID	NO_2^- -N	TON	NH_4^+ -N	Boron	Calcium	Iron	Mg^{2+}	Mn^{2+}
2.1	0.0014142	0.01	0.04	0.018	11.6	4.03	8.38	0.325
2.3	0.003	0.01	0.21	0.038	20.7	13.3	3.92	0.507
3.1	0.0014142	3.09	0.007071	0.016	8.53	0.378	2.09	0.093
3.2	0.0014142	0.34	0.58	0.043	11.1	8.99	3.97	0.229
3.3	0.01	5.19	0.02	0.029	15.3	0.326	3.69	0.152
4.1	0.009	2.85	0.01	0.03	8.16	0.04	2.88	0.208
4.2	0.003	5.51	0.03	0.017	9.01	0.364	4.09	0.169
4.3	0.0014142	3.6	0.01	0.01	3.84	0.254	2.41	0.054
5.1	0.0014142	0.1	0.07	0.028	10.6	2	4.78	1.14
5.2	0.007	0.02	1.35	0.105	75	11	21.9	0.695
5.3	0.008	6.77	0.02	0.054	11.6	1.39	6.97	0.32
7.1	0.0014142	0.32	0.13	0.016	15.9	1.03	7.18	0.541
8.3	0.01	11.5	0.06	0.024	16.1	0.112	6.22	0.143
11.2	0.011	7.9	0.05	0.02	13.6	1.22	5.91	0.168
11.3	0.0014142	0.01	0.99	0.453	19.1	0.218	4.99	0.15
12.3	0.01	8.38	0.02	0.039	21.7	0.916	7.42	0.254
13.3	0.009	0.02	4.06	0.304	28.3	9.4	11.7	1.66
14.2	0.003	1.35	0.02	0.036	19.4	0.201	8.84	0.459
18.1	0.0014142	1.76	1.92	1.17	18.3	3.49	6.31	0.116
18.2	0.0014142	0.008	0.49	0.041	25.6	9.36	12.3	2.58
21.2	0.01	1.32	0.007071	0.047	14.1	0.667	2.84	0.077
21.3	0.006	4.2	0.02	0.013	11.9	0.607	2.28	0.136
22.1	0.0014142	1.64	0.02	0.029	9.13	0.167	3.67	0.013
22.2	0.009	0.02	2.24	0.045	15.7	8.96	7.19	0.95
23.3	0.0014142	0.01	1.25	0.094	62.9	16.8	7.31	0.343
24.1	0.0014142	4.66	0.01	0.009	10.5	0.037	3.79	0.048
25.1	0.008	0.47	0.02	0.047	20.7	0.495	4.57	0.376
25.2	0.0014142	0.02	0.09	0.04	21.9	1.82	6.75	1.01
29.3	0.024	14.6	0.04	0.05	34.4	0.405	10.5	0.071
30.1	0.0014142	1.48	0.2	0.04	13.6	3.61	5.59	0.155
30.2	0.0014142	0.007	0.99	0.048	13	13.2	8.09	1.56
30.3	0.0014142	0.68	0.05	0.05	15.3	0.074	4	0.066
31.1	0.017	1.05	0.03	0.03	10.9	0.074	6.78	0.405
50.1	0.003	5.16	0.02	0.019	6.32	0.649	3.29	0.17
50.2	0.0014142	0.01	0.04	0.05	11.9	1.18	5.05	0.37
50.3	0.0014142	0.01	2.35	0.812	48.3	2.89	15.7	0.813
50.5	0.0014142	5.16	0.007071	0.033	12	0.008	4.49	0.005
50.6	0.062	15.4	0.09	0.036	20.9	0.042	6.26	0.555
50.8	0.007	0.02	0.08	0.049	57.8	9.28	10.6	0.388
50.9	0.001	0.02	0.11	0.017	6.17	3.91	2.61	0.205
51.1	0.001	0.44	0.01	0.027	6.23	0.14	2.51	0.14
51.4	0.001	0.2	0.34	0.032	7.15	3.83	5.39	0.202
52.1	0.001	3.79	0.03	0.02	34.9	0.255	15.4	0.058
D/L	0.002	0.002	0.01	0.005	0.01	0.005	0.01	0.005

NO_2^- -N = Nitrite nitrogen (mg L^{-1})
TON = Total organic nitrogen (mg L^{-1})
NH_4^+-N = Ammoniacal nitrogen (mg L^{-1})
Mg^{2+} = Magnesium (mg L^{-1})
Mn^{2+} = Manganese (mg L^{-1})

SiteID	Potassium	Sodium	Silica	Total Dissolved P	Dissolved Reactive P	Arsenic	pH
2.1	3.76	12	22.3	0.003535534	0.003535534	0.000707	5.4
2.3	1.48	8.81	25.5	0.021	0.003535534	0.008	6.02
3.1	2.81	7.51	11.5	0.003535534	0.003535534	0.000707	5.33
3.2	2.36	7.77	17.9	0.003535534	0.003535534	0.003	5.64
3.3	3.07	9.24	12.7	0.026	0.003535534	0.000707	5.53
4.1	2.19	9.4	15.4	0.03	0.011	0.000707	5.81
4.2	2.47	9.59	16.6	0.003535534	0.003535534	0.000707	5.83
4.3	1.37	9.06	19.2	0.003535534	0.003535534	0.000707	5.67
5.1	2.57	15.8	35	0.003535534	0.003535534	0.000707	6.09
5.2	6.7	60.2	50.9	0.031	0.017	0.008	7.1
5.3	4.49	16	16.9	0.017	0.003535534	0.000707	5.91
7.1	2	14.2	27	0.04	0.044	0.001	6.73
8.3	1.7	15.2	24.9	0.121	0.122	0.000707	6.02
11.2	3.74	10.6	18	0.003535534	0.003535534	0.000707	5.91
11.3	6.23	94.8	15.7	0.018	0.017	0.001	7.95
12.3	3.61	22.8	18.3	0.028	0.003535534	0.000707	5.93
13.3	6.46	95.7	49.7	0.032	0.007	0.006	6.86
14.2	3.25	17.5	26.7	0.007	0.006	0.000707	5.82
18.1	6.81	248	61.4	0.118	0.115	0.009	7.81
18.2	1.61	24.7	24.8	6	0.003535534	0.004	5.87
21.2	5.37	10.4	15.7	0.017	0.003535534	0.000707	5.52
21.3	3.29	8.37	10.2	0.003535534	0.003535534	0.000707	5.49
22.1	3.54	10.5	25.2	0.02	0.02	0.000707	5.91
22.2	5.24	21.6	65	0.025	0.014	0.000707	6.43
23.3	5.19	50.3	54.7	0.005	0.003535534	0.003	6.55
24.1	1.06	5.41	14.1	0.003535534	0.003535534	0.000707	5.77
25.1	2.88	14.7	28.2	0.016	0.009	0.000707	6.07
25.2	2.18	21.6	32.6	0.003535534	0.003535534	0.000707	6.11
29.3	1.87	15.9	15.2	0.034	0.003535534	0.000707	6.15
30.1	4.88	12.1	10.4	0.003535534	0.003535534	0.003	5.82
30.2	2.81	31.4	48.4	0.003535534	0.003535534	0.057	6.66
30.3	1.37	13.4	12.7	0.017	0.016	0.000707	7.25
31.1	2.21	14.1	22.9	0.006	0.006	0.001	6.94
50.1	2.09	6.97	16.3	0.003535534	0.003535534	0.000707	5.9
50.2	1.02	28.8	21.7	0.009	0.007	0.000707	5.87
50.3	7.44	418	30	0.029	0.008	0.042	7.31
50.5	4.81	15.3	16.7	0.015	0.015	0.000707	5.64
50.6	3.95	16	24.1	0.012	0.009	0.000707	5.96
50.8	3.38	23	28.1	0.026	0.003535534	0.002	6.03
50.9	1.61	7.23	18.4	0.003535534	0.003535534	0.000707	5.38
51.1	1.21	9.89	17.3	0.007	0.007	0.000707	5.7
51.4	1.51	16.1	36.2	0.005	0.003535534	0.002	6.03
52.1	2.92	41.7	18.6	0.005	0.006	0.000707	5.52
D/L	0.01	0.02	0.02	0.005	0.005	0.001	

Total Dissolved P = Total dissolved phosphorus (mg L^{-1})

Dissolved Reactive P = Dissolved reactive phosphorus (mg L^{-1})

SiteID	DO %sat	DO mg/L	pH	*Eh*	ORP	SPCond	Salinity	Resistance
2.1	0.71	0.07	5.4	284.580	84.58	239.41	0.1	5190.2
2.3	0.5	0.05	6.02	150.800	-49.2	229.8	0.1	5167
3.1	67.125	6.51	5.325	277.950	77.95	122.125	0.1	9820.5
3.2	0.9	0.08	5.64	-2.200	-202.2	176.2	0.1	6514
3.3	34.6	3.36	5.53	251.100	51.1	186.2	0.1	6591
4.1	65.2	6.42	5.81	264.600	64.6	121.9	0.1	10481
4.2	74.2	7.02	5.83	234.600	34.6	146.7	0.1	8128
4.3	64.5	6.22	5.67	238.300	38.3	101.8	0	12028
5.1	3.6	0.3	6.09	-1.400	-201.4	188.5	0.1	5431
5.2	2.1	0.21	7.1	-72.400	-272.4	823.5	0.4	1550
5.3	71.5	7.13	5.91	185.700	-14.3	230.2	0.1	5396
7.1	2.2	0.21	6.73	-25.900	-225.9	221	0.1	5443
8.3	11.5	1.1	6.02	216.500	16.5	233.1	0.1	5190
11.2	32.1	3.07	5.91	155.100	-44.9	214.2	0.1	5593
11.3	0.4	0.03	7.95	-66.700	-266.7	620.5	0.3	1726
12.3	35.2	3.35	5.93	201.600	1.6	305	0.1	3853
13.3	5.1	0.48	6.86	130.600	-69.4	697.6	0.3	1687
14.2	11.6	1.11	5.82	141.000	-59	288.6	0.1	4089
18.1	3.3	0.28	7.81	121.700	-78.3	1443	0.7	724
18.2	51.2	4.64	5.87	194.900	-5.1	388.7	0.2	2912
21.2	16.1	1.5	5.52	178.000	-22	166	0.1	6971
21.3	25.5	2.47	5.49	235.000	35	155.5	0.1	7918
22.1	50.56	5	5.91	321.400	121.4	150.3	0.1	8335
22.2	2.7	0.26	6.43	179.500	-20.5	276.9	0.1	4307
23.3	1.4	0.14	6.55	142.500	-57.5	703.3	0.3	1773
24.1	53.72	4.97	5.77	269.600	69.6	127.9	0.1	9126
25.1	10.6	1.03	6.07	73.500	-126.5	218.9	0.1	5497
25.2	3.4	0.34	6.11	25.300	-174.7	295.8	0.1	4276
29.3	0.8	0.07	6.15	231.600	31.6	383.9	0.2	3216
30.1	19.6	1.82	5.82	3.800	-196.2	225.2	0.1	5141
30.2	6.6	0.65	6.66	-198.000	-398	355.3	0.2	3445
30.3	59.5	5.65	7.25	168.800	-31.2	184.9	0.1	6361
31.1	15.5	1.42	6.94	33.300	-166.7	191.9	0.1	6020
50.1	67.78	6.5	5.9	256.500	56.5	114.8	0.1	10479
50.2	51.5	4.89	5.87	164.700	-35.3	252	0.1	4682
50.3	18.2	1.6	7.31	113.400	-86.6	2587.4	1.4	423
50.5	37.2	3.77	5.64	318.400	118.4	208.6	0.1	6014
50.6	64.4	5.67	5.96	260.300	60.3	271.3	0.1	4030
50.8	0.6	0.06	6.03	187.000	-13	531.5	0.3	2239
50.9	10.3	1.04	5.38	182.100	-17.9	107.4	0.1	11724
51.1	36.2	3.4	5.7	301.500	101.5	104.1	n/a	n/a
51.4	2.4	0.23	6.03	-71.800	-271.8	177	0.1	6866
52.1	92	8.77	5.52	378.500	178.5	564.1	0.3	2091

DO %sat = percent saturation of dissolved oxygen
DO mg/L = Dissolved oxygen (mg L^{-1})
Eh = Redox potential (mV)
ORP = Oxidation reduction potential (mV)
SPCond = Specific conductivity (µS cm^{-1})

SiteID	TDS	HCO_3^-	TA_mgCaCO3	TA_meq/L	TitrantVol	TitrantTemp	TApH	TaTemp
2.1	0	62.666	50.537	1.011	2.349	19.9	5.55	19.7
2.3	0	103.083	83.131	1.663	3.864	21	6.13	21
3.1	0	16.407	13.231	0.265	0.615	16.8	5.41	16.4
3.2	0	71.283	57.486	1.15	2.672	18.9	5.91	18.4
3.3	0	31.426	25.344	0.507	1.178	18.1	5.59	17.8
4.1	0	35.455	28.592	0.572	1.329	18.2	5.86	17.9
4.2	0	32.493	26.204	0.524	1.218	18.9	6.14	18.7
4.3	0	24.624	19.858	0.397	0.923	21.2	5.91	20
5.1	0	145.500	117.339	2.347	5.454	21.1	6.35	21.3
5.2	1	401.420	323.725	6.475	15.047	19.8	7.19	19.8
5.3	0	27.691	22.232	0.477	1.038	18.1	5.99	18.1
7.1	0	143.126	115.424	2.308	5.365	20.5	6.92	20.2
8.3	0	52.715	42.512	0.85	1.976	18.5	6.09	18.1
11.2	0	90.197	72.74	1.455	3.381	20.3	6.00	20.2
11.3	0	437.461	352.791	7.056	16.398	20.9	8.07	21.1
12.3	0	78.432	63.252	1.265	2.94	17.5	6.10	16.9
13.3	0	411.771	332.073	6.641	15.435	18.7	6.78	17.4
14.2	0	74.351	59.96	1.199	2.787	19	5.97	18.7
18.1	1	666.943	537.857	10.757	25	20.6	8.03	20
18.2	0	237.698	191.692	3.834	8.91	19.7	6.09	19.7
21.2	0	36.815	29.69	0.594	1.38	19.9	5.67	19.9
21.3	0	28.892	23.3	0.466	1.083	18.1	5.57	17.7
22.1	0	55.490	44.75	0.895	2.08	20.3	6.08	20.8
22.2	0	254.265	205.053	4.101	9.531	20.3	6.60	20
23.3	0	403.127	325.102	6.502	15.111	21.2	6.61	21
24.1	0	34.894	28.141	0.563	1.308	16.5	5.89	16.1
25.1	0	140.111	112.993	2.26	5.252	20	6.21	19.7
25.2	0	124.718	100.579	2.012	4.675	19.3	6.27	18
29.3	0	71.336	57.529	1.151	2.674	19.1	6.32	11.8
30.1	0	26.598	21.54	0.429	0.997	20.5	5.88	20.2
30.2	0	158.145	127.537	2.551	5.928	22.2	6.53	21.8
30.3	0	91.478	73.772	1.475	3.429	22	7.22	21.8
31.1	0	91.398	73.708	1.474	3.426	17.9	7.42	17.4
50.1	0	25.637	20.675	0.414	0.961	16.3	6.03	16
50.2	0	116.368	93.845	1.877	4.362	19.5	6.11	19
50.3	2	574.718	463.482	9.27	21.543	20.8	7.45	20.6
50.5	0	54.609	44.04	0.881	2.047	18	5.93	17.6
50.6	0	99.374	80.141	1.603	3.725	19.8	6.49	19.8
50.8	0	447.305	360.73	7.215	16.767	21.5	7.59	21
50.9	0	26.518	21.385	0.428	0.994	19.8	5.65	19.7
51.1		48.153	38.833	0.777	1.805	20.8	5.95	20.5
51.4	0	56.263	45.374	0.907	2.109	19.9	6.09	19.6
52.1	0	12.138	9.789	0.196	0.455	20.1	6.73	19.8

TDS = Total dissolved solids (ppt)
TA_meq/L = Alkalinity (milliequivalents)
TitrantVol = Titrant volume (ml)
TApH = Total alkalinity analysis titrant pH
HCO_3^- = Bicarbonate
TitrantTemp = Titrant temperature (°C)
TaTemp = Temperature at total alkalinity analysis (°C)
TA_mgCaCO3 = Total alkalinity as calcium carbonate (mg)

SiteID	Density	Baro	Temp	SpActual	Salinity	Pressure	AirTemp	SampleDate
2.1	0.999	989.8	14.8	192.69	0.1	-0.0074	20.36	15-Nov-16
2.3	0.999	1008	16.73	193.5	0.1	-0.013	38.5	19-Dec-16
3.1	0.999	1002.2	16.3	101.825	0.1	0.0005	0.00375	05-Dec-16
3.2	0.999	1004.3	18.26	153.6	0.1	-0.002	35.6	17-Dec-16
3.3	0.999	982.8	15.33	151.8	0.1	-0.01	21.3	28-Nov-16
4.1	0.999	961.9	13.64	95.5	0.1	-0.018	16.9	17-Nov-16
4.2	0.999	982.7	16.55	123.1	0.1	0.008	33.8	18-Nov-16
4.3	0.999	978.1	15.39	83.1	0	-0.021	24.9	20-Dec-16
5.1	0.997	994.2	23.8	184.2	0.1	-0.0003	50.1	03-Dec-16
5.2	1	991.7	13.66	645.1	0.4	0	16.1	13-Oct-16
5.3	0.999	998.2	14.81	185.4	0.1	-0.007	19.2	29-Sep-16
7.1	0.999	973.6	16.22	184	0.1	-0.0008	27.1	18-Dec-16
8.3	0.999	972.9	15.97	192.9	0.1	-0.01	23.4	28-Nov-16
11.2	0.999	989.7	16.35	178.8	0.1	0	31.1	07-Dec-16
11.3	0	986.7	21.59	579.9	0.3	-0.004	29.7	07-Dec-16
12.3	0.999	1004.3	17.21	259.6	0.1	0.0007	40.7	01-Dec-16
13.3	0.999	996.7	17.14	592.9	0.3	-0.02	21.1	01-Nov-16
14.2	0.1	1004.7	17.01	244.6	0.1	-0.009	20.2	02-Dec-16
18.1	0.998	999	22.76	1381.4	0.7	-0.015	31	01-Nov-16
18.2	0.999	987.8	18.9	343.4	0.2	-0.012	24	25-Nov-16
21.2	0.999	1000.5	17.91	143.5	0.1	-0.006	34.4	08-Nov-16
21.3	0.999	978.9	15.19	126.3	0.1	-0.017	24.6	28-Nov-16
22.1	0.999	990.8	14.44	120	0.1	0.01	13.1	05-May-17
22.2	0.999	988.1	16.55	232.2	0.1	-0.019	24	31-Oct-16
23.3	0.999	994.8	14.63	563.9	0.3	0.026	16.8	04-May-17
24.1	0.999	980.6	17.51	109.6	0.1	0.006	30.7	06-Dec-16
25.1	0.999	1001.9	15.96	181.9	0.1	0.005	24.5	13-Oct-16
25.2	0.999	1005	14.32	234	0.1	-0.016	17.8	02-Dec-16
29.3	0.999	1000.4	15.04	310.9	0.2	-0.007	20.8	22-Nov-16
30.1	0.999	1000.3	18.23	196.3	0.1	0.024	24	11-Apr-17
30.2	0.999	1002.3	15.41	290.2	0.2	0.026	18.6	27-Apr-17
30.3	0.999	999.9	17.15	111.9	0.1	0.02	23.1	28-Apr-17
31.1	0.999	978.8	18	166.1	0.1	-0.005	18.9	19-Nov-16
50.1	0.999	981.9	16.16	95.4	0.1	0.006	29.8	06-Dec-16
50.2	0.999	996.5	17.02	213.6	0.1	0.01	35	24-Nov-16
50.3	0.999	999.3	20.49	2364.6	1.4	-0.007	22.1	25-Nov-16
50.5	0.999	1003.2	14.36	166.3	0.1	2.594	31	01-Dec-16
50.6	0.998	990	20.56	248.2	0.1	-0.02	27	04-Dec-16
50.8	0.999	1009.9	16.63	446.6	0.3	-0.012	27.2	21-Dec-16
50.9	0.999	992	14.25	85.3	0.1	-0.02	22.8	21-Dec-16
51.1	n/a	1002.2	16.9	n/a	n/a	n/a	n/a	10-Apr-17
51.4	0.999	976.3	15.72	145.7	0.1	0.015	17.6	30-Apr-17
52.1	0.999	1002.2	17.04	487.4	0.3	0.021	24.1	10-Apr-17

Baro = Barometric pressure (kPa)
Temp = Temperature (°C)
SpActual = Actual conductivity (µS cm^{-1})
AirTemp = Ambient temperature at time of sampling (°C)

Table 24: Laboratory Analysis Results for existing wells dataset collected in the Tararua GWMZ from February to March 2014.

QualarcID	SiteID	DOC	DIC	Chloride	Bromide	NO_3^--N	Sulphate	NO_2^--N
20140609	319002	0.220	5.168	7.072	0.026	0.156	4.344	0.006
20140597	319004	0.310	5.350	7.107	0.030	0.193	4.683	0.001
20140811	329032	1.530	31.180	10.341	0.050	0.001	0.004	0.005
20140593	329092	3.420	91.550	74.946	0.308	0.001	0.028	0.001
20140406	338005	1.070	19.700	49.583	0.252	0.131	11.146	0.001
20140509	338006	1.000	26.670	12.414	0.080	0.053	11.073	0.001
20140508	338066	1.300	29.960	24.273	0.110	0.002	0.004	0.001
20140527	339001	1.800	10.020	57.861	0.217	4.652	31.041	0.001
20140531	339008	1.800	28.740	20.988	0.090	1.080	6.921	0.016
20140529	339013	1.100	41.370	62.776	0.207	0.001	2.282	0.001
20140530	339047	1.600	23.180	22.541	0.100	0.055	16.344	0.002
20140669	347023	0.300	13.640	12.845	0.068	0.868	6.320	0.003
20140523	347031	0.800	11.650	16.050	0.085	0.599	7.525	0.001
20140761	347053	0.300	11.210	7.109	0.054	0.072	5.082	0.006
20140590	348028	0.106	24.320	14.600	0.098	2.158	10.915	0.001
20140380	348134	0.670	10.790	14.420	0.077	2.898	17.506	0.001
20140506	348137	0.900	6.640	10.163	0.057	0.529	5.877	0.001
20140385	348138	8.750	6.310	46.420	0.117	0.424	19.773	0.002
20140760	349011	0.640	25.600	47.049	0.143	0.003	30.812	0.001
20140591	349012	1.190	30.180	77.992	0.360	0.007	18.617	0.001
20140525	349013	0.800	24.140	37.049	0.143	0.027	27.274	0.001
20140386	356043	0.360	2.060	15.429	0.113	4.129	9.421	0.001
20140387	357058	0.650	2.870	8.796	0.046	0.455	4.383	0.011
20140453	357103	0.300	7.210	12.328	0.093	3.351	3.176	0.001
20140456	357109	0.300	7.030	13.817	0.103	5.037	10.289	0.003
20140382	357111	0.350	3.090	9.900	0.059	1.605	8.668	0.001
20140374	357114	0.300	5.250	14.141	0.099	5.318	10.161	0.001
20140370	357115	0.300	6.770	11.208	0.081	3.860	9.058	0.001
20140375	357116	0.300	7.090	14.149	0.102	5.426	10.154	0.001
20140381	357117	0.62	3.53	8.9782	0.0518	0.332	4.8077	0.00141
20140504	357118	0.300	4.844	8.735	0.051	0.595	4.815	0.001
20140455	357119	0.400	9.120	13.043	0.096	3.797	9.983	0.007
20140503	366076	0.300	11.040	16.663	0.108	1.006	8.925	0.001
20140642	367006	1.000	14.870	13.051	0.094	5.032	15.680	0.004
20140641	367017	0.300	19.800	53.388	0.294	0.348	2.961	0.009
20140639	402001	0.3	25.44	15.6113	0.0692	0.002	14.5018	0.002
20140605	402029	0.140	17.400	16.711	0.100	0.001	2.238	0.005
20140688	410050	2.210	48.670	17.180	0.073	0.001	4.322	0.006
20140813	411043	0.400	11.530	10.482	0.056	0.001	15.207	0.004
20140607	412001	2.200	120.300	35.657	0.128	1.026	160.885	0.284
20140608	412016	0.550	35.180	18.981	0.097	0.007	15.284	0.007
20140814	420057	1.140	46.000	24.802	0.103	5.100	32.651	0.025
20140594	420075	1.070	23.370	25.524	0.144	0.003	6.589	0.001
20140595	420087	1.320	26.590	21.555	0.115	15.827	39.039	0.003
20140606	421003	0.970	63.940	46.654	0.144	0.006	6.946	0.007
20140546	430001	1.300	29.730	25.430	0.138	0.003	20.047	0.001
20140544	430005	1.500	13.310	20.193	0.092	1.013	15.414	0.001
20140545	430008	1.500	35.670	18.418	0.140	0.007	9.902	0.001
20140551	430016	1.000	16.890	28.596	0.114	11.620	20.690	0.003
20140758	798002	0.59	9.6	10.9563	0.0685	0.4886	6.7443	0.00141
20140759	798003	0.800	16.320	16.799	0.109	3.138	14.076	0.003
20140810	798004	0.530	21.750	9.203	0.104	0.001	5.482	0.005
20140644	799002	2.010	24.880	11.271	0.166	0.271	13.281	0.014

20140670	799003	0.300	15.030	18.008	0.090	2.962	9.953	0.003
20140689	799004	0.300	5.340	5.690	0.022	0.101	4.280	0.009
20140690	799005	0.300	5.030	5.692	0.019	0.035	4.690	0.006

DOC = Dissolved organic carbon (mg L^{-1})
DIC = Dissolved inorganic carbon (mg L^{-1})
NO_3^--N = Nitrate nitrogen (mg L^{-1})
NO_2^--N = Nitrite nitrogen (mg L^{-1})

SiteID	NH_4^+-N	Boron	Calcium	Iron	Magnesium	Manganese	Potassium
319002	0.007	0.000	4.994	0.005	1.255	0.004	0.832
319004	0.007	0.000	5.540	0.004	1.270	0.004	0.704
329032	1.440	0.000	9.456	0.039	5.720	0.362	3.950
329092	2.300	0.000	7.048	0.037	4.630	0.004	3.550
338005	0.024	0.000	20.998	0.036	5.324	0.004	3.188
338006	0.030	0.000	16.720	1.059	3.946	0.243	2.487
338066	0.929	0.000	16.133	0.194	5.771	0.362	1.713
339001	0.007	0.000	19.600	0.010	6.848	0.004	3.298
339008	0.036	0.000	21.890	0.358	5.780	0.940	2.886
339013	0.115	0.000	45.990	0.030	6.750	0.066	1.802
339047	0.007	0.000	16.470	1.856	4.338	0.108	4.210
347023	0.007	0.000	7.210	0.013	1.820	0.004	0.852
347031	0.007	0.000	2.896	0.016	1.600	0.016	5.406
347053	0.093	0.000	3.020	6.190	0.842	0.284	0.465
348028	0.007	0.000	32.080	0.004	2.950	0.004	1.871
348134	0.007	0.000	18.401	0.004	4.350	0.004	2.023
348137	0.007	0.000	7.338	0.004	1.699	0.004	1.452
348138	0.134	0.000	13.910	0.289	4.995	1.007	3.931
349011	0.168	0.000	24.100	0.800	8.450	0.417	3.160
349012	0.209	0.000	36.400	2.056	10.100	0.843	3.096
349013	0.027	0.000	18.100	0.132	7.640	0.095	2.605
356043	0.013	0.000	7.885	0.005	2.065	0.024	2.140
357058	0.007	0.000	4.005	0.004	1.161	0.004	1.553
357103	0.010	0.000	1.913	0.004	1.754	0.007	1.214
357109	0.007	0.000	6.710	0.037	2.590	0.011	2.930
357111	0.007	0.000	4.820	0.004	1.950	0.004	1.653
357114	0.007	0.000	9.616	0.004	3.050	0.004	1.880
357115	0.007	0.000	8.220	0.004	2.564	0.004	2.108
357116	0.007	0.000	9.641	0.004	3.288	0.004	1.368
357117	0.021	0	4.671	0.00354	1.29	0.00354	1.187
357118	0.007	0.000	4.449	0.004	1.198	0.004	1.005
357119	0.007	0.000	10.298	0.009	2.063	0.008	3.038
366076	0.007	0.000	3.366	0.030	2.671	0.014	0.946
367006	0.007	0.000	13.550	0.004	1.980	0.043	3.890
367017	0.142	0.000	10.320	0.251	3.010	0.224	1.380
402001	0.253	0	21.44	0.052	11.59	0.662	1.97
402029	0.076	0.000	11.614	0.064	7.634	0.593	1.085
410050	3.968	0.000	3.010	0.077	1.380	0.046	5.350
411043	0.044	0.000	8.810	2.180	4.670	0.257	2.060
412001	7.374	0.000	76.239	0.009	35.271	0.083	21.640
412016	0.046	0.000	22.742	0.157	14.952	0.982	1.893
420057	0.007	0.000	85.060	0.005	6.160	0.022	2.130
420075	0.158	0.000	11.100	5.530	4.940	0.561	1.710
420087	0.007	0.000	17.400	0.004	7.550	0.004	13.800
421003	0.627	0.000	0.263	0.034	0.026	0.004	5.579
430001	0.256	0.000	23.700	0.216	9.210	0.480	2.470
430005	0.007	0.000	12.100	0.004	5.020	0.004	3.020
430008	0.076	0.000	22.300	0.076	11.500	1.346	1.819
430016	0.007	0.000	23.300	0.008	10.100	0.024	2.280
798002	0.007071	0	9.65	0.00354	2.04	0.00354	1.65
798003	0.007	0.000	10.690	0.004	3.280	0.004	3.590
798004	0.288	0.000	15.100	1.140	6.540	0.693	2.880
799002	0.279	0.000	31.990	0.247	2.910	0.289	6.070
799003	0.012	0.000	10.370	0.004	3.940	0.004	4.330
799004	0.015	0.000	4.990	0.004	1.230	0.004	0.794
799005	0.007	0.000	5.990	0.004	1.310	0.004	0.669

SiteID	Sodium	Silica	pH	HCO_3^-	DO mg/L	*Eh*	ORP	SPCond
319002	5.152	10.086	6.180	20.736	9.050	440.600	240.600	70.000
319004	5.770	9.090	6.310	25.614	8.820	418.400	218.400	73.500
329032	39.500	57.100	7.040	160.868	0.070	125.000	-75.000	295.800
329092	205.365	11.800	8.350	473.029	0.180	97.800	-102.200	929.000
338005	20.326	22.758	5.900	70.754	0.410	353.300	153.300	303.300
338006	13.400	27.660	5.920	81.733	0.570	262.700	62.700	202.100
338066	35.400	36.800	6.640	146.337	0.210	155.000	-45.000	329.600
339001	32.100	21.250	5.900	34.157	7.410	465.600	265.600	362.600
339008	23.700	32.500	6.530	120.739	0.400	157.900	-42.100	292.200
339013	49.900	29.810	6.750	201.190	0.370	27.400	-172.600	523.600
339047	17.000	25.870	5.940	67.094	0.660	175.700	-24.300	226.600
347023	17.870	37.390	6.170	48.792	5.740	348.900	148.900	141.100
347031	14.580	81.277	5.380	25.619	5.430	369.100	169.100	122.400
347053	6.450	11.400	6.030	14.638	0.620	236.700	36.700	93.000
348028	14.200	13.200	6.010	87.831	4.260	344.500	144.500	224.300
348134	11.160	13.390	6.020	59.773	5.380	356.700	156.700	207.400
348137	7.550	7.940	5.810	30.498	4.590	360.700	160.700	99.900
348138	21.393	12.310	5.700	36.598	0.150	368.000	168.000	269.300
349011	30.900	31.700	6.200	86.606	0.210	156.100	-43.900	369.200
349012	37.500	39.500	6.200	123.201	0.250	198.900	-1.100	114.600
349013	31.770	26.600	5.990	86.612	0.570	297.900	97.900	326.600
356043	8.197	9.560	5.100	8.540	4.240	532.100	332.100	130.700
357058	5.554	6.460	6.020	14.638	4.710	425.900	225.900	71.200
357103	9.371	15.700	5.080	6.100	7.200	448.700	248.700	92.200
357109	8.807	10.840	5.340	10.980	8.540	469.100	269.100	135.600
357111	6.826	10.170	5.460	17.079	5.280	361.700	161.700	95.100
357114	8.873	11.800	5.310	9.760	8.500	554.300	354.300	146.900
357115	7.636	10.270	5.250	9.760	7.690	400.600	200.600	124.500
357116	8.589	11.240	5.350	9.760	8.350	515.600	315.600	147.900
357117	5.503	7.08	5.8	19.5184	3.55	371.1	171.1	77.2
357118	5.837	7.840	5.760	17.079	5.070	366.200	166.200	73.500
357119	8.119	11.290	5.960	28.057	5.700	256.700	56.700	147.600
366076	10.570	16.837	5.030	12.200	2.850	425.700	225.700	108.400
367006	8.740	8.220	5.320	17.080	2.140	505.800	305.800	154.000
367017	48.550	24.080	6.540	86.590	1.960	305.400	105.400	316.700
402001	14.67	45.71	6.95	124.3278	0.24	38.5	-161.5	274.2
402029	10.921	44.365	6.570	76.831	0.230	90.900	-109.100	189.500
410050	94.370	62.300	7.920	257.794	0.210	28.000	-172.000	114.100
411043	10.800	57.400	6.310	46.350	0.570	185.100	-14.900	155.700
412001	135.120	28.682	7.450	591.336	0.430	292.200	92.200	1308.000
412016	20.807	35.924	6.440	154.898	0.220	115.300	-84.700	333.700
420057	18.500	21.790	7.360	236.157	1.490	246.000	46.000	115.900
420075	23.800	35.300	6.160	76.849	0.330	114.800	-85.200	244.800
420087	47.100	19.200	6.060	93.929	1.300	391.200	191.200	435.600
421003	146.210	65.090	6.940	307.183	0.120	204.800	4.800	642.000
430001	28.500	32.700	6.610	136.585	0.180	137.700	-62.300	352.800
430005	13.700	16.300	5.920	45.136	4.960	377.900	177.900	186.700
430008	23.200	31.200	6.260	150.033	0.200	210.300	10.300	313.700
430016	19.200	19.600	5.830	54.896	3.240	333.500	133.500	322.100
798002	8.72	9.09	5.97	34.1564	5.21	350.8	150.8	114.6
798003	13.100	16.900	5.530	32.939	2.510	342.700	142.700	171.400
798004	10.960	66.100	6.590	95.123	0.130	113.700	-86.300	208.900
799002	7.240	9.070	6.560	103.662	0.210	277.700	77.700	241.600
799003	14.280	26.130	5.810	42.697	2.170	352.800	152.800	175.300

799004	4.850	10.550	6.050	19.517	6.490	351.600	151.600	63.900
799005	5.020	10.080	6.650	24.387	8.650	333.000	133.000	68.400

HCO_3^- = Bicarbonate (mg L^{-1})
Eh = Redox potential (mV)
SPCond = Specific conductivity (µS cm^{-1})
DO mg/L = Dissolved oxygen (mg L^{-1})
ORP = Oxidation reduction potential (mV)
NH_4^+-N = Ammoniacal nitrogen (mg L^{-1})

Appendix G: Charge Balance Analysis

G.1 Charge Balance Equations for Both Datasets

Table 25: Charge Balance Equations for Both Direct-Push and Existing Well Data.

Site	Sum of Anions	Sum of Cations	CBE
2.1	2.895	2.034	-17.473
5.1	2.959	1.752	-25.620
5.2	9.103	8.824	-1.557
11.2	2.773	1.769	-22.114
11.3	8.245	5.725	-18.038
13.3	7.723	7.329	-2.619
18.1	13.916	12.656	-4.742
22.2	4.646	2.929	-22.666
25.1	3.038	2.141	-17.323
50.3	26.292	22.346	-8.115
50.6	3.478	2.363	-19.095
50.8	10.600	5.181	-34.336
329092	9.868	9.922	0.270
412001	14.121	13.663	-1.648
421003	6.496	6.564	0.517

Red text indicates the site exhibited a high negative CBE, Bold text indicates the sample also plotted as an outlier with SPSS.

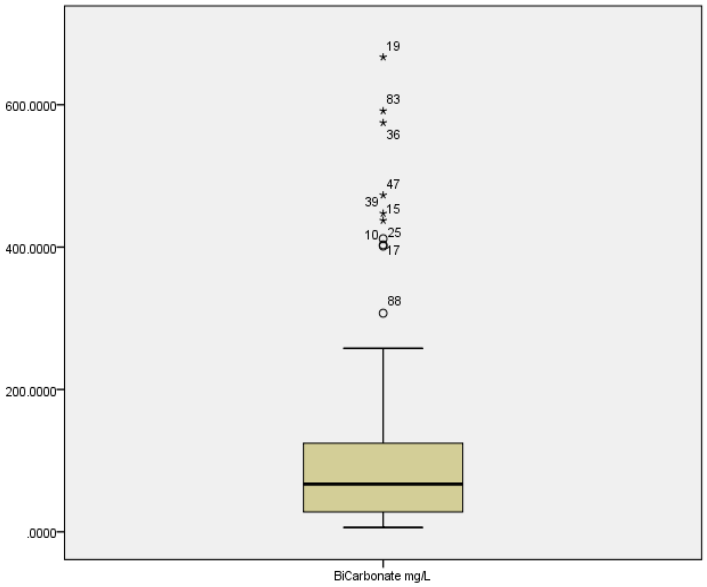

Figure 113: Boxplot of HCO_3^-. Outliers are sites 2.1, 5.2, 11.3, 13.3, 18.1, 23.3, 50.3, 50.8, 329092, 412001, and 421003.

Appendix H: Analytes Exceeding MAV

H.1 Groundwater Analytes Exceeding MAV's and GV's

Table 26: Groundwater analytes exceeding MAV's and GV's (n = 99) collected between February 2014 and May 2016.

Analyte	MAV	GV	units	SiteID	Value	Units
As	0.01	--	mg L^{-1}	30.2	0.06	mg L^{-1}
				50.3	0.04	
NH_4^+ -N	--	1.50	mg L^{-1}	5.2	1.74	mg L^{-1}
				13.3	5.23	
				18.1	2.47	
				22.2	2.89	
				23.3	1.61	
				50.3	3.03	
				410050	5.11	
Fe^{2+}	--	0.20	mg L^{-1}	47 sites	Fe^{2+} > 0.2	mg L^{-1}
Mn^{2+}	0.05		mg L^{-1}	60 sites	Mn^{2+} > 0.5	mg L^{-1}
Na^+	--	200	mg L^{-1}	18.1	248.00	mg L^{-1}
				50.3	418.00	
NO_3^- -N	11.3	--	mg L^{-1}	8.3	11.5	mg L^{-1}
				29.3	14.6	
				50.6	15.3	
				420087	15.83	
				430016	11.62	
pH	--	7.0 - 8.5	pH	87 sites	pH < 7.0	pH

As = Arsenic

B = Boron

Mn^{2+} = Manganese

NO_3^- -N = Nitrate nitrogen

NH_4^+ -N = Ammoniacal nitrogen

Fe^{2+} = Ferric iron

Na^+ = Sodium

Appendix I: QMap Lithological Classes

I.1 Description of QMap Lithological Classes

Table 27: QMap Lithological Classes used in this Study

QMap Class	Grouping Level	Relevant Classes
MAIN_ROCK	Highest	1. Coquina (includes limestone). 2. Gravel. 3. Greywacke. 4. Mudstone (includes claystone). 5. Sandstone.
SUBROCK	Subordinate rock types found with mainrocks	1. Conglomerate, mudstone, limestone. 2. Limestone. 3. Mudstone, tephra, loess. 4. Sand, loess, silt. 5. Sand, mud, peat. 6. Sand, silt, clay. 7. Sand, silt, pumice, clay. 8. Sandstone, conglomerate, coquina, tephra. 9. Sandstone, mudstone, tephra, silt, lignite.
SUBROCK_ Simpl	Sub rocks simplified and condensed	1. Conglomerate, mudstone, limestone. 2. Mudstone, tephra, loess. 3. Sand, loess, silt. 4. Sand, mud, peat. 5. Sand, silt, clay. 6. Sand, silt, pumice, clay. 7. Sandstone, conglomerate, coquina, tephra. 8. Sandstone, mudstone, tephra, silt, lignite.
SIM_NAME	Combines stratigraphic age and depositional environment	6. Holocene river deposits. 7. Late Pleistocene river deposits. 8. Middle Pleistocene - Late Pleistocene river deposits. 9. Middle Pleistocene river deposits. 10. Early Pleistocene river, lake, and shoreline deposits. 11. Neogene sedimentary rocks.

		12. Basement sedimentary rocks.
KEY_NAME	Combines stratigraphic age, stratigraphic name, and lithological information	1. OIS1 (Holocene) river deposits. 2. OIS2 (Late Pleistocene) river deposits. 3. OIS3 (Late Pleistocene) river deposits. 4. Late Pliocene Limestones (e.g.) Totaranui, Otope, Pori, Ngaruru, Kumeroa, from the Mangamaire Group[1] 5. OIS6-OIS2 (Middle Pleistocene - Late Pleistocene) river deposits. 6. OIS6 (Middle Pleistocene) river deposits. 7. Middle Pleistocene river deposits. 8. Early Pleistocene river, lake and intertidal deposits (Kidnappers Group). 9. Pliocene sandstone and siltstone (Mangaheia Group)[2] 10. Pliocene mudstone (Mangamaire Group, Mangahea Group, Te Aute Group, Hurupi Group, Eketahuna Group, Moa Group, Makuri Group, Onoke Group)[3]. 11. Esk Head sandstone and mudstone.

[1] Simplified in chart legends to Late Pliocene Limestones.

[2] Simplified in chart legends to Pliocene sandstone and siltstone.

[3] Simplified in chart legends to Pliocene mudstone

Appendix J: Attenuation Classes

J.1 Parameters used to Derive Attenuation Factors

	QMap layers				FSL layers				
	Water Type	Slope Class	Subrocks Carbon	Rocks Drainage	Soil Gravel Class	Soil pH	Soil Drainage	Soil Texture	Soil Carbon
Combination All	X	X	X	X	X	X	X	X	X
Combination 2			X	X	X	X	X	X	X
Combination 3			X		X	X	X	X	X
Combination 4			X		X		X	X	X
Combination 5			X				X	X	X
Combination 6			X		X		X	X	X
Combination 7	X		X		X	X	X	X	X
Combination 8	X	X			X		X	X	X
Combination 9	X							X	X